New Tools Derived from the Solvatochromic 4-*N,N*-Dimethylamino-1,8-naphthalimide Fluorophore for the Detection of Biomolecular Interactions

by

Galen Loving

B.S. Chemistry
University of Kansas, 2003

MASSACHUSETTS INSTITUTE OF TECHNOLOGY
SEP 2 2 2009
LIBRARIES

Submitted to the Department of Chemistry
in Partial Fulfillment of the Requirements for the
Degree of Doctor of Philosophy

at the

ARCHIVES

Massachusetts Institute of Technology

August 2009

© 2009 Massachusetts Institute of Technology
All rights reserved

Signature of Author:_____
Department of Chemistry
August 31, 2009

Certified by:_____
Barbara Imperiali
Class of 1922 Professor of Chemistry and Professor of Biology
Thesis Supervisor

Accepted by:_____
Robert W. Field
Haslam and Dewey Professor of Chemistry
Chairman, Committee on Graduate Students

This doctoral thesis has been examined by a committee of the Department of Chemistry as follows:

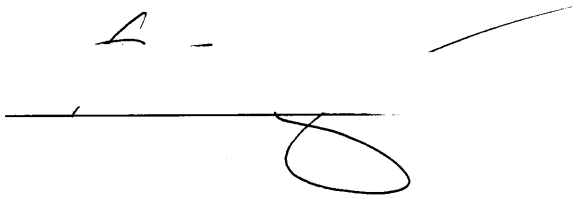

Alice Y. Ting
Chair
Professor of Chemistry
Massachusetts Institute of Technology

Barbara Imperiali
Thesis Supervior
Professor of Chemistry and Professor of Biology
Massachusetts Institute of Technology

Sarah E. O'Connor
Professor of Chemistry
Massachusetts Institute of Technology

New Tools Derived from the Solvatochromic 4-*N,N*-Dimethylamino-1,8-naphthalimide Fluorophore for the Detection of Biomolecular Interactions

by

Galen Loving

Submitted to the Department of Chemistry
on August 31, 2009 in partial fulfillment of the
requirements for the Degree of Doctor of
Philosophy in Organic Chemistry

Abstract

The concept that complex cellular behavior is driven by an intricate network of biomolecular interactions, which emerged through billions of years of evolution, is one of the great wonders of nature. Living cells must constantly assimilate vital information from the surrounding environment and respond appropriately. Such responses include growth, proliferation, migration, and even death. Much of this activity is tightly regulated through elaborately integrated signal transduction pathways — sometimes involving hundreds of cellular components.

In order to further our understanding of the basic molecular machinery responsible for coordinating life processes at the cellular level, new tools are required. Fluorescence methods have formed a cornerstone of modern cell biology and have allowed researchers to interrogate the dynamics of many biomolecular events in real-time. However, the criteria for a good fluorescent probe are often numerous and demanding, particularly when considering applications in complex chemical environments like that of a living cell. Tradeoffs often exist between variables such as good extinction coefficients, suitable wavelengths of excitation and emission, thermal and photochemical stability, size, and others.

Here in, we report a new series of fluorescent tools based on the solvatochromic 4-*N,N*-dimethylamino-1,8-naphthalimide (4-DMN) fluorophore for the study of biomolecular interactions. This fluorophore is distinctive in that it yields very few compromises by combining many of the key elements required of a good fluorescent tool. It can be excited in the visible spectrum (400-450 nm), thus minimizing the damaging effects of high-energy UV light; derivatives of the dye can be prepared in few synthetic steps for facile incorporation into peptides and proteins; it is highly stable to a wide range of chemical conditions; and it possesses extremely sensitive switch-like fluorescent properties capable of responding to subtle changes in the local solvent environment. This thesis chronicles the design and validation of a new fluorescent amino acid of the 4-DMN dye as well as a series of thiol-modifying agents for application in protein and peptide studies. The power of these new tools is demonstrated using the calcium binding protein calmodulin as a model system. Ongoing work to develop a sensitive sensor of Cdc42 activity is also described.

Thesis Supervisor: Barbara Imperiali
Title: Class of 1922 Professor of Chemistry and Professor of Biology

Acknowledgments

I can easily identify the most profound influences that have led me to this point in my life's journey as the lessons learned in childhood from my loving and infinitely supportive family. To my parents, David and Linda, I thank you for always being there for me throughout the bumps and curves of these many years. The uniqueness of my story begins with you. By all accounts, I should not have made it this far. We started in a small farm town in Kansas as an average working class family where I watched the two of you, exhausted and frayed from working your long day jobs, muster the remainder of your energy in the evenings to manage the small apartment complex on Liberty Street. And though we sometimes struggled to make ends meet, our home was more than amply supplied with love, encouragement, and the security of knowing we had each other. You were there when it became clear to my teachers that my school work was hindered by a severe, yet paradoxical learning disability. Though I excelled at reading, which merited placement in an advanced reading class, I utterly lacked the ability to recognize whether the words I saw were correctly spelled. You sought the much needed help and attention that I required in those early years of grade school and remained strong advocates of special education. Your caring and devotion to my academic development ensured that such limitations would not stand in the way of me reaching my dreams. To my brothers, Brian and Jason, you were the trailblazers. We were the first generation in our family to have the extraordinary opportunity to attend college and to see the immense intellectual satisfaction that higher education can provide. Without your guidance, I would be lost. I could not imagine being luckier than to be blessed with two mentors as gifted and brilliant as you. Brian, I forgive the endless teasing about my afro from childhood. It only made me stronger for when I would later enter the Navy. I've always admired your ability to detach yourself from the stresses of work and I try my best to live by your credo: Don't sweat the small stuff because after all, it's all small stuff. I'll get back to you as soon as I figure out how to manage that one. Jason, I don't know what type of scientist I would have been without you. Many times, I think back to the excited discussions we would have about science, mathematics, and engineering. Your presence has been deeply missed these last few years. I'm quite certain that much of my experiences in graduate school have been shaded by the tremendous sense of loss that I bear from your passing. I sorely miss those opportunities to share with you my discoveries as well as failings. But none the less, your impact in my life has been extraordinary, positive, and unforgettable. Your memory lives in my heart.

Kathryn, I've told you this on more than one occasion, but it's well worth repeating: you are my true hero. Although it sounds odd coming from me, you have had an enormous calming effect on my typically high-strung personality. Your warmth and devotion to me and my wellbeing has been of great comfort during these last few years. So much of the strength and courage that I have expressed through my actions is derived from you. I will always love and be inspired by you. Thank you for being such an important part of my life.

To friends and colleagues. Dr. Seung-Jib Choi — You've always struck me as a man of pleasant contradictions. Your outwardly stoic character is nothing more than a paper-thin veil barely masking your true nature as a deeply compassionate and thoughtful friend. I too enjoyed our many morning coffee trips and expansive discussions regarding all things mundane and profound. You are a remarkably well-balanced renaissance intellectual and I do hope we meet again soon. Drs. Eranthie Weerapana and Mary O'Reilly — Years from now when I'm old and infirm, clinging to the few memories of my life that I cherish the most, without question that

precious collection will include the many late nights we spent joking and storytelling at the darkest and dingiest pubs in all of Cambridge. Those were periods of great personal growth for me and I am thankful that I had you there. Dr. Jebrell Glover — I don't know if you fully realize how much you've shaped my thinking and sharpened my skills as a scientist. You were a terrific mentor in life as well as in the laboratory. You are a true scientist and I greatly admire your ethic. Dr. Joel Moore — Over the years, you have been my roommate, my friend, and even my neighbor. But, most importantly, I feel that you have also been like another brother to me. I have relied on you for more than just help with chemistry homework. You are a role model of decency and integrity and are an incredibly remarkable person in ways that cannot adequately be stated in words (note – my definition of 'decency' is fairly relaxed with respect to the colloquial usage of the term). I must also express my deepest gratitude to those special professors from my undergraduate years, Dr. Helen Alexander, Dr. Bryan Foster, and especially Dr. Richard Givens. All of you were instrumental in helping me find the path that led me to where I am now. I saw the passion for science and discovery in each of you, and you saw and cultivated that same passion in me. Thank you for your excellence in teaching and for pushing me to reach further than I ever thought possible. Kale Laverentz — I've always found it difficult to pursue my life's aspirations while maintaining the close friendships that mean so much to me. You have never wavered in our friendship and the bond we share stretches far into our past lives when we were just two kids killing time at the babysitters by setting things on fire in the front yard using a magnifying glass. I still have the scare on my hand where you extinguished a smoldering cigarette butt that we lit. Don't worry; I'm still thinking of a way to get you back. Anyway, you're a quality friend and our bond is stronger than ever. Dr. Langdon Martin — You are the sweetest and most admirable person I know. I am so glad that I had the opportunity to work with you, learn from you, and laugh endlessly at your awful jokes. Dr. Elvedin Lukovic — You were alright at times. I wish we could have gotten to know each other better. You were just so quiet and tightlipped about your personal life. Maybe if you shared more of my penchant for drinking, profanity, and dancing lasciviously to Madonna, we could have hit it off better. Are you certain you want to be a medical doctor? You just don't strike me as a "people-person." Angelyn Larkin — You're seriously the best! I think it's your innocence and pureness of heart that I admire the most. That's why I'm always so careful not to use my blue words in your presence. Dr. Matthieu Sainlos — It has truly been an honor to work with such a gifted and creative chemist as you. I owe much of my success here to you and thank you for all the help you've given me. Brenda Goguen — I've always been impressed by you. You are clearly a deep thinking person and a remarkable scientist. Don't ever change. Meredith Hartley — Thank you for your indomitable spirit. You always cheer me up. Drs. Mark Chen and Jay Troutman — One of you always fills me with great optimism for life and the other is a constant reminder of all that is gloomy. Hee, hee. Just kidding. Drs. James Morrison and Cliff Stains — Thanks for all the great scientific conversations. Michelle Chang and Michael Morrison — Good luck with your graduate careers. I know you're both well on your way to success. Marcie Jaffee — Just when I think have enough lifelong friends, I'm always amazed to find there's room for one more. You're the coolest. Too ALL of you… I love you… I'll miss you… and I'll never forget you.

And last, Professor Barbara Imperiali, I want to thank you for the unbelievable opportunity you've given me these last few years. This has been an incredible experience and you've taught me so much. I look forward to the new and exciting opportunities that await me, but I will always be grateful for the time I had here to explore and mature into the chemist that I am today.

Table of Contents

List of Figures

List of Tables

List of Schemes

List of Abbreviations

4-DAPA	4-*N,N*-dimethylaminophthalimidoalanine
4-DMAP	4-*N,N*-dimethylaminophthalimide
4-DMN	4-*N,N*-dimethylamino-1,8-naphthalimide
4-DMNA	4-*N,N*-dimethylamino-1,8-naphthalimidoalanine
6-DMN	6-*N,N*-dimethylamino-2,3-naphthalimide
6-DMNA	6-*N,N*-dimethylamino-2,3-naphthalimidoalanine
ALADAN/DANA	6-(2-dimethylaminonaphthoyl)alanine
amu	atomic mass unit
a. u.	arbitrary units
Boc	*t*-butoxycarbonyl
BSA	bovine serum albumin
C. I.	confidence interval
CaM	calmodulin
DCM	Dichloromethane
DIPEA	*N,N*-diisopropylethylamine
DMAP	4-dimethylaminopyridine
DMF	*N,N*-dimethylformamide
DMSO	dimethyl sulfoxide
DTT	dithiothreitol
ε	extinction coefficient or molar absorbtivity
EDT	1,2-ethanedithiol
EDTA	ethylenediaminetetraacetic acid
ESI-MS	electrospray ionization mass spectrometry
$E_T(30)$	2,6-diphenyl-(2,4,6-triphenyl-l-pyridinio)phenolate
Φ	quantum yield
FCS	fluorescence correlation spectroscopy
FP	fluorescence polarization
FRET	Förster resonance energy transfer
Fmoc	9-fluorenylmethoxycarbonyl
GAP	GTPase activating protein
GB1	immunoglobulin binding domain B1 of streptococcal protein G
GBD	GTPase-binding domain
GDF	GDI displacement factor
GDI	GDP dissociation inhibitor
GDP	guanosine-5'-diphosphate
GEF	guanine nucleotide exchange factor
GTP	guanosine-5'-triphosphate
GTPase	guanosine triphosphatase
h	Plank's constant
HBTU	O-(Benzotriazol-1-yl)-N,N,N',N'-tetramethyluronium hexafluorophosphate
HOBt	1-hydroxybenzotriazole
HPLC	high performance liquid chromatography
HRMS	high resolution mass spectrometry

ICT	Internal charge transfer
ISC	Intersystem crossing
ITC	isothermal titration calorimetry
K_d	dissociation constant
λ_{em}	emission wavelength
λ_{ex}	excitation wavelength
MALDI-TOF MS	matrix-assisted laser desorption ionization time-of-flight mass spectrometry
MeCN	acetonitrile
MESNA	2-mercaptoethane sulfonate sodium
Mmt	4-methoxytrityl
ν	frequency
NBD	7-nitrobenz-2-oxa-1,3-diazol-4-yl amine
NMR	nuclear magentic resonance
NMP	*N*-methylpyrrolidinone
PBS	phosphate-buffered saline
PDB	protein data bank
PRODAN	6-Propionyl-2-(dimethylamino)naphthalene
S^0	electronic ground state
S^1	excited singlet state
SDS-PAGE	sodium dodecyl sulfate polyacrylamide gel electrophoresis
SPPS	solid-phase peptide synthesis
std. dev.	standard deviation
T^1	excited triplet state
TCEP	*tris*(2-carboxyethyl)phosphine
TFA	trifluoroacetic acid
TIS	triisopropylsilane
TNBS	2,4,6-trinitrobenzene sulfonic acid
Tris	2-amino-2-hydroxymethyl-propane-1,3-diol
Trt	trityl
UV-Vis	ultraviolet-visible

Chapter 1: Introduction of solvatochromic fluorophores as tools for studying biomolecular interactions

1-1. The scope

Fluorescence techniques have become a vital component to the fields of molecular cell biology and protein biochemistry. Many of these techniques include principles of fundamental importance such as Förster resonance energy transfer (FRET),[1] fluorescence polarization (FP),[2] and fluorescence correlation spectroscopy (FCS)[3] as well as a broad assortment of fluorescent dyes exhibiting unique and varied photophysical properties.[4] Innovations in instrumentation have enabled the application of many of these techniques in a wide array of formats ranging from high throughput screening assays[5] for drug discovery to the latest in state-of-the-art super resolution microscopy[6] for *in cellulo* studies. Of particular interest are fluorescent dyes that possess emission properties that are highly responsive to physical changes in the local environment. Such environmental factors can include temperature, pH, viscosity, certain biological analytes, and solvent polarity. By conjugating probes of this type to biologically relevant molecules, it is possible to obtain valuable information regarding the functions, activities, and interactions of such species in the context of living systems with great spatial and temporal resolution.

This introductory chapter focuses on recent advances in the development and application of a specific class of environment sensitive fluorophores that display a property known as solvatochromism. Particular attention is devoted to the incorporation of these tools into peptides and proteins to develop powerful sensors of biomolecular dynamics. In surveying a selection of these applications, various methods that have been developed for the incorporation of such tools are presented along with a brief analysis of the associated advantages and limitations.

1-2. Solvatochromism

Solvatochromic fluorophores possess emission properties (*e.g.* fluorescence lifetimes, emission wavelengths, and fluorescence quantum yields) that are highly sensitive to the nature of the immediate solvent environment. These effects are often most dramatic when comparing these species in solvents of different polarities. The origin of this phenomenon is generalized in the Jablonski diagram of Figure 1-1, which depicts the energies of the different electronic states of the system. Beginning in the bottom left corner of the diagram, the fluorophore (large oval) resides in the electronic ground state (S^0) surrounded by a sphere of solvent molecules (small ovals). The electric dipole moment of the fluorophore is indicated by the black arrow with the "+" sign at the positive terminus of the dipole. Upon absorbing a photon of appropriate energy ($h\nu_A$), the system is rapidly promoted to an excited singlet state (S^1). During this event, the system adopts a new electronic configuration with a dipole moment that differs significantly from that of the ground state. In this case, the dipole has increased in magnitude. As described by the Frank–Condon principle, the process of electronic excitation occurs on a time scale that is much faster than that of the motions of atomic nuclei.[7] Over a period of picoseconds, the dipoles of the solvent sphere molecules reorient to accommodate the now larger dipole of the fluorophore, resulting in a more highly ordered arrangement (upper left corner). This step, termed solvent relaxation, ultimately lowers the energy of the excited singlet state while simultaneously destabilizing the ground state thereby narrowing the energetic gap between the two states. When the system finally returns to the ground state through a fluorescence event, the emitted photon is of a much longer wavelength (*i.e.* lower energy, $h\nu_F$) than that which was originally absorbed during excitation. The degree of solvent relaxation increases with increasing solvent polarity.

In some instances, the fluorophore will return spontaneously to the ground electronic state through a thermal (non-radiative) decay process (k_{nr}) that competes with fluorescence. A common feature among many solvatochromic fluorophores is the tendency to exhibit a marked increase in non-radiative decay as the energy gap separating the S^0 and S^1 states is reduced. This effect is particularly apparent in polar protic solvents such as water, resulting in a decrease of the fluorescence quantum yield. The mechanisms for such processes are varied and can include a range of events such as internal charge transfer (ICT), tautomerization, isomerization, and intersystem crossing (ISC) to an excited triplet state (T^1).[8] When non-radiative decay competes strongly with fluorescence in polar solvents, the fluorophore can exhibit sensitive "switch-like" emission properties upon perturbations to the ordering of the solvent sphere.

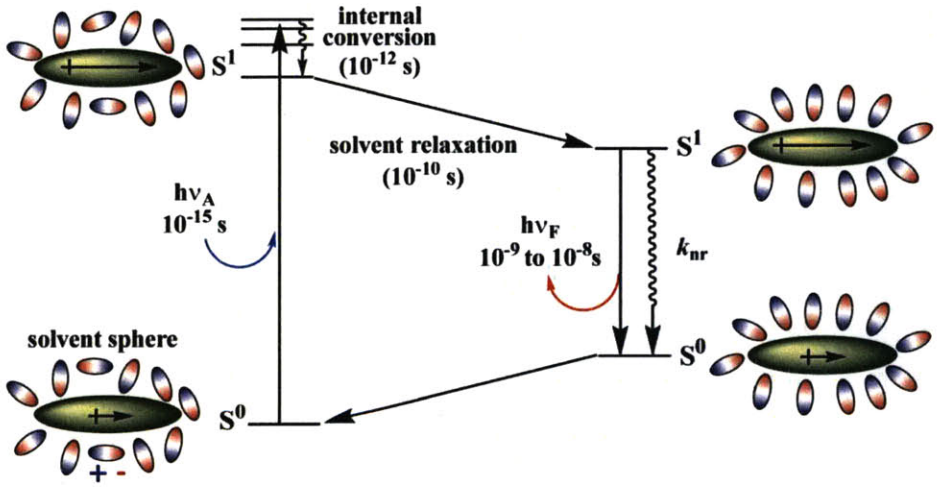

Figure 1-1. Jablonski diagram depicting the effects of solvent relaxation on the emission properties of a typical solvatochromic fluorophore (large oval). The molecules that comprise the immediate solvent sphere (small ovals) are shown surrounding the fluorophore. Both the fluorophore and solvent molecules possess electric dipole moments indicated by the large black arrow bearing a "+" at the positive end of the dipole for the fluorophore and the red-blue poles for the solvent molecules.[8]

1-3. Solvatochromic fluorophores commonly used in biological studies

The dynamic emission properties of solvatochromic fluorophores make these species particularly well suited as potential tools for probing a variety of biomolecular interactions. For instance, if the fluorophore were appended to the surface of a protein at a site that mediates a transient protein-protein interaction, then the probe could report binding provided that the event results in partial or complete extrusion of the surrounding solvent sphere. This basic strategy has been successfully applied in the design of a number of fluorescent biosensors and has led to the emergence of a host of solvatochromic probes with diverse properties, many of which are currently available through commercial sources.[9]

Selecting the appropriate fluorophore for a particular application involves a variety of factors that must be considered. These factors can include such properties as extinction coefficient, wavelengths of excitation and emission, quantum yields of fluorescence, size, hydrophobicity, chemical stability, and reactivity. Often, it is difficult to identify a species that possesses all of the desired attributes required for a given application. Fortunately, a number of well established solvatochromic fluorophores (Chart 1-1) possessing overlapping subsets of these traits have been developed offering researchers more choice over which compromises to accept.

For example, the merocyanine dyes[10] possess exceptionally large extinction coefficients with very long wavelengths of excitation that are ideal for *in cellulo* studies due to the minimization of damaging effects of UV light and the potential for signal interference by autofluorescence. However, these dyes are also large and exhibit rather subtle changes in both fluorescence quantum yields and emission wavelengths in response to solvent polarity. A fluorophore like PRODAN,[9] on the other hand, is much smaller by comparison and can exhibit wavelength shifts as great as 100 nm in the emission spectrum. The smaller chromophore size

reduces the likelihood that the probe will negatively impact the native function or activity of the attached biomolecule. However, unlike the merocyanine derivatives, PRODAN is excited at wavelengths below 400 nm and has an appreciably smaller extinction coefficient.

Chart 1-1. Established solvatochromic fluorophores used in peptide and protein studies

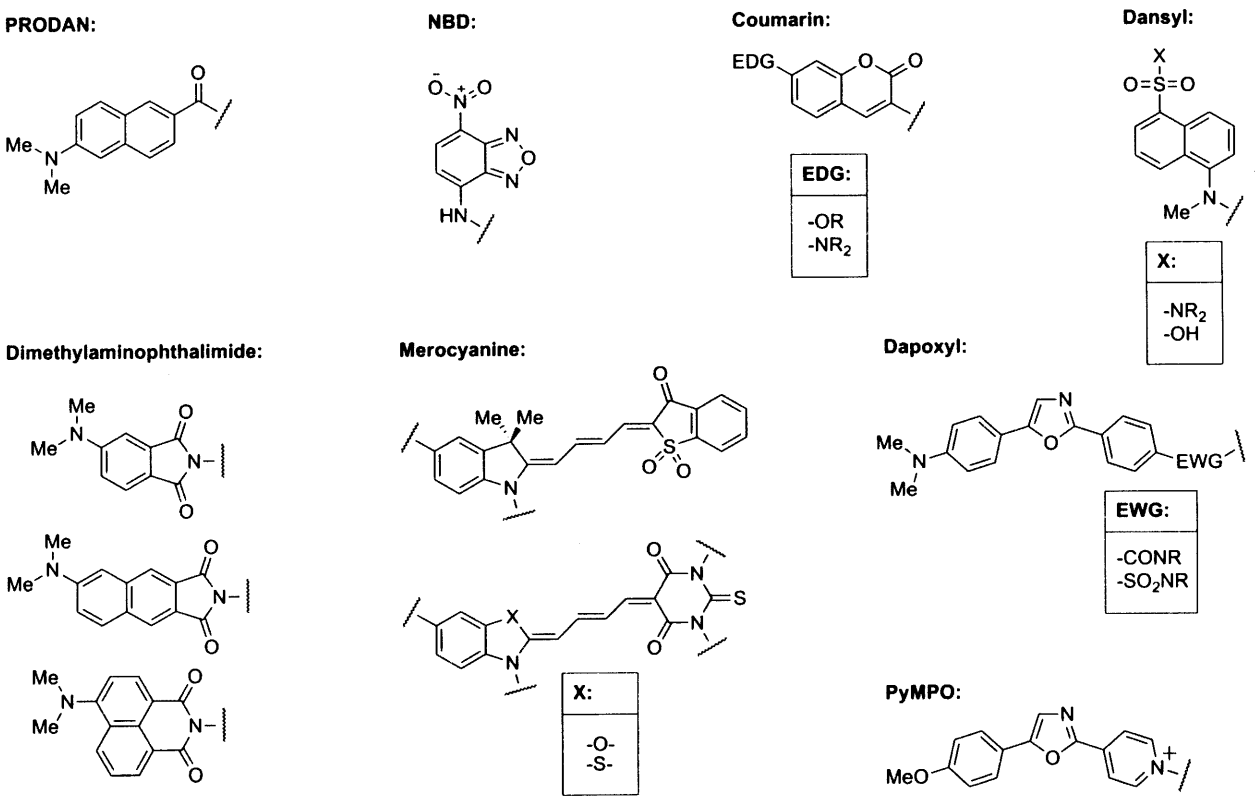

The variation of the emission properties of many solvatochromic fluorophores are difficult to directly compare as most of the studies have been conducted in different laboratories under varying conditions and using different metrics (*i.e.* Lippert-Mataga plots[8] versus the $E_T(30)$ scale[11]). Typically, comparisons are made by measuring the emission properties of the fluorophores in a range of solvents or solvent mixtures. However, these studies are sometimes

complicated by the fact that the solubility of many of these species is restricted to a very narrow range of solvents. Methods to overcome this limitation have been developed whereby the dye is conjugated to another molecule to enhance solubility;[12] however the need still exists for a standardized system by which the solvatochromic properties of all fluorophores may be compared more directly and without bias. With that stated, there are a number of generalities that can be made regarding each species without resorting to meta-analysis. For example, the dimethylaminophthalimide dyes exhibit extremely weak fluorescence in aqueous buffers[12] providing the advantage of low background signal until the occurrence of an event that perturbs the local environment. This creates the effect of "switch-like" fluorescence changes with the potential to produce 1000-fold increases in emission intensity. The dapoxyl® dyes are noted for the ability to exhibit shifts in emission wavelength greater than 200 nm in response to changes in solvent polarity alone.[13] Other important properties for consideration are provided in Table 1-1.

Table 1-1. Physical properties of several solvatochromic fluorophore families

fluorophore family	**extinction coeff. ε (cm^{-1} M^{-1})**	**excitation maximum exc_{max} (nm)**	**MW range (g mol^{-1})**	**charge z (+/-)**	**Refs**
PRODAN	2.0×10^4	390	200	neutral	9
NBD[a]	2.5×10^4	480	180	neutral	9
Coumarin derivatives	$2.4 \times 10^4 - 5.0 \times 10^4$	376 – 419	160 – 215	neutral	9
Dansyl derivatives	$4.1 \times 10^3 - 5.7 \times 10^3$	336 – 340	235 – 265	– / neutral	9
Dimethylamino-phthalimides	$6.5 \times 10^3 - 8.8 \times 10^3$	378 – 408	190 – 240	neutral	12,14,15
Merocyanines	$1.1 \times 10^5 - 2.2 \times 10^5$	570 – 605	440 – 500	+ / – / neutral	10
Dapoxyl® derivatives	2.7×10^4	366 – 370	280 – 330	neutral	13
PyMPO[b]	2.3×10^4	412	250	+	9

(a) 7-nitrobenz-2-oxa-1,3-diazol-4-yl amine.
(b) 1-(2-maleimidylethyl)-4-(5-(4-methoxyphenyl)oxazol-2-yl)-pyridinium methanesulfonate.

1-4. Methods of incorporation into peptides and proteins

The same methods developed to introduce solvatochromic fluorophores into peptides and proteins have been used in a multitude of applications for incorporating other unique functionalities. These methods can broadly be divided into three categories: 1) direct covalent modification of proteins; 2) incorporation of unnatural amino acids *via* expressed protein ligation; and 3) incorporation of unnatural amino acids *via* suppression of the amber (TAG) stop codon. Here, only a brief description of each approach is provided as these have been thoroughly reviewed elsewhere.[9,16,17]

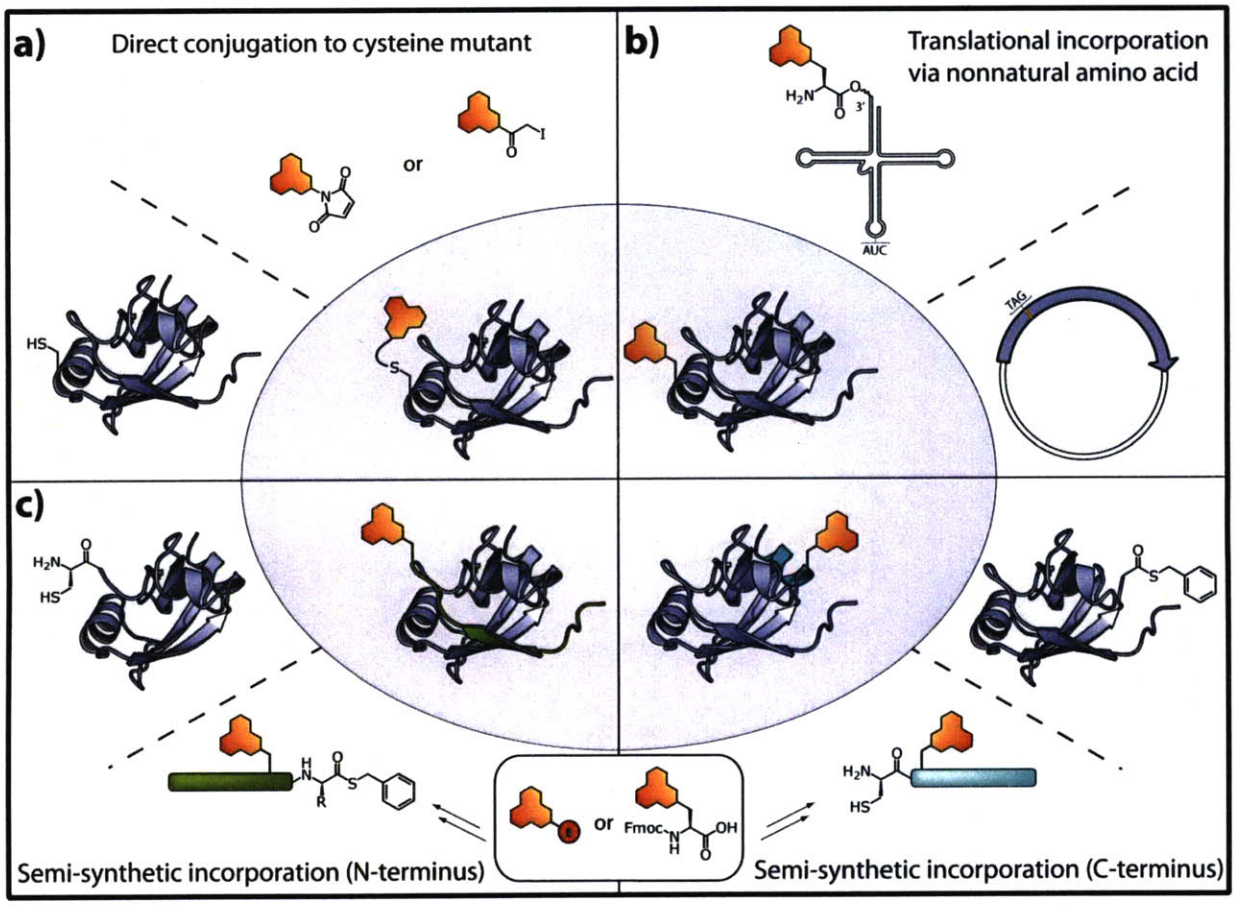

Figure 1-2. Methods for site-selective and site-specific incorporation of solvatochromic fluorophores into protein. (a) Direct labeling of a solvent exposed cysteine residue using a thiol-reactive agent.[9,16] (b) Incorporation of an unnatural amino acid possessing a solvatochromic fluorophore as the side chain group *via* suppression of the amber stop codon. A tRNA molecule designed to recognize and read-through the amber codon is charged with the

unnatural amino acid.[17,18] (c) Expressed protein ligation involves a semisynthetic approach requiring either the N- or C-terminal end of the protein to be prepared by solid phase peptide synthesis. The peptides are then ligated to the portion of the protein construct that was expressed from a recombinant gene product.[19-21]

Direct covalent modification of proteins. A large number of methods for chemically modifying proteins with various extrinsic fluorophores have been developed over the years.[9,16] However, not all of these methods are particularly effective for the design and development of fluorescent protein sensors that rely on solvatochromic dyes. The reason for this resides in the necessity for the dye to be located at a site on the protein surface that is within range of detecting a key biomolecular event through some form of direct physical interaction. Protein labeling methods that require specific peptide or protein motifs to direct labeling[22,23] may not offer sufficient latitude in dye placement, which is typically required for optimizing the fluorescent response. Lysine and cysteine reactive agents offer a convenient and direct method for labeling proteins and have been used extensively to conjugate a myriad of auxiliary groups into proteins. Most common among these are the thiol-selective electrophiles such as maleimides and α-halocarbonyl compounds, along with the amine-selective acylating agents such as the *O*-succinimidyl esters (Figure 1-2a).

Cysteine residues are ideal for site-specific labeling of proteins as this amino acid occurs relatively infrequently in many proteins[17] and possesses excellent nucleophilic properties under most physiological conditions. This permits one to introduce the codon for a cysteine residue site-specifically within a gene sequence of interest using standard molecular biology techniques. In contrast, lysine residues are far more abundant in proteins[17] making selective site-specific labeling of recombinant proteins less straightforward. Additionally, it is possible for amine-reactive derivatives to label the α-amino group of the N-terminal residue of the protein.

Incorporation of unnatural amino acids via expressed protein ligation. Expressed protein ligation (EPL)[19-21] is a powerful semisynthetic approach for incorporating non-native elements into proteins site-specifically. The technique, which has been used extensively, involves expressing a truncated form of the desired protein construct to which a synthetically prepared peptide is ligated at either the N- or C-terminus. The synthetic peptide that is prepared then constitutes the omitted portion of the native protein, but includes an unnatural amino acid in place of another residue. The most commonly employed ligation method requires one of the two fragments to contain an N-terminal cysteine residue while the complementary fragment bears a C-terminal thioester. The N-terminal cysteine residue facilitates ligation through an initial, reversible transthioesterification step, followed immediately by an irreversible intramolecular S→N acyl transfer resulting in the formation of an amide bond (Figure 1-2c).

Many solvatochromic fluorophores have been developed into unnatural amino acids for incorporation into both peptide and protein biosensors through synthetic and semisynthetic aproaches.[12,14,15,24-28] The technique of EPL offers the advantage of yielding materials of greater homogeneity than is typically achieved through direct chemical modification using thiol- or amine-reactive labeling agents. However, EPL does require more synthetic steps and can be limited by low yields of the desired product. Additionally, most applications of EPL have been confined to modification of amino acids within approximately 40 residues of the N- and C-termini of proteins. While methods have been developed to incorporate peptide inserts between two recombinant protein fragments, this practice is less common due to the cumbersome nature of performing sequential ligation steps.[29]

Incorporation of unnatural amino acids via suppression of the amber stop codon. Methods to expand the genetic code to include additional unnatural amino acids have been the

source of intense study by several research groups.[17] One of the more successful approaches utilizes the amber stop codon (TAG) to code for a new amino acid.[18] The infrequent occurrence of this codon in the genes of protein-expression systems like *E. coli* makes it ideally suited for reassignment.[30] Early embodiments of the method involved the semisynthesis of an artificial tRNA molecule designed to recognize the amber codon through base pairing of the anticodon loop. Although different methods have been applied to prepare the suppressor $tRNA_{CUA}$ molecule, one of the more straightforward approaches utilizes a technique termed run-off transcription.[18] The $tRNA_{CUA}$ is transcribed from a DNA template such that it lacks the last two nucleotides of the 3'-terminus. These components are then prepared synthetically as a dinucleotide (pdCpA) charged with the desired unnatural amino acid. Using an enzymatic reaction that requires T4 RNA ligase, the two fragments are then joined together generating the final product. Once obtained, the artificial tRNA is introduced to a specially prepared cell extract derived from *E. coli* (or in other cases derived from yeast or rabbit reticulocyte lysates) that is rich in the molecular machinery necessary for protein synthesis. The gene of interest, which has been mutated to incorporate the amber codon site-specifically, is then translated with the unnatural amino acid successfully integrated into the peptide backbone at the desired position (Figure 1-2b).

Drawbacks to the *in vitro* translation approach include the difficulty of synthesizing the aminoacylated dinucleotide (AA-pdCpA) and the fact that protein yield is limited stoichiometrically to the quantity of the suppressor $tRNA_{CUA}$ added to the reaction. Furthermore, suppression efficiency is generally low on average (20-30%)[17] and can vary widely depending on the nature of the amino acid, the gene to be expressed, the site within the gene that the amber codon is located, and the protein expression system being used.

Currently, a great deal of attention is being focused on expanding the utility of this approach by evolving novel aminoacyl-tRNA synthetase/suppressor tRNA pairs in *E. coli*,[31] yeast[32] and mammalian cell[33] lines that may recognize unnatural amino acids. This *in vivo* approach shows greater promise in yielding usable quantities of protein and has been utilized for the incorporation of a wide range of tyrosine derivatives. However, the unnatural amino acid of interest must first meet several criteria. It must be passively or actively transported into the host cell and lack any toxic activity. Furthermore, it should be orthogonal to the native aminoacyl-tRNA synthetases of the host such that it is not recognized as a substrate and used to misacylate one of the endogenous tRNAs.

1-5. Design considerations when incorporating solvatochromic fluorophores into proteins

The design of a useful fluorescent protein or peptide biosensor often requires an empirical approach guided by any available structural information regarding the interaction of interest. On some occasions, the optimal placement of a solvatochromic fluorophore is readily identified in that a well-defined hydrophobic pocket is already known, which can readily accommodate the dye. An excellent example of this was the development of a series of fluorogenic probes to detect peptide loading onto class II MHC proteins involved in the activation of the adaptive immune response (Figure 1-3).[34] Crystallographic data of the class II MHC protein, HLA-DR1, in complex with a short peptide fragment (HA) derived from influenza revealed a pronounced hydrophobic pocket (P1) that can bind large aliphatic or aromatic side chains such as tyrosine. This position in the HA peptide chain was replaced with the fluorescent amino acids 4-*N,N*-dimethylaminophthalimidoalanine (4-DAPA)[15] and 6-*N,N*-dimethylamino-2,3-naphthalimidoalanine (6-DMNA).[14] Upon binding to HLA-DR1, the peptide probes

exhibited 10^2 to 10^3-fold increases in fluorescence intensity without disrupting the binding affinity or biological activity of the native complex.

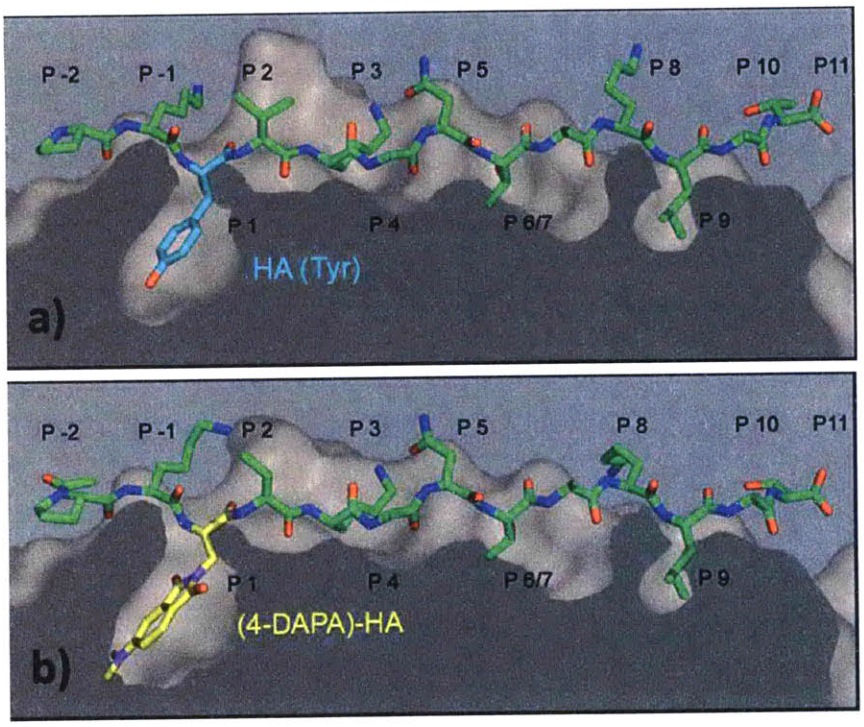

Figure 1-3. Crystal structures of the class II MHC protein, HLA-DR1, in complex with (a) the native influenza-derived HA peptide (PDB entry 1JWU) and (b) the HA peptide containing the 4-DAPA amino acid (PDB entry 2IPK). This figure was reproduced from Venkatraman *et al.*[34]

However, in most cases, determining the optimal site of fluorophore placement is challenging even when exceptional structural data is available. Additionally, the pockets and clefts that form the interface of an interaction can be of differing size, shape and charge thereby admitting some fluorophores while prohibiting others. This has lead many researchers to resort to screening-based methods to examine both placement and fluorophore type simultaneously.

When utilizing cysteine modifying agents to introduce a solvatochromic fluorophore, the key is to identify residues that may be mutated without significantly disrupting the native structure or function of the protein. Furthermore, it is important that the appended fluorophore is

positioned appropriately such that it is capable of producing an adequate signal without negatively interfering with the interaction of interest. Recently, Zhu *et al.* reported the results of a screening approach that produced an effective fluorescent sensor for the detection of a signaling molecule used in bacterial quorum sensing.[35] A variety of cysteine mutants were prepared from two protein receptors known to bind different forms of the bacterial autoinducer II (AI-2). The receptors, LuxP and LsrB, exhibit structural similarity and consist of two domains linked together by a hinge region with the ligand-binding site located at the interface. The cysteine residues introduced at the periphery of this site were labeled with an assortment of solvatochromic fluorophores, including derivatives of dansyl, PRODAN, NBD, dapoxyl®, and PyMPO. One construct, a LuxP mutant (T137C) labeled with a dapoxyl derivative, was identified to possess the desired optical properties. It was then compared with the wild-type receptor by isothermal titration calorimetry (ITC). Although the cysteine mutation had a negligible impact on AI-2 binding, after labeling with the dapoxyl fluorophore, the LuxP-T137C mutant exhibited a seven-fold deterioration in the measured dissociation constant. This was not a major limitation with regard to the intended application of the biosensor, but it does illustrate an important caveat that should be anticipated when introducing a solvatochromic fluorophore.

In addition to the fluorophore type and placement, the linker length, between the fluorophore and the target biomolecule, represents another essential variable to be explored when optimizing the fluorescent response of a biosensor. This matter is treated in greater detail later in Chapter 5. Though it suffices to say the nature of the linker connecting the dye to the biomolecule can exert a dramatic influence on both the measured fluorescence change and the degree of background emission generated by the construct.

The engineering of fluorescently labeled peptides typically offers more flexibility in the design due to the modular nature of solid phase peptide synthesis (SPPS).[36] Peptide libraries of moderate size can be generated quickly and screened for the desired fluorescent properties. Using this approach the fluorophore may be introduced either as an unnatural amino acid building block or attached through covalent modification of an unprotected side chain residue.

The development of short fluorogenic peptides containing solvatochromic fluorophores is more straightforward in some ways in that these molecules typically lack the higher order structures can that occur in globular proteins. A feature common to most solvatochromic fluorophores is the tendency to exhibit altered fluorescence properties when appended to proteins than when freely dissolved in water. This is primarily due to local interactions with the protein surface that can ultimately result in a high degree of background fluorescent signal, limiting the utility of the probe. Since small peptides generally lack the ability to form such structural elements, the fluorophore remains largely exposed to the solvent environment until the probe interacts with another biomolecule.

1-6. Applications of solvatochromic fluorophores

The power and versatility of solvatochromic fluorophores to address problems relating to various biomolecular interactions has been demonstrated repeatedly in a host of applications. These include the sensitive detection of changes in protein structure[37-42] as cited above in the case of the AI-2 receptor LuxP.[35] Often, structural modifications can be quite subtle as described by De Lorimier *et al.*[43] in their work to construct a family of fluorescent biosensors from different bacterial periplasmic binding proteins (bPBPs). These proteins undergo highly localized conformational changes in the presence of specific analytes such as carbohydrates,

amino acids, dipeptides, cations, and anions.[43] Work has also been reported on successful attempts to detect various forms of posttranslational modifications ranging from cysteine prenylation[44] of peptide substrates to protein phosphorylation.[45]

Another important class of applications involves the development of sensors for protein-protein and protein-peptide interactions. Research in this area is intensely active as many biomolecular events of this type constitute a cornerstone of intracellular signal processing. The temporal and spatial dynamics of these events are still poorly understood and yet are known to play a vital role in governing both normal and aberrant cellular behavior. Excellent examples include sensors of Cdc42 activation,[46] actin polymerization,[47] and phosphorylation driven binding events.[14,15,48]

1-7. Dimethylaminopthalimides as powerful tools for the study of biomolecular interactions

Over the past few years, our group has developed and investigated the application of novel amino acids that possess solvatochromic fluorophores as the side-chain group.[14,15,34,49] Amino acid derivatives of 4-*N,N*-dimethylaminophthalimide (4-DMAP) and 6-*N,N*-dimethylamino-2,3-naphthalimide (6-DMN) are of particular interest (Chart 1-2) due to the exceptionally low fluorescence quantum yields that they exhibit in polar protic solvents such as water compared to that in non-polar solvents. This offers the advantage of a greater signal-to-noise ratio over that of other commercially available solvatochromic fluorophores. With sizes comparable to tryptophan, the fluorescent amino acid analogues, 4-*N,N*-dimethylaminophthalimidoalanine (4-DAPA) and 6-*N,N*-dimethylamino-2,3-naphthalimidoalanine (6-DMNA) (Chart 1-2), can be incorporated into the primary sequence of a peptide or protein without introducing a significant perturbation to the overall surface topology

of the native structure. The 4-DAPA and 6-DMNA amino acids have been incorporated into peptide motifs that are recognized by 14-3-3 proteins,[15] SH2 domains,[14] PDZ domains,[50] opioid receptors,[51] and the class II MHC proteins[34] and have proven very effective as probes for monitoring binding. However, due to the intrinsic strain of the five-membered phthalimide ring systems of 4-DMAP and 6-DMN, these fluorophores are susceptible to nucleophilic attack leading to the formation of ring-opened byproducts.

Chart 1-2: Dimethylaminophthalimidoalanine Series of Solvatochromic Amino Acids

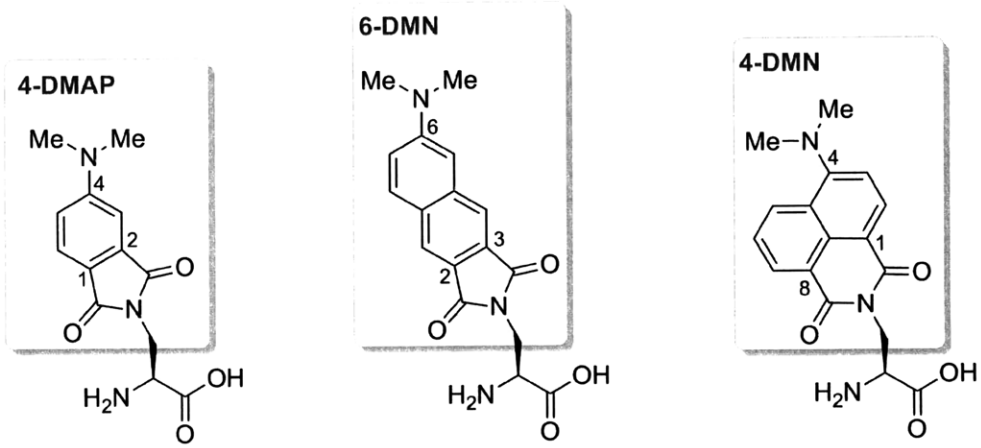

4-DAPA **6-DMNA** **4-DMNA**

Recently, we have developed a new solvatochromic amino acid, 4-*N,N*-dimethylamino-1,8-naphthalimidoalanine (4-DMNA),[12] to complement 4-DAPA and 6-DMNA. This amino acid offers several distinct advantages over the previous congeners while retaining many of the same excellent solvatochromic properties that are characteristic of the dimethylaminophthalimide series. The six-membered imide ring of 4-*N,N*-dimethylamino-1,8-naphthalimide (4-DMN, Chart 1-2) eliminates angle strain on the sp^2 hybridized nuclei resulting in much greater chemical stability. This allows the flexibility to expose the fluorophore to a

wider range of conditions (*i.e.* pH, temperature, buffers, *etc.*) that bear physiological relevance for much longer durations, thus greatly expanding the scope of possible applications. In addition to the fluorescent amino acid, a series of thiol-reactive agents derived from 4-DMN were developed and characterized. Through the studies presented in this thesis we demonstrate that these tools nicely complement — and in some instances surpass — the array of fluorescent probes currently employed in biological studies and will be of great utility in the design of future experiments for many researchers.

The earliest reports of the fluorescent properties of 4-DMN can be traced to studies involving derivatives of the parent 4-amino-1,8-naphthalimide group, which were beginning to draw interest for their brilliant yellow and orange colors.[52] Since that time, the fluorophore has been utilized in a wide range of technologies[53-55] and its photophysical properties have been studied extensively.[56-61] However, biological applications of 4-DMN are comparatively scarce.[62-64]

This thesis chronicles the body of work devoted to the development of a new suite of fluorescent tools derived from the 4-DMN fluorophore. In Chapter 2, we examine the sequence of events that led to a fundamental discovery regarding the chemical stability of the 4-DMAP and 6-DMN dyes. This finding was the impetus for considering alternative fluorophores that ultimately drew our attention to 4-DMN. Chapter 3 details some of the challenges encountered in designing synthetic routes to the molecules described in subsequent chapters. Chapters 4 and 5 present studies that explore many of the key principles that influence the successful design of biosensors that incorporate the properties of solvatochromic fluorophores while simultaneously illustrating the excellent advantages offered by the dimethylaminophthalimide dyes. Chapter 4 focuses exclusively on the use of fluorescent amino acids in peptides with the potential to be

applied in proteins. Chapter 5 delves into the many benefits of using thiol-reactive derivatives of 4-DMN. Here, particular consideration is allocated to the importance of linker-type when attempting to optimize a fluorescent probe. Finally, Chapter 6 discusses ongoing work to develop a new probe for detecting the activation of Cdc42 of the Rho-family GTPases.

References

(1) Jares-Erijman, E. A.; Jovin, T. M. FRET imaging. *Nat. Biotechnol.* **2003**, *21*, 1387-1395.

(2) Goulko, A. A.; Zhao, Q.; Guthrie, J. W.; Zou, H.; Le, X. C. In *Springer Series on Fluorescence*; 1st ed.; Wolfbeis, O. S., Ed.; Springer: New York, 2008; Vol. 5, p 303-322.

(3) Krichevsky, O.; Bonnet, G. Fluorescence correlation spectroscopy: the technique and its applications. *Rep. Prog. Phys.* **2002**, *65*, 251-297.

(4) Lavis, L. D.; Raines, R. T. Bright Ideas for Chemical Biology. *ACS Chem. Biol.* **2008**, *3*, 142-155.

(5) Janzen, W. P. *High throughput screening: methods and protocols*; Humana Press: Totowa, N.J., 2002.

(6) Fernandez-Suarez, M.; Ting, A. Y. Fluorescent probes for super-resolution imaging in living cells. *Nat. Rev. Mol. Cell Biol.* **2008**, *9*, 929-943.

(7) Condon, E. U. Nuclear motions associated with electron transitions in diatomic molecules. *Phys. Rev.* **1928**, *32*, 858-872.

(8) Lakowicz, J. R.; 3rd ed.; Springer: New York, 2006, p 205-235.

(9) Haugland, R. P.; Spence, M. T. Z.; Johnson, I. D.; Basey, A. *The handbook : a guide to fluorescent probes and labeling technologies*; 10th ed.; Molecular Probes: Eugene, OR, 2005.

(10) Toutchkine, A.; Kraynov, V.; Hahn, K. Solvent-sensitive dyes to report protein conformational changes in living cells. *J. Am. Chem. Soc.* **2003**, *125*, 4132-4145.

(11) Reichardt, C. Solvatochromic dyes as solvent polarity indicators. *Chem. Rev.* **1994**, *94*, 2319-2358.

(12) Loving, G.; Imperiali, B. A versatile amino acid analogue of the solvatochromic fluorophore 4-*N,N*-dimethylamino-1,8-naphthalimide: A powerful tool for the study of dynamic protein interactions. *J. Am. Chem. Soc.* **2008**, *130*, 13630-13638.

(13) Diwu, Z.; Lu, Y. X.; Zhang, C. L.; Klaubert, D. H.; Haugland, R. P. The spectral properties and biological applications of solvatochromic Dapoxyl (TM) dyes. *Proceedings Of Advances in Fluorescence Sensing Technology IV* **1999**, *3602*, 256-264.

(14) Vazquez, M. E.; Blanco, J. B.; Imperiali, B. Photophysics and biological applications of the environment-sensitive fluorophore 6-*N,N*-dimethylamino-2,3-naphthalimide. *J. Am. Chem. Soc.* **2005**, *127*, 1300-1306.

(15) Vazquez, M. E.; Rothman, D. M.; Imperiali, B. A new environment-sensitive fluorescent amino acid for Fmoc-based solid phase peptide synthesis. *Org. Biomol. Chem.* **2004**, *2*, 1965-1966.

(16) Hermanson, G. T. *Bioconjugate techniques*; Academic Press: San Diego, 1996.
(17) de Graaf, A. J.; Kooijman, M.; Hennink, W. E.; Mastrobattista, E. Nonnatural amino acids for site-specific protein conjugation. *Bioconjug. Chem.* **2009**, *20*, 1281-1295.
(18) Ellman, J.; Mendel, D.; Anthonycahill, S.; Noren, C. J.; Schultz, P. G. Biosynthetic Method for Introducing Unnatural amino-acids site-specifically into proteins. *Meth. Enzymol.* **1991**, *202*, 301-336.
(19) Dawson, P. E.; Muir, T. W.; Clark-Lewis, I.; Kent, S. B. Synthesis of proteins by native chemical ligation. *Science* **1994**, *266*, 776-779.
(20) Hackeng, T. M.; Griffin, J. H.; Dawson, P. E. Protein synthesis by native chemical ligation: expanded scope by using straightforward methodology. *Proc. Natl. Acad. Sci. U.S.A.* **1999**, *96*, 10068-10073.
(21) Muir, T. W.; Sondhi, D.; Cole, P. A. Expressed protein ligation: A general method for protein engineering. *Proc. Natl. Acad. Sci. U.S.A.* **1998**, *95*, 6705-6710.
(22) Chen, I.; Ting, A. Y. Site-specific labeling of proteins with small molecules in live cells. *Curr. Opin. Biotechnol.* **2005**, *16*, 35-40.
(23) Wu, P.; Shui, W. Q.; Carlson, B. L.; Hu, N.; Rabuka, D.; Lee, J.; Bertozzi, C. R. Site-specific chemical modification of recombinant proteins produced in mammalian cells by using the genetically encoded aldehyde tag. *Proc. Natl. Acad. Sci. U.S.A.* **2009**, *106*, 3000-3005.
(24) Summerer, D.; Chen, S.; Wu, N.; Deiters, A.; Chin, J. W.; Schultz, P. G. A genetically encoded fluorescent amino acid. *Proc. Natl. Acad. Sci. U.S.A.* **2006**, *103*, 9785-9789.
(25) Wang, J.; Xie, J.; Schultz, P. G. A genetically encoded fluorescent amino acid. *J. Am. Chem. Soc.* **2006**, *128*, 8738-8739.
(26) Cohen, B. E.; McAnaney, T. B.; Park, E. S.; Jan, Y. N.; Boxer, S. G.; Jan, L. Y. Probing protein electrostatics with a synthetic fluorescent amino acid. *Science* **2002**, *296*, 1700-1703.
(27) Turcatti, G.; Nemeth, K.; Edgerton, M. D.; Meseth, U.; Talabot, F.; Peitsch, M.; Knowles, J.; Vogel, H.; Chollet, A. Probing the structure and function of the Tachykinin Neurokinin-2 receptor through biosynthetic incorporation of fluorescent amino acids at specific sites. *J. Biol. Chem.* **1996**, *271*, 19991-19998.
(28) Dufau, I.; Mazarguil, H. Design of a fluorescent amino acid derivative usable in peptide synthesis. *Tetrahedron Lett.* **2000**, *41*, 6063-6066.
(29) Cotton, G. J.; Ayers, B.; Xu, R.; Muir, T. W. Insertion of a synthetic peptide into a recombinant protein framework: A protein biosensor. *J. Am. Chem. Soc.* **1999**, *121*, 1100-1101.
(30) Nakamura, Y.; Gojobori, T.; Ikemura, T. Codon usage tabulated from international DNA sequence databases: status for the year 2000. *Nucleic Acids Res.* **2000**, *28*, 292-292.
(31) Wang, L.; Brock, A.; Herberich, B.; Schultz, P. G. Expanding the genetic code of Escherichia coli. *Science* **2001**, *292*, 498-500.
(32) Chin, J. W.; Cropp, T. A.; Anderson, J. C.; Mukherji, M.; Zhang, Z. W.; Schultz, P. G. An expanded eukaryotic genetic code. *Science* **2003**, *301*, 964-967.
(33) Liu, W.; Brock, A.; Chen, S.; Schultz, P. G. Genetic incorporation of unnatural amino acids into proteins in mammalian cells. *Nat. Methods* **2007**, *4*, 239-244.
(34) Venkatraman, P.; Nguyen, T. T.; Sainlos, M.; Bilsel, O.; Chitta, S.; Imperiali, B.; Stern, L. J. Fluorogenic probes for monitoring peptide binding to class II MHC proteins in living cells. *Nat. Chem. Biol.* **2007**, *3*, 222-228.

(35) Zhu, J.; Pei, D. A LuxP-based fluorescent sensor for bacterial autoinducer II. *ACS Chem. Biol.* **2008**, *3*, 110-119.
(36) Chan, W. C.; White, P. D. *Fmoc solid phase peptide synthesis: a practical approach*; Oxford University Press: New York, 2000.
(37) Hibbs, R. E.; Talley, T. T.; Taylor, P. Acrylodan-conjugated cysteine side chains reveal conformational state and ligand site locations of the acetylcholine-binding protein. *J. Biol. Chem.* **2004**, *279*, 28483-28491.
(38) Cohen, B. E.; Pralle, A.; Yao, X. J.; Swaminath, G.; Gandhi, C. S.; Jan, Y. N.; Kobilka, B. K.; Isacoff, E. Y.; Jan, L. Y. A fluorescent probe designed for studying protein conformational change. *Proc. Natl. Acad. Sci. U.S.A.* **2005**, *102*, 965-970.
(39) Hahn, K.; Debiasio, R.; Taylor, D. L. Patterns of elevated free calcium and calmodulin activation in living cells. *Nature* **1992**, *359*, 736-738.
(40) Dattelbaum, J. D.; Looger, L. L.; Benson, D. E.; Sali, K. M.; Thompson, R. B.; Hellinga, H. W. Analysis of allosteric signal transduction mechanisms in an engineered fluorescent maltose biosensor. *Protein Sci.* **2005**, *14*, 284-291.
(41) SchauerVukasinovic, V.; Cullen, L.; Daunert, S. Rational design of a calcium sensing system based on induced conformational changes of calmodulin. *J. Am. Chem. Soc.* **1997**, *119*, 11102-11103.
(42) Tamrazi, A.; Carlson, K. E.; Katzenellenbogen, J. A. Molecular sensors of estrogen receptor conformations and dynamics. *Mol. Endocrinol.* **2003**, *17*, 2593-2602.
(43) de Lorimier, R. M.; Smith, J. J.; Dwyer, M. A.; Looger, L. L.; Sali, K. M.; Paavola, C. D.; Rizk, S. S.; Sadigov, S.; Conrad, D. W.; Loew, L.; Hellinga, H. W. Construction of a fluorescent biosensor family. *Protein Sci.* **2002**, *11*, 2655-2675.
(44) Cassidy, P. B.; Dolence, J. M.; Poulter, C. D. Continuous fluorescence assay for protein prenyltransferases. *Meth. Enzymol.* **1995**, *250*, 30-43.
(45) Post, P. L.; Trybus, K. M.; Taylor, D. L. A genetically-engineered, protein-based optical biosensor of myosin-II regulatory light-chain phosphorylation. *J. Biol. Chem.* **1994**, *269*, 12880-12887.
(46) Nalbant, P.; Hodgson, L.; Kraynov, V.; Toutchkine, A.; Hahn, K. M. Activation of endogenous Cdc42 visualized in living cells. *Science* **2004**, *305*, 1615-1619.
(47) Marriott, G.; Zechel, K.; Jovin, T. M. Spectroscopic and functional-characterization of an environmentally sensitive fluorescent actin conjugate. *Biochemistry* **1988**, *27*, 6214-6220.
(48) Wang, Q.; Lawrence, D. S. Phosphorylation-driven protein-protein interactions: a protein kinase sensing system. *J. Am. Chem. Soc.* **2005**, *127*, 7684-7685.
(49) Nitz, M.; Mezo, A. R.; Ali, M. H.; Imperiali, B. Enantioselective synthesis and application of the highly fluorescent and environment-sensitive amino acid 6-(2-dimethylaminonaphthoyl) alanine (DANA). *Chem. Commun. (Camb.)* **2002**, 1912-1913.
(50) Sainlos, M.; Iskenderian, W. S.; Imperiali, B. A General screening strategy for peptide-based fluorogenic ligands: probes for dynamic studies of PDZ domain-mediated interactions. *J. Am. Chem. Soc.* **2009**, *131*, 6680-6682.
(51) Vazquez, M. E.; Blanco, J. B.; Salvadori, S.; Trapella, C.; Argazzi, R.; Bryant, S. D.; Jinsmaa, Y.; Lazarus, L. H.; Negri, L.; Giannini, E.; Lattanzi, R.; Colucci, M.; Balboni, G. 6-*N,N*-Dimethylamino-2,3-naphthalimide: A new environment-sensitive fluorescent probe in δ- and μ-selective opioid peptides. *J. Med. Chem.* **2006**, *49*, 3653-3658.

(52) Alexiou, M. S.; Tychopoulos, V.; Ghorbanian, S.; Tyman, J. H. P.; Brown, R. G.; Brittain, P. I. The UV-visible absorption and fluorescence of some substituted 1,8-naphthalimides and naphthalic anhydrides. *J. Chem. Soc. Perkin Trans. II* **1990**, 837-842.
(53) Grabchev, I.; Meallier, P.; Konstantinova, T.; Popova, M. Synthesis of some unsaturated 1,8-naphthalimide dyes. *Dyes Pigm.* **1995**, *28*, 41-46.
(54) Tomasz, M.; Krzysztof, F.; Hanka, M.; Ewa, M.; Eryk, W.; Danuta, B.; Jozef, Z., Ed.; SPIE: 1995; Vol. 2372, p 317-322.
(55) Jun, L.; Changchun, M.; Quanguo, Z.; Yanxiang, C.; Lixiang, W.; Dongge, M.; Xiabin, J.; Fosong, W. Blue light-emitting polymer with polyfluorene as the host and highly fluorescent 4-dimethylamino-1,8-naphthalimide as the dopant in the sidechain. *Applied Physics Letters* **2006**, *88*, 083505.
(56) Kollar, J.; Hrdlovic, P.; Chmela, S.; Sarakha, M.; Guyot, G. Synthesis and transient absorption spectra of derivatives of 1,8-naphthalic anhydrides and naphthalimides containing 2,2,6,6-tetramethylpiperidine; triplet route of deactivation. *J. Photochem. Photobiol. A Chem.* **2005**, *170*, 151-159.
(57) Saha, S.; Samanta, A. Influence of the structure of the amino group and polarity of the medium on the photophysical behavior of 4-amino-1,8-naphthalimide derivatives. *J. Phys. Chem. A* **2002**, *106*, 4763-4771.
(58) Grabchev, I.; Guittonneau, S.; Konstantinova, T.; Meallier, P. Photochemistry of naphthalenic dyes. *Bull. Soc. Chim. Fr.* **1994**, *131*, 828-830.
(59) Zhang, W.; Wang, Y. L.; Xu, Y. F.; Qian, X. H. New fluorescent conjugates of uridine nucleoside and substituted 1,8-naphthalimide: Synthesis, weak interactions and solvent effects on spectra. *Monatsh. Chem.* **2003**, *134*, 393-402.
(60) Banthia, S.; Samanta, A. Influence of structure on the unusual spectral behavior of 4-dialkylamino-1,8-naphthalimide. *Chem. Lett.* **2005**, *34*, 722-723.
(61) Grabtchev, I.; Philipova, T.; Meallier, P.; Guittonneau, S. Influence of substituents on the spectroscopic and photochemical properties of naphthalimide derivatives. *Dyes Pigm.* **1996**, *31*, 31-34.
(62) Berque-Bestel, I.; Soulier, J. L.; Giner, M.; Rivail, L.; Langlois, M.; Sicsic, S. Synthesis and characterization of the first fluorescent antagonists for human 5-HT4 receptors. *J. Med. Chem.* **2003**, *46*, 2606-2620.
(63) Singh, S.; Singh, R. Synthesis and fluorescence studies of some new fluorophores and their effect on hybridization of oligodeoxyribonucleotides. *J. Fluoresc.* **2007**, *17*, 139-148.
(64) Gryzunov Iu, A.; Miller Iu, I.; Dobretsov, G. E.; Pestova, A. B. Fluorescent method of determining mass concentration of human serum albumin. *Klin. Lab. Diagn.* **1994**, 27-31.

Chapter 2: Comparative studies on the chemical stability of the dimethylamino-phthalimide fluorophores

A significant portion of the work described in this chapter has been published in:

Loving, G.; Imperiali, B. A versatile amino acid analogue of the solvatochromic fluorophore 4-*N,N*-dimethylamino-1,8-naphthalimide: A powerful tool for the study of dynamic protein interactions. *J. Am. Chem. Soc.* **2008**, *130*, 13630-13638.

Introduction

A major initiative in the Imperiali laboratory over the last few years has focused on the development and application of novel biochemical tools for probing the dynamics of biomolecular events involved in cell biology. Many aspects of cellular behavior are controlled or regulated through a complex network of transient interactions amongst proteins, nucleic acids, carbohydrates, and other biomolecules.[1] Although many of these interactions have been identified and even characterized in great structural detail using NMR and X-ray crystallographic methods, the highly choreographed regulation of such events within the context of living cells is less clearly understood. One approach to access this information in real-time is to exploit the highly sensitive emission properties of certain solvatochromic fluorophores. While this method has been utilized for many years — particularly in regard to *in vitro* studies[2] — we have developed a number of novel solvatochromic amino acids[3-6] (Chart 2-1) that can be incorporated directly into the peptide backbone of proteins using the various methods introduced earlier in Chapter 1 and, which due to the greatly improved photophysical properties, can potentially be employed in highly complex systems.

Chart 2-1. Unnatural amino acids of solvatochromic fluorophores developed *in-house*[3-5,7]

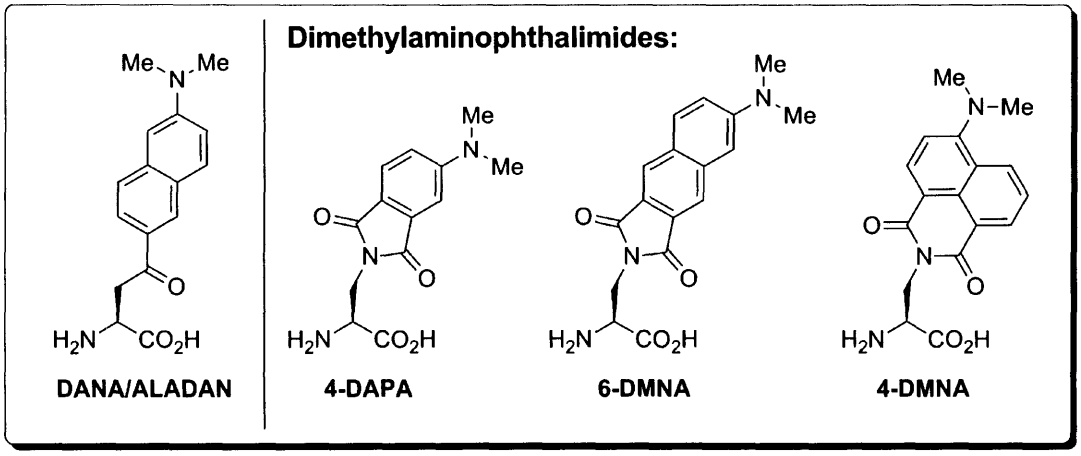

The concept of using unnatural amino acids to serve as probes for detecting various protein-mediated interactions has been supported by numerous reports in the literature in which the natural amino acid tryptophan[8-10] was used to measure the occurrence of such events. Exemplary applications include the detection of changes in protein structure as well as protein-protein binding. Tryptophan possesses a fluorescent indole heterocycle as the side chain group, which exhibits sensitive solvatochromic properties.[8] If a protein containing this residue undergoes a transformation of some form that alters the exposure of the indole group to the aqueous environment, then an associated change in the emission properties would be observed. Unfortunately, tryptophan lacks the key attributes required to make it an effective probe for the detection of biomolecular interactions in complex environments such as living cells. This is due to the fact that the natural abundance of this amino acid within cells would overshadow any useful fluorescent signal by interference from other proteins. Additionally, the excitation maximum of tryptophan occurs at 280 nm. This wavelength is particularly damaging to nucleic acids and select coenzymes and can potentially be lethal to the cell if overexposed. Therefore, unnatural fluorescent amino acids that possess superior photophysical properties to tryptophan could greatly benefit the field of live cell imaging.

Early endeavors by our group to develop a solvatochromic amino acid were pioneered by Dr. Mark Nitz who developed an enantioselective synthesis of the PRODAN derivative 6-(2-dimethylaminonaphthoyl) alanine (DANA) (Chart 2-1).[3] Similar work by Cohen *et al.* was also reported in the same period using the synonym ALADAN in reference to the identical amino acid.[7] The PRODAN fluorophore exhibits excellent solvatochromic properties compared to other amino acid derivatives available at that time, such as that derived from 7-nitrobenz-2-oxa-

1,3-diazol-4-yl amine (NBD).[11] However, it is limited to some extent by the high degree of intrinsic fluorescence the fluorophore exhibits in water.[12] This issue is discussed in greater detail later in Chapter 4.

In view of this success, researchers of the Imperiali group began to explore an alternative class of solvatochromic fluorophores capable of producing more pronounced changes in their emission properties. Members of the dimethylaminophthalimide family of fluorophores possess fluorescence quantum yields that are extremely sensitive to solvent polarity. This is primarily due to an internal charge transfer (ICT) process that occurs with high efficiency when these species are dissolved in polar protic solvents like water.[13] Charge transfer processes that occur in the excited state of fluorophores often lead to intersystem crossing (ISC) and return to the electronic ground state via non-radiative decay. The amino acid derivative 4-DAPA (Chart 2-1), which was introduced by Dr. Eugenio Vázquez,[5] contains the solvatochromic fluorophore 4-*N,N*-dimethylaminophthalimide (4-DMAP) as the side chain group. This amino acid offers several distinct advantages over DANA. Foremost, it exemplifies the dramatic changes in fluorescence quantum yield that are characteristic of the dimethylaminophthalimide family. This property is demonstrated later in Chapter 4. The size of the chromophore is more comparable to that of the aromatic side chain of tryptophan making it less likely to interfere with the native activity of a peptide or protein into which it is introduced (Figure 2-1). Additionally, the synthetic route developed to prepare 4-DAPA is relatively straightforward in that the anhydride precursor (**2-1**) can be directly conjugated to the side chain of a protected (S)-2,3-diaminopropanoic acid derivative (**2-2**). This transformation makes use of the "chiral pool" and thus circumvents the need to generate a new stereocenter as was required for the preparation of DANA.

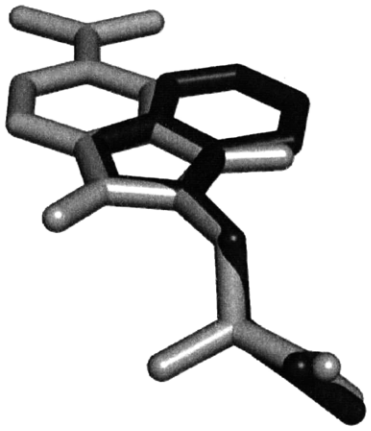

Figure 2-1. 3-Dimensional overlay of the 4-DAPA amino acid (grey) with tryptophan (black).

Scheme 2-1. Synthesis of allyl protected Fmoc-4-DAPA building block.

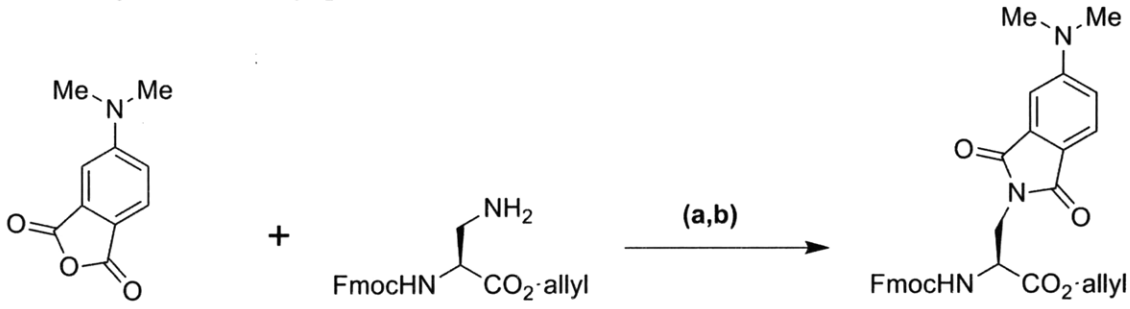

4-DMAP anhydride, 2-1 **2-2** **2-3**

Reagents and conditions: (a) DIPEA, DMF, room temperature, 30 min; (b) HBTU/HOBt, overnight, 63% overall yield for both steps.

Following the development of 4-DAPA, Vázquez attempted to improve upon the properties of the 4-DMAP by extending the π-system of the chromophore to that of a naphthalene ring.[4] It was anticipated that increasing the conjugation of the system would reduce the energy gap separating the HOMO and LUMO thereby increasing the wavelengths of excitation and emission. In his work to characterize the photophysical properties of the new fluorescent amino acid 6-DMNA (Chart 2-1), Vázquez was able to show that this new probe exhibits a larger shift in emission wavelength (>100 nm) in response to changes in solvent

polarity. However, the excitation band for 6-DMNA curiously appears at a shorter wavelength (375 nm) compared to that of 4-DAPA (395 nm).

While exploring new applications of the 6-DMNA amino acid in small peptide probes for protein motifs such as SH2 domains and PDZ[14] domains, it was observed by Dr. Matthieu Sainlos that an anomalous emission band around 460-470 nm would increase steadily in intensity in aqueous solutions of 6-DMNA samples over the time course of a few hours. The emission band had originally been reported by Vázquez in his initial characterization of 6-DMNA,[4] but it was noted that although the intensity of the band differed from peptide to peptide, it was almost invariant throughout the course of his titration experiments. Believing the band to be an intrinsic feature of 6-DMN, he proposed that the second emission band could potentially be a useful reference for ratiometric measurements (Figure 2-2). However, as the investigation into the matter continued it was eventually demonstrated by Sainlos that the aberrant band that appeared in the emission spectrum was actually the result of a degradation product. Due to the intrinsic strain of the five-membered phthalimide ring system of 6-DMN, the fluorophore is highly susceptible to nucleophilic attack leading to the formation of ring-opened byproducts.[6] In this instance, the product was the result of hydrolysis (Figure 2-3a) and happened to be highly fluorescent compared to that of the ring-closed state.

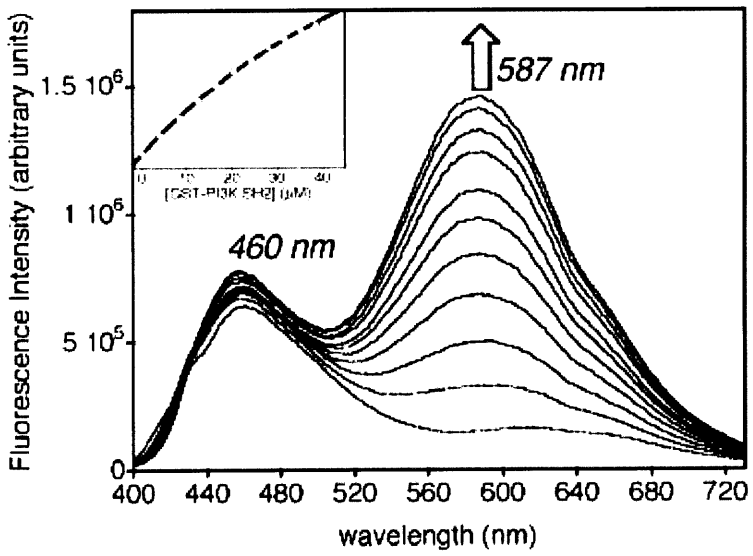

Figure 2-2. Titration of a fluorogenic peptide probe containing the 6-DMNA amino acid with an SH2 domain of a Phosphoinositide 3-kinase (PI3K). The series of fluorescence spectra correspond to increasing concentration of the SH2 domain. The aberrant emission peak is visible at 460 nm. (Figure reproduced from Vázquez et al.)[4]

The difficulty in determining the underlying chemistry responsible for this phenomenon was the lack of an apparent byproduct. Although the intensity of the anomalous emission band would increase several fold over the course of a single hour, this actually represented a very small percentage of conversion of the 6-DMN fluorophore to the corresponding naphthalamic acid. When a sample of this peptide solution was then examined by analytical HPLC, UV-vis, and mass spectrometry, the results always appeared to confirm that no chemical transformation had occurred. Eventually, Sainlos was able to force the reaction to completion by incubating a peptide containing 6-DMNA in an aqueous buffer overnight at 42 °C (Figure 2-3b). This treatment of the peptide sample dramatically increased the magnitude of the emission band at 460 nm. It also had an obvious effect on the UV-spectrum of the chromophore with a shift in the absorption band from 390 nm down to 315 nm. Furthermore, mass spectral analysis plainly indicated a new mass corresponding to that of the original peptide with the addition of 18 amu.

The combined data strongly suggested that hydrolysis of the imide ring system was involved. To confirm this hypothesis, Sainlos independently synthesized the putative ring-opened byproduct and compared the absorption and emission spectra. The results matched that of the byproduct.

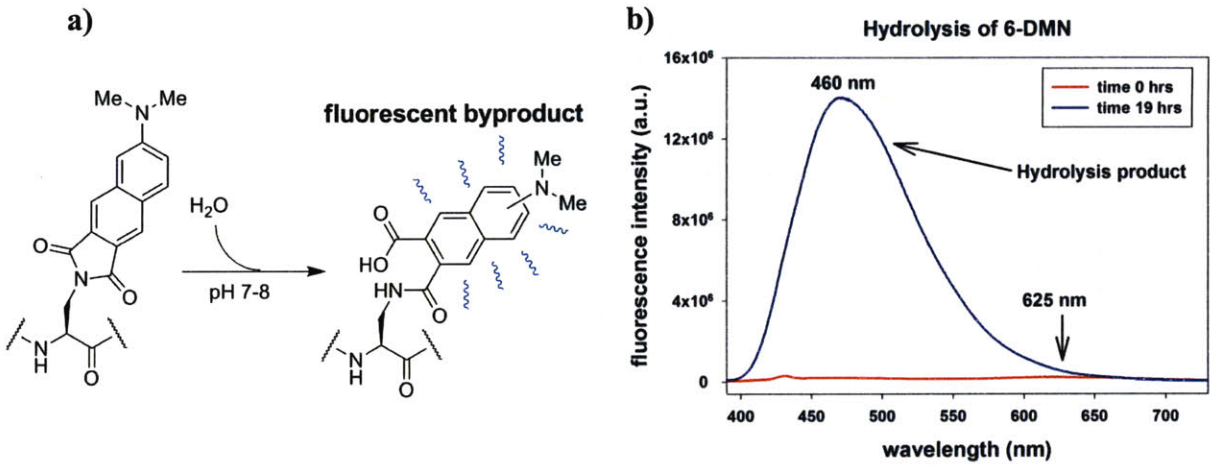

Figure 2-3. (a) Hydrolysis of the five-membered imide ring system of 6-DMNA leading to the highly fluorescent naphthalamic acid byproduct. (b) Fluorescence spectra of a 6-DMNA containing peptide in a phosphate buffered saline solution before and after being heated at 42 °C for 19 hrs. The 6-DMN fluorophore exhibits very little fluorescence in water and possesses an emission maximum at 625 nm. By contrast, the hydrolysis product is highly fluorescent in water and exhibits an emission maximum at 625 nm. (Data were obtained by Dr. Matthieu Sainlos).

During this period it was also discovered that the fluorophore 4-DMAP exhibited similar susceptibility toward hydrolysis. This was less of a problem since the corresponding byproduct of this reaction was non-fluorescent. Still, the lack of chemical stability exhibited by the 4-DMAP and 6-DMN fluorophores presented a potentially fundamental limitation that had to be addressed. If these tools were to eventually be incorporated into proteins, it was determined that further evolution of the fluorophores was essential. It was this context that ultimately led us to investigate the potential applications of a new fluorescent amino acid also derived from the dimethylaminophthalimide family of solvatochromic fluorophores. The experiments described in this chapter demonstrate the robustness of the new 4-DMNA amino acid while qualitatively

defining the limitations presented by 4-DAPA and 6-DMNA. This work also reveals important parameters that should be considered when designing experiments that utilize the 4-DMAP and 6-DMN fluorophores.

Results and Discussion

2-1. Stability of 4-DMNA to hydrolysis

Very often proteins are limited to a narrow range of conditions in which they are stable or functional (*e.g.* pH, temperature, detergents, *etc.*). Because these conditions are sometimes extremely restrictive, it is important to have fluorescent tools devoid of additional environmental constraints. As stated earlier, a principal vulnerability of the 4-DMAP and 6-DMN fluorophores is the tendency to hydrolyze over time at high pH. While hydrolysis of the imide ring of 4-DMAP leads to a non-fluorescent byproduct, the hydrolysis of 6-DMN results in a fluorescent species with an emission maximum observed at 460 nm. This produces a gradual increase in background fluorescence that strongly interferes with the signal of interest.

A comparison of 4-DMAP to 4-DMN was performed to demonstrate the enhanced stability of 4-DMN toward hydrolysis. Both fluorophores were incorporated into a pair of model peptides rich in lysine and arginine residues (termed the KR peptides) to facilitate solubility. The KR_{4DMAP} peptide was screened at various concentrations in PBS buffer at three different pH levels (pH 6, 7, and 8). Since 4-DMAP undergoes a loss of fluorescence upon hydrolysis, the percent conversion of the fluorophore was simply defined as the percent loss of fluorescence from the initial starting point of the reaction. These same conditions were also applied to the

KR_{4DMN} peptide. The reactions were monitored in a 96-well plate over the course of 24 hrs (see Experimental section for details).

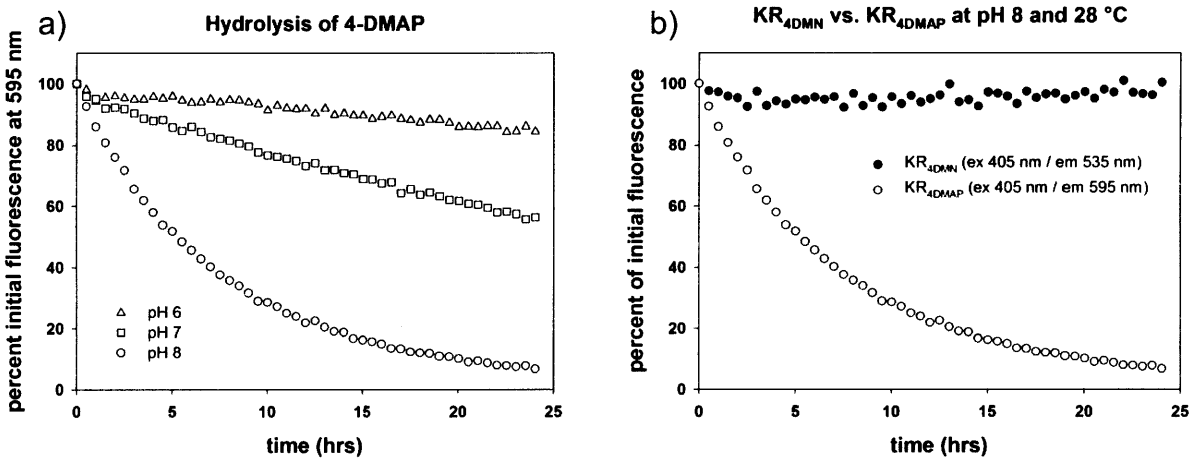

Figure 2-4. (a) The graph depicts the loss of fluorescence due to imide-ring hydrolysis of 4-DMAP in the KR_{4DMAP} peptide (40 μM) over 24 hrs in PBS buffer at 28 °C. The data reveals the rate enhancement observed at higher pH levels. (b) This side-by-side comparison of 4-DMN versus 4-DMAP shows that no significant change in fluorescence was observed for 4-DMN under the harshest conditions anticipated for its use. No hydrolysis byproduct was detected by ESI MS for the treated KR_{4DMN} peptide.

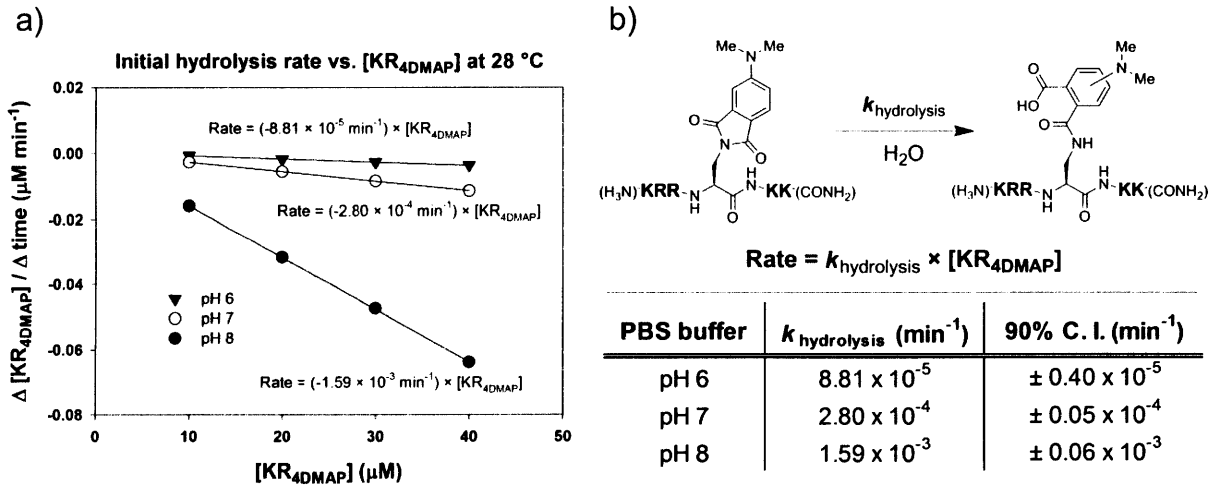

PBS buffer	$k_{hydrolysis}$ (min^{-1})	90% C. I. (min^{-1})
pH 6	8.81×10^{-5}	$\pm 0.40 \times 10^{-5}$
pH 7	2.80×10^{-4}	$\pm 0.05 \times 10^{-4}$
pH 8	1.59×10^{-3}	$\pm 0.06 \times 10^{-3}$

Figure 2-5. (a) Graph depicts the pseudo first-order dependence of the hydrolysis of 4-DMAP based on the initial rates measured at four concentrations of the KR_{4DMAP} peptide. The reaction was examined at three different pH levels (pH 6, 7, and 8). Regression lines were set to intercept the y-axis at zero. (b) Shown are the calculated rate constants for the hydrolysis of the KR_{4DMAP} peptide with the reaction scheme and rate law (omitting the contribution of $[H_2O]$) depicted above. (C. I. – Confidence Interval)

Here, a clear trend emerges from the data of the KR_{4DMAP} peptide. The rate of hydrolysis is relatively modest at low pH, but increases considerably as the pH is raised (Figures 2-4 and 2-5). By measuring the initial rates at four different concentrations of the peptide, a pseudo first-order rate constant was calculated for the reaction at each pH level (Figure 2-5). The results of this experiment were comparable to those measured for the KR_{6DMN} peptide indicating that the imide ring size was the dominant driving force for the observed reactivity and that the proximity of the dimethylamino group bears little impact on the rate of reaction (see Experimental section for details). By comparison, the KR_{4DMN} peptide showed no signs of degradation under any of the applied conditions. This is especially apparent in Figure 2-4b, where the fluorescence emission of the KR_{4DMN} peptide was unchanged after 24 hrs while the fluorescent signal from the KR_{4DMAP} peptide was almost completely abolished.

2-2. Compatibility of the Fmoc-4DMNA amino acid with standard solid phase peptide synthesis (SPPS)

A significant drawback to the use of 4-DAPA and 6-DMNA amino acids in SPPS is the reactivity toward nucleophilic bases such as piperidine analogues like 4-methylpiperidine,[15] which are commonly used for Fmoc group deprotection. While the formation of ring-opened piperidine adducts of these two amino acids can be circumvented by substituting bases like 4-methylpiperidine with 1,8-diazabicyclo[5.4.0]undec-7-ene (DBU),[16] caution must be exercised with sequences containing certain Asp-Xaa motifs due to the potential for aspartimide formation.[17] By contrast, the Fmoc amino acid of 4-DMNA has been used for the preparation of a number of fluorescent peptides and shows no susceptibility to attack by 4-methylpiperidine. The following experiment illustrates the enhanced stability of 4-DMNA by treating a series of

model peptides (KR_{4DMAP}, KR_{6DMN}, and KR_{4DMN}) with 4-methylpiperidine while still bound to the solid support (Figure 2-6). The conditions used simulate a standard Fmoc-deprotection cycle. Samples of the treated and untreated peptides were then cleaved from the resin under acidic conditions and the crude mixtures were analyzed by HPLC and mass spectrometry (see Experimental section for details).

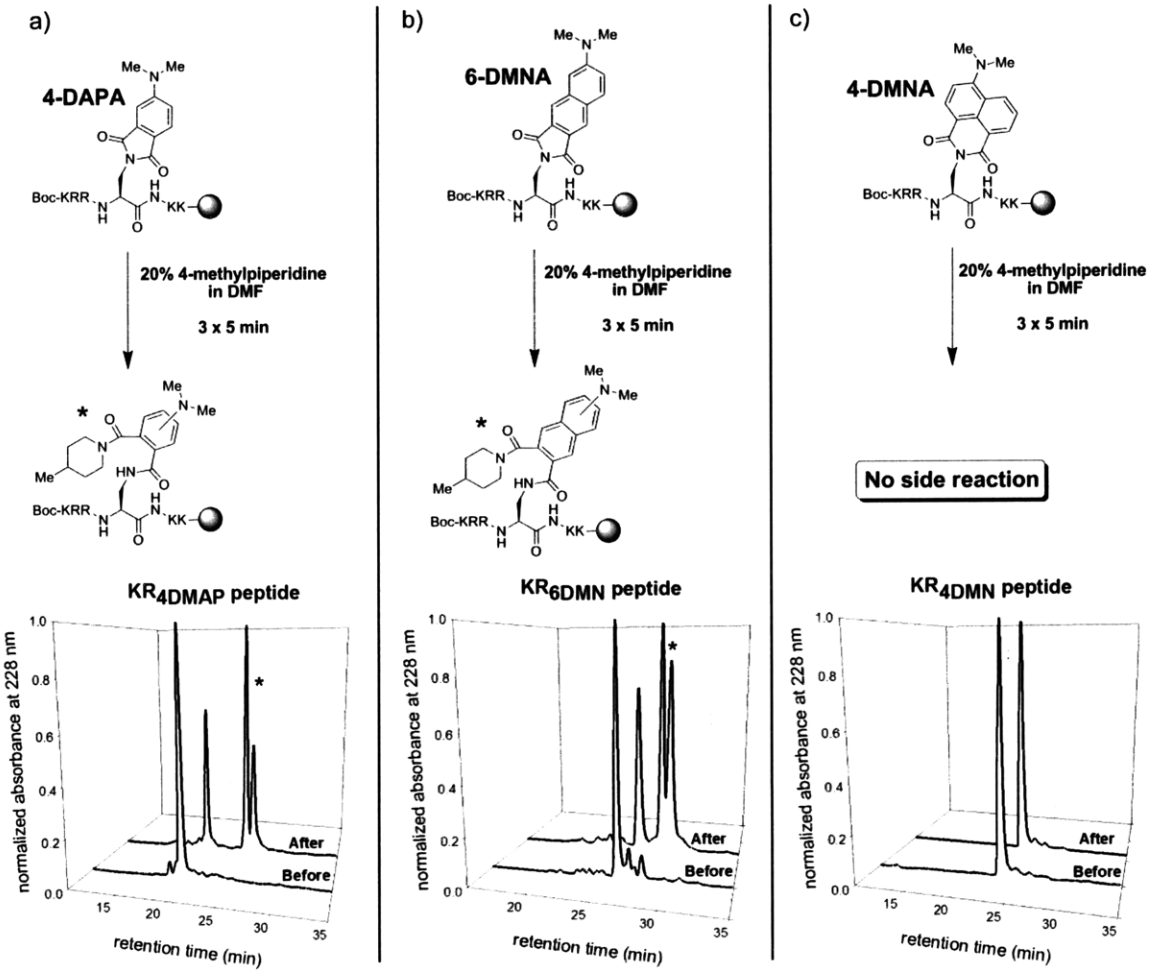

Figure 2-6. Panels (a) and (b) illustrate the susceptibility of the amino acids 4-DAPA and 6-DMNA to nucleophilic attack by bases such as 4-methylpiperidine leading to ring-opened byproducts. The HPLC traces (shown bottom) depict the model KR peptides cleaved before and after exposure to the base. The addition of 4-methylpiperidine to the imide rings of 4-DMAP and 6-DMN gives a mixture of two regioisomers (*) as shown in the HPCL traces after treatment. Panel (c) shows that the amino acid, 4-DMNA, exhibits no sign of degradation under these same conditions. The identities of the peaks were determined by a combination of MALDI and ESI mass spectrometry.

The HPLC traces of Figure 2-6a and 2-6b clearly exhibit the presence of two new peaks that elute later than those of the desired products after treatment with 4-methylpiperidine. These new peaks correspond to the masses of the ring-opened adducts that occur as a mixture of regioisomers. By contrast, the KR_{4DMN} peptide yielded virtually identical HPLC traces before and after treatment with 4-methylpiperidine and showed no signs of degradation. The robustness of 4-DMNA allows for multiple Fmoc-deprotection cycles to be performed subsequent to its incorporation into a peptide obviating the need for the use of bases like DBU.

Conclusion

Due to the reactivity of the 4-DMAP and 6-DMN fluorophores in aqueous buffers above pH 7, we have found that it is important to maintain peptide probes that contain these dyes in a frozen and lyophilized state for long-term storage. However, such conditions are often incompatible for many proteins. By contrast, 4-DMN has been observed to remain stable for multiple days in aqueous buffers at room temperature. This robustness to a wide range of conditions opens the window to many potential future applications as we aim to incorporate this tool into full-length proteins for *in cellulo* studies.

Experimental

Kinetic measurements of 4-DMAP and 6-DMN hydrolysis:

The KR_{4DMAP} peptide was screened at four concentrations (10 μM, 20 μM, 30 μM, and 40 μM) and three different pH levels (pH 6, 7, and 8) in PBS buffer at 28 °C. Since 4-DMAP undergoes a loss of fluorescence upon hydrolysis, the percent conversion of the fluorophore can be defined as the percent loss of fluorescence from time zero. These same conditions were also applied to the KR_{6DMN} and KR_{4DMN} peptides. The experiments were performed using a PerkinElmer® HTS 7000 plate reader with NUNC™ 96-well black PolySorb plates for both the KR_{4DMAP} and KR_{4DMN} peptides and a Falcon™ 96-well black/clear bottom Optilux™ plate for the KR_{6DMN} peptide. The plates were assembled such that each condition was repeated a total of four times. A series of blank samples (PBS buffer without peptide added) were also added to measure the background, which would later be subtracted from the fluorescence/absorbance measurements. The wells were loaded with 200 μL of each sample and then topped with 80 μL of white, light, mineral oil (Mallinckrodt Chemicals) to prevent evaporation. After assembly, the plates were placed in the plate reader and monitored at 30 min intervals over the course of 24 hrs. The 4-DMAP and 4-DMN fluorophores were both excited at 405 nm using a 10 nm band-pass filter. The fluorescence emission of 4-DMAP and 4-DMN was measured using a 595 nm filter and 535 nm filter, respectively. Since the byproduct of 6-DMN hydrolysis is highly fluorescent, the reaction rates were determined by measuring the absorbance at 405 nm (see Figures 2-7 and 2-8 for results). At this wavelength, the ring-closed product absorbs to an appreciable extent while the ring-opened product does not absorb at all. Four concentrations for the KR_{6DMN} peptide were screened (31 μM, 63 μM, 94 μM, and 125 μM).

After the data was recorded, it was plotted as a function of time. Trend lines were fit to the initial time points using the least-squares method and used to calculate the initial rates. The initial rates were then plotted as a function of peptide concentration. Again, a trend line was fit to these plots for each pH level to compute the pseudo first-order rate constants. The trend lines gave excellent fits ($R^2 > 0.99$) when the Y-intercept was set at zero. While the 4-DMAP and 6-DMN fluorophores showed significant signs of hydrolysis over 24 hrs, no change was observed for 4-DMN. (Note – This experiment was conducted using potassium phosphate buffers containing 0.2 M phosphate).

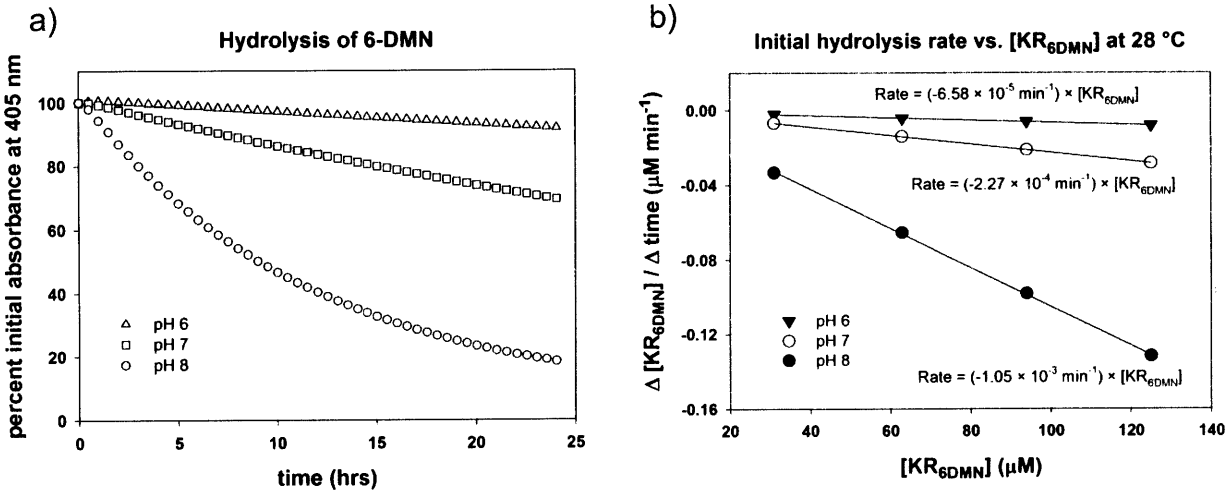

Figure 2-7. Hydrolysis data for the 6-DMN fluorophore. Panel (a) depicts the absorbance of 6-DMN at 405 nm over time at three pH levels. The decrease is due to conversion of the fluorescent species to the ring-opened byproduct. Panel (b) indicates the rate dependence of the hydrolysis reaction on the initial fluorophore concentration.

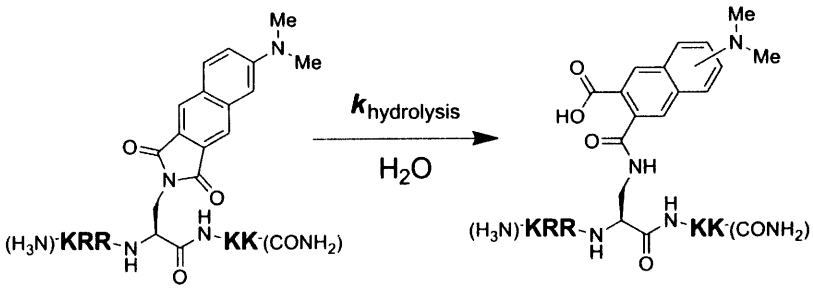

Rate = $k_{hydrolysis}$ × [KR_{6DMN}]

PBS buffer	$k_{hydrolysis}$ (min^{-1})	90% C. I. (min^{-1})
pH 6	6.58×10^{-5}	$\pm 0.40 \times 10^{-5}$
pH 7	2.27×10^{-4}	$\pm 0.05 \times 10^{-4}$
pH 8	1.05×10^{-3}	$\pm 0.06 \times 10^{-3}$

Figure 2-8. Measured rate constants of 6-DMN hydrolysis. The results represent the average of four trials. (C. I. – Confidence Interval)

Treatment of KR peptide series with 4-methylpiperidine:

Approximately 20 mg of Pal-PEG resin for each of the three KR peptides was transferred to a small 2 mL spin column (Bio-Rad) and treated with a 20% solution of 4-methylpiperidine in DMF (3 × 5 min) to simulate the conditions of a typical Fmoc deprotection step in SPPS. Following this, the resin was washed thoroughly with fresh DMF and finally with DCM before cleaving the peptides from the resin using a solution of 96:2:2 TFA/H_2O/EDT for 2.5 hrs. The resin was then filtered off and the TFA removed by evaporation. The crude products were then dissolved in 200 µL of dH_2O and analyzed by MALDI-MS, HPLC, and ESI-MS. Due to the highly polar nature of KR peptides, a slow gradient (95:5 to 55:45 H_2O/MeCN with 0.1% TFA over 35 min) was used to resolve the starting material from the 4-methylpiperidine adducts. The HPLC method monitored the absorbance at 228 nm and 280 nm. The isolated products were then further analyzed by ESI-MS to confirm their identity.

Table 2-1. Evidence of 4-methylpiperidine adducts to 4-DMAP and 6-DMN

4-methylpiperidine adducts of KR peptides	$[M+xH]^{x+}$ Calcd.	MALDI MS $[M+H]^{1+}$ found	ESI MS $[M+xH]^{1+}$ found
KR_{4DMAP}	1073.1 (1+)	1073.5 (1+)	—
	537.1 (2+)	—	536.9 (2+)
	358.4 (3+)	—	358.3 (3+)
KR_{6DMN}	1123.2 (1+)	1123.6 (1+)	—
	562.1 (2+)	—	562.0 (2+)
	375.1 (3+)	—	375.0 (3+)
KR_{4DMN}	No adducts observed		

Acknowledgments

This research was supported by NSF CHE-0414243 (BI), the NIH Cell Migration Consortium (GM064346), and the Biotechnology Training Program (T32-GM08334). I thank Dr. Eugenio Vázquez and Dr. Matthieu Sainlos (MIT) for their helpful advice and insight. The Biophysical Instrumentation Facility for the Study of Complex Macromolecular Systems (NSF-0070319) is also gratefully acknowledged.

References

(1) Pawson, T.; Nash, P. Assembly of cell regulatory systems through protein interaction domains. *Science* **2003**, *300*, 445-452.

(2) Lakowicz, J. R.; 3rd ed.; Springer: New York, 2006, p 205-235.

(3) Nitz, M.; Mezo, A. R.; Ali, M. H.; Imperiali, B. Enantioselective synthesis and application of the highly fluorescent and environment-sensitive amino acid 6-(2-dimethylaminonaphthoyl) alanine (DANA). *Chem. Commun. (Camb.)* **2002**, 1912-1913.

(4) Vazquez, M. E.; Blanco, J. B.; Imperiali, B. Photophysics and biological applications of the environment-sensitive fluorophore 6-*N,N*-dimethylamino-2,3-naphthalimide. *J. Am. Chem. Soc.* **2005**, *127*, 1300-1306.

(5) Vazquez, M. E.; Rothman, D. M.; Imperiali, B. A new environment-sensitive fluorescent amino acid for Fmoc-based solid phase peptide synthesis. *Org. Biomol. Chem.* **2004**, *2*, 1965-1966.

(6) Loving, G.; Imperiali, B. A versatile amino acid analogue of the solvatochromic fluorophore 4-*N,N*-dimethylamino-1,8-naphthalimide: A powerful tool for the study of dynamic protein interactions. *J. Am. Chem. Soc.* **2008**, *130*, 13630-13638.

(7) Cohen, B. E.; McAnaney, T. B.; Park, E. S.; Jan, Y. N.; Boxer, S. G.; Jan, L. Y. Probing protein electrostatics with a synthetic fluorescent amino acid. *Science* **2002**, *296*, 1700-1703.

(8) Lakowicz, J. R.; 3rd ed.; Springer: New York, 2006, p 529-575.

(9) Vivian, J. T.; Callis, P. R. Mechanisms of tryptophan fluorescence shifts in proteins. *Biophysical Journal* **2001**, *80*, 2093-2109.

(10) Weljie, A. M.; Vogel, H. J. Tryptophan fluorescence of calmodulin binding domain peptides interacting with calmodulin containing unnatural methionine analogues. *Protein Engineering* **2000**, *13*, 59-66.

(11) Turcatti, G.; Nemeth, K.; Edgerton, M. D.; Meseth, U.; Talabot, F.; Peitsch, M.; Knowles, J.; Vogel, H.; Chollet, A. Probing the structure and function of the Tachykinin Neurokinin-2 receptor through biosynthetic incorporation of fluorescent amino acids at specific sites. *J. Biol. Chem.* **1996**, *271*, 19991-19998.

(12) Prendergast, F. G.; Meyer, M.; Carlson, G. L.; Iida, S.; Potter, J. D. Synthesis, spectral properties, and use of 6-acryloyl-2-dimethylaminonaphthalene (Acrylodan). A thiol-selective, polarity-sensitive fluorescent probe. *J. Biol. Chem.* **1983**, *258*, 7541-7544.

(13) Saroja, G.; Soujanya, T.; Ramachandram, B.; Samanta, A. 4-Aminophthalimide derivatives as environment-sensitive probes. *J. Fluoresc.* **1998**, *8*, 405-410.

(14) Sainlos, M.; Iskenderian, W. S.; Imperiali, B. A General screening strategy for peptide-based fluorogenic ligands: probes for dynamic studies of PDZ domain-mediated interactions. *J. Am. Chem. Soc.* **2009**, *131*, 6680-6682.

(15) Hachmann, J.; Lebl, M. Alternative to piperidine in Fmoc solid-phase synthesis. *J. Comb. Chem.* **2006**, *8*, 149-149.

(16) Sainlos, M.; Imperiali, B. Tools for investigating peptide-protein interactions: peptide incorporation of environment-sensitive fluorophores through SPPS-based 'building block' approach. *Nat. Protoc.* **2007**, *2*, 3210-3218.

(17) Wade, J. D.; Mathieu, M. N.; Macris, M.; Tregear, G. W. Base-induced side reactions in Fmoc-solid phase peptide synthesis: Minimization by use of piperazine as N-alpha-deprotection reagent. *Lett. Pept. Sci.* **2000**, *7*, 107-112.

Chapter 3: Design and synthesis of versatile 4-DMN derivatives for biochemical studies

A significant portion of the work described in this chapter has been published or submitted for publication in:

Loving, G.; Imperiali, B. A versatile amino acid analogue of the solvatochromic fluorophore 4-*N,N*-dimethylamino-1,8-naphthalimide: A powerful tool for the study of dynamic protein interactions. *J. Am. Chem. Soc.* **2008**, *130*, 13630-13638.

Loving, G.; Imperiali, B. Thiol-reactive derivatives of the solvatochromic 4-*N,N*-dimethylamino-1,8-naphthalimide fluorophore: A highly sensitive toolset for the detection of biomolecular interactions. *Bioconjug. Chem.* Submitted on July 17, 2009.

Introduction

As described in the previous chapter, it was deemed necessary to address important limitations to the 4-DMAP and 6-DMN dyes in the design and development of superior probes with advantageous properties for diverse applications. Both of the fluorophores exhibit the tendency to hydrolyze in aqueous buffers over prolonged periods rendering them unsuitable for certain applications in biochemical studies. While considering various approaches to reduce the reactivity of the imide ring system, it was discovered that the 4-DMN fluorophore was a much more stable alternative. This chapter details the research involved in developing a new series of fluorescent tools based on the 4-DMN fluorophore to greatly expand the scope of potential applications.

The synthetic route originally developed by Vázquez *et al.*[1] to prepare the anhydride precursor of the 6-DMN fluorophore required seven steps. This protocol was relatively labor intensive and involved two low-yielding transformations, one of which utilizing sublimation to generate and isolate the anhydride ring-system of the final product. This step was difficult to perform on large scales and commonly required multiple days to obtain sufficient material for downstream applications. Furthermore, the method resulted in a significant loss of starting material through degradation. Although an improved procedure was later developed to replace the sublimation step (see Appendix), the time invested in preparing this precursor made it extremely precious and limited broad applicability. In seeking to develop new synthetic routes leading to derivatives of the 4-DMN fluorophore, one goal was to avoid similar limitations.

In research that focused on examining the triplet route of deactivation for 4-substituted 1,8-naphthalic acid anhydrides Kollár *et al.*[2] developed a highly efficient one-step synthesis (Scheme 3-1) of the fluorescent 4-dimethylamino-1,8-naphthalic acid anhydride (**3-1**). The

method yields a highly pure crystalline solid with near quantitative conversion. This approach represented a significant advantage over the methods that we were employing to prepare the anhydride precursors of 4-DMAP[3] and 6-DMN.[1] With easy access to gram quantities of material, the possibilities were now open for synthesizing a wide range of fluorescent derivatives as well as carrying out detailed photophysical studies.

Scheme 3-1. Synthesis of 4-DMN anhydride (**3-1**)[2]

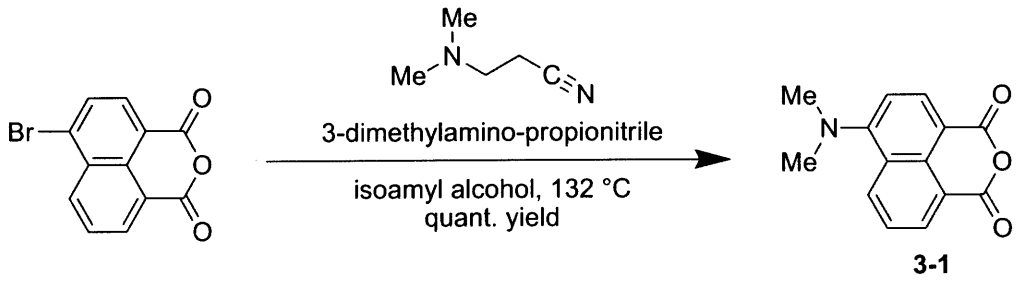

3-1

An unexpected drawback that was encountered however was the remarkable lack of reactivity exhibited by this electrophile. In retrospect, it is clear that the stability of **3-1** can be attributed to the same factors responsible for the enhanced stability of the corresponding imide ring-system of 4-DMN (Chapter 2). All initial attempts to react the anhydride with primary amines failed under the conditions commonly used for the 4-DMAP and 6-DMN anhydrides. Although this issue was eventually overcome, early efforts to prepare fluorescent derivatives of 4-DMN began with the more reactive electrophile 4-nitro-1,8-naphthalic anhydride (**3-2**). In this case, the electron withdrawing nature of the nitro group in **3-2** activates the anhydride ring toward nucleophilic attack allowing the reaction to proceed at room temperature.

This chapter highlights the challenges encountered in the synthesis of the fluorescent tools **3-3** through **3-7** (Chart 3-1), which constitute the primary focus of this thesis and presents the approaches that were ultimately developed for their syntheses. The discussion begins with

the development of cysteine modifying agents where particular attention is devoted to compounds **3-4** and **3-5**. The information gained in preparing these derivatives ultimately guided the successful syntheses of compounds **3-3** and **3-6**. The chapter concludes with a brief description of the experiments that led to a refined synthesis of the Fmoc-4DMNA building block **3-7**.

Chart 3-1. Fluorescent tools including the 4-DMN fluorophore

cysteine modifying agents:

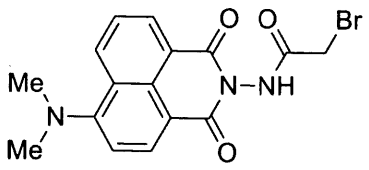

3-3

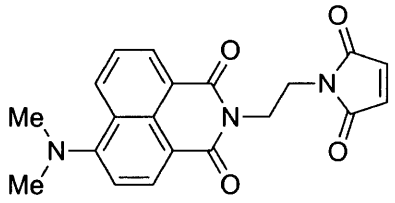

3-4

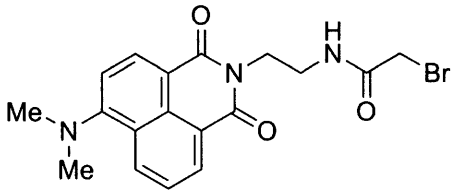

3-5

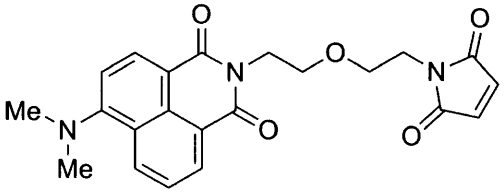

3-6

Fmoc building block:

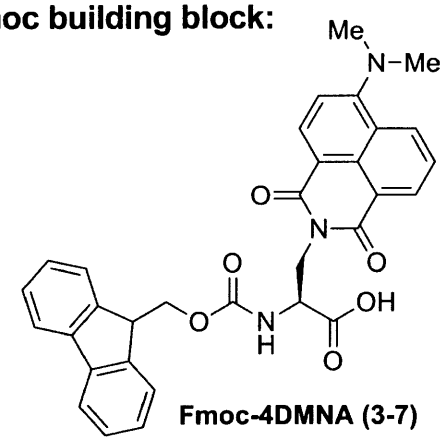

Fmoc-4DMNA (3-7)

Results and Discussion

3-1. Synthesis of the 4-DMN cysteine modifying agents

In developing a synthetic route to the cysteine modifying agents **3-4** and **3-5**, the anhydride **3-2** was first coupled with *N*-Boc-ethylenediamine to give **3-8**. With the linker installed, reductive amination was performed to convert nitro group to the dimethylamino group of **3-9** (Scheme 3-2). This reaction was typically sluggish and required the presence of acetic acid and gentle warming (50 °C) to observe any product formation over 24 hrs. It was determined that the rate limiting step was the introduction of the second methyl group at the 4-amino position. The basis for this was attributed to a disadvantageous steric effect due to the unfavorable *peri*-interaction that results following addition of the first methyl group. Ultimately, this approach was abandoned due to the low yield and the fact that it produced a number of additional byproducts that proved difficult to separate.

Scheme 3-2. Synthesis of compound **3-9**

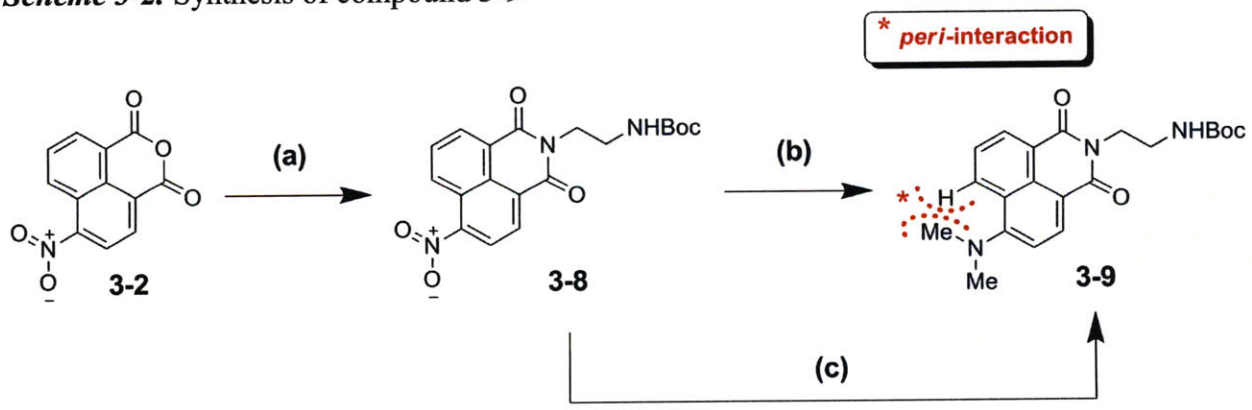

Reagents and conditions: (a) 1st N-Boc-ethylenediamine, DIPEA, DMF, room temperature, 1 hr, 2nd HOBt/HBTU (1:1), room temperature, overnight, 72% yield; (b) H_2 (1 atm), Pd/C 10 wt. %, acetic acid/dioxane (2:1), formalin 37% aq., 50 °C, 24 hrs, 30% yield; (c) 3-dimethylamino-propionitrile, isoamyl alcohol, Δ, N_2 (1 atm), 22 hrs, 74% yield.

An alternative approach, inspired by the reaction of Scheme 3-1, was found to afford the desired product with a much higher yield. Specifically, by refluxing **3-8** in isoamyl alcohol in the presence of 3-dimethylamino-propionitrile, the nitro group is eliminated smoothly without formation of by-products. Once **3-9** was obtained, the Boc protecting group was removed using a 1:1 solution of TFA/DCM and isolated as the free amine, **3-10**, for subsequent reactions.

Initial attempts to synthesize compound* 3-4*: The maleimide/isomaleimide dichotomy. Using a standard approach to introduce the maleimide group[4,5] of compound **3-4**, the amine **3-10** was reacted with maleic anhydride to generate the maleamic acid intermediate **3-11** (Scheme 3-3). Next, this intermediate was refluxed with acetic anhydride in the presence of sodium acetate in an attempt to close the ring. However, for reasons that were not resolved, the reaction failed to yield any conversion of the starting material. Strong dehydrating agents such as HBTU were also used in combination with catalytic nucleophiles such as HOBt and DMAP, but this led to rapid degradation of the product. The cause was attributed to the fact that the maleimide group exhibits high reactivity toward must nucleophilic species. Therefore, the use of HOBt and DMAP was avoided in subsequent experiments.

Scheme 3-3. Attempted synthesis of **3-4** via the maleamic acid intermediate **3-11**

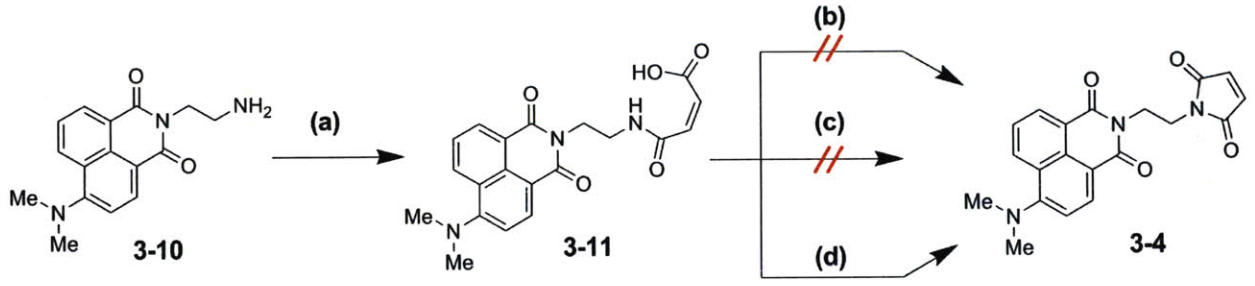

Reagents and conditions: (a) maleic anhydride, DIPEA, DCM, quant. yield; (b) Ac_2O, NaOAc, Δ, Ar (1 atm), no conversion; (c) HOBt/HBTU (1:1), DMF, rapid degradation of starting material; (d) EDC, DCM, room temperature, 15% yield.

Finally, it was discovered that 1-ethyl-3-(3-dimethylaminopropyl) carbodiimide (EDC) alone was capable of promoting quantitative conversion of **3-11** to the product according to TLC and ESI-MS analysis. However, the product was highly unstable showing a strong tendency to revert back to the ring-opened maleamic acid when attempting to isolate it by flash column chromatography on silica gel. This resulted in exceptionally low yields of desired product. The reason for the unexpected lack of stability was revealed by the ^{1}H NMR of the isolated product, which exhibited a set of anomalous signals for the maleimide protons (Figure 3-1). The two protons displayed asymmetry with a 0.65 ppm difference in chemical shift. The protons were also coupled to each other (J = 5.6 Hz). It was ultimately determined that the isolated product was not the maleimide **3-4**, but instead a structural isomer known as an isomaleimide (**3-12**).

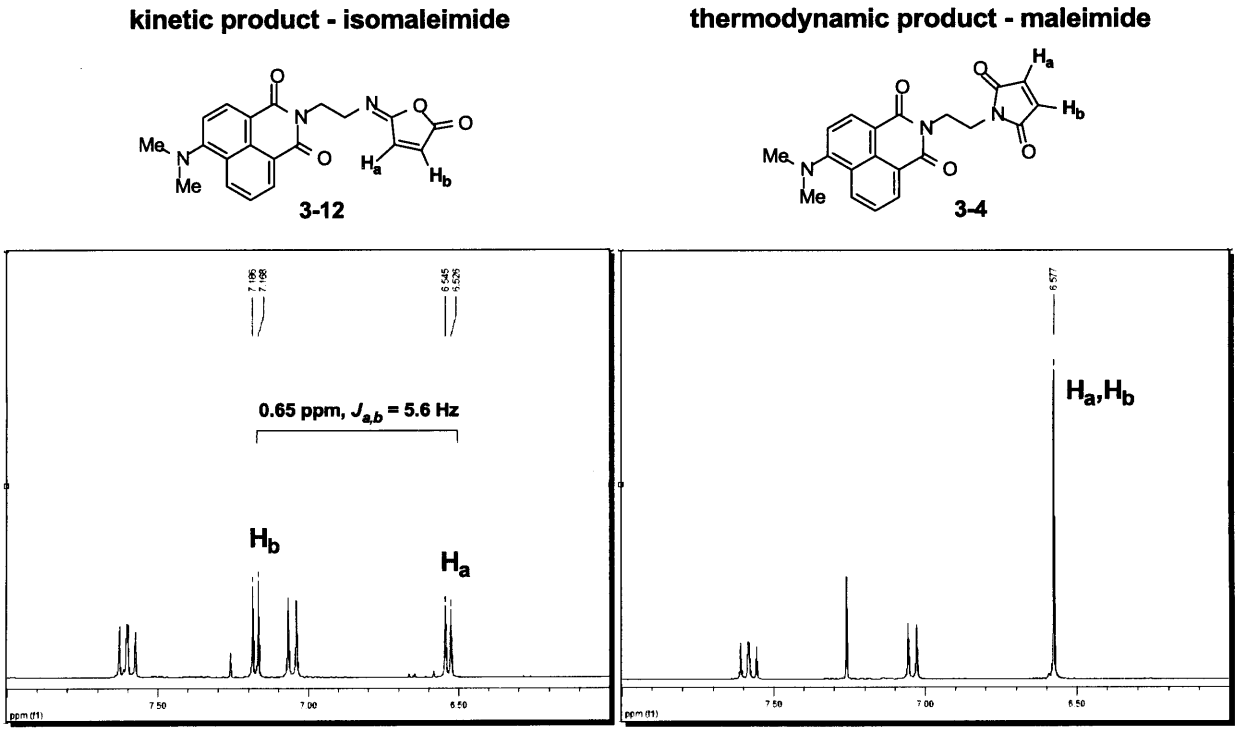

Figure 3-1. ^{1}H NMR (300 MHz, $CDCl_3$) of the structural isomers **3-12** and **3-4**. The two spectra show the region corresponding to the chemical shifts of the maleimide and isomaleimide protons (H_a and H_b). The isomaleimide is the kinetic product that results from activation of maleamic acid by strong dehydrating agents like EDC.

The isomaleimide is the kinetic product formed when activating a maleamic acid using powerful dehydrating agents such as phosgene, carbodiimides, acid chlorides, and others.[6] Although isomaleimides are highly reactive electrophiles that may be used for protein labeling, they lack specificity and are capable of *N*-acylation of lysine side chains.[7] Therefore, this approach to preparing **3-4** was abandoned in favor of an alternative route.

Synthesis of the maleimide* 3-4 *via a modified Mitsunobu reaction. Shortly after the difficulties encountered when exploring methods to condense maleic anhydride with compound **3-10,** it was discovered that compound **3-1** reacts readily with simple primary amines when refluxed in ethanol (Scheme 3-4). This reaction proved to be extremely useful in that it reliably furnished the desired products (**3-13** through **3-15**) with near quantitative yields and relatively few impurities. The excess unreacted amine can easily be removed through extraction or by placing the crude product under high vacuum overnight. The chief limitation is that the reaction is restricted to ethanol-soluble amines. Therefore, it was not applicable to the synthesis of the Fmoc-4DMNA building block **3-7**.

The primary alcohol of compound **3-13** offered a useful handle for inserting the maleimide group. Work by Walker[8] had shown that the Mitsunobu reaction could be adapted to directly alkylate phenethyl alcohol using maleimide as the nucleophile. When the method was applied to **3-13** the reaction conditions gave a modest yield (Scheme 3-5). However, the quantity of material obtained was more than sufficient for all of the downstream applications described in later chapters. The same Mitsunobu conditions were also applied to **3-14** with similar results. The isolated products, **3-4** and **3-6**, both exhibited significantly greater stability than that of the previously obtained isomaleimide **3-12**.

Scheme 3-4. Coupling of amines to 4-DMN anhydride (**3-1**)

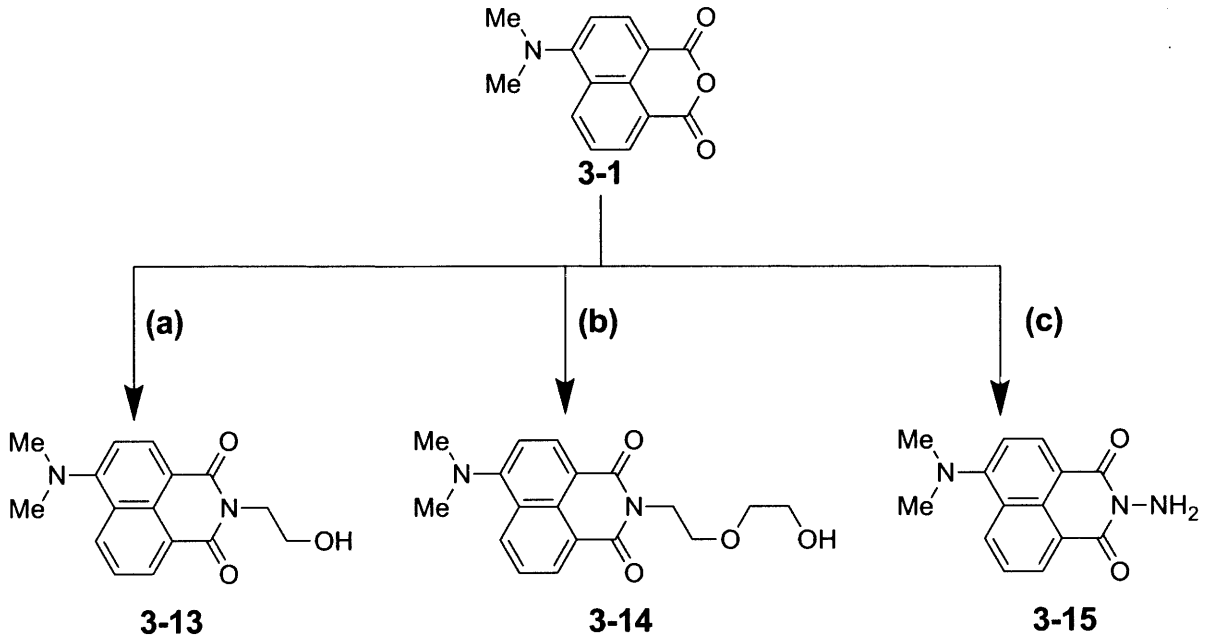

Reagents and conditions: (a) ethanolamine, ethanol, Δ, N_2 (1 atm), quant. yield; (b) 2-(2-aminoethoxy)-ethanol, ethanol, Δ, N_2 (1 atm), 98% yield; (c) hydrazine monohydrate, ethanol, Δ, N_2 (1 atm), 87% yield.

Scheme 3-5. Synthesis of the maleimide **3-4** and **3-6** via a modified Mitsunobu reaction

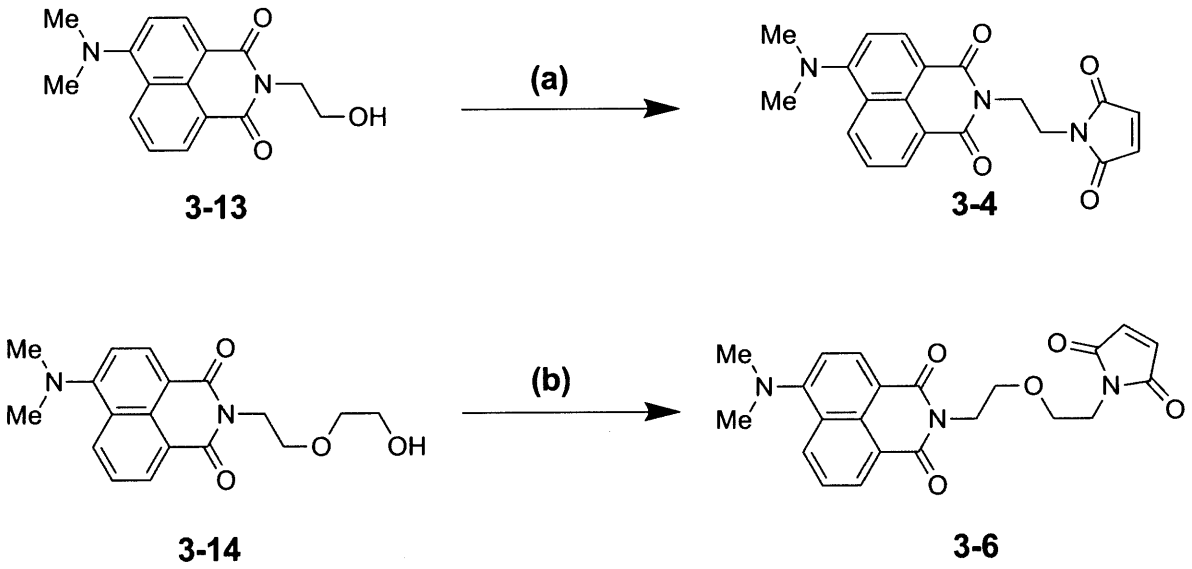

Reagents and conditions: (a) 1st PPh_3, DEAD, -78 °C, N_2 (1 atm), THF, 2nd neopentyl alcohol, maleimide, -78 °C to room temperature, overnight, 22% yield; (b) 1st PPh_3, DEAD, -78 °C, N_2 (1 atm), THF, 2nd neopentyl alcohol, maleimide, -78 °C to room temperature, overnight, 24% yield.

***Synthesis of the bromoacetamide* 3-5.** In preparing this series of cysteine-modifying agents, the type of electrophilic group used to append the labeling agents to protein was also investigated. Returning to compound **3-10**, an attempt was made to acetylate the free amino group using the symmetric anhydride of bromoacetic acid (Scheme 3-6). The anhydride was synthesized using a standard protocol[9] in the same reaction vessel to which **3-10** would subsequently be added. Upon addition of the amine, the reaction appeared to proceed directly to the desired product as determined by TLC.

Scheme 3-6. Acetylation of **3-10** using the symmetric anhydride of bromoacetic acid

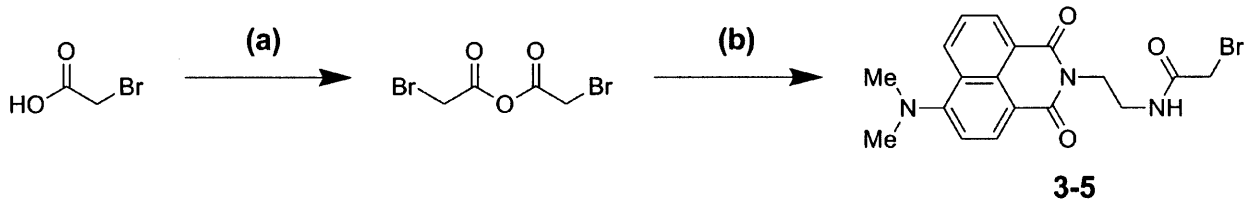

Reagents and conditions: (a) EDC, DCM (anhydrous), Ar (1 atm), 0 °C; (b) **3-10**, DIPEA, DCM, 92% overall yield.

However, upon isolating the product, the ^{1}H NMR exhibited an unexpected feature. The resonance corresponding to the methylene protons of the acetamide group was split as was that of the amide proton. After obtaining the high-resolution mass spectrum, it was clear that what appeared to be a single product isolated by flash column chromatography was actually a mixture of the chloro- and bromoacetamides, **3-16** and **3-5** (Figure 3-2). The presence of the byproduct was puzzling at first as the mixture was determined to contain a precise 1:2 ratio of the chloro- versus bromoacetamide.

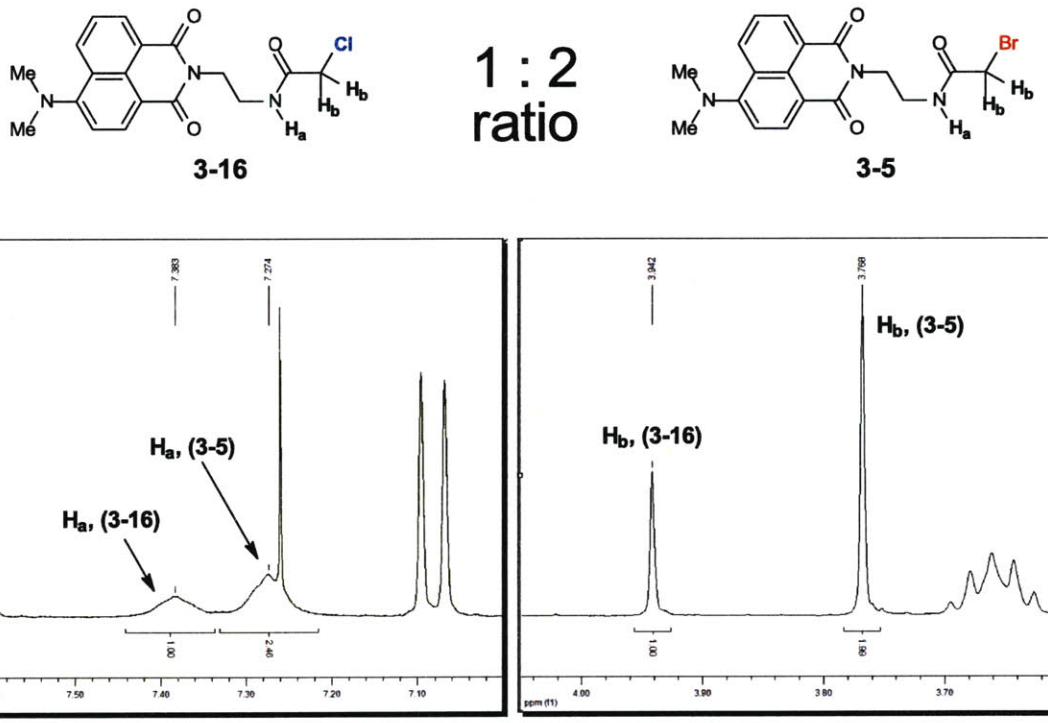

Figure 3-2. ^{1}H NMR (300 MHz, $CDCl_3$) of the product mixture isolated from the reaction of Scheme 3-6. The indicated protons of **3-16** and **3-4** reveal a 1:2 ratio of the two compounds.

It was later determined that the source of the problem originated with the use of the carbodiimide, EDC, to generate the anhydride of bromoacetic acid. The EDC used in the reaction was obtained as a hydrochloride salt. One equivalent of this salt was used with two equivalents of the bromoacetic acid in the reaction. It was therefore deduced that as the coupling reaction was allowed to proceed, a concomitant halide exchange reaction (Finkelstein reaction) was also occurring that ultimately yielded a statistical ratio of the two products of Figure 3-2. In order to avoid this complication, bromoacetyl bromide was substituted as the acylating agent giving the final product in excellent yield (Scheme 3-7).

Scheme 3-7. Acylation of **3-10** and **3-15** with bromoacetyl bromide

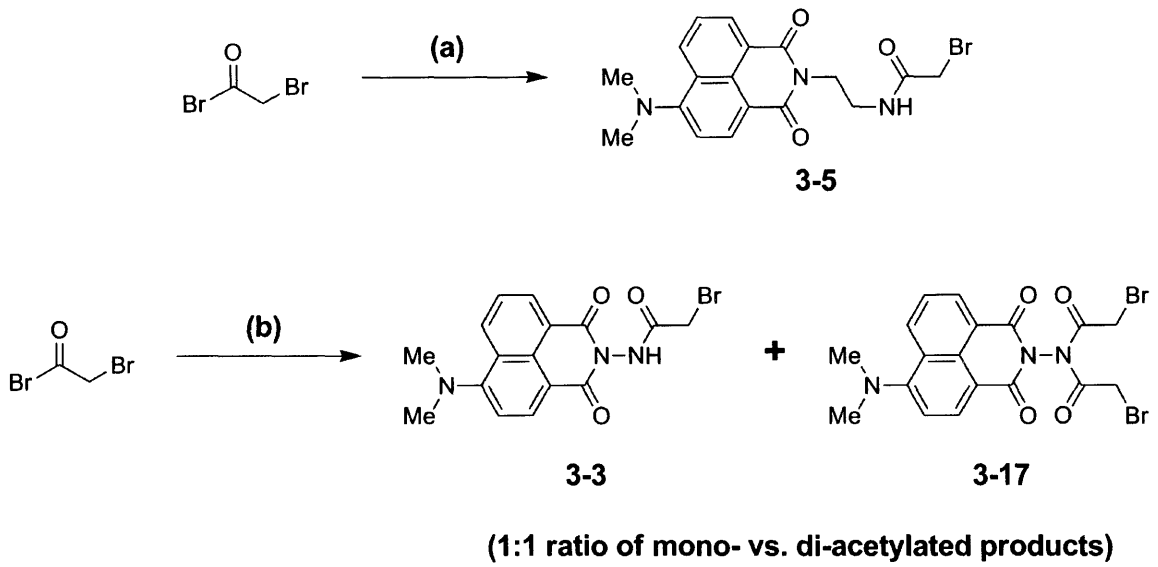

Reagents and conditions: (a) **3-10**, DIPEA, -15 °C to room temperature, N_2 (1 atm), DCM (anhydrous), 1.5 hrs, 91% yield; (b) **3-15**, DIPEA, -15 °C to room temperature, N_2 (1 atm), DCM (anhydrous), overnight, 48% yield of the mono-acetylated product **3-3**.

The same reaction was also performed on compound **3-15** using 1.5 equivalents of the acylating agent. This method also proceeded in a high yield, but resulted in a mixture of the mono- and di-acetylated products. This was not a significant problem, however, since the two products were easily separated by flash column chromatography and enough of the desired product, **3-3**, was obtained for later applications. Furthermore, the byproduct could easily be avoided in future reactions by reducing the quantity of bromoacetyl bromide added to the reaction.

3-2. Synthesis of N-α-Fmoc-(4-N,N-dimethylamino-1,8-naphthalimido)-alanine (3-7)

The development of a synthetic route leading to Fmoc-4DMNA (**3-7**) proved to be more challenging than the cysteine modifying agents since the anhydride **3-1** was unreactive toward (S)-2,3-diaminopropanoic acid (Dap) derivatives, which were protected at the 2-amino position.

Attempts were made to couple the fluorophore to the amino acid using a variety of solvents (e.g. ethanol, chloroform, dioxane, toluene) under reflux conditions. However, conversion of the starting material was not observed. Catalytic nucleophiles such as HOBt, DMAP, and 2-pyridone were also employed in an unsuccessful effort to facilitate the reaction by ring-opening of the anhydride. Finally, it was discovered that the reaction could proceed using a mixed solvent system consisting of dioxane and water. The nucleophile, (S)-3-amino-2-(Boc-amino)-propionic acid, was dissolved in water under basic conditions while a solution of the anhydride **3-1** is prepared in dioxane. The two solutions were then combined and brought to reflux. Although much of the anhydride was hydrolyzed to the diacid, the desired product (**3-18**) was formed in reasonable yield. The subsequent reactions involving the removal of the Boc group and addition of the Fmoc amino protecting group proceeded efficiently using standard conditions (Scheme 3-8).[10]

Scheme 3-8. Synthesis of Boc-4DMNA (**3-18**) and Fmoc-4DMNA (**3-7**)

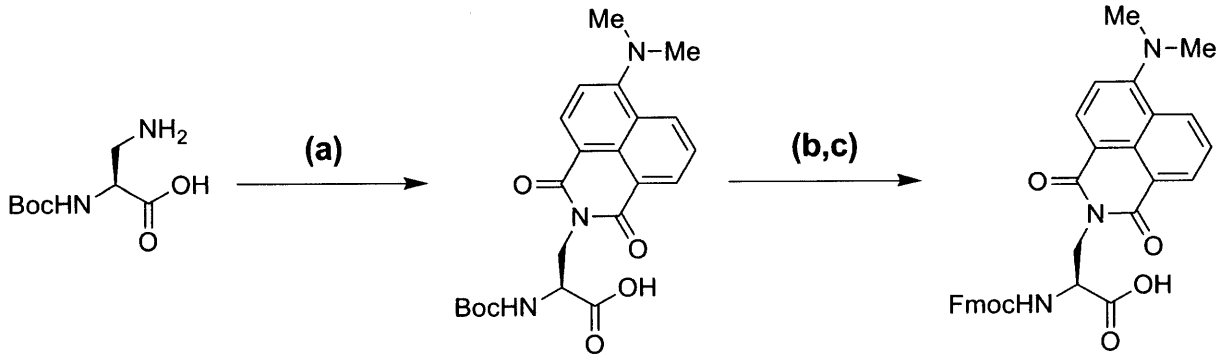

3-18 **3-7**

Reagents and conditions: (a) $NaHCO_3$, **3-1**, dioxane/water (5:1), Δ, N_2 (1 atm), 30 min, 55% yield; (b) TFA/DCM (1:1), room temperature, 1.5 hrs; (c) Fmoc-OSu, $NaHCO_3$, dioxane/water (5:1), room temperature, 2 hrs, 83% overall yield for steps b and c.

After the development of this synthetic route, an additional series of experiments were conducted on small scales (50 mg of **3-1**) to identify improved conditions for the preparation of **3-18**. Recently, it was discovered that heating 3-amino-2-(Boc-amino)-propionic acid with **3-1**, DIPEA, and a catalytic amount of DMAP (0.1 eq.) in NMP (70 °C) for 6 hrs will afford the desired product with a quantitative yield. Further experiments will have to be conducted to determine if the reaction yield can be conducted on larger scales.

Conclusions

This chapter describes reliable and facile syntheses of the tools presented in this thesis. The protocols presented within the Experimental section afford ample quantities — ranging from milligrams to grams — of the desired products required for any future applications. Furthermore, many of these tools can be prepared in as few as three to four synthetic steps with a minimal investment of time.

Experimental

Synthesis of 4-*N*,*N*-dimethyl-1,8-naphthalimide cysteine modifying reagents:

NMR and FT-MS of the following derivatives: ^{1}H and ^{13}C NMR spectra were recorded on a Varian Mercury 300 MHz NMR and Varian Inova 500 MHz NMR spectrometer. Chemical shifts (δ) for ^{1}H and ^{13}C NMR spectra are reported in parts per million (ppm) and are referenced to residual proton in the deuterated solvent. Coupling constants (*J*) are reported in Hertz (Hz) and multiplicities are abbreviated as singlet (s), doublet (d), triplet (t), and multiplet (m). High-resolution mass spectra were obtained using a Bruker Daltonics APEXIV 4.7 Tesla Fourier Transform Ion Cyclotron Resonance Mass Spectrometer (FT-ICR-MS).

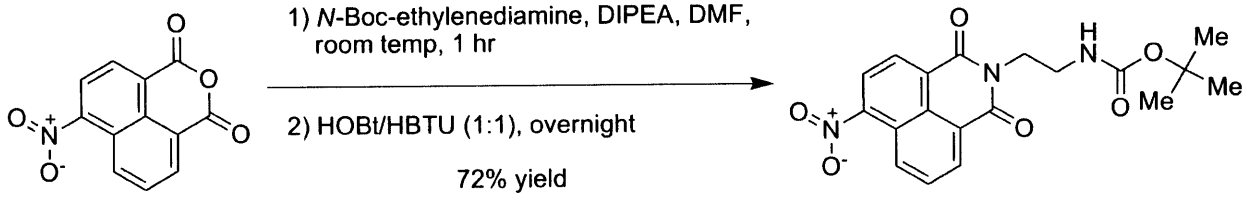

3-2 **3-8**

4-Nitro-*N*-(2-*tert*-butoxycarbonylamino-ethyl)-1,8-naphthalimide (3-8). Dissolved 4-nitro-1,8-naphthalic anhydride, **3-2** (9.2 g, 37.7 mmol), in 50 mL of DMF, then added DIPEA (17.9 mL, 102.9 mmol). In a separate flask, *N*-Boc-ethylenediamine was dissolved in another 50 mL DMF and added over 4 min to the solution containing the anhydride via an addition funnel. The reaction was allowed to proceed for 1 hr at ambient temperature before adding the coupling reagents HOBt/HBTU (100 mL, 0.58 M each in DMF) to facilitate closure of the imide ring

system. The reaction was allowed to proceed overnight. The next day, the reaction mixture was poured into a large separatory funnel containing 400 mL of diethyl ether and washed with brine (3 × 200 mL) to remove DMF (note- some precipitation of the product from the organic layer may be observed if left for extended periods of time). The organic layer was then dried with $MgSO_4$, filtered, and concentrated to dryness. The crude product was then purified by flash column chromatography using 3:1 hexanes/ethyl acetate to give a light cream colored solid (9.56 g, 24.8 mmol, 72.3% yield, R_f = 0.1 in 3:1 hexanes/EtOAc).

^{1}H NMR (300 MHz, $CDCl_3$, δ): 1.21 (s, 9H), 3.53 (m, 2H), 4.34 (t, 2H, J = 5.7 Hz), 4.97 (m, 1H), 7.94 (dd, 1H, J_1 = 8.7 Hz, J_2 = 7.5 Hz), 8.36 (d, 1H, J = 8.1 Hz), 8.65 (d, 1H, J = 8.1 Hz), 8.69 (dd, 1H, J_1 = 7.4 Hz, J_2 = 1.1 Hz), 8.77 (dd, 1H, J_1 = 8.7 Hz, J_2 = 0.9 Hz).

^{13}C NMR (300 MHz, $CDCl_3$, δ): 28.4, 39.3, 40.7, 79.5, 123.0, 123.7, 124.1, 127.0, 129.3, 129.5, 130.1, 130.1, 132.7, 149.7, 156.3, 163.0, 163.8.

HRMS-ESI (*m/z*): $[M+Na]^+$ calcd for $C_{19}H_{19}N_3O_6$, 408.1166; found, 408.1188.

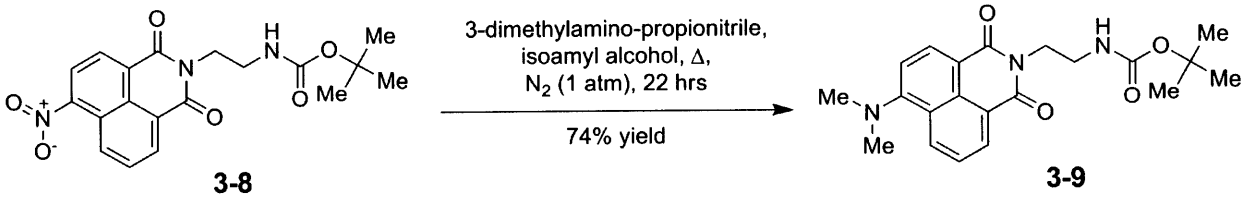

3-8 **3-9**

4-*N*,*N*-Dimethylamino-*N*-(2-*tert*-butoxycarbonylamino-ethyl)-1,8-naphthalimide (3-9). The 4-nitro-*N*-(2-*tert*-butoxycarbonylamino-ethyl)-1,8-naphthalimide, **3-8** (2.00 g, 5.19 mmol), was added to a 250 mL two-necked round-bottom flask equipped with a reflux condenser, rubber septum, and magnetic stir bar. The assembled reaction vessel was then

charged with and inert atmosphere by evacuating the air under reduced pressure and purging with N_2 gas (3×). The flask then received 52 mL of isoamyl alcohol transferred by syringe through the rubber septum. The suspension was stirred as the temperature was raised to 132 °C. Once the starting material dissolved, 3-dimethylamino-propionitrile (2.35 mL, 20.8 mmol) was added by syringe through the septum of the reaction vessel. The reaction was refluxed for 22 hrs before stopping by concentrating the reaction mixture to dryness by rotary evaporation. The crude was then purified by flash chromatography using 7:3 hexanes/ethyl acetate to give an orange solid (1.47 g, 3.83 mmol, 74% yield, R_f = 0.25 in 1:1 hexanes/ethyl acetate).

^{1}H NMR (300 MHz, $CDCl_3$, δ): 1.31 (s, 9H), 3.10 (s, 6H), 3.51 (m, 2H), 4.34 (t, 2H, J = 5.6 Hz), 5.09 (br, 1H), 7.09 (d, 1H, J = 8.1 Hz), 7.64 (dd, 1H, J_1 = 8.6 Hz, J_2 = 7.4 Hz), 8.42 (dd, 1H, J_1 = 8.4 Hz, J_2 = 1.2 Hz), 8.46 (d, 1H, J = 8.1 Hz), 8.56 (dd, 1H, J_1 = 7.4 Hz, J_2 = 1.1 Hz).

^{13}C NMR (500 MHz, $CDCl_3$, δ): 28.2, 39.4, 39.8, 44.7, 78.9, 113.1, 114.5, 122.7, 124.7, 125.1, 130.2, 131.1, 131.2, 132.8, 156.0, 157.0, 164.3, 164.9.

HRMS-ESI (*m/z*): $[M+H]^+$ calcd for $C_{21}H_{25}N_3O_4$, 384.1923; found, 384.1932.

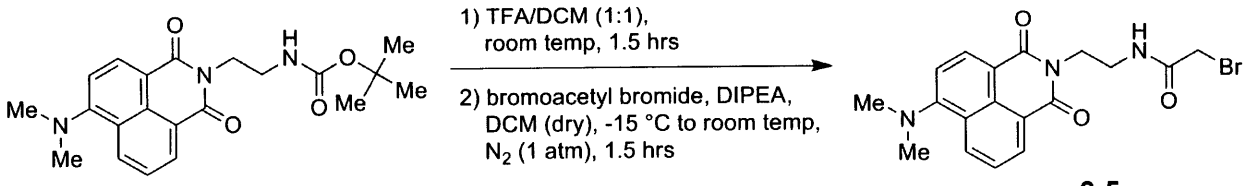

3-9 **3-5**

4-*N*,*N*-Dimethylamino-*N*-[2-(2-bromo-acetylamino)-ethyl]-1,8-naphthalimide (3-5). Dissolved **3-9** (0.50 g, 1.30 mmol) in dichloromethane (22.0 mL) in a 100 mL round-bottom flask. Cold trifluoroacetic acid (22.0 mL) was then added slowly over 5 min by addition funnel

while stirring the reaction. The reaction was allowed to proceed at room temperature for 1.5 hrs before concentrating to dryness by rotary evaporation. The crude solid was redissolved in dichloromethane (100 mL) and washed with 2% $NaHCO_3$ aq. solution (100 mL). The aqueous layer was back-extracted with fresh dichloromethane (2 × 100 mL) and the organic layers were combined (total volume of 300 mL). The organic layer was dried with $MgSO_4$, filtered and concentrated to give the free amine as an orange solid. The free base was then transferred to a 250 mL Schlenk flask under an atmosphere of nitrogen and dissolved in dry dichloromethane (100 mL). The Schlenk flask was cooled to -15 °C in a 1:3 sodium chloride/ice bath. The bromoacetyl bromide (0.40 g, 1.96 mmol) was then added dropwise by syringe followed by *N,N*-diisopropylethylamine (0.25 mL, 1.43 mmol). The reaction was allowed to run for 5 min at -15 °C before warming to room temperature. After 1.5 hrs, the reaction mixture was diluted to a total volume of 100 mL in dichloromethane and washed with 2% $NaHCO_3$ aq. solution (100 mL) followed by a second wash with brine (100 mL). The organic layer was dried with $MgSO_4$, filtered, and concentrated by rotary evaporation. The product was purified by flash chromatography using 2:3 hexanes/ethyl acetate to give an orange solid (0.48 g, 1.19 mmol, 91% yield, R_f = 0.10 in 2:3 hexanes/ethyl acetate). The product was stored as solid at -20 °C.

^{1}H NMR (300 MHz, $CDCl_3$, δ): 3.11 (s, 6H), 3.67 (m, 2H), 3.78 (s, 2H), 4.43 (t, 2H, J = 5.4 Hz), 7.09 (d, 1H, J = 8.1 Hz), 7.27 (br s, 1H), 7.64 (dd, 1H, J_1 = 8.6 Hz, J_2 = 7.4 Hz), 8.43 (dd, 1H, J_1 = 8.7 Hz, J_2 = 1.2 Hz), 8.46 (d, 1H, J = 8.4 Hz), 8.56 (dd, 1H, J_1 = 7.4 Hz, J_2 = 1.1 Hz).

^{13}C NMR (300 MHz, $CDCl_3$, δ): 28.9, 38.5, 40.4, 44.6, 113.1, 114.0, 122.4, 124.7, 124.9, 130.2, 131.2, 131.5, 133.0, 157.2, 164.4, 165.0, 166.0.

HRMS-ESI (*m/z*): $[M+H]^+$ calcd for $C_{18}H_{18}BrN_3O_3$, 404.0610; found 404.0612.

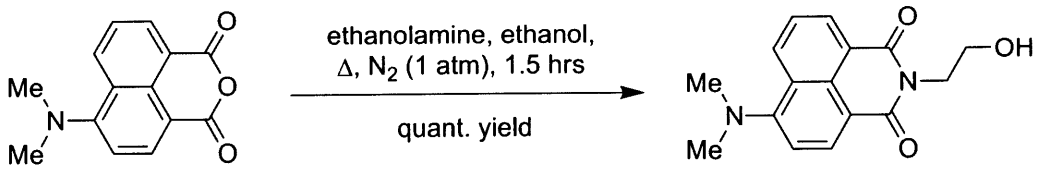

3-1 **3-13**

4-*N*,*N*-Dimethylamino-*N*-(2-hydroxy-ethyl)-1,8-naphthalimide (3-13). Added 4-*N*,*N*-dimethylamino-1,8-naphthalic anhydride, **3-1** (1.00 g, 4.15 mmol), to a 200 mL two-necked round-bottom flask equipped with a reflux condenser, magnetic stir bar, and rubber septum. The reaction vessel was then evacuated of air by applying vacuum and flushing with N_2 gas (3×). Anhydrous ethanol (42 mL) was then added to the flask by syringe. The suspension was stirred as the temperature was raised to reflux. The anhydride was still present as a solid as the suspension reached reflux until the addition of ethanolamine (0.28 mL, 4.56 mmol) by syringe. The slurry then turned to a clear deep orange solution. The reaction was allowed to proceed at reflux for 1.5 hrs then stopped by cooling to room temperature. The solvent was then removed using rotary evaporation and the crude placed under high vacuum overnight to remove excess ethanolamine. The product obtained was an orange solid requiring no further purification (1.18 g, 4.15 mmol, quantitative yield).

^{1}H NMR (300 MHz, $CDCl_3$, δ): 2.70 (br s, 1H), 3.10 (s, 6H), 3.95 (t, 2H, J = 5.3 Hz), 4.42 (t, 2H, J = 5.3 Hz), 7.06 (d, 1H, J = 8.1 Hz), 7.62 (dd, 1H, J_1 = 8.6 Hz, J_2 = 7.4 Hz), 8.40 (dd, 1H, J_1 = 8.4 Hz, J_2 = 1.2 Hz), 8.42 (d, 1H, J = 8.4 Hz), 8.52 (dd, 1H, J_1 = 7.5 Hz, J_2 = 1.2 Hz).

^{13}C NMR (300 MHz, $CDCl_3$, δ): 42.7, 44.7, 62.1, 113.1, 114.2, 122.6, 124.8, 124.9, 130.2, 131.3, 131.5, 132.9, 157.1, 164.9, 165.4.

HRMS-ESI (*m/z*): $[M+Na]^+$ calcd for $C_{16}H_{16}N_2O_3$, 307.1053; found, 307.1059.

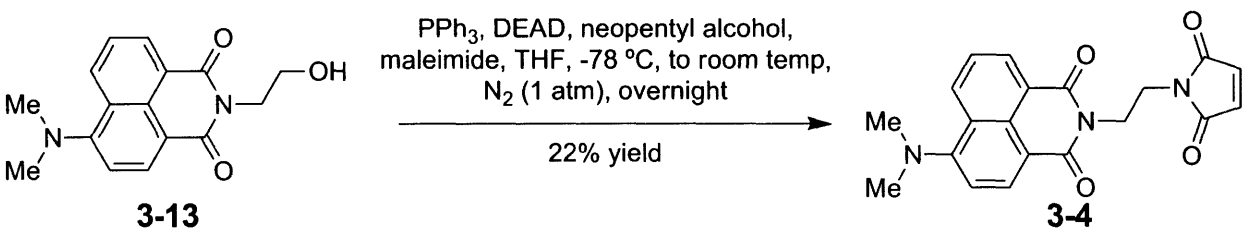

4-*N*,*N*-Dimethylamino-*N*-(2-maleimidyl-ethyl)-1,8-naphthalimide (3-4). Solid triphenylphosphine (0.42 g, 1.60 mmol) was added to an oven-dried 100 mL Kjeldahl-style Schlenk flask equipped with a magnetic stir bar and rubber septum. The flask was evacuated of air under high vacuum and charged with N_2 gas (3×). The triphenylphosphine was then dissolved in freshly distilled anhydrous THF. The reaction vessel was then cooled to -78 °C by immersing the Schlenk flask in a dry ice/isopropanol bath. Next, diethyl azodicarboxylate (0.696 mL, 40% solution in toluene, 1.60 mmol) was added dropwise via syringe over 1.5 min. The mixture was allowed to stir for approximately 5 min to allow formation of the betaine. At this point, the reaction mixture was a pale yellow color. The alcohol, **3-13** (0.50 g, 1.8 mmol), was then added as a solid followed by neopentyl alcohol (0.07 g, 0.8 mmol) to form the oxyphosphonium ion intermediate. Once the two alcohols were fully dissolved, maleimide was added as a solid and the reacting mixture was allowed to warm to room temperature. The reaction was allowed to proceed at room temperature overnight before stopping by concentrating to dryness using a rotary evaporator. TLC indicated that the reaction only preceded 30-40%. The product was isolated by flash column chromatography using toluene with 5% methanol.

The product was a bright yellow solid (0.13 g, 0.36 mmol, 22.4% yield, R_f = 0.24 in 1:1 hexanes/ethyl acetate) and was dissolved in DMSO for storage at -80 °C in 100 mM aliquots.

^{1}H NMR (300 MHz, $CDCl_3$, δ): 3.06 (s, 6H), 3.94 (t, 2H, J = 5.1 Hz), 4.36 (t, 2H, J = 5.1 Hz), 6.58 (s, 2H), 7.04 (d, 1H, J = 8.4 Hz), 7.58 (dd, 1H, J_1 = 8.6 Hz, J_2 = 7.4 Hz), 8.36 (d, 1H, J = 8.1 Hz), 8.38 (dd, 1 H, J_1 = 8.7 Hz, J_2 = 1.2 Hz), 8.46 (dd, 1H, J_1 = 7.4 Hz, J_2 = 1.1 Hz).

^{13}C NMR (300 MHz, $CDCl_3$, δ): 36.2, 38.6, 44.6, 113.1, 114.3, 122.4, 124.7, 125.1, 130.2, 131.0, 131.3, 132.6, 133.9, 156.8, 164.0, 164.6, 170.7.

HRMS-ESI (*m/z*): $[M+H]^+$ calcd for $C_{20}H_{17}N_3O_4$, 364.1292; found, 364.1308.

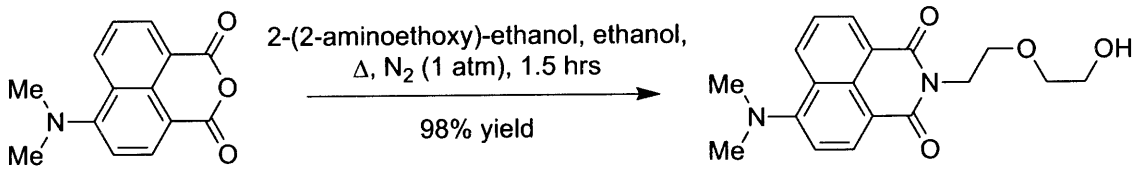

3-1 **3-14**

4-*N*,*N*-Dimethylamino-*N*-[2-(2-hydroxy-ethoxy)-ethyl]-1,8-naphthalimide (3-14). Added 4-*N*,*N*-dimethylamino-1,8-naphthalic anhydride, **3-1** (1.00 g, 4.15 mmol), to a 200 mL two-necked round-bottom flask equipped with a reflux condenser, magnetic stir bar, and rubber septum. The reaction vessel was then evacuated of air by applying vacuum and flushing with N_2 gas (3×). Anhydrous ethanol (42 mL) was then added to the flask by syringe. The suspension was stirred as the temperature was raised to reflux. The anhydride was still present as a solid as the suspension reached reflux until the addition of 2-(2-aminoethoxy)-ethanol (0.454 mL, 4.56 mmol) by syringe. The slurry then turned to a clear deep orange solution. The reaction was allowed to proceed at reflux for 1.5 hrs then stopped by cooling to room temperature. The

solvent was removed by rotary evaporation and the crude mixture placed under high vacuum overnight to remove excess 2-(2-aminoethoxy)-ethanol. The product was isolated by flash column chromatography using a gradient of 1:3 to 1:4 hexanes/ethyl acetate. The product was a dark orange oil (1.33 g, 4.05 mmol, 97.7% yield, R_f = 0.1 in 1:3 hexanes/ethyl acetate).

^{1}H NMR (300 MHz, $CDCl_3$, δ): 2.76 (br s, 1H), 3.07 (s, 6H), 3.66 (m, 4H), 3.82 (t, 2H, J = 5.6 Hz), 4.39 (t, 2H, J = 5.7 Hz), 7.05 (d, 1H, J = 8.4 Hz), 7.60 (dd, 1H, J_1 = 8.3 Hz, J_2 = 7.4 Hz), 8.38 (dd, 1H, J_1 = 8.6 Hz, J_2 = 1.1 Hz), 8.42 (d, 1H, J = 8.4 Hz), 8.51 (dd, 1H, J_1 = 7.4 Hz, J_2 = 1.1 Hz).

^{13}C NMR (300 MHz, $CDCl_3$, δ): 39.2, 44.6, 61.7, 68.4, 72.1, 113.1, 114.4, 122.7, 124.7, 125.0, 130.2, 131.1, 131.3, 132.8, 157.0, 164.2, 164.8.

HRMS-ESI (*m/z*): $[M+H]^+$ calcd for $C_{18}H_{20}N_2O_4$, 329.1496; found, 329.1506.

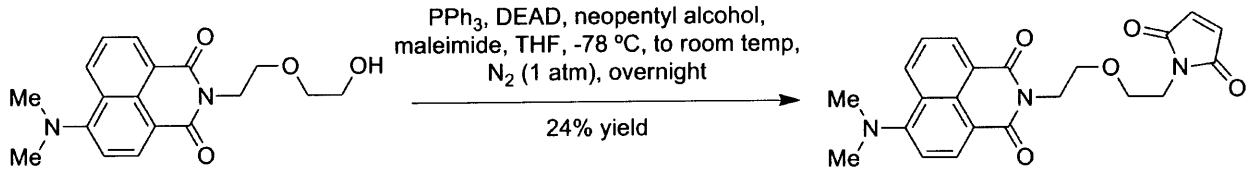

3-14 **3-6**

4-*N*,*N*-Dimethylamino-*N*-[2-(2-maleimidyl-ethoxy)-ethyl]-1,8-naphthalimide (3-6). Prior to assembling the Mitsunobu reaction, the alcohol, **3-14** (0.50 g, 1.51 mmol), was transferred to a 50 mL pear-shaped flask equipped with rubber stopper and placed under high vacuum overnight to remove trace water that may inhibit the reaction. An oven-dried 100 mL Kjeldahl-style Schlenk flask equipped with a magnetic stir bar and rubber septum was charged with solid triphenylphosphine (0.36 g, 1.37 mmol). The Schlenk flask was then evacuated of air

by placing under high vacuum and charged with N_2 gas (3×). Freshly distilled dry THF (4 mL) was then transferred to the Schlenk flask by syringe and the triphenylphosphine stirred at ambient temperature until completely dissolved. This solution was then lowered to -78 °C by immersing in a dry ice/isopropanol bath. Next, diethyl azodicarboxylate (0.597 mL, 40% solution in toluene, 1.37 mmol) was added dropwise via syringe over 2 min. The mixture was allowed to stir for approximately 5 min to allow formation of the betaine. At this point, the reaction mixture was a pale yellow color. Meanwhile, a solution of the alcohol, **3-14**, was prepared by dissolving in 6 mL of freshly distilled dry THF. This solution was then transferred very slowly to the reaction vessel by syringe to avoid raising the temperature. Once the transfer was complete, neopentyl alcohol (0.06 g, 0.69 mmol) was added as a solid. The reaction was allowed to stir approximately 5 min to allow formation of the oxyphosphonium ion intermediate. Solid maleimide (0.13 g, 1.37 mmol) was then added and the reaction was allowed to warm to room temperature and stirred overnight. The reaction was stopped by concentrating to dryness on the rotary evaporator and the product was isolated by flash column chromatography using 1:2 hexanes/ethyl acetate. The product was a bright yellow solid (0.15 g, 0.37 mmol, 24.4 % yield, R_f = 0.22 in 1:2 hexanes/ethyl acetate) and was dissolved in DMSO for storage at -80 °C in 100 mM aliquots.

^{1}H NMR (300 MHz, $CDCl_3$, δ): 3.09 (s, 6H), 3.65 (m, 4H), 3.74 (t, 2H, J = 6.0 Hz), 4.34 (t, 2H, J = 5.9 Hz), 6.50 (s, 2H), 7.09 (d, 1H, J = 8.1 Hz), 7.63 (dd, 1H, J_1 = 8.4 Hz, J_2 = 7.2 Hz), 8.42 (apparent d, 2H, J = 8.1 Hz), 8.51 (dd, 1H, J_1 = 7.5 Hz, J_2 = 1.2 Hz).

^{13}C NMR (300 MHz, $CDCl_3$, δ): 37.2, 38.8, 44.7, 67.2, 67.6, 113.2, 114.9, 122.9, 124.8, 125.1, 130.2, 131.0, 131.1, 132.6, 133.8, 156.6, 163.9, 164.4, 170.5.

HRMS-ESI (*m/z*): $[M+H]^+$ calcd for $C_{22}H_{21}N_3O_5$, 408.1554; found, 408.1567.

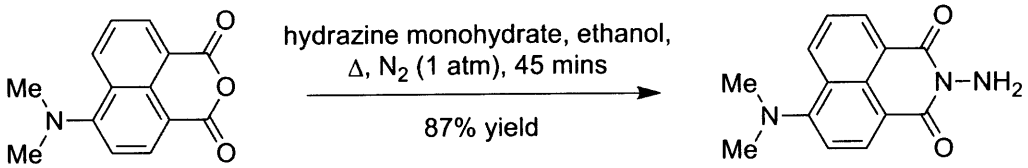

***N*-Amino-4-*N*,*N*-dimethylamino-1,8-naphthalimide (3-15).** Added 4-*N*,*N*-dimethylamino-1,8-naphthalic anhydride, **3-1** (1.00 g, 4.14 mmol), to a 200 mL two-necked round-bottom flask equipped with a reflux condenser, magnetic stir bar, and rubber septum. The reaction vessel was then evacuated of air by applying vacuum and flushing with N_2 gas (3×). Anhydrous ethanol (42 mL) was then added to the flask by syringe. The suspension was stirred as the temperature was raised to reflux. The anhydride was still present as a solid as the suspension reached reflux until the addition of hydrazine monohydrate (0.402 mL, 8.29 mmol) by syringe. The slurry then turned to a clear deep orange solution. The reaction was allowed to proceed at reflux for 45 min then stopped by cooling to room temperature. The reaction mixture was diluted to a final volume of 200 mL with cold water to precipitate the product, which was then filtered and purified by flash chromatography using 1:3 hexanes/ethyl acetate. The product was a bright yellow solid (0.925 g, 3.624 mmol, 87.4 % yield, R_f = 0.23 in 1:3 hexanes/ethyl acetate).

^{1}H NMR (300 MHz, $CDCl_3$, δ): 3.09 (s, 6H), 5.26 (br s, 2H), 7.02 (d, 1H, J = 8.4 Hz), 7.58 (dd, 1H, J_1 = 8.4 Hz, J_2 = 7.5 Hz), 8.37 (dd, 1H, J_1 = 8.6 Hz, J_2 = 0.8 Hz), 8.38 (d, 1H, J = 8.4 Hz), 8.49 (dd, 1H, J_1 = 7.4 Hz, J_2 = 0.8 Hz).

^{13}C NMR (300 MHz, $CDCl_3$, δ): 44.8, 113.0, 113.4, 121.9, 124.6, 124.9, 128.7, 131.0, 131.5, 132.8, 157.3, 160.7, 161.0.

HRMS-ESI (*m/z*): $[M+H]^+$ calcd for $C_{14}H_{13}N_3O_2$, 256.1081; found, 256.1083.

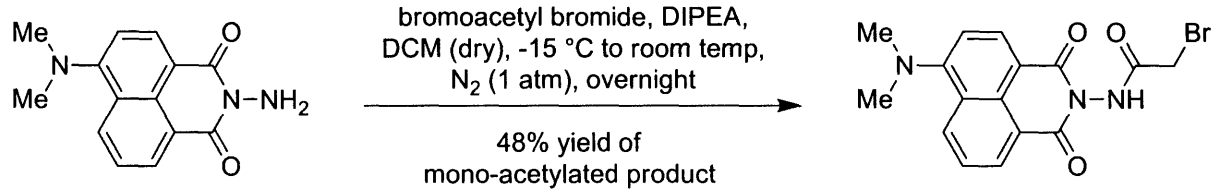

3-15 **3-3**

4-*N*,*N*-Dimethylamino-*N*-[2-bromoacetamido]-1,8-naphthalimide (3-3). The solid *N*-amino-4-*N*,*N*-dimethylamino-1,8-naphthalimide, **3-15** (0.50 g, 1.96 mmol), was transferred to an oven-dried 100 mL Schlenk flask along with a magnetic stir bar. The flask was then capped with a rubber septum and evacuated of air by placing under high vacuum followed by charging with N_2 gas (3×). The starting material was then partially dissolved in dry dichloromethane (39 mL) and stirred as *N*,*N*-diisopropylethylamine (0.357 mL, 2.15 mmol) was added through the septum via syringe. The Schlenk flask was then cooled to -15 °C in an ice bath of 3:1 ice/NaCl. Once cooled, bromoacetyl bromide (0.255 mL, 2.94 mmol) was added to the suspension dropwise via syringe and stirred for 5 min before bringing the reaction vessel back to room temperature. A white solid, presumed to be a bromide salt, was observed precipitating from the reaction mixture over time. After allowing the reaction to run overnight, the mixture was diluted to a total volume of 100 mL in dichloromethane and washed with $NaHCO_3$ (3 × 50 mL). The organic layer was dried with $MgSO_4$, filtered, and concentrated on the rotary evaporator. The desired product was isolated by flash chromatography using 1:1 hexanes/ethyl acetate. The reaction yielded two

products: the desired monoacylated product, **3-3** (0.24 g, 0.93 mmol, 47.6% yield, R_f = 0.10 in 1:1 hexanes/ethyl acetate), and a diacylated byproduct in nearly a 1:1 ratio. The desired product was stored as a solid at -20 °C.

^{1}H NMR (300 MHz, $CDCl_3$, δ): 3.13 (s, 6H), 4.31 (s, 2H), 7.08 (d, 1H, J = 8.4Hz), 7.64 (dd, 1H, J_1 = 8.6 Hz, J_2 = 6.9 Hz), 8.44 (dd, 1H, J_1 = 8.4 Hz, J_2 = 1.2 Hz), 8.46 (d, 1H, J = 8.1 Hz), 8.57 (dd, 1H, J_1 = 7.5 Hz, J_2 = 1.2 Hz), 8.62 (br s, 1H).

^{13}C NMR (500 MHz, $CDCl_3$, δ): 26.5, 44.7, 113.2, 113.5, 122.3, 124.8, 125.1, 130.4, 132.0, 132.3, 133.7, 157.8, 161.6, 162.2, 164.5.

HRMS-ESI (*m/z*): $[M+H]^+$ calcd for $C_{16}H_{14}BrN_3O_3$, 376.0291; found, 376.0304.

Synthesis of 4-*N*,*N*-dimethyl-1,8-naphthalimide derivatives and characterization:

All reagents and solvents were procured from Sigma-Aldrich unless otherwise stated.

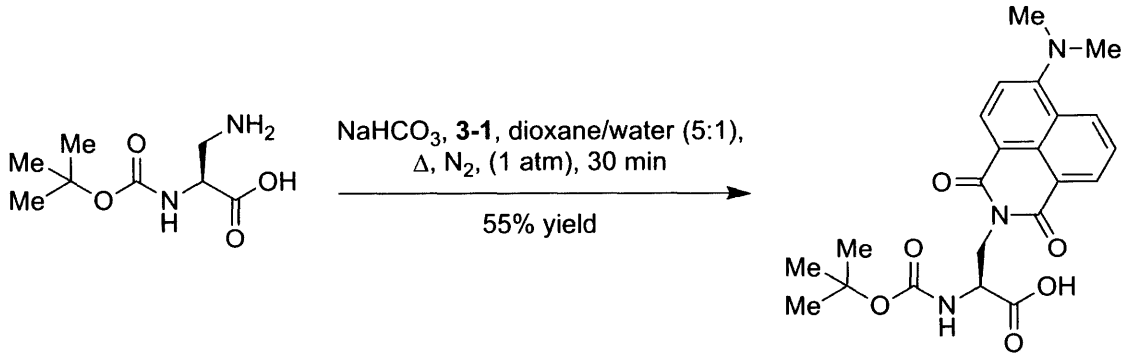

3-18

***N*-α-Boc-(4-*N*,*N*-dimethylamino-1,8-naphthalimido)-alanine (3-18).** Dissolved (S)-3-amino-2-(Boc-amino)-propionic acid (2.00 g, 9.79 mmol) (Cat. No. A-3220, Bachem) and $NaHCO_3$ (4.11 g, 48.97 mmol) together in dH_2O (49 mL) and transferred to a 60 mL addition

funnel. Next, added solid 4-*N,N*-dimethylamino naphthalic anhydride **3-1** (2.60 g, 10.77 mmol) to a 500 mL three-necked round-bottom flask equipped with a magnetic stir bar and reflux condenser. The reaction vessel was evacuated of air by placing under high vacuum, then charging with N_2 gas (3×). Dioxane (245 mL) was then transferred to the reaction vessel via syringe through the rubber septum. The suspension was stirred vigorously as the temperature was raised to reflux. Once at reflux, the aqueous solution of the amino acid was added slowly over 5 min. The reaction was allowed to proceed at reflux for 30 min before allowing cooling to room temperature. The reaction was then concentrated on the rotary evaporator to remove most of the dioxane before diluting to 200 mL with dH_2O and washing with ether to remove unreacted anhydride. The aqueous layer was then acidified with 6 N HCl and extracted with DCM (3 × 100 mL). The organic layers were combined, dried with $MgSO_4$, filtered, and concentrated. The crude was purified by flash column chromatography using ethyl acetate with 0.5% acetic acid as the solvent system. The fractions containing the desired product were combined and azeotroped in toluene (3 × 100 mL) to remove residual acetic acid. The product was isolated as a bright orange solid (2.31 mg, 5.40 mmol, 55% yield, R_f = 0.2 in EtOAc with 0.5% AcOH).

^{1}H-NMR (500 MHz, $CDCl_3$, δ): 1.26 (s, 9H), 3.12 (s, 6H), 4.61 (m, 2H), 4.81 (m, 1H), 5.67 (d, 1H, J = 7.0 Hz), 7.11 (d, 1H, J = 8.5 Hz), 7.65 (apparent triplet, 1H, J = 8.0 Hz), 8.44 (d, 1H, J = 8.0 Hz), 8.48 (d, 1H, J = 8.0 Hz), 8.56 (d, 1H, J = 7.0 Hz).

^{13}C-NMR (300 MHz, $CDCl_3$, δ): 173.7, 165.0, 164.5, 157.1, 156.0, 133.2, 131.6, 131.5, 130.4, 125.0, 124.9, 122.5, 114.1, 113.3, 80.2, 52.8, 44.7, 40.7, 28.0.

HRMS-ESI (m/z): [M+H$^+$] calcd for $C_{22}H_{25}N_3O_6$ 428.1816, found, 428.1814.

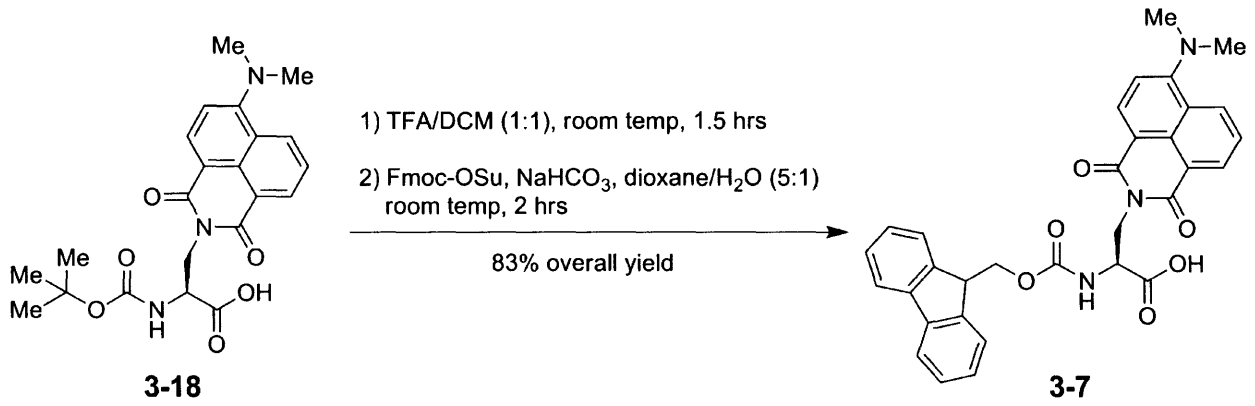

3-18 **3-7**

***N*-α-Fmoc-(4-*N*,*N*-dimethylamino-1,8-naphthalimido)-alanine (3-7).** The solid Boc-4DMNA **3-18** (2.0 g, 4.68 mmol) was dissolved in dichloromethane (47 mL) and stirred in a 250 mL round-bottom flask as cold TFA (47 mL) was added by addition funnel over 5 min. The reaction was allowed to proceed at ambient temperature for 1.5 hrs before concentrating to dryness and azeotroping with chloroform (3 × 50 mL) to remove residual TFA. The crude was then placed under high vacuum overnight. The crude was redissolved in dH_2O (23 mL) with $NaHCO_3$ (1.97 g, 23.40 mmol). The pH was tested to ensure the solution was basic. A solution of *N*-(9-fluorenylmethoxycarbonyloxy) succinimide (1.74 g, 5.15 mmol) was then prepared in dioxane (117 mL) and slowly added to the stirring solution of the amino acid. The reaction was allowed to proceed for 2 hrs before concentrating to remove most of the dioxane and re-diluting to a total volume of 150 mL in dH_2O. The aqueous layer was washed with diethyl ether (1 × 50 mL) to remove excess Fmoc-OSu. The aqueous layer was acidified with 6 N HCl and the product extracted into dichloromethane (3 × 100 mL). The organic layers were combined, dried with $MgSO_4$, filtered, and concentrated. The product was purified by flash column chromatography using 3:1 ethyl acetate/hexanes with 0.5% acetic acid as the solvent system.

The product is an orange solid (2.14 g, 3.89 mmol, 83% yield, R_f = 0.2 in EtOAc with 5% AcOH). Note: the final product contained a small amount of toluene as a result of azeotroping to ensure the complete removal of residual acetic acid following the purification. (Note — Both the ^{13}C-NMR and ^{1}H-NMR of this compound exhibit anisochronous resonances for nine of the ten aromatic carbons and all eight of the aromatic protons of the 9-fluorenyl group. A variable temperature experiment showed no coalescence of these aromatic protons at 80 °C. The cause of this apparent asymmetry is presumed to be the result of partial overlap of one side to the 9-fluorenyl ring system with that of the fluorescent side-chain of the amino acid. These nuclei would therefore lack chemical equivalence producing the observed spectra).

^{1}H-NMR (500 MHz, $CDCl_3$, δ): 3.02 (s, 6H), 3.95 (t, 1H, J = 7.3 Hz), 4.11 (dd, 1H, J_1 = 10.5 Hz, J_2 = 8.0 Hz), 4.21 (dd, 1H, J_1 = 10.8 Hz, J_2 = 7.3 Hz), 4.72 (d, 2H, J = 6.5 Hz), 4.99 (apparent dd, 1H, J_1 = 14.8 Hz, J_2 = 7.3 Hz), 6.17 (d, 1H, J = 8.0 Hz), 6.96 (d, 1H, J = 8.5 Hz), 7.16 (apparent t, 1H, J = 7.5 Hz), 7.21 (apparent t, 1H, J = 8.0 Hz), 7.31 (apparent t, 2H, J = 7.3 Hz), 7.45 (d, 1H, J = 7.5 Hz), 7.5 (d, 1H, J = 7.5 Hz), 7.57 (apparent t, 1H, J = 8.0 Hz), 7.66 (apparent t, 2H, J = 6.5 Hz), 8.34 (d, 1H, J = 8.0 Hz), 8.41 (d, 1H, J = 8.5 Hz), 8.54 (d, 1H, J = 7.5 Hz).

^{13}C-NMR (500 MHz, $CDCl_3$, δ): 173.6, 165.1, 164.6, 157.2, 156.3, 143.9, 143.6, 141.0, 133.4, 131.7, 131.6, 130.3, 129.0, 128.2, 127.4, 127.0, 126.9, 125.3, 125.1, 124.8, 124.7, 122.2, 119.7, 119.6, 113.7, 113.1, 67.3, 53.2, 46.9, 44.6, 40.6.

HRMS-ESI (m/z): [M+H$^+$] calcd for $C_{32}H_{27}N_3O_6$ 550.1973, found, 550.1959.

Acknowledgements

This research was supported by NSF CHE-0414243 (BI), the NIH Cell Migration Consortium (GM064346), and the Biotechnology Training Program (T32-GM08334). I thank Dr. Matthieu Sainlos, Dr. Andreas Aemissegger, and Dr. Bianca Sculimbrene for their helpful advice and guidance in the synthesis of these tools. The Department of Chemistry Instrumentation Facility (NSF CHE-9808061, DBI-9729592, and CHE-0234877) is also gratefully acknowledged.

References

(1) Vazquez, M. E.; Blanco, J. B.; Imperiali, B. Photophysics and biological applications of the environment-sensitive fluorophore 6-*N,N*-dimethylamino-2,3-naphthalimide. *J. Am. Chem. Soc.* **2005**, *127*, 1300-1306.

(2) Kollar, J.; Hrdlovic, P.; Chmela, S.; Sarakha, M.; Guyot, G. Synthesis and transient absorption spectra of derivatives of 1,8-naphthalic anhydrides and naphthalimides containing 2,2,6,6-tetramethylpiperidine; triplet route of deactivation. *J. Photoch. Photobio. A* **2005**, *170*, 151-159.

(3) Vazquez, M. E.; Rothman, D. M.; Imperiali, B. A new environment-sensitive fluorescent amino acid for Fmoc-based solid phase peptide synthesis. *Org. Biomol. Chem.* **2004**, *2*, 1965-1966.

(4) Chi, Y.; Zhang, H.; Huang, W.; Zhou, J.; Zhou, Y.; Qian, H.; Ni, S. Microwave-assisted solid phase synthesis, PEGylation, and biological activity studies of glucagon-like peptide-1(7-36) amide. *Bioorg. Med. Chem.* **2008**, *16*, 7607-7614.

(5) Yamashita, S.; Mase, N.; Takabe, K. Chemoenzymatic total synthesis and determination of the absolute configuration of (S)-nebracetam. *Tetrahedron Asymmetry* **2008**, *19*, 2115-2118.

(6) Haval, K. P.; Mhaske, S. B.; Argade, N. P. Cyanuric chloride: decent dehydrating agent for an exclusive and efficient synthesis of kinetically controlled isomaleimides. *Tetrahedron* **2006**, *62*, 937-942.

(7) Corrie, J. E. T.; Moore, M. H.; Wilson, G. D. Product diversity in cyclisations of maleamic acids: The imide-isoimide dichotomy. *J. Chem. Soc. Perkin Trans. I* **1996**, 777-781.

(8) Walker, M. A. A high-yielding synthesis of N-alkyl maleimides using a novel modification of the Mitsunobu reaction. *J. Org. Chem.* **1995**, *60*, 5352-5355.

(9) Brown, E.; Sheppard, R. C.; Williams, B. J. Peptide-Synthesis .4. Solid-phase syntheses of peptides related to Gastrin. *J. Chem. Soc. Perkin Trans. I* **1983**, 75-82.

(10) Wuts, P. G. M.; Greene, T. W.; 4th ed.; Wiley-Interscience: Hoboken, N.J., 2007, p 712-713, 725-732.

^{1}H NMR and ^{13}C NMR spectra

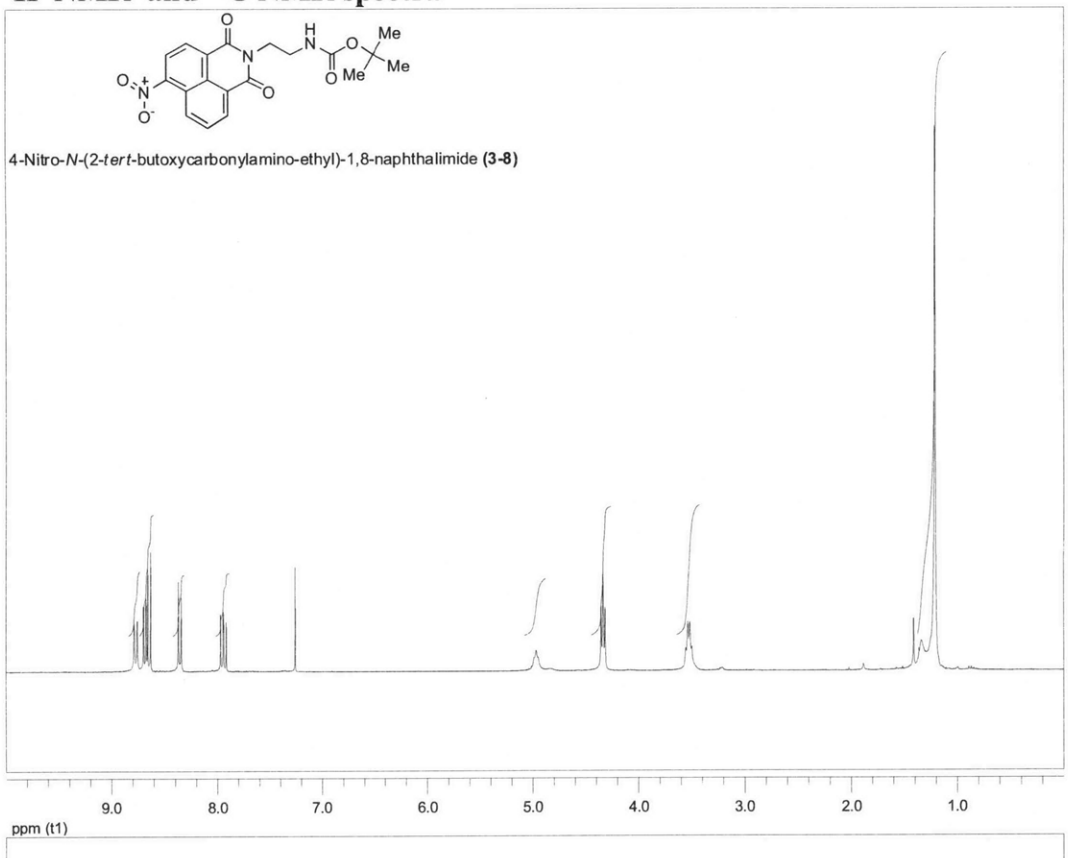

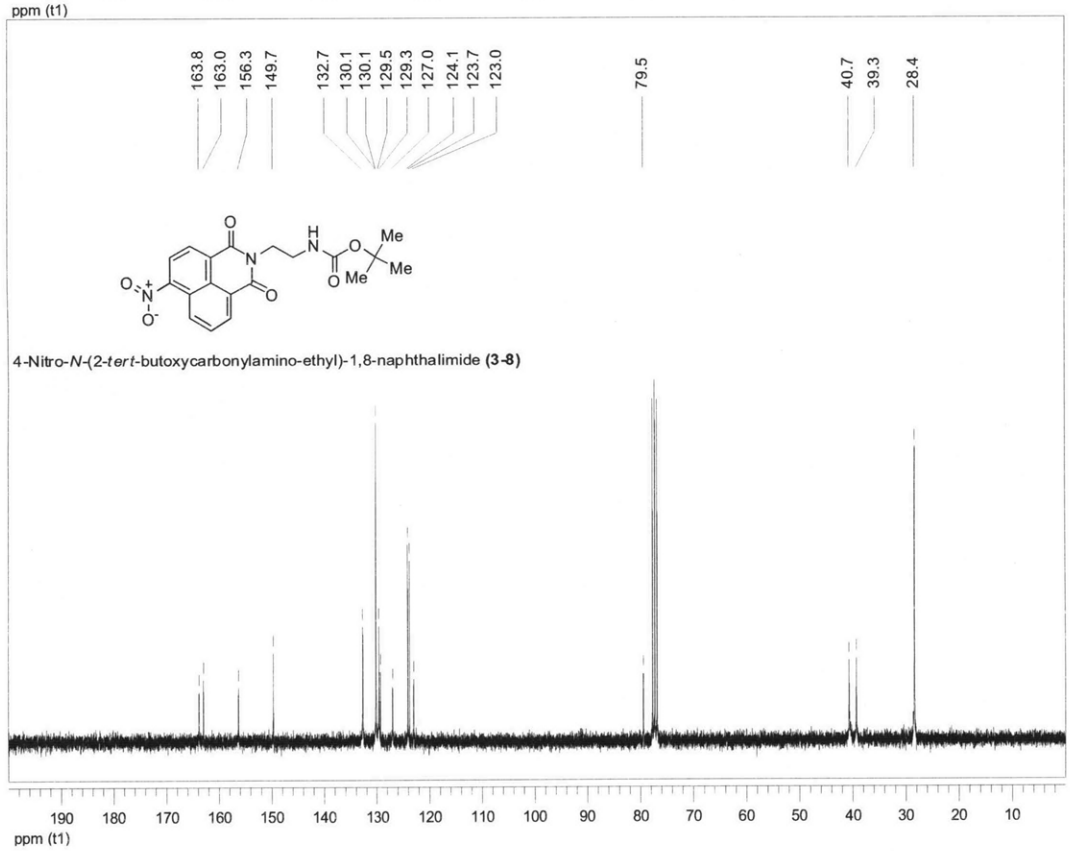

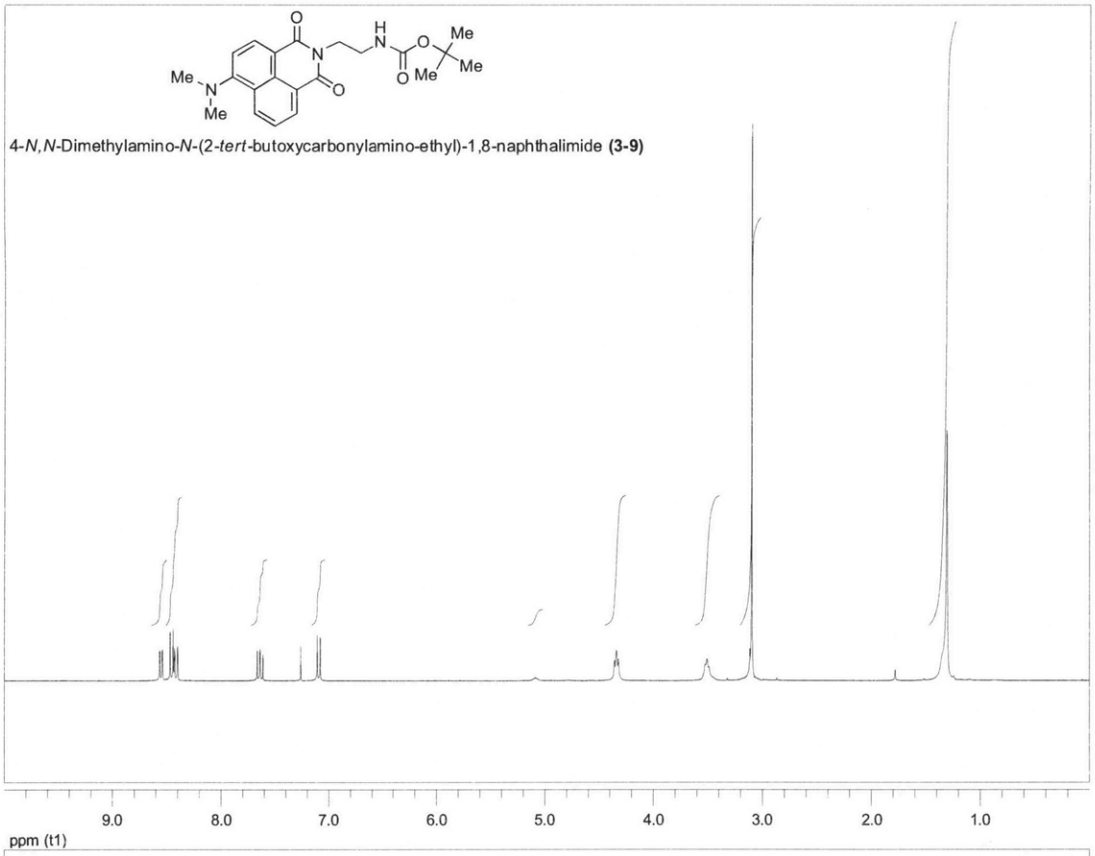
4-N,N-Dimethylamino-N-(2-tert-butoxycarbonylamino-ethyl)-1,8-naphthalimide (3-9)
9.0
8.0
7.0
6.0
5.0
4.0
3.0
2.0
1.0
ppm (t1)

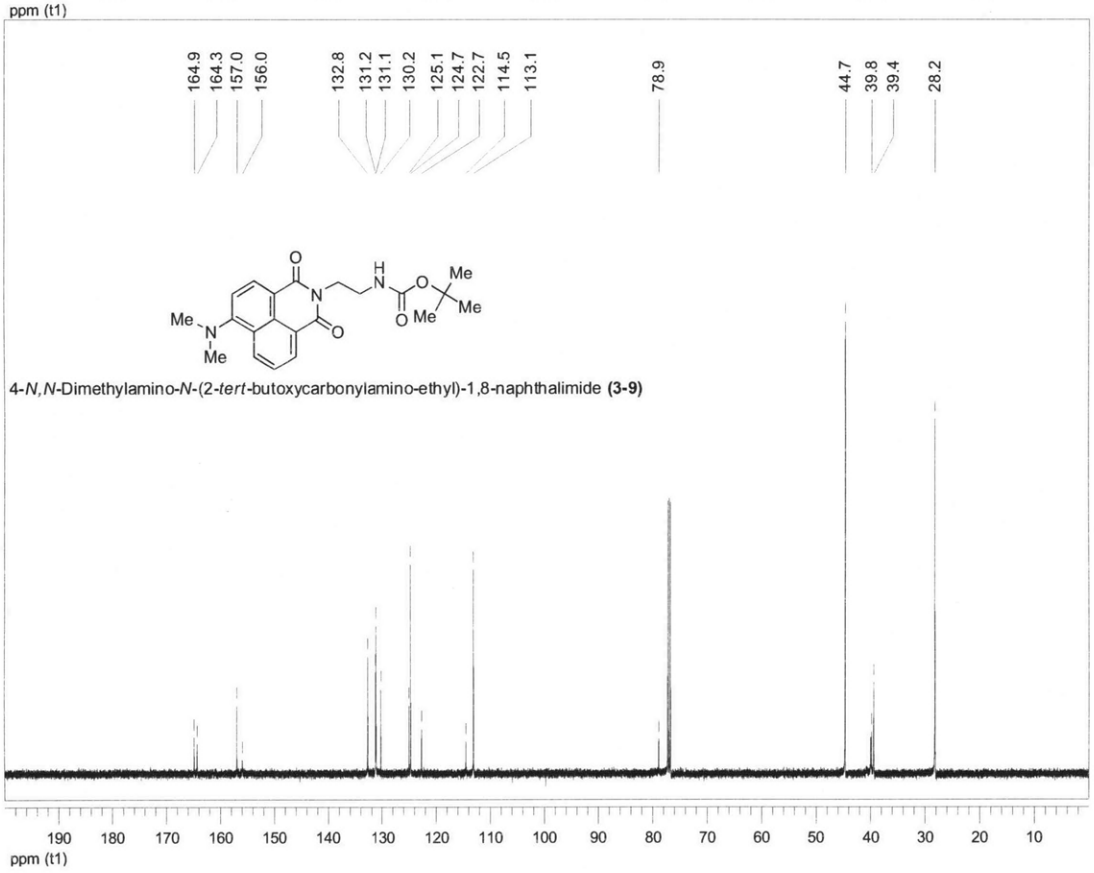
164.9
164.3
157.0
156.0
132.8
131.2
131.1
130.2
125.1
124.7
122.7
114.5
113.1
78.9
44.7
39.8
39.4
28.2
4-N,N-Dimethylamino-N-(2-tert-butoxycarbonylamino-ethyl)-1,8-naphthalimide (3-9)
190
180
170
160
150
140
130
120
110
100
90
80
70
60
50
40
30
20
10
ppm (t1)

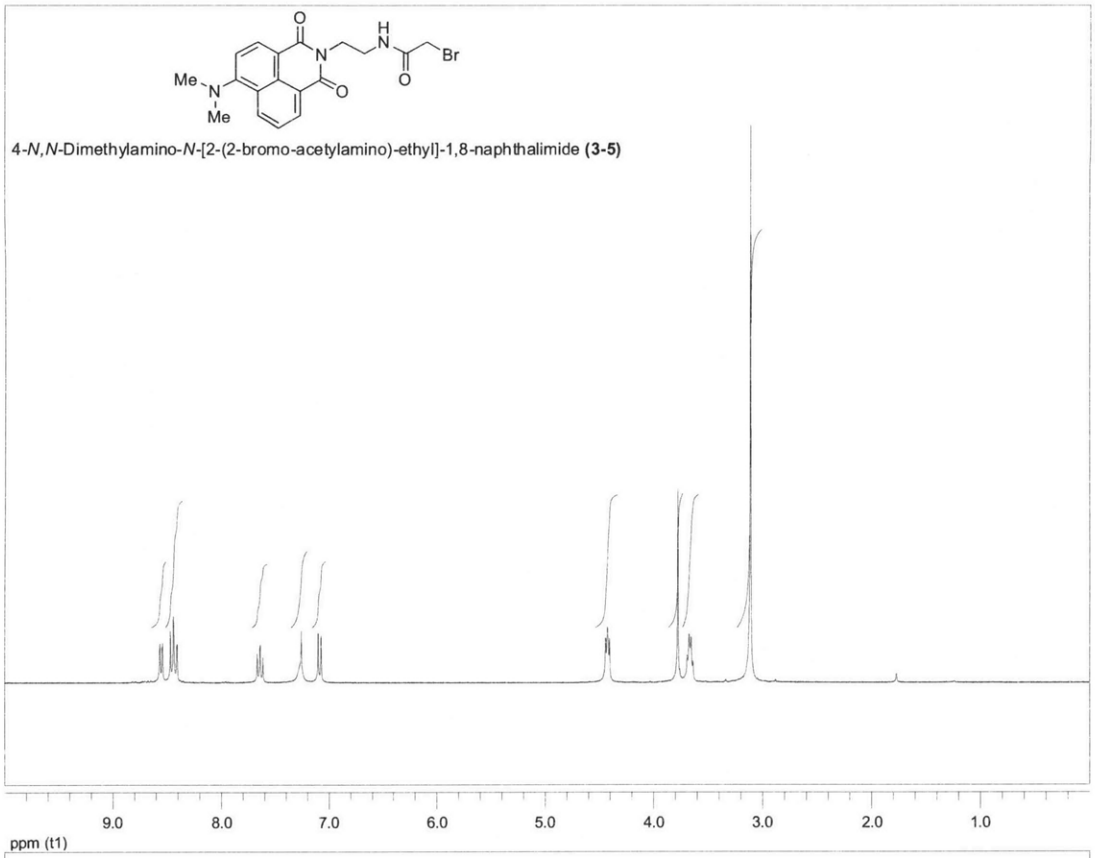
4-N,N-Dimethylamino-N-[2-(2-bromo-acetylamino)-ethyl]-1,8-naphthalimide (3-5)
9.0
8.0
7.0
6.0
5.0
4.0
3.0
2.0
1.0
ppm (t1)

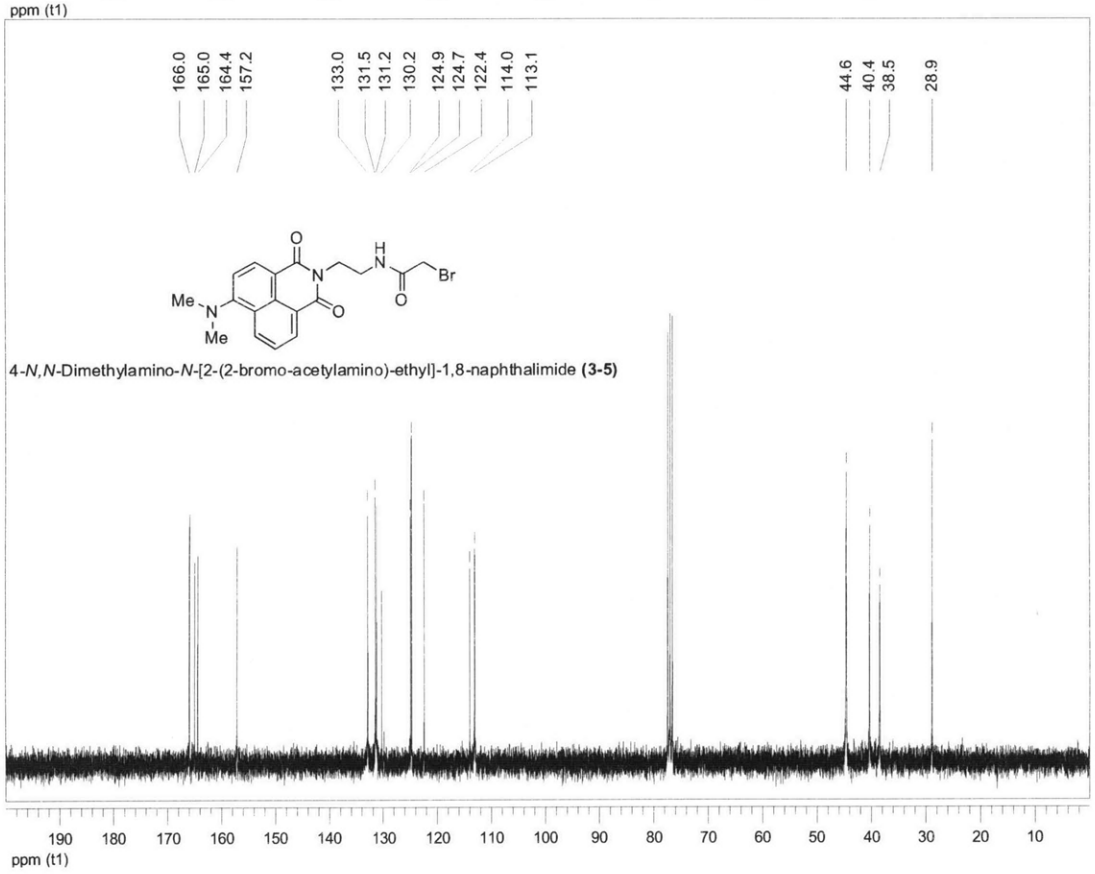
166.0
165.0
164.4
157.2
133.0
131.5
131.2
130.2
124.9
124.7
122.4
114.0
113.1
44.6
40.4
38.5
28.9
4-N,N-Dimethylamino-N-[2-(2-bromo-acetylamino)-ethyl]-1,8-naphthalimide (3-5)
190
180
170
160
150
140
130
120
110
100
90
80
70
60
50
40
30
20
10
ppm (t1)

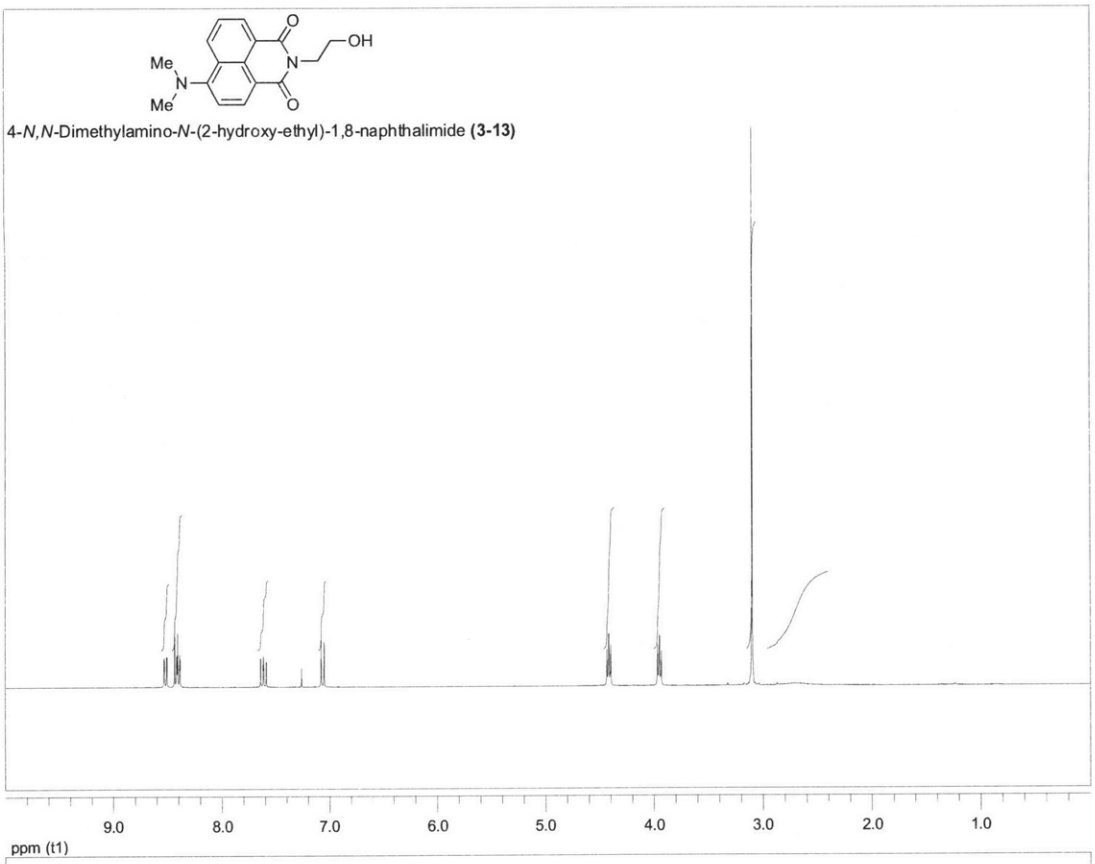
Me
N
Me
O
N
OH
O
4-*N*,*N*-Dimethylamino-*N*-(2-hydroxy-ethyl)-1,8-naphthalimide **(3-13)**
9.0
8.0
7.0
6.0
5.0
4.0
3.0
2.0
1.0
ppm (t1)

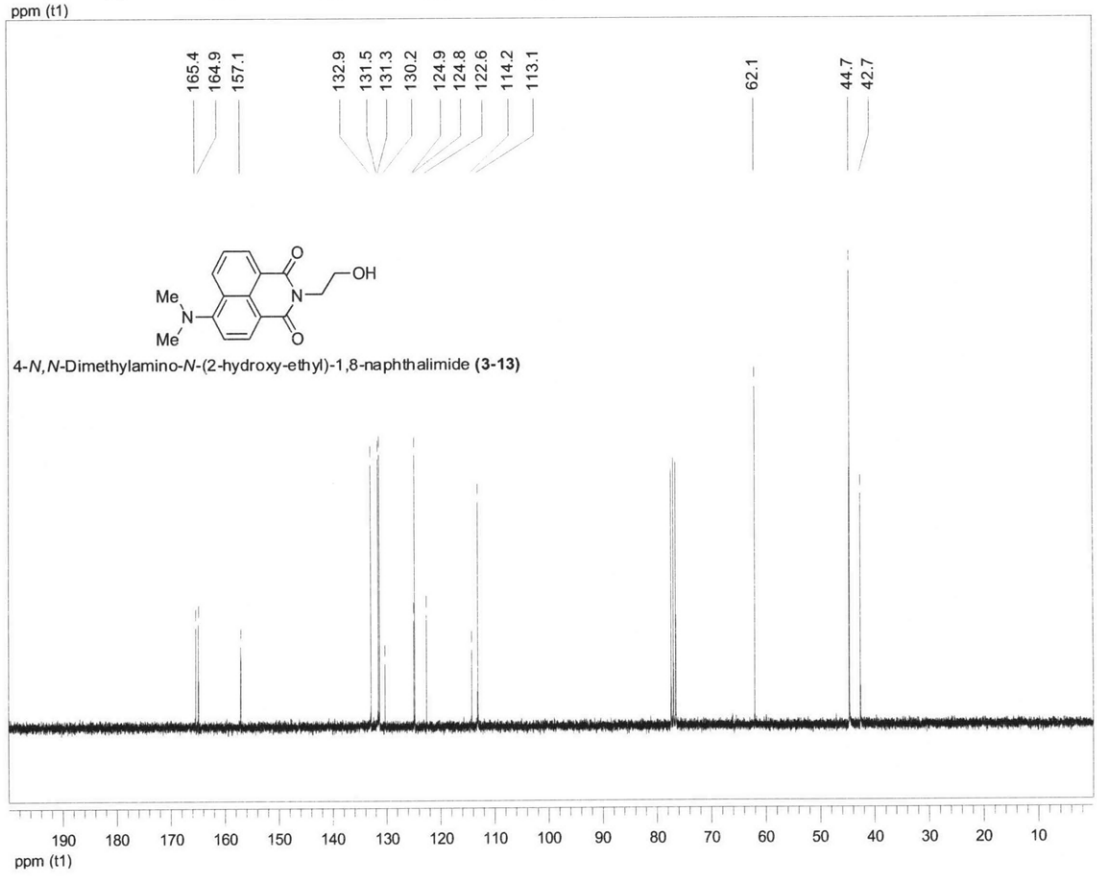
165.4
164.9
157.1
132.9
131.5
131.3
130.2
124.9
124.8
122.6
114.2
113.1
62.1
44.7
42.7
Me
N
Me
O
N
OH
O
4-*N*,*N*-Dimethylamino-*N*-(2-hydroxy-ethyl)-1,8-naphthalimide **(3-13)**
190
180
170
160
150
140
130
120
110
100
90
80
70
60
50
40
30
20
10
ppm (t1)

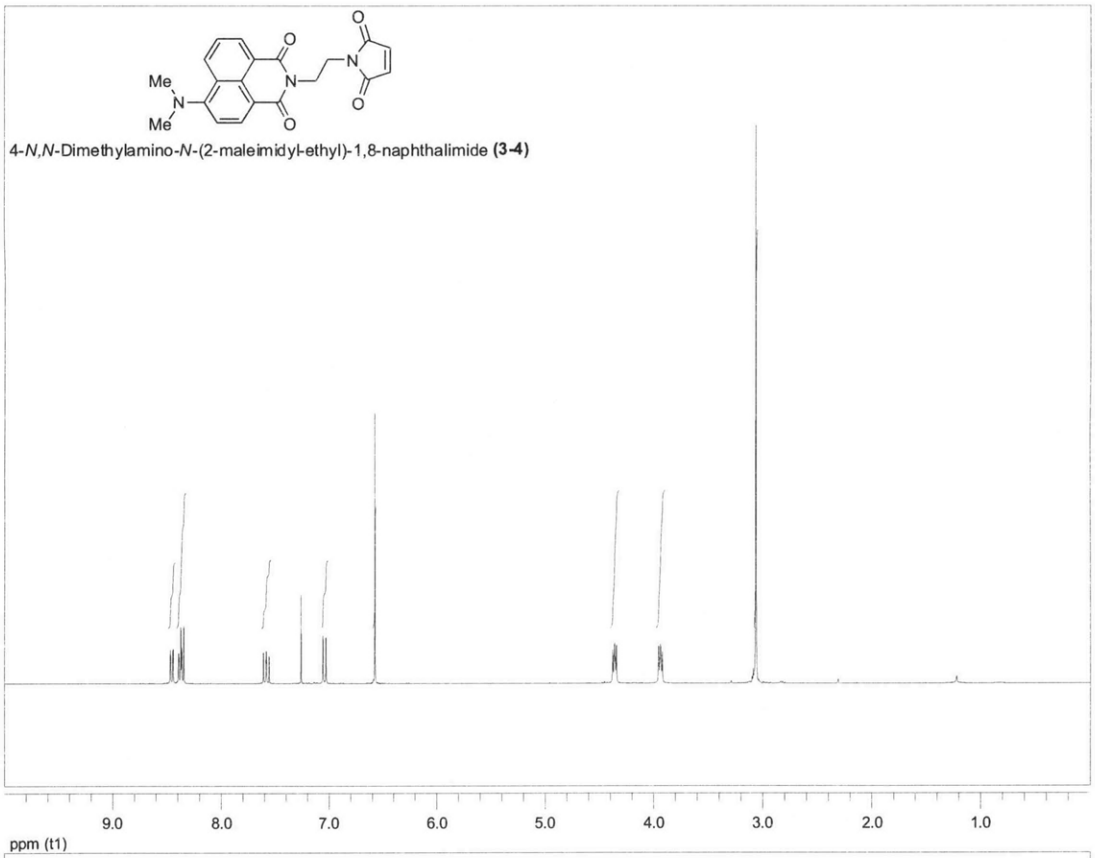
4-N,N-Dimethylamino-N-(2-maleimidyl-ethyl)-1,8-naphthalimide (3-4)
9.0
8.0
7.0
6.0
5.0
4.0
3.0
2.0
1.0
ppm (t1)

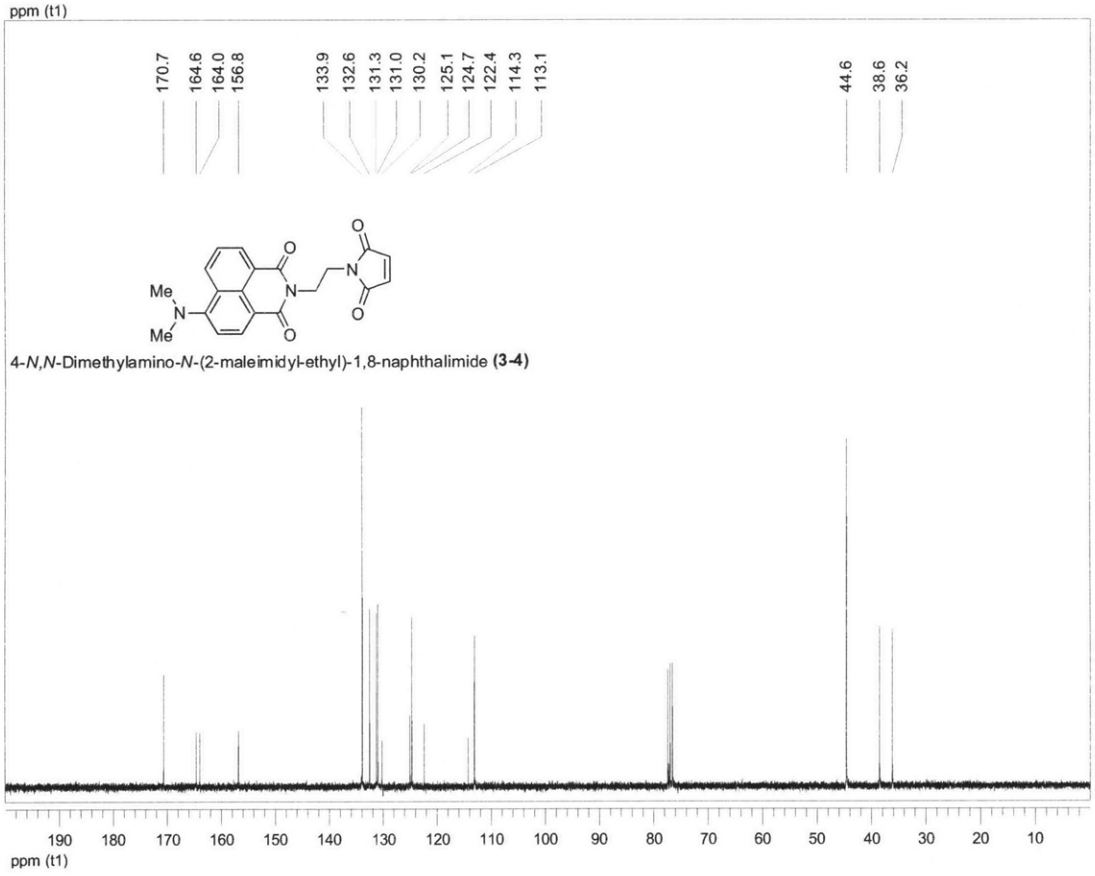
170.7
164.6
164.0
156.8
133.9
132.6
131.3
131.0
130.2
125.1
124.7
122.4
114.3
113.1
44.6
38.6
36.2
4-N,N-Dimethylamino-N-(2-maleimidyl-ethyl)-1,8-naphthalimide (3-4)
190
180
170
160
150
140
130
120
110
100
90
80
70
60
50
40
30
20
10
ppm (t1)

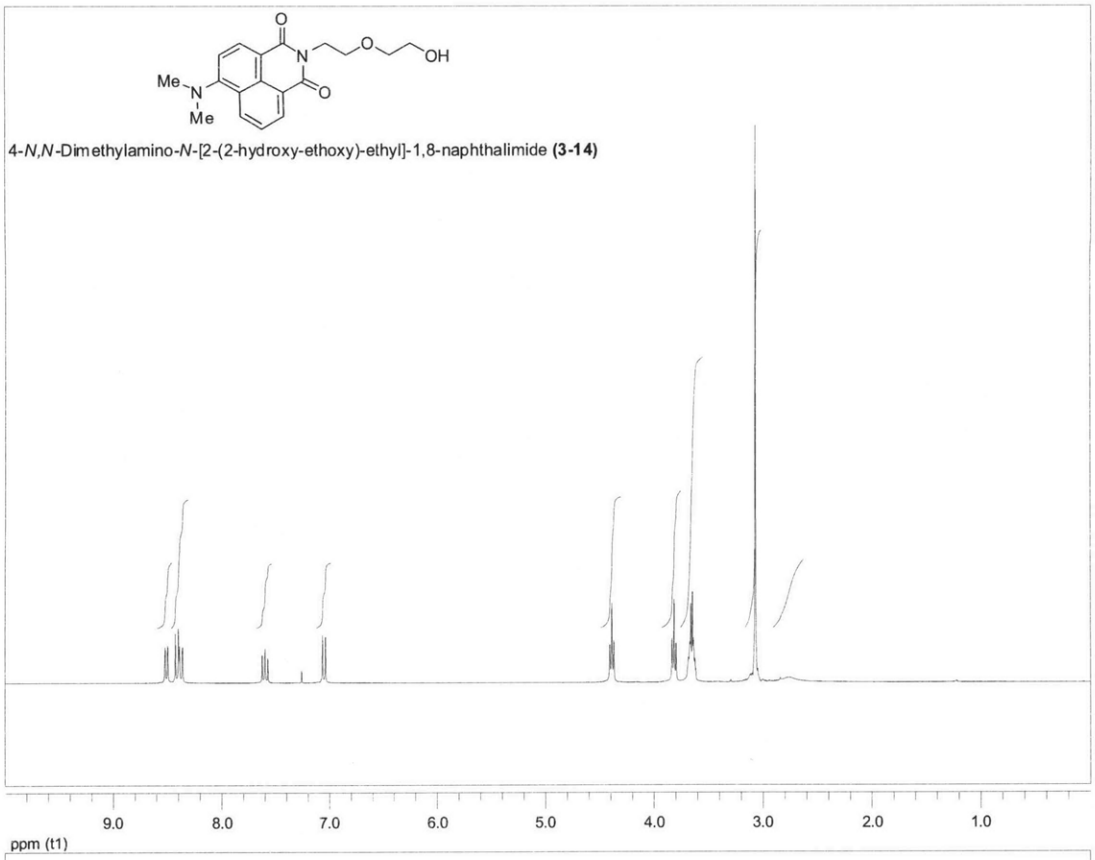
4-N,N-Dimethylamino-N-[2-(2-hydroxy-ethoxy)-ethyl]-1,8-naphthalimide (3-14)
9.0
8.0
7.0
6.0
5.0
4.0
3.0
2.0
1.0
ppm (t1)

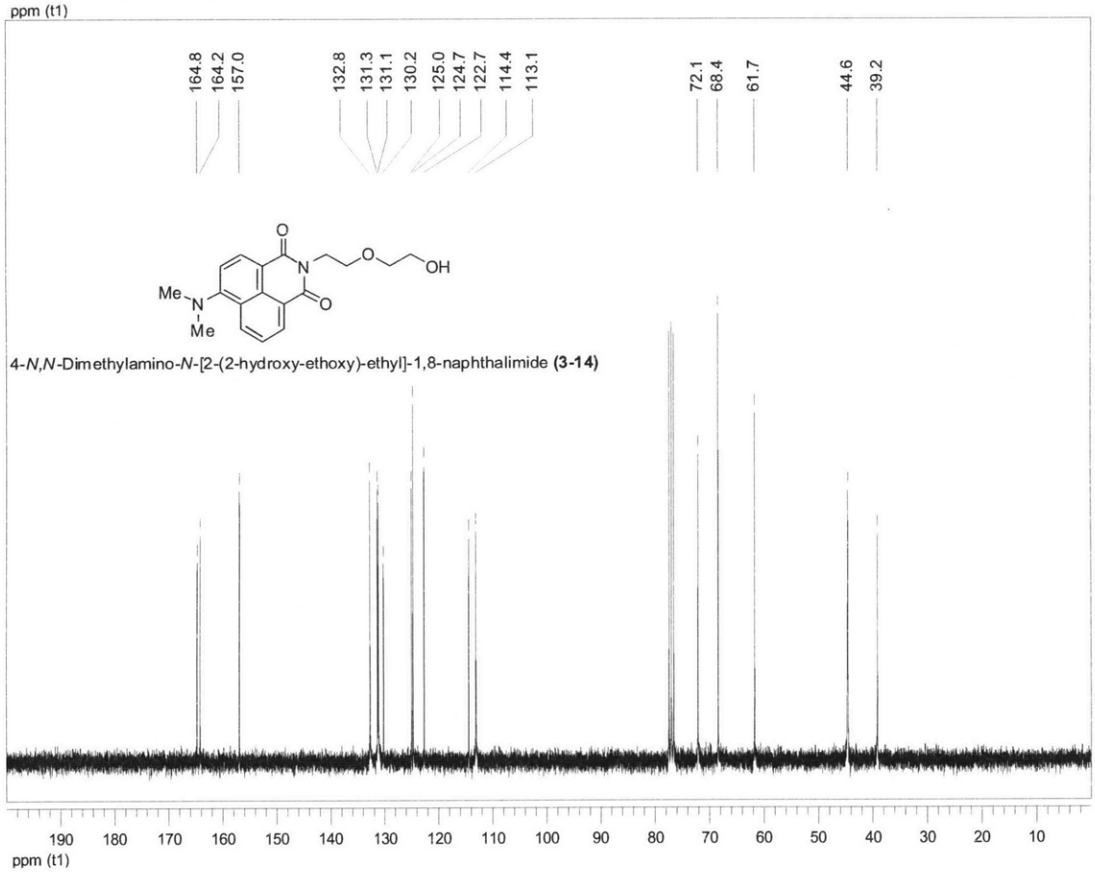
164.8
164.2
157.0
132.8
131.3
131.1
130.2
125.0
124.7
122.7
114.4
113.1
72.1
68.4
61.7
44.6
39.2
4-N,N-Dimethylamino-N-[2-(2-hydroxy-ethoxy)-ethyl]-1,8-naphthalimide (3-14)
190
180
170
160
150
140
130
120
110
100
90
80
70
60
50
40
30
20
10
ppm (t1)

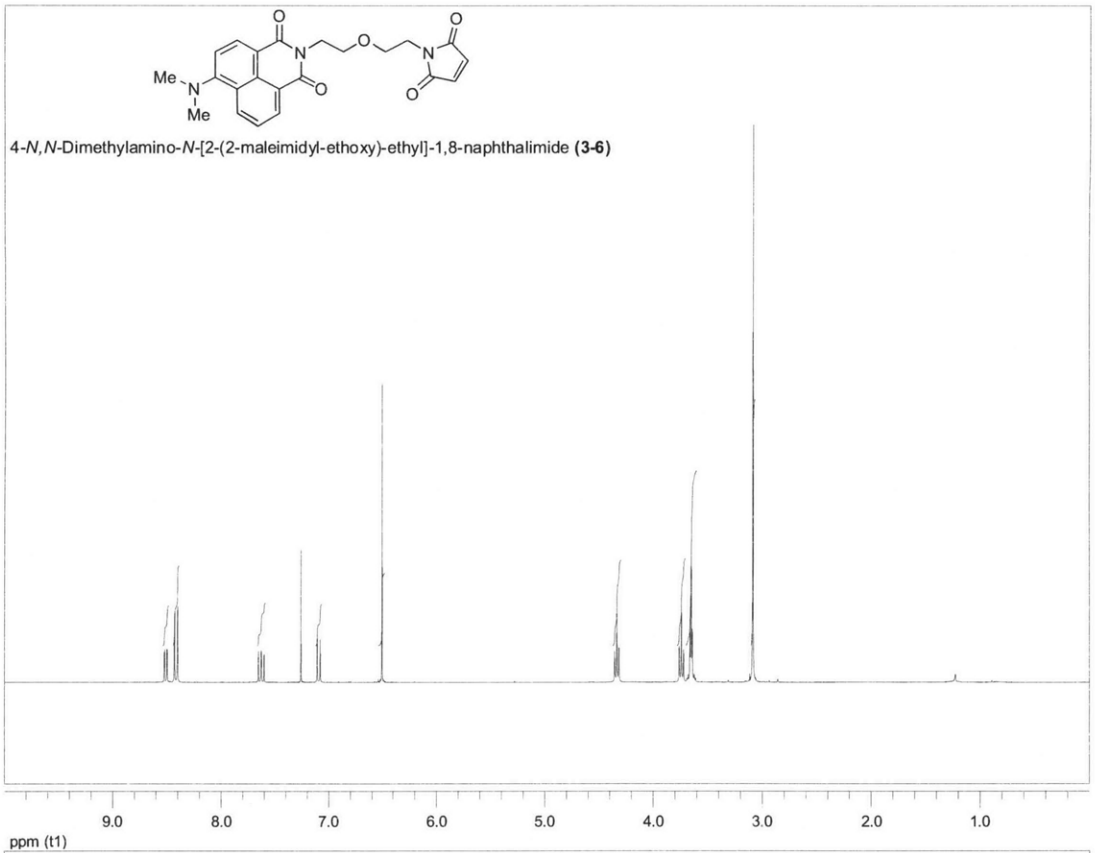
4-N,N-Dimethylamino-N-[2-(2-maleimidyl-ethoxy)-ethyl]-1,8-naphthalimide (3-6)
9.0
8.0
7.0
6.0
5.0
4.0
3.0
2.0
1.0
ppm (t1)

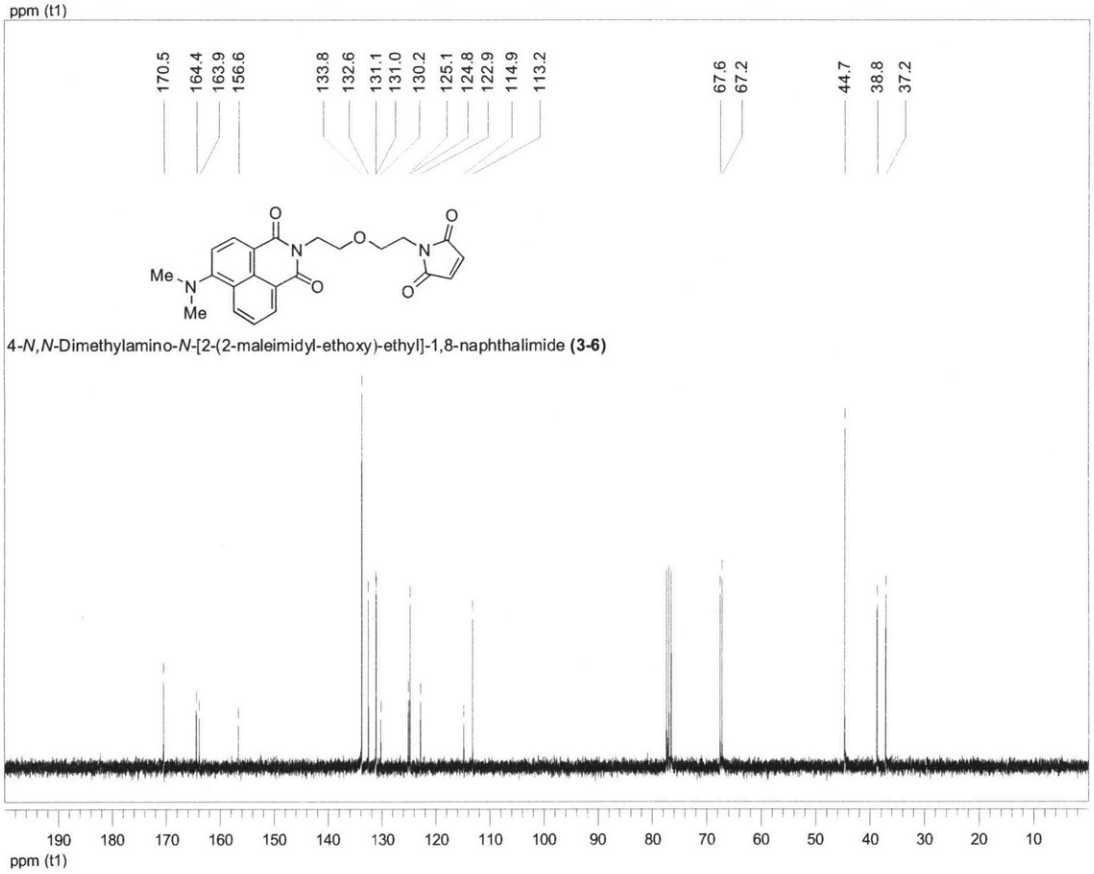
170.5
164.4
163.9
156.6
133.8
132.6
131.1
131.0
130.2
125.1
124.8
122.9
114.9
113.2
67.6
67.2
44.7
38.8
37.2
4-N,N-Dimethylamino-N-[2-(2-maleimidyl-ethoxy)-ethyl]-1,8-naphthalimide (3-6)
190
180
170
160
150
140
130
120
110
100
90
80
70
60
50
40
30
20
10
ppm (t1)

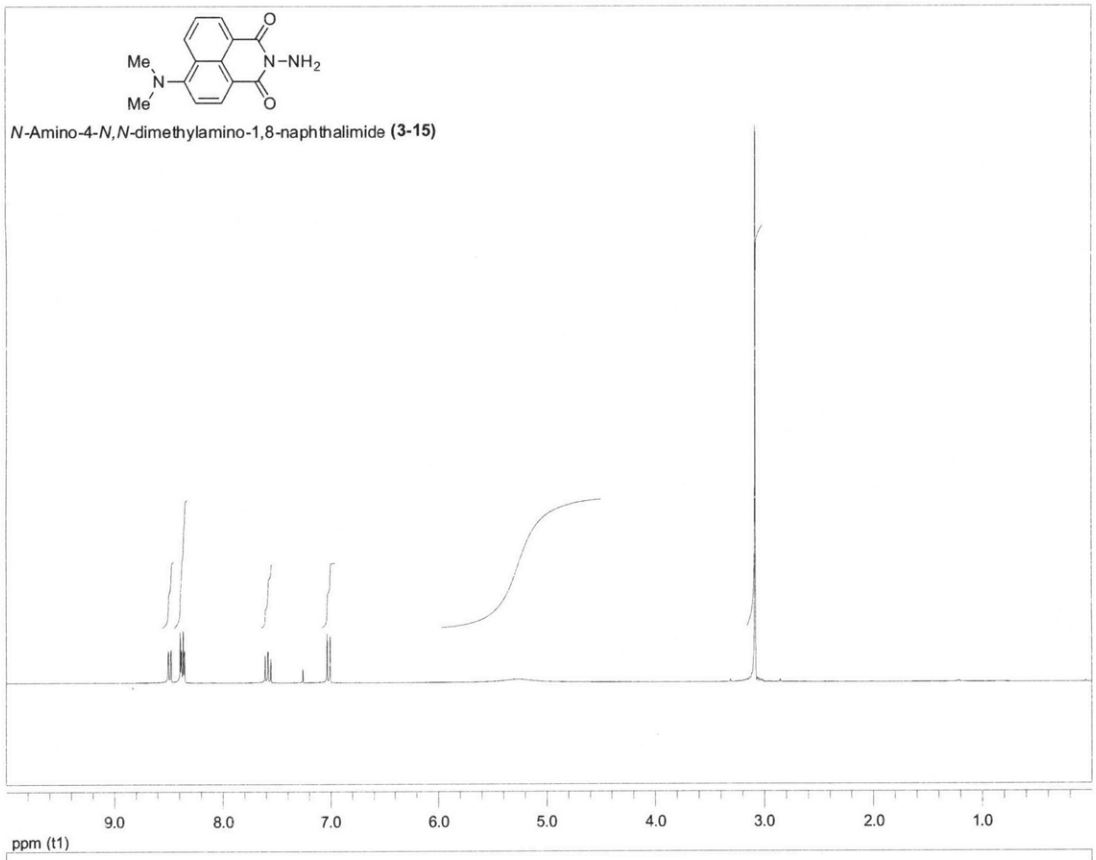
Me
N
Me
O
N–NH2
O
N-Amino-4-N,N-dimethylamino-1,8-naphthalimide (3-15)
9.0
8.0
7.0
6.0
5.0
4.0
3.0
2.0
1.0
ppm (t1)

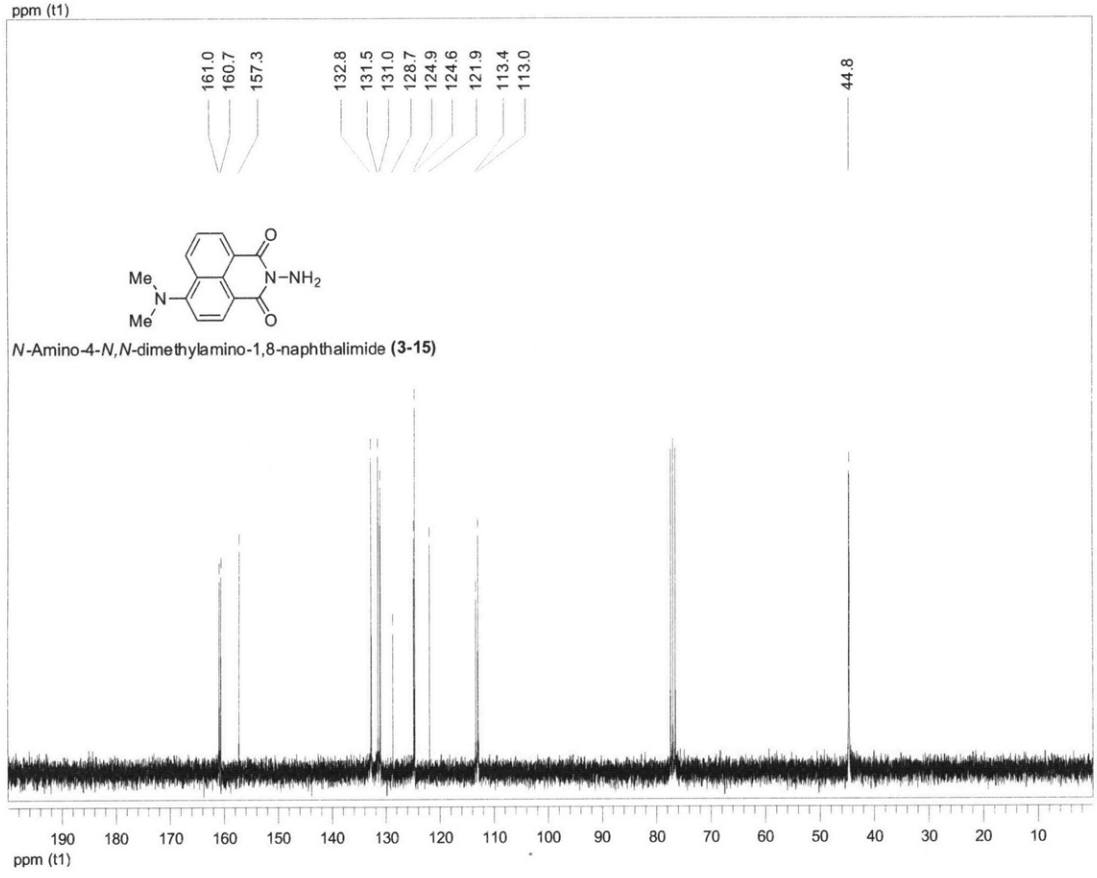
161.0
160.7
157.3
132.8
131.5
131.0
128.7
124.9
124.6
121.9
113.4
113.0
44.8
Me
N
Me
O
N–NH2
O
N-Amino-4-N,N-dimethylamino-1,8-naphthalimide (3-15)
190
180
170
160
150
140
130
120
110
100
90
80
70
60
50
40
30
20
10
ppm (t1)

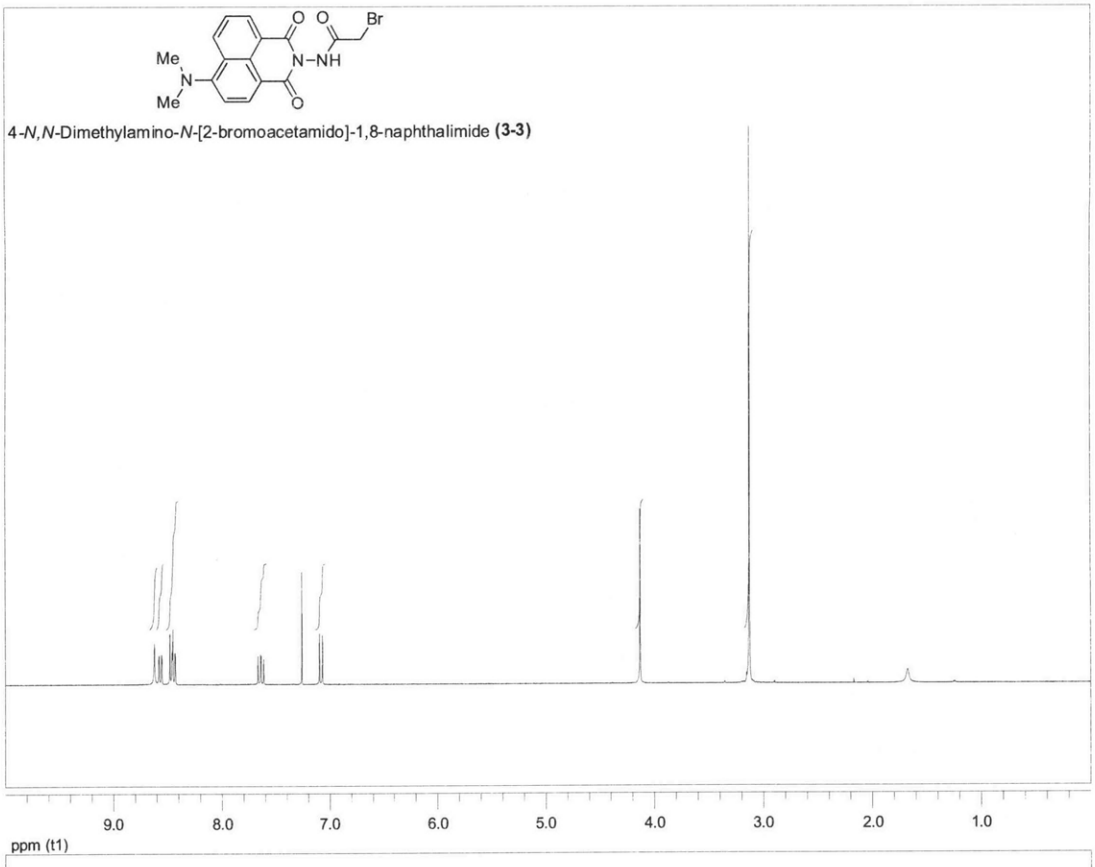
Me
N
Me
O
O
N–NH
O
Br
4-N,N-Dimethylamino-N-[2-bromoacetamido]-1,8-naphthalimide (3-3)
9.0
8.0
7.0
6.0
5.0
4.0
3.0
2.0
1.0
ppm (t1)

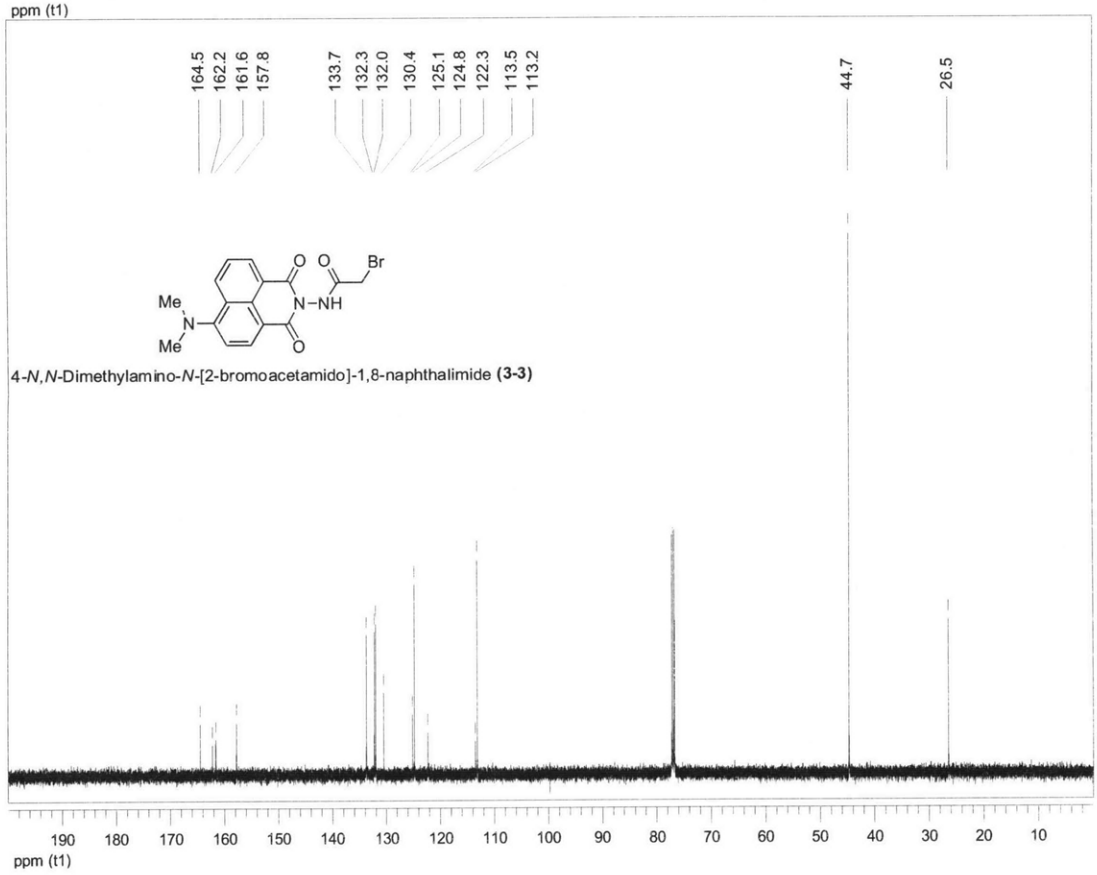
164.5
162.2
161.6
157.8
133.7
132.3
132.0
130.4
125.1
124.8
122.3
113.5
113.2
44.7
26.5
Me
N
Me
O
O
N–NH
O
Br
4-N,N-Dimethylamino-N-[2-bromoacetamido]-1,8-naphthalimide (3-3)
190
180
170
160
150
140
130
120
110
100
90
80
70
60
50
40
30
20
10
ppm (t1)

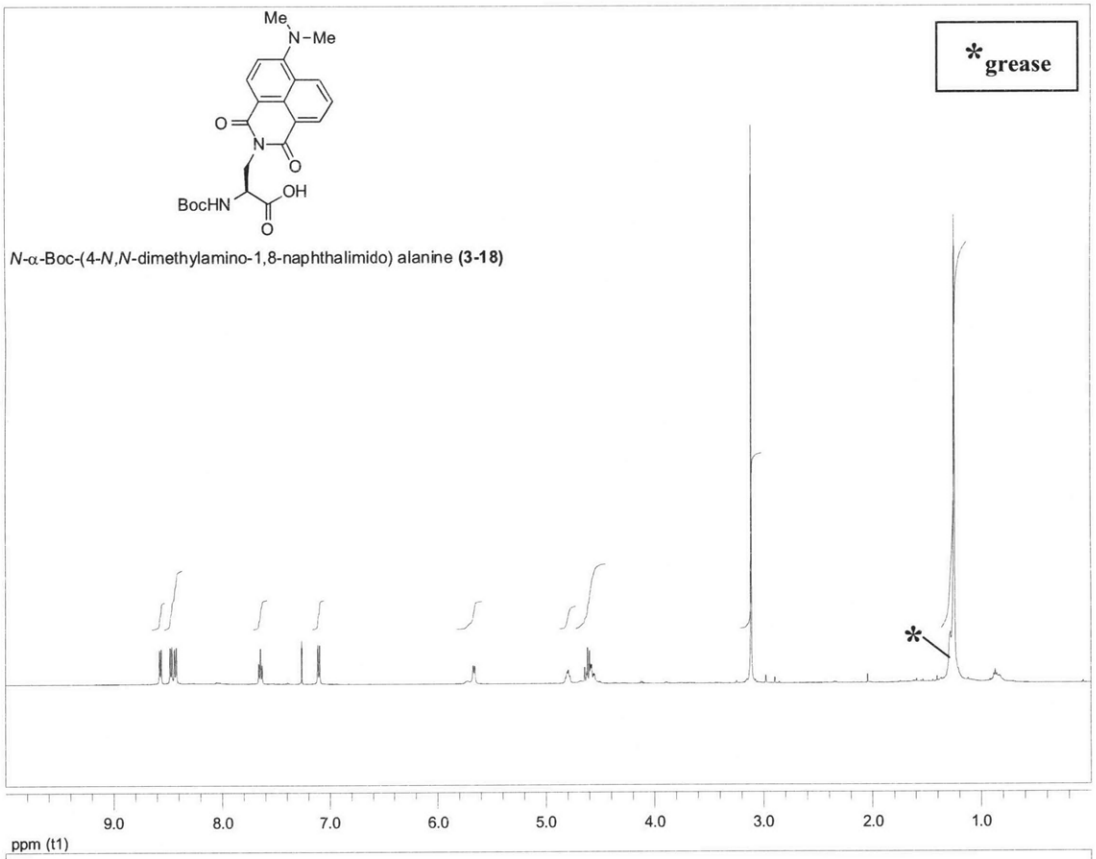

N-α-Boc-(4-*N*,*N*-dimethylamino-1,8-naphthalimido) alanine **(3-18)**

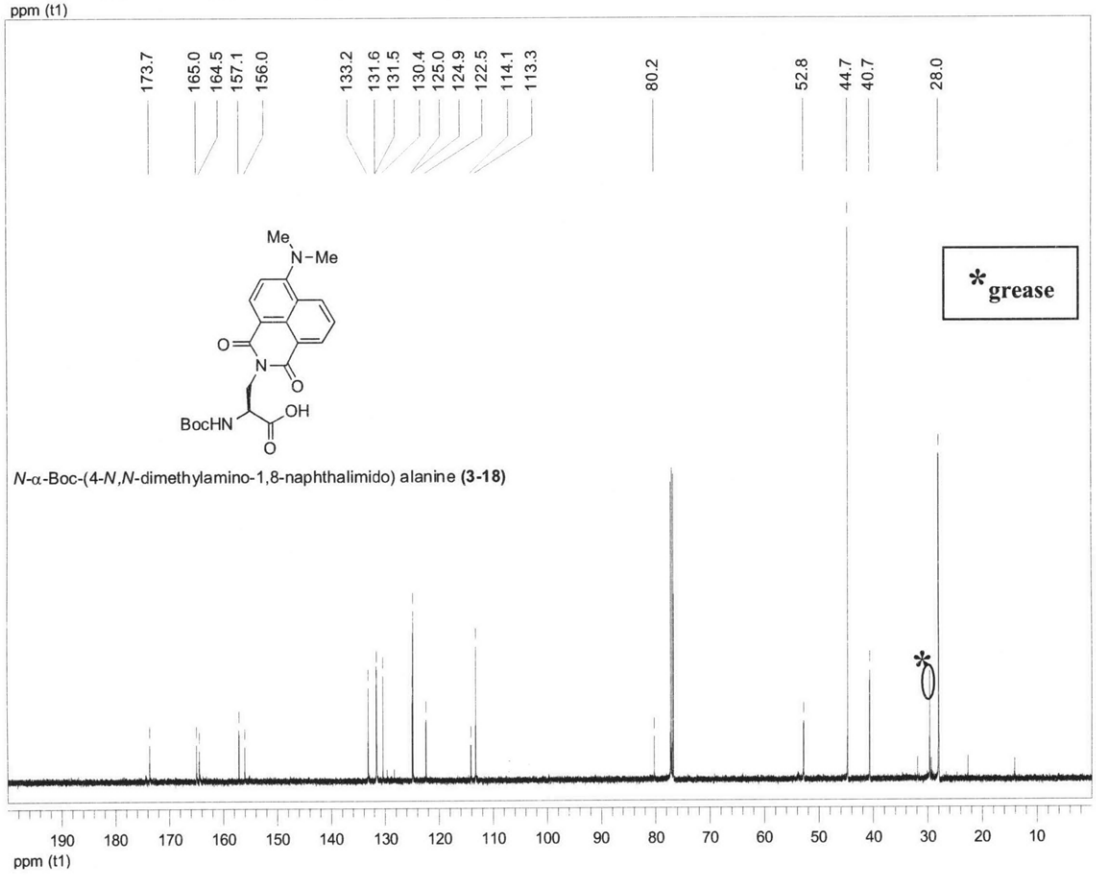

N-α-Boc-(4-*N*,*N*-dimethylamino-1,8-naphthalimido) alanine **(3-18)**

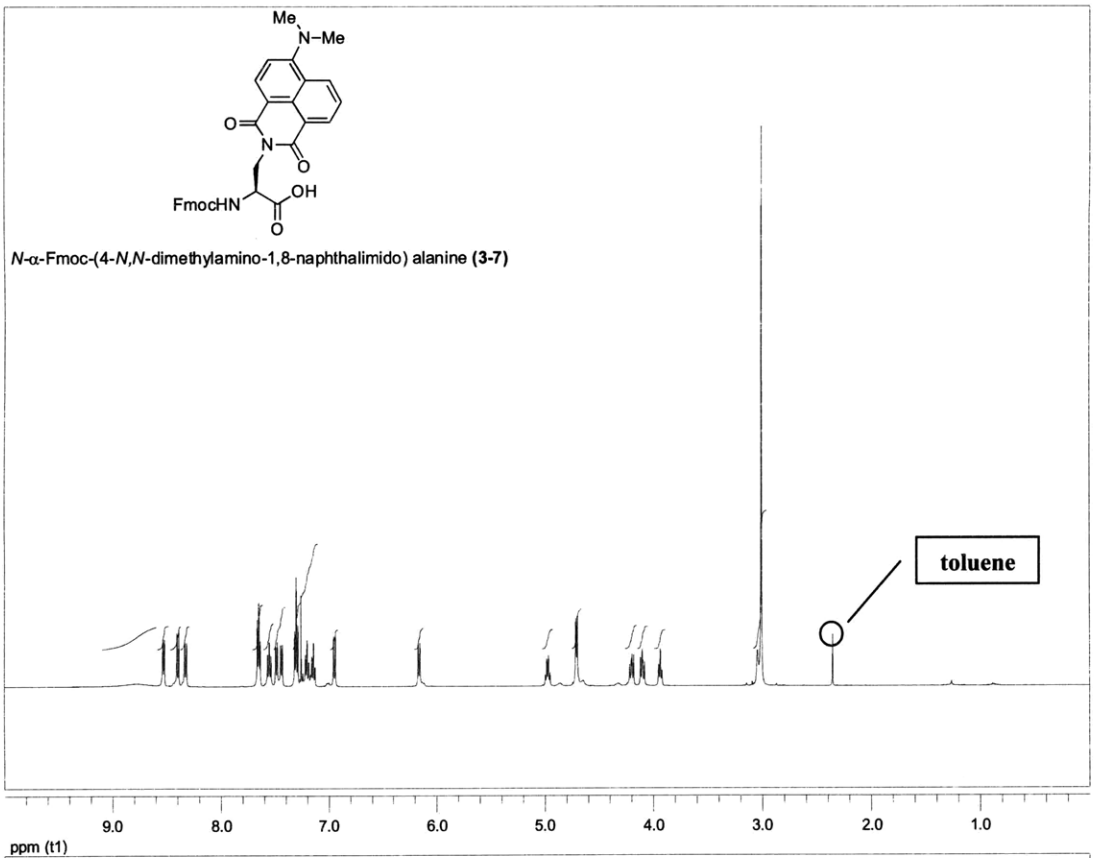

N-α-Fmoc-(4-*N*,*N*-dimethylamino-1,8-naphthalimido) alanine **(3-7)**

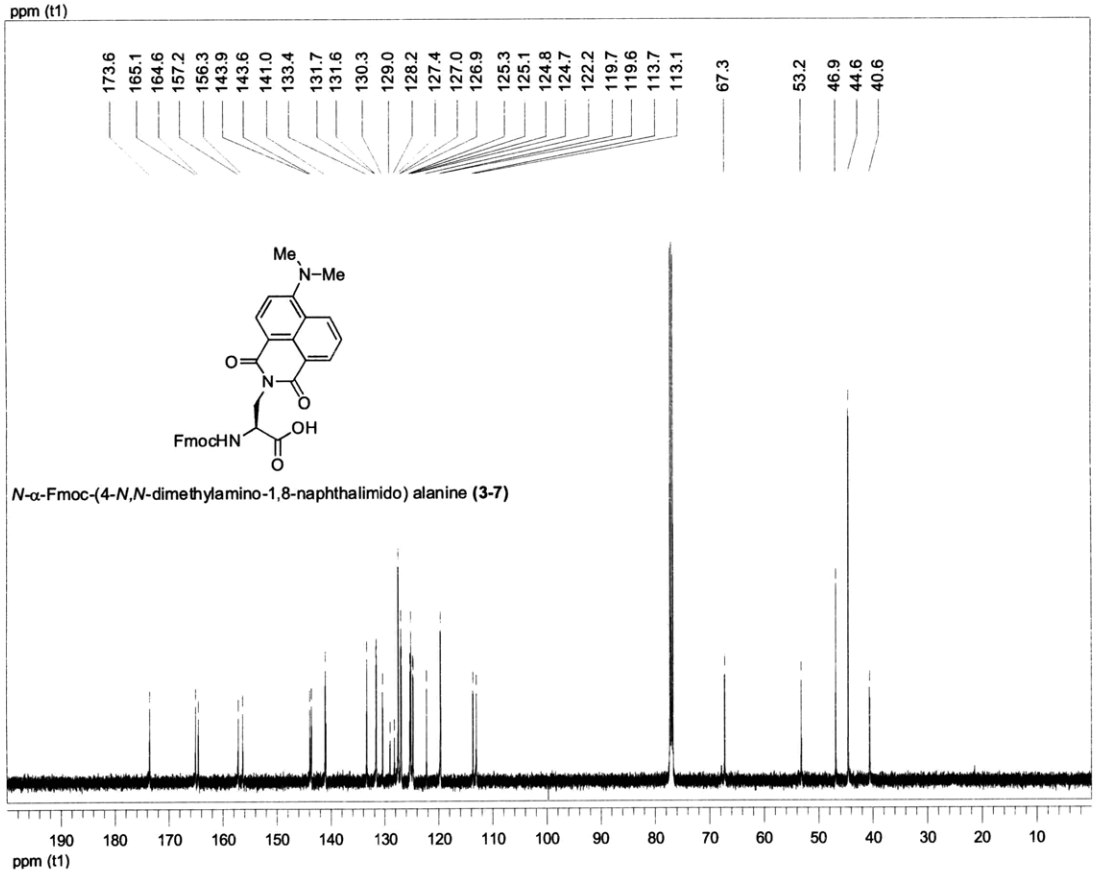

N-α-Fmoc-(4-*N*,*N*-dimethylamino-1,8-naphthalimido) alanine **(3-7)**

Chapter 4: Comparative studies of the dimethylaminophthalimide amino acids with other commercial solvatochromic fluorophores

A significant portion of the work described in this chapter has been published:

Loving, G.; Imperiali, B. A versatile amino acid analogue of the solvatochromic fluorophore 4-*N,N*-dimethylamino-1,8-naphthalimide: A powerful tool for the study of dynamic protein interactions. *J. Am. Chem. Soc.* **2008**, *130*, 13630-13638.

Introduction

Dynamic protein-protein interactions within the cell play a critical and pervasive role in nature. Many signal transduction pathways are mediated through the binding and dissociation of key proteins in a tightly regulated fashion.[1] The dynamics of these interactions are also vital to the controlled assembly and disassembly of many functional ensembles such as the actin filament component of the cytoskeleton[2] or the focal adhesions involved in mammalian cell migration.[3] As such, concentrated efforts to better understand these interactions have led to the development of a wide range of techniques that are now commonplace in the field of protein biochemistry. These techniques span a broad spectrum from purely *in vitro* biophysical methods such as isothermal titration calorimetry[4] and analytical ultracentrifugation[5] to ones more amenable to *in cellulo* studies like yeast two-hybrid assays[6] and photoaffinity labeling.[7] While each of the approaches are indispensible for the unique information that they provide, many of these methods are limited in the ability to yield spatial and temporal information regarding dynamic interactions and are often necessarily destructive to the cell. Consequently, a vast number of questions regarding the temporal and spatial significance of various protein-protein interactions within living cells remain unanswered and require the continual development of new generations of tools if further advances are to be made.

An ideal tool for addressing these questions should be one that can sensitively detect the transient nature of various protein-protein interactions in a reversible manner. By this measure, Förster Resonance Energy Transfer (FRET) has become increasingly more popular in the literature and stands as one of the preferred methods for *in cellulo* studies.[8] An alternative approach is the use of solvatochromic fluorophores, which feature emission properties that exhibit a significant dependence on changes in solvent polarity, solvent relaxation rates,

orientation to electric fields, and rigidity of the local environment.[9] The effects of these environmental factors on the photophysical properties of the fluorophore typically manifest as shifts in the wavelength of maximum emission, changes in the magnitude of the observed fluorescence lifetime or alterations in the quantum yield. In many instances all three properties, which constitute the dynamic range of the fluorophore, are affected simultaneously.

Chart 4-1. Dimethylaminophthalimidoalanine series of solvatochromic amino acids

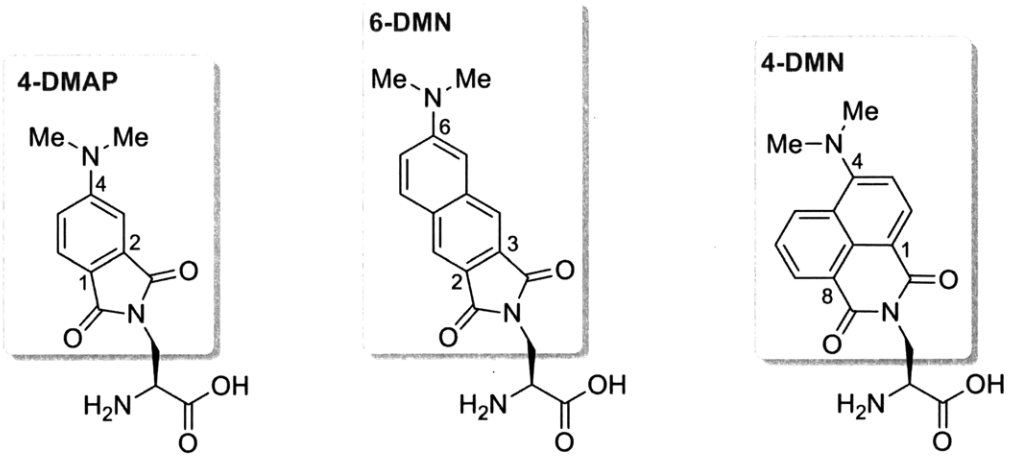

In this chapter, the new solvatochromic amino acid 4-DMNA is introduced as an alternative to the 4-DAPA[10] and 6-DMNA[11] amino acids previously reported by the Imperiali laboratory. The experiments described herein demonstrate the potential of 4-DMN to be utilized as a tool for detecting biomolecular interactions. The improved stability (Chapter 2), the ease of synthesis (Chapter 3), and the longer wavelength of excitation of 4-DMNA over that of the amino acids 4-DAPA and 6-DMNA will greatly expand the range of potential applications. A comparative study is provided that evaluates the photophysical properties of 4-DMN relative to

those of 6-DMN and 4-DMAP as well as other frequently used solvatochromic fluorophores that are commercially available: BADAN, dansyl, and NBD.[12]

Results and Discussion

4-1. Comparison of the solvatochromic properties of the N,N-dimethylaminophthalimide series with BADAN, dansyl, and NBD

Since their discovery, reactive derivatives of solvatochromic fluorophores including dansyl chloride (5-(dimethylamino)-naphthalene-1-sulfonyl chloride),[13,14] BADAN (6-bromoacetyl-2-dimethylaminonaphthalene),[15-17] and NBD fluoride (4-fluoro-7-nitrobenzofurazan)[18-20] have been used extensively in the areas of cell biology and protein biochemistry. All three fluorophores exhibit hypsochromic shifts (blue-shifts) in the emission spectra upon changing from a polar to nonpolar environment. Additionally, these display greater fluorescence quantum yields in hydrophobic solvents than in aqueous buffers. The same trends also apply to the dimethylaminophthalimide series of fluorophores, although these probes have the notable advantage of possessing much larger differences in fluorescence quantum yields in response to the solvent environment.

To evaluate the properties of 4-DMN, we incorporated the 4-DMNA amino acid into a test peptide via SPPS. The test peptide consists of a six-residue sequence rich in lysine and arginine residues, dubbed the KR peptide motif in reference to the single-letter notation for amino acids. This peptide motif was selected specifically to ensure complete solubility of the fluorophores in both solvent systems for accurate fluorescence measurements. While the highly charged peptides are naturally soluble in aqueous buffers such as TBS (pH 7.4), the peptides can easily be dissolved in dioxane in the presence of 18-crown-6, which forms very strong

complexes with protonated primary amines such as those of the lysine residues and N-terminus. We also prepared the same peptide with amino acid derivatives of 4-DMAP, 6-DMN, BADAN, dansyl and NBD. Each member of the KR peptide series contained one of the six fluorophores located at the fourth position within the six-residue sequence (Chart 4-2). The peptides were studied in different solvent systems (dioxane and water) to encompass two extremes of the solvent-polarity spectrum (see Experimental section for details).

Chart 4-2: The KR Peptide Series of Solvatochromic Fluorophores

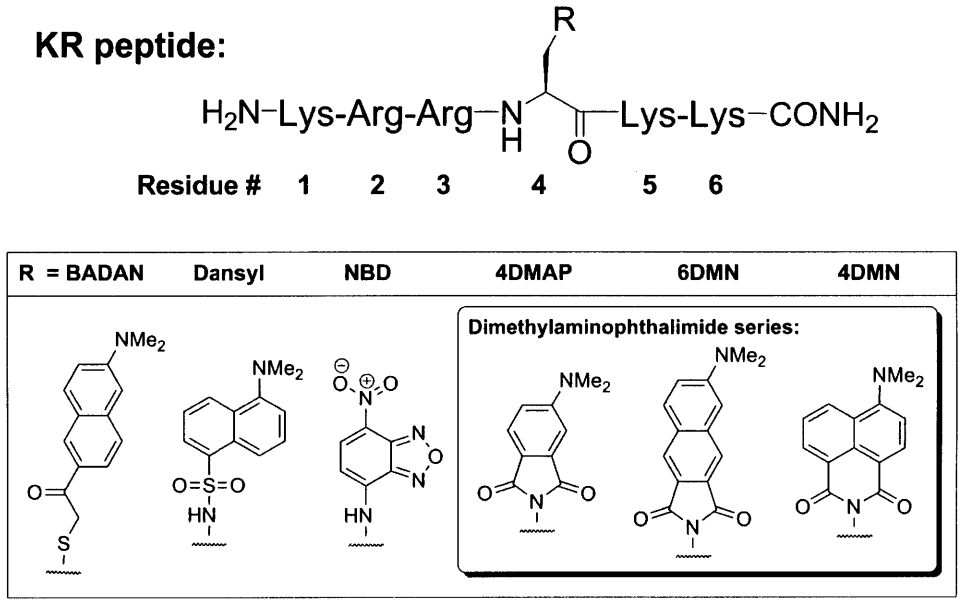

The most striking trend to emerge from this study was the substantial difference in fluorescence intensities exhibited by the dimethylaminophthalimide series between the two solvent systems. In each case, the ratio of the fluorescence intensity was greater than 1000-fold at the wavelength of maximum emission in dioxane (Table 4-1). This was significantly greater than that observed for dansyl and NBD. The magnitude of this ratio is attributed primarily to the

extremely low fluorescence quantum yields of the dimethylaminophthalimides in polar protic solvents creating the appearance of virtually no fluorescence in TBS buffer as plotted in the graphs of Figure 4-1. BADAN, a derivative of PRODAN[21] that has long been considered state-of-the-art for applications in biological studies, also displayed a significant fluorescent response between water and dioxane despite its large quantum yield of fluorescence in water (Φ_{water} = 0.18).[22] However, even with this excellent performance under these idealized conditions, such absolute changes are rarely achieved in actual biological applications. This experiment merely demonstrates the potential dynamic range of each fluorophore under optimal conditions. In protein studies, where the conditions are typically far from optimal, even the smallest degree of background fluorescence can strongly limit the magnitude of the observed fluorescence change.

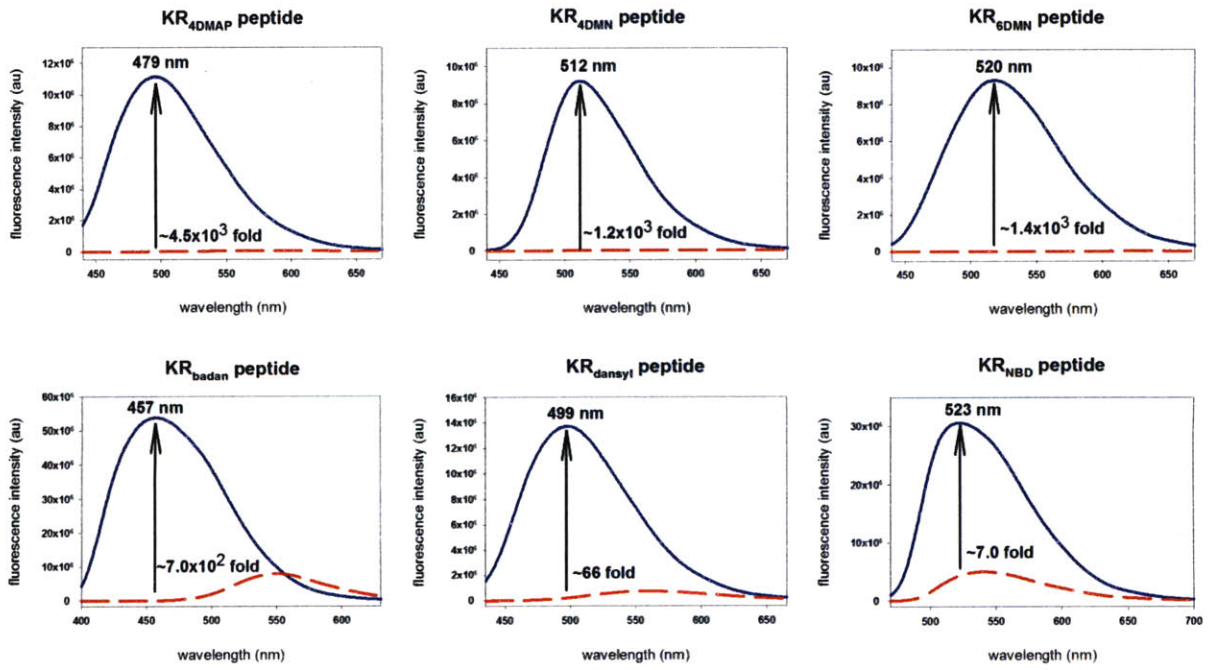

Figure 4-1. Fluorescence spectra of the KR peptides (5 μM) measured in TBS buffer at pH 7.4 (– – –) and 1,4-dioxane with 5 mM 18-crown-6 (——). Each spectrum is the average of three independent measurements corrected for background. The fold-increase in fluorescence is reported at the wavelength of maximum emission in the 1,4-dioxane solution. All measurements were made at 25 °C.

Table 4-1. Photophysical properties of the fluorescent KR peptide series

Peptide	λ_{abs} (nm)	ε (M^{-1} cm^{-1})	λ_{exc} (nm)	TBS λ_{em} (nm)	dioxane λ_{em} (nm)	$I_{dioxane}/I_{TBS}$ at λ_{em} in dioxane[a]
KR_{4DMAP}	421	6.5×10^3	390	580	497	$4.5 \times 10^3 \pm 1.4 \times 10^3$
KR_{4DMN}	440	8.8×10^3	408	554	512	$1.2 \times 10^3 \pm 0.2 \times 10^3$
KR_{6DMN}	390	8.0×10^3	378	625	520	$1.4 \times 10^3 \pm 0.2 \times 10^3$
KR_{BADAN}	391	2.0×10^4	365	550	457	$7.0 \times 10^2 \pm 0.2 \times 10^2$
KR_{dansyl}	337	5.3×10^3	345	564	499	66 ± 1
KR_{NBD}	465	2.2×10^4	455	543	523	7.0 ± 0.3

[a] This ratio was calculated by integrating the fluorescence intensity in both solvent systems over a 5 nm window centered on the wavelength of maximum emission in dioxane. The area of the measured region in dioxane was then divided by that measured in TBS buffer. The listed errors represent the 90% confidence interval from three trials.

4-2. Preparation of M13 peptide mutants and binding studies with calmodulin

To examine the behavior of these fluorophores in a more biologically relevant context, another peptide series was prepared (Table 4-2). This series of peptides was derived from the previously reported M13 peptide,[23] which contains the calmodulin binding domain of skeletal muscle myosin light chain kinase (skMLCK). Calmodulin (CaM) binds the M13 peptide in a calcium-dependent manner with a reported K_d on the order of 10^{-9} to 10^{-10} M.[24] The structural details of this interaction have been extremely well characterized and shown to include many hydrophobic contacts as the protein literally wraps around the peptide binding partner (Figure 4-2).[24] Hence, the calcium-dependent CaM-M13 interaction has served as a model system for evaluating many new methods for detecting protein-protein interactions.[25-28]

Table 4-2. The mutant M13 peptide series containing the solvatochromic fluorophores

	Residue #:[a]																		
M13 mutant:	N-term	2	3	4[c]	5	6	7	8[b]	9	10	11	12	13	14	15	16	17[c]	18	19	C-term
$M13_{4DMAP}$	H_2N-	R	R	**W**	K	K	N	**Dap(4DMAP)**	I	A	V	S	A	A	N	R	**F**	K	K	-$CONH_2$
$M13_{4DMN}$	H_2N-	R	R	**W**	K	K	N	**Dap(4DMN)**	I	A	V	S	A	A	N	R	**F**	K	K	-$CONH_2$
$M13_{6DMN}$	H_2N-	R	R	**W**	K	K	N	**Dap(6DMN)**	I	A	V	S	A	A	N	R	**F**	K	K	-$CONH_2$
$M13_{Dansyl}$	H_2N-	R	R	**W**	K	K	N	**Dap(dansyl)**	I	A	V	S	A	A	N	R	**F**	K	K	-$CONH_2$
$M13_{NBD}$	H_2N-	R	R	**W**	K	K	N	**Dap(NBD)**	I	A	V	S	A	A	N	R	**F**	K	K	-$CONH_2$
$M13_{BADAN}$	H_2N-	R	R	**W**	K	K	N	**Cys(BADAN)**	I	A	V	S	A	A	N	R	**F**	K	K	-$CONH_2$

[a] The residue numbering refers to the original M13 fragment reported by Blumenthal et al.[23]

[b] The fluorophore, indicated in parentheses, is appended to the 3-amino group of Dap or, in the case of the $M13_{BADAN}$ mutant, the side-chain of the cysteine residue. The wild-type M13 peptide contains a phenylalanine residue at this position.

[c] Trp 4 and Phe 17 (bold face) are the key residues that bind in the hydrophobic pockets of the C- and N-terminal domain, respectively, forming important contacts that may establish the orientation of the α-helical peptide in the complex.[29]

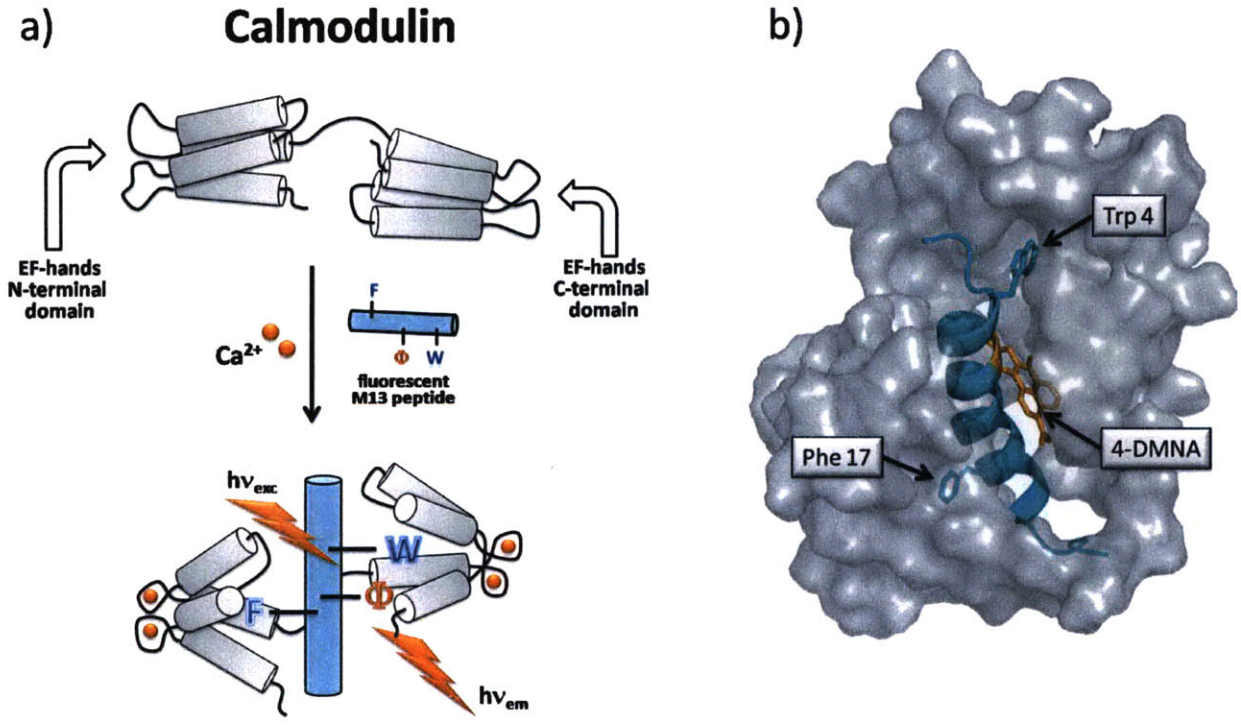

Figure 4-2. (a) A graphical depiction of the Ca^{2+} activation and binding of CaM (grey) to an M13 peptide mutant (cyan) that contains a residue with an environment sensitive fluorophore as the side-chain (Φ). Upon complex formation, the fluorophore exhibits a measurable change in fluorescence. The Trp 4 and Phe 17 residues are indicated in this panel using the single-letter notation for amino acids. (b) NMR structure of the Ca^{2+}-CaM-M13 peptide complex deposited by Ikura et al. in the Brookhaven Protein Data Bank (2BBM).[24] The structure indicates

the solvent exposed surface of CaM (grey) surrounding the M13 peptide (cyan). Superimposed over the side-chain of residue Phe 8 is 4-DMN (gold) as it might be oriented in the $M13_{4DMN}$ peptide mutant.[30]

Based on the structural information available for the Ca^{2+}-CaM-M13 complex, the phenylalanine residue located at position 8 of the wild-type M13 sequence was selected as the site for introducing the fluorescent probes. This residue is known to make a number of hydrophobic contacts with Ca^{2+}-CaM. Furthermore, reports of other peptide sequences that bind CaM through a mode similar to that of the M13 peptide have shown that CaM is tolerant of most hydrophobic residues at this position.[29] The mutant M13 peptides of Table 2 represent abridged versions of the original 27-residue M13 peptide reported by Blumenthal et al.[23] The peptides of this study consist only of the span of residues required for binding. The CaM construct used in this investigation contained a C-terminal hexahistidine tag used for purification and as an epitope for Western Blot analysis. The fluorescence spectra for the mutant M13 peptides were recorded in the presence of saturating CaM, $CaCl_2$, and CaM with $CaCl_2$ (see Experimental section for details). These results were then compared to the spectra of the peptides alone (Figure 4-3).

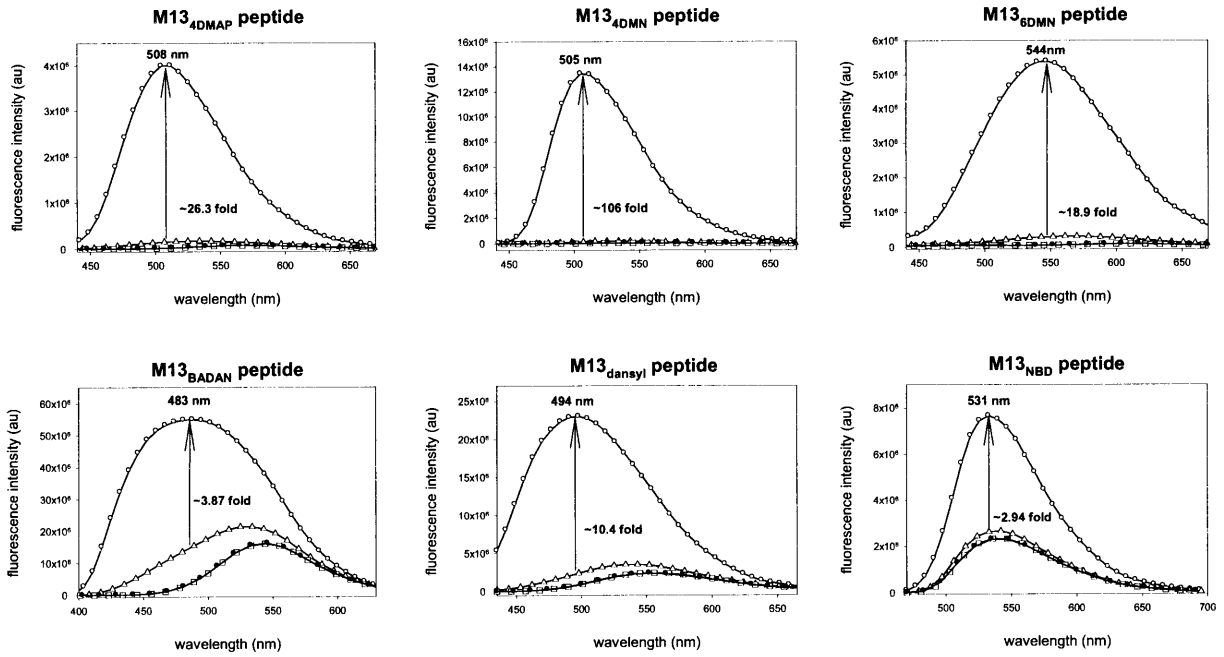

Figure 4-3. Fluorescence spectra of the M13 mutant peptide series measured in TBS buffer at pH 7.4, 25 °C with EDTA (40 μM). Four separate conditions were examined for each member of the series shown above: ●, M13 peptide (10 μM); △, M13 peptide (10 μM) + CaM (15 μM); ○, M13 peptide (10 μM) + CaM (15 μM) + Ca^{2+} (200 μM); □, M13 peptide (10 μM) + Ca^{2+} (200 μM). Each spectrum represents the average of three independent measurements corrected for background. The fold-increase in fluorescence indicated by the arrows represents the fluorescence ratio between conditions '○' and '△' at the wavelength of maximum emission (λ_{em}) in condition '○'.

Table 4-3. Observed Fluorescence Changes for M13 Mutants in the Presence of CaM and Ca^{2+}-CaM

Peptide	λ_{exc} (nm)	Free M13 peptide λ_{em} (nm)[a]	Ca^{2+}-CaM-M13 complex λ_{em} (nm)[b]	$I_{(○)}/I_{(△)}$ at λ_{em}[c]	$I_{(○)}/I_{(●)}$ at λ_{em}[c]
$M13_{4DMAP}$	390	567	508	26.3 ± 7.4	183 ± 3
$M13_{4DMN}$	408	550	505	106 ± 7	963 ± 100
$M13_{6DMN}$	378	608	544	18.9 ± 1.2	119 ± 4
$M13_{BADAN}$	365	542	483	3.87 ± 0.05	17.9 ± 0.7
$M13_{dansyl}$	345	553	494	10.4 ± 0.1	33.3 ± 2.3
$M13_{NBD}$	455	541	531	2.94 ± 0.14	3.41 ± 0.20

[a] Measurements made in TBS buffer (pH 7.4. 25 °C) with the M13 peptide concentration at 10 μM.

[b] Measurements made in TBS buffer (pH 7.4, 25 °C) with M13 peptide (10 μM), CaM (15 μM) and $CaCl_2$ (200 μM).

[c] The measured fluorescence intensity ratios are indicated by the subscripted symbols: ●, M13 peptide alone; △, M13 peptide + CaM; and ○, M13 peptide + CaM + Ca^{2+}. The listed errors represent the 90% confidence interval from an average of three trials.

In contrast to the previous study that examined the fluorescent properties of the fluorophores in dioxane versus water, the measured spectra in this experiment reflect a complex array of variables extending well beyond solvent polarity. Here, the fluorophores are sequestered within a highly restricted microenvironment upon binding of the M13 peptide mutants to calcium-activated CaM. Such microenvironments lack the homogeneity of a fluid medium of uniform dielectric constant. The packing of each fluorophore within the binding interface is strongly influenced by its size, shape and hydrophobicity. A deeply buried solvatochromic fluorophore, stripped of a surrounding solvation sphere, will no longer experience the effects of solvent relaxation, which reduces the energy gap between the ground and excited electronic states.[9] The rigidity of the microenvironment can also impact the observed fluorescence quantum yields by restricting certain vibrational modes within the fluorophore excited state that may lead to the ground state through nonradiative decay processes.[9] Bearing in mind that each fluorophore can respond differently to a particular microenvironment and that the nature of such microenvironments can vary widely depending on the protein interaction of interest, the results of this type of comparative study are relative and some caution should be exercised when making generalizations. Nevertheless, basic trends do emerge providing guidelines for gauging the efficacy of these tools in future applications.

With the exception of the $M13_{4DMN}$ peptide, all members of this series showed a significantly smaller hypsochromic shift in their emission maxima between the bound and unbound states (Table 4-3) compared to that observed in water versus dioxane (Table 4-1) with the corresponding KR peptides. This observation is fairly typical of environment-sensitive fluorophores since changes in the local solvent environment are often more subtle in studies of this type. Despite this fact, the dimethylaminophthalimide series still exhibited the greatest

overall changes in fluorescence intensity. Furthermore, the $M13_{4DMN}$ peptide produced the most dramatic results, yielding a greater than 900-fold increase in fluorescence intensity in the presence of saturating CaM and Ca^{2+} compared to that of the peptide alone. The magnitude of this change, which was approximately 5-8 times greater than that of 4-DMAP and 6-DMN, may be due to the more effective sequestering of the fluorophore within the peptide-protein complex.

All of the M13 peptide mutants exhibited small increases in fluorescence intensities in the presence of CaM alone, with the largest change being observed for the $M13_{4DMN}$ peptide (~9-fold). Initially, this was thought to be the result of some contaminating calcium that was activating a fraction of the total calmodulin toward binding of the fluorescent peptides. However, control experiments that were performed, using chelating agents like EDTA to sequester free calcium, showed this was not the cause of the observed increases. Rather, it was concluded that the increases in fluorescent signal were due to the weak association constant that exists for the CaM-M13 complex in the absence of calcium. It has previously been reported that the K_d of the CaM-M13 complex is approximately two-million-fold higher than that of the Ca^{2+}-CaM-M13 complex.[31] Based on our determination of the K_d of the Ca^{2+}-CaM-$M13_{4DMN}$ complex shown later in Figure 4-4, we estimated that the calcium-independent K_d is on the order of 150-200 μM. This would imply that roughly 7% of the mutant M13 peptide is bound by CaM under these experimental concentrations. Consequently, two different ratios are reported in Table 3: the fluorescence increase upon the addition of calcium when CaM was already present ($I_{(○)}/I_{(△)}$); and the overall fluorescence increase observed when comparing the Ca^{2+}-CaM-M13 complex to that of the M13 mutant alone ($I_{(○)}/I_{(●)}$).

The results of Figure 4-3 exemplify the importance of having low-background fluorescence for the unbound probe. If the measured hypsochromic shift is small, such that the

emission spectrum of the Ca^{2+}-CaM-M13 complex partially or fully overlaps with that of the lone peptide, then a large quantum yield of fluorescence in water may drastically limit the magnitude of the measured fluorescence increase. Since the dimethylaminophthalimide series exhibits very little fluorescence in aqueous environments, even a modest shift in the emission wavelength will typically be accompanied by a significant change in fluorescence intensity. Hence, these probes closely mimic switch-like or "on-off" emission properties making them excellent tools for cell microscopy by eliminating the need for extensive washing to remove unbound probe in order to reduce background signal.[32] Furthermore, these probes may readily be adapted for ratiometric measurements by introducing a secondary non-solvatochromic fluorophore of a different emission wavelength to afford more quantitative information within the highly compartmentalized environment of living cells.

4-3. Titration of the $M13_{4DMN}$ Peptide with Calcium Activated CaM

One caveat of incorporating unnatural structural elements into proteins is the potential to disrupt a native binding interaction. A titration of the $M13_{4DMN}$ peptide with Ca^{2+}-CaM was performed to demonstrate that that the presence of the unnatural amino acid, **3**, has a negligible impact on the affinity of the complex (Figure 4-4). The K_d for the wild-type M13 peptide has previously been reported by several groups using various techniques that place the value within the low nanomolar to high picomolar range.[23,33,34] In this study, the K_d for the Ca^{2+}-CaM-$M13_{4DMN}$ complex was determined to be 86 ± 25 pM, indicating an extremely tight interaction (see Experimental section for details). Therefore, it was concluded that the presence of 4-DMNA at position 8 in the M13 peptide sequence does not significantly impact the protein-peptide interaction.

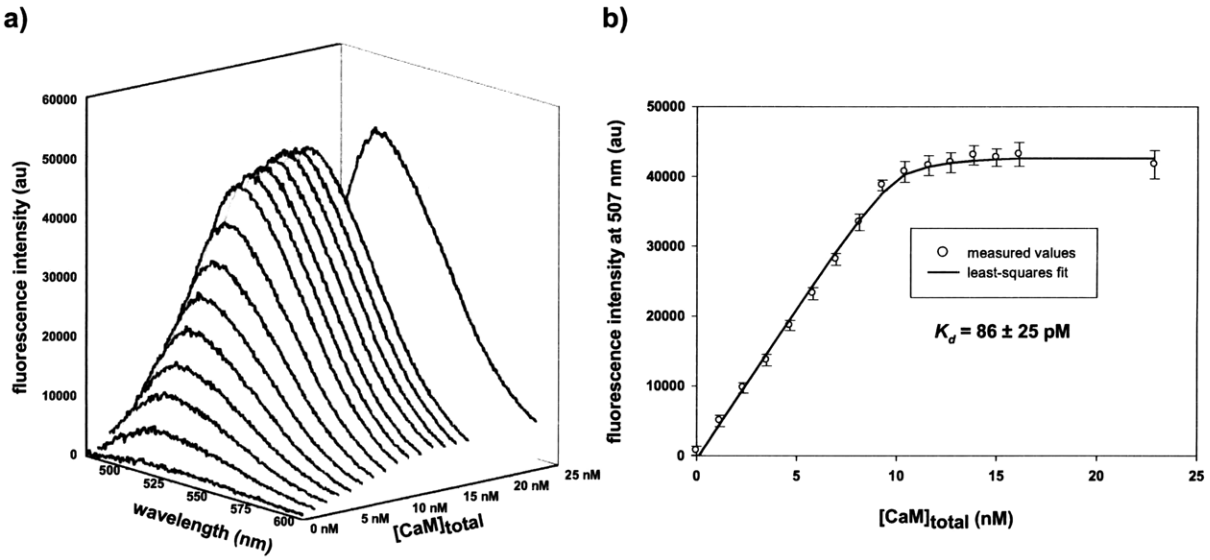

Figure 4-4. (a) Fluorescence spectra collected from 475 nm to 600 nm as the $M13_{4DMN}$ peptide (10 nM) was titrated with CaM in the presence of 200 μM $CaCl_2$. The fluorophore was excited at 408 nm. Each spectrum represents the average of nine measurements after background correction. (b) The titration curve of the $M13_{4DMN}$ peptide measured at 507 nm. The error bars shown for the measured values represent the 95% confidence interval based on the average of nine trials. The solid line indicates the least-squares fit to the measured data. The interval shown for the K_d of the complex was also calculated at the 95% confidence level.

Conclusions

While there are a number of known solvatochromic fluorophores that have been developed into amino acids,[17,35-39] it is rare for a single species to meet all of the criteria for obtaining optimal results in protein studies. Tradeoffs often exist between variables such as good extinction coefficients, suitable wavelengths of excitation and emission, thermal and photochemical stability, size, and many others. The 4-DMNA amino acid is unique in that this species appears to demonstrate very few compromises by combining many of the key elements required of a good fluorescent tool. It can be excited in the visible spectrum (400-450 nm), thus minimizing the damaging effects of high-energy UV light; the Fmoc building block, **3-7**, can be prepared in few synthetic steps and offers facile incorporation into peptides; the fluorescent side-

chain is significantly more stable than those of 4-DAPA and 6-DMNA; and it possesses the same switch-like fluorescent properties that are characteristic of the dimethylaminophthalimide series. Like 4-DAPA and 6-DMNA, the comparative size of 4-DMNA to the natural aromatic amino acid tryptophan allows it to be incorporated into peptides or proteins without significantly altering the native surface topology. This is critical in developing new fluorescent probes like the $M13_{4DMN}$ peptide, which we have shown to have a binding affinity for Ca^{2+}-CaM similar to that reported for the wild-type system. The combination of these properties into this single amino acid opens the window to many potential future applications as we aim to incorporate this tool into full-length proteins for *in cellulo* studies.

Experimental

PBS and TBS buffers:

Phosphate-buffered saline. All references to solutions prepared in PBS buffer pertain to the following recipe.

10 × PBS Buffer:

80.0 g NaCl
2.0 g KCl
14.4 g Na_2HPO_4
2.4 g KH_2PO_4

Dissolved the measured salts in 800 mL of distilled H_2O (pH should be approximately 6.8). Adjust to final volume of 1 L. Upon diluting the 10× PBS buffer ten-fold with distilled H_2O, the pH should be 7.4. The final 1× PBS concentrations should be 137 mM NaCl, 10 mM phosphate, and 2.7 mM KCl.

Tris-buffered saline. All references to solutions prepared in TBS buffer pertain to the following recipe.

10× TBS Buffer:

60.6 g Tris-HCl
87.7 g NaCl

Dissolve the measured salts in 800 mL of distilled H_2O and adjust the pH to 7.3 with concentrated HCl. Then increase the volume to 1 L. Upon diluting the 10× TBS buffer ten-fold with distilled H_2O, the pH should be 7.4. The final 1× TBS concentrations are 50 mM Tris-HCl, 150 mM NaCl, and pH 7.4.

Synthesis of the KR peptide series:

The KR peptide series was prepared using standard Fmoc-based solid-phase peptide synthesis techniques (SPPS).[40] Each peptide was prepared using 0.21 mmol/g loading Fmoc-PAL-PEG-PS resin (Cat. No. GEN913383, Applied Biosystems) in a Poly-Prep® chromatography column (Cat. No. 731-1550, Bio-Rad). Fmoc-protected amino acids with the standard side-chain protecting groups were used: Fmoc-Arg(Pbf)-OH and Fmoc-Lys(Boc)-OH. A Boc-Lys(Boc)-OH residue was incorporated at the N-terminus of each member of the series in order to yield the free α-amino group following cleavage of the peptides from the solid support. The KR peptides of 4-DMAP, 6-DMN, dansyl, and NBD were all prepared from the parent $KR_{Dap(alloc)}$ peptide while KR_{BADAN} was prepared from the $KR_{Cys(Mmt)}$ peptide. The (S)-2-(Fmoc-amino)-3-(alloc-amino)-propionic acid (Fmoc-Dap(alloc)-OH) and the Fmoc-Cys(Trt)-OH residues were both incorporated at position 4 within the $KR_{Dap(alloc)}$ and $KR_{Cys(Mmt)}$ peptides, respectively. Synthesis of the $KR_{Dap(alloc)}$ peptide was performed on a 105 μmole scale and the $KR_{Cys(Mmt)}$ peptide was prepared on a 21 μmole scale. Amide couplings were executed using 6 equiv of each amino acid with exception to position 4. Here, only 3 equiv of the Fmoc-Dap(alloc)-OH and Fmoc-Cys(Mmt)-OH residues were used. All of the amino acids were dissolved to a final concentration of 50 mM in DMF containing a 1:1 mixture of HOBt/HBTU (50 mM each) with *N,N*-diisopropylethylamine (100 mM, 12 equiv). Each coupling reaction was allowed to proceed at room temperature for 30-45 min. The coupling was monitored by a colormetric assay for detecting free primary amines known as the 2,4,6-trinitrobenzenesulphonic acid (TNBS) test.[41] Removal of the Fmoc group prior to each coupling step was performed using a 20% 4-methylpiperidine solution[42] in DMF (3 × 5 min). Once the syntheses of the $KR_{Dap(alloc)}$ and $KR_{Cys(Mmt)}$ peptides were complete, the Dap and Cys residues were selectively

deprotected in order to append the desired fluorophores. Removal of the Alloc group was performed according to the previously described protocol.[43] The Mmt group was removed using a 1% trifluoroacetic acid (TFA) solution in dichloromethane with 5% triisopropylsilane added as a cation scavenger (4 × 15 min). The side chains of the Dap and Cys residues were then alkylated with the appropriate fluorophores. The KR_{BADAN} peptide was prepared by first dissolving 6-bromoacetyl-2-dimethylaminonaphthalene (BADAN, AnaSpec) (3.3 equiv) in *N*-methylpyrrolidone with 1,8-diazabicyclo[5.4.0]undec-7-ene (DBU) (1 equiv). The solution was then added directly to the resin-bound KR_{Cys} peptide. The coupling reaction was allowed to proceed overnight in the dark at room temperature. The KR_{4DMAP} and KR_{6DMN} peptides were prepared by coupling the anhydride precursors of 4-DMAP and 6-DMN to the side chain of Dap according to the previously described protocol.[43] The KR_{dansyl} and KR_{NBD} peptides were prepared by treating the resin-bound KR_{Dap} peptide with a 50 mM solution of 5-(dimethylamino)-naphthalene-1-sulfonyl chloride (dansyl chloride, 2 equiv) and 4-fluoro-7-nitrobenzofurazan (NBD fluoride, 2 equiv) dissolved in DMF with *N,N*-diisopropylethylamine (2 equiv). The reactions were allowed to proceed at room temperature overnight in the dark. Preparation of the KR_{4DMN} peptide was unique among the series in that it was prepared using the Fmoc-4DMNA building block (**3-7**) instead of coupling the fluorophore to the fully assembled peptide. The KR peptides were cleaved from the resin using a solution of 96:2:2 TFA/H_2O/EDT for 3 hrs. The cleavage cocktail was then filtered and evaporated. The crude peptides were triturated with cold diethyl ether (3 × 10 mL) and purified by high-performance liquid chromatography (HPLC) using a Waters 600E HPLC with a Waters 600 automated control module and Waters 2487 dual wavelength absorbance detector set at 228 and 280 nm. The separations were performed using a preparative YMC-pack, C_{18}, 20 × 250 mm reverse-phase

column. A YMC-pack, C_{18}, 4.6 ×150 mm reverse-phase column was used for analytical HPLC. The following analytical HPLC method was used to verify purity of the peptides:

Time (min)	Flow Rate (mL/min)	% H_2O (with 0.1% TFA)	% acetonitrile (with 0.1% TFA)	Gradient
initial	1.00	95	5	linear
5	1.00	95	5	linear
40	1.00	55	45	linear

Table 4-4. Characterization of purified KR peptide series

KR peptides	Peptide Sequence								HPLC Ret. Time (min)	$[M+xH]^{x+}$ Calc.	$[M+xH]^{x+}$ found
	N-term	1	2	3	4	5	6	C-term			
KR_{4DMAP}	H_2N-	K	R	R	**Dap(4DMAP)**	K	K	-$CONH_2$	21.2	974.0 (1+)	973.7 (1+)
KR_{4DMN}	H_2N-	K	R	R	**Dap(4DMN)**	K	K	-$CONH_2$	23.4	1024.1 (1+)	1023.6 (1+)
KR_{6DMN}	H_2N-	K	R	R	**Dap(6DMN)**	K	K	-$CONH_2$	24.0	1024.1 (1+)	1023.7 (1+)
KR_{BADAN}	H_2N-	K	R	R	**Cys(BADAN)**	K	K	-$CONH_2$	26.9	1029.1 (1+)	1029.7 (1+)
KR_{Dansyl}	H_2N-	K	R	R	**Dap(dansyl)**	K	K	-$CONH_2$	20.2	1034.0 (1+)	1034.2 (1+)
KR_{NBD}	H_2N-	K	R	R	**Dap(NBD)**	K	K	-$CONH_2$	16.1	482.5 (2+) 322.0 (3+)	482.4 (2+)[α] 321.9 (3+)[α]

[α] Peptide mass determined by ESI-MS on a Mariner electrospray mass spectrometer (PerSeptive Biosystems). All other KR peptides in this series were confirmed by MALDI mass spectroscopy on a PerSeptive Biosystems Voyager MALDI-TOF instrument using a 2,5-dihydroxybenzoic acid matrix.

Synthesis of the M13 mutant peptide series:

The M13 mutant peptide series was prepared using standard Fmoc-based solid-phase peptide synthesis techniques (SPPS).[40] The peptides were prepared using 0.17 mmol/g loading Fmoc-NovaPEG Rink Amide resin LL (Cat. No. 01-64-0483, Novabiochem®). Fmoc-protected amino acids with the standard side-chain protecting groups were used: Fmoc-Ala-OH, Fmoc-Phe-OH, Fmoc-Ile-OH, Fmoc-Lys(Boc)-OH, Fmoc-Asn(Trt)-OH, Fmoc-Arg(Pbf)-OH, Fmoc-

Ser(tBu)-OH, Fmoc-Val-OH, and Fmoc-Trp(Boc)-OH. The M13 peptide mutants containing 4-DMAP, 6-DMN, Dansyl, and NBD were all prepared from the parent $M13_{Dap(alloc)}$ peptide while $M13_{BADAN}$ was prepared from the $M13_{Cys(Mmt)}$ peptide. Synthesis of all the peptides of this series began by coupling the first seven residues (positions 13-19) with an ABI 431A peptide synthesizer (Applied Biosystems). The synthesis was performed on the 40 μmol scale using 4 equiv of the Fmoc amino acids in each cycle. It had previously been discovered from earlier attempts at making these peptides that the coupling efficiency was extremely low for residues incorporated after the alanine at position 10 in the M13 sequence. This problem was overcome by using a pseudoproline dipeptide, Fmoc-Val-Ser($\Psi^{Me,Me}$pro)-OH (Cat. No. 05-20-1001, Novabiochem), at positions 11-12 in place of Fmoc-Val-OH and Fmoc-Ser(tBu)-OH. The remaining residues were all coupled manually using 6 equiv of the Fmoc amino acids. All of the building blocks were dissolved to a final concentration of 50 mM in DMF containing a 1:1 mixture of HOBt/HBTU (50 mM each) with *N,N*-diisopropylethylamine (100 mM, 12 equiv). Each coupling reaction was allowed to proceed at room temperature for 30-45 min. The coupling efficiency was monitored using the TNBS test.[41] Removal of the Fmoc group prior to each coupling step was performed using a 20% 4-methylpiperidine solution[42] in DMF (3 × 5 min). After the incorporation of Fmoc-Ile-OH at position 9, the resin was split into three aliquots. The Fmoc-Dap(alloc)-OH, Fmoc-Cys(Mmt)-OH, and Fmoc-4DMNA building blocks were then coupled at position 8. A Boc-Arg(Pbf)-OH residue was incorporated at the N-terminus of the $M13_{Dap(alloc)}$, $M13_{Cys(Mmt)}$, and $M13_{4DMN}$ peptides in order to yield the free α-amino group following cleavage from the solid support. Once the syntheses of the $M13_{Dap(alloc)}$ and $M13_{Cys(Mmt)}$ peptides were complete, the Dap and Cys residues were selectively deprotected in order to append the desired fluorophores. Removal of the Alloc group was performed

according to the previously described protocol.[43] The Mmt group was removed using a 1% TFA solution in dichloromethane with 5% triisopropylsilane added as a cation scavenger (4 × 15 min). The side chains of the Dap and Cys residues were then modified with the appropriate fluorophores. The $M13_{BADAN}$ peptide was prepared by first dissolving BADAN (3.3 equiv) in *N*-methylpyrrolidone with 1,8-DBU (1 equiv). The solution was then added directly to the resin-bound $M13_{Cys}$ peptide. The coupling reaction was allowed to proceed overnight in the dark at room temperature. The $M13_{4DMAP}$ and $M13_{6DMN}$ peptides were prepared by coupling the anhydride precursors of 4-DMAP and 6-DMN to the side chain of Dap according to the previously described protocol.[43] The $M13_{dansyl}$ and $M13_{NBD}$ peptides were prepared by treating the $M13_{Dap}$ peptide with a 50 mM solution of dansyl chloride (2 equiv) and NBD fluoride (2 equiv) dissolved in DMF with *N,N*-diisopropylethylamine (2 equiv). The reactions were allowed to proceed at room temperature overnight in the dark. Preparation of the $M13_{4DMN}$ peptide was unique among the series in that it was prepared using the Fmoc-4DMNA building block (**3-7**) instead of coupling the fluorophore to the fully constructed peptide. The M13 mutant peptides were cleaved from the resin using a solution of 96:2:2 TFA/H_2O/EDT for 3 hrs. The cleavage cocktail was then filtered and evaporated. The crude peptides were triturated with cold diethyl ether (3 × 10 mL) and purified by HPLC using a Waters 600E HPLC with a Waters 600 automated control module and Waters 2487 dual wavelength absorbance detector set at 228 and 280 nm. The separations were performed using a preparative YMC-pack, C_{18}, 20 × 250 mm reverse-phase column. A YMC-pack, C_{18}, 4.6 ×150 mm reverse-phase column was used for analytical HPLC. The following analytical HPLC method was used to characterize the peptides:

Time (min)	Flow Rate (mL/min)	% H_2O (with 0.1% TFA)	% acetonitrile (with 0.1% TFA)	Gradient
initial	1.00	95	5	linear
5	1.00	95	5	linear
40	1.00	55	45	linear

Table 4-5. Characterization of purified M13 mutant peptide series

M13 peptide mutants	Peptide Sequence																				HPLC Ret. Time (min)	$[M+xH]^{x+}$ Calc.	$[M+xH]^{x+}$ found
	N-term	2	3	4	5	6	7	8	9	10	11	12	13	14	15	16	17	18	19	C-term			
$M13_{4DMAP}$	H_2N-	R	R	W	K	K	N	Dap(4DMAP)	I	A	V	S	A	A	N	R	F	K	K	-$CONH_2$	34.8	2332.6 (1+)	2332.2 (1+)
$M13_{4DMN}$	H_2N-	R	R	W	K	K	N	Dap(4DMN)	I	A	V	S	A	A	N	R	F	K	K	-$CONH_2$	36.0	2382.6 (1+)	2383.1 (1+)
$M13_{6DMN}$	H_2N-	R	R	W	K	K	N	Dap(6DMN)	I	A	V	S	A	A	N	R	F	K	K	-$CONH_2$	37.0	2382.6 (1+)	2382.3 (1+)
$M13_{BADAN}$	H_2N-	R	R	W	K	K	N	Cys(BADAN)	I	A	V	S	A	A	N	R	F	K	K	-$CONH_2$	33.0	2387.6 (1+)	2388.6 (1+)
$M13_{Dansyl}$	H_2N-	R	R	W	K	K	N	Dap(dansyl)	I	A	V	S	A	A	N	R	F	K	K	-$CONH_2$	38.1	2392.6 (1+)	2393.6 (1+)
$M13_{NBD}$	H_2N-	R	R	W	K	K	N	Dap(NBD)	I	A	V	S	A	A	N	R	F	K	K	-$CONH_2$	34.0	774.9 (3+)	774.4 (3+)[α]
																						581.4 (4+)	581.1 (4+)[α]
																						465.3 (5+)	465.1 (5+)[α]

[α] Peptide mass determined by ESI-MS on a Mariner electrospray mass spectrometer (PerSeptive Biosystems). All other M13 peptide mutants in this series were confirmed by MALDI mass spectroscopy on a PerSeptive Biosystems Voyager MALDI-TOF instrument using a 2,5-dihydroxybenzoic acid matrix.

Expression and purification of CaM-His_6:

The CaM-His_6 construct was transformed in BL21-Gold(DE3) competent cells from which a 20% glycerol stock was prepared for subsequent protein expression. The stock was used to inoculate a 5 mL LB-broth starter culture containing carbenicillin (50 μg/mL). The starter culture was allowed to grow overnight in a 37 °C shaker at 225 rpm. The next day, the starter culture was used to inoculate a 1 L LB-broth culture containing carbenicillin (50 μg/mL) and grown at 37 °C with agitation at 225 rpm. The culture was allowed to grow to an $OD_{600nm} \approx$ 0.5 after which the 1 L shaker flask was transferred to a 25 °C shaker (225 rpm) for induction. The cells were induced with 0.1 mM IPTG and shaken for 4 hrs before harvesting at 5000 × g (4

°C). The pellet was then resuspended in 0.9% NaCl aqueous solution (30 mL) and transferred to a 50 mL conical tube and repelleted for storage at -80 °C.

On the day of the protein preparation, the pellet was thawed at room temperature and resuspended in the following lysis buffer:

4 mL	10× PBS buffer
400 µL	NP-40 Alternative
4 mL	glycerol
40 mg	lysozyme
6 mg	dithiothreitol
40 µL	Protease Cocktail III (Calbiochem)
40 mL	final vol. after diluting with dH_2O

Once the pellet was fully resuspended, the cells were sonicated using a Branson Sonifier 450 at 50% power with a 30% duty cycle for 2 min at 4 °C. The lysate was then transferred to 45 mL polycarbonate bottle and spun at 100,000 × g in a Type 28 rotor from Beckman Coulter to pellet DNA and other cellular debris. Meanwhile, a 5 mL bed of Ni-NTA agarose resin obtained from Qiagen was pre-equilibrated in PBS buffer. After the spin, the clarified supernatant was transferred to a clean 50 mL conical tube where it received the pre-equilibrated Ni-NTA agarose resin and was tumbled gently on a rotisserie at 4 °C for 1 hr. The resin was then recovered by passing the lysate through 20 mL spin column obtained from Bio-Rad. The resin was washed first with 4 mL of PBS buffer, then 4 mL of 10 mM imidazole in PBS buffer and then with 4 mL of 20 mM imidazole in PBS buffer at 4 °C. The protein was then eluted in 6 × 1.5 mL fractions of 250 mM imidazole in PBS buffer at 4 °C. The fractions were assayed for protein and combined appropriately. The imidazole was removed by dialysis using a 3.5 kDa MWCO Slide-A-Lyzer dialysis cassette from Pierce. The protein solution was dialyzed against 3 × 2 L changes of TBS buffer. The protein was quantified using the Bio-Rad protein assay solution. Protein yield was ~150 mg/L for the purified CaM mutant.

SDS PAGE (15% polyacrylamide) analysis was performed on the protein to confirm purity by Coomassie staining. Western blotting of the gel also confirmed the presence of the poly-histidine tag when probed with the mouse anti-his IgG. After transferring to nitrocellulose for 1 hr at 4 °C at 100 V, the nitrocellulose was blocked with nonfat dry milk (3 g) in TBS buffer (30 mL) for approximately 4 hrs. The milk solution was then poured off and washed with TBST buffer (3 × 30 mL for 5 min each wash). Next, a 1:10,000 dilution in TBST (15 mL) of the mouse anti-his IgG was added to the nitrocellulose and incubated for 1 hr. The antibody solution was poured off and the nitrocellulose sheet was again washed with TBST buffer (3 × 30 mL) for 5 min each wash). A 1:10,000 dilution of the goat anti-mouse IgG(H+L) alkaline phosphatase conjugate in TBST (15 mL) was added to the nitrocellulose and incubated for 1 hr. The antibody solution was poured off and the nitrocellulose sheet was again washed with TBST buffer (3 × 30 mL) for 5 min each wash). Last, 10 mL of 1-Step™ NBT/BCIP from Pierce was added and incubated with the nitrocellulose until the band was visible. The nitrocellulose was then washed with dH_2O and blotted dry (Figure 4-5).

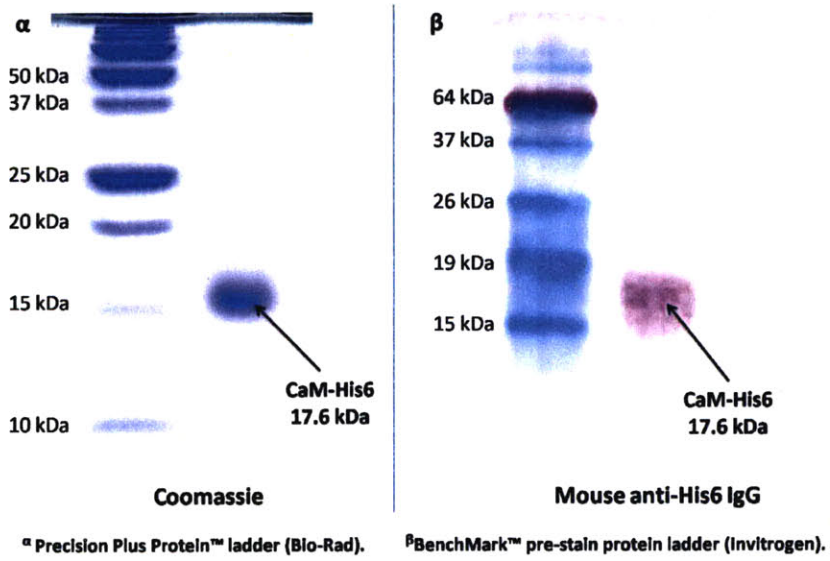

Figure 4-5. Coomassie and western blot of the CaM-His_6 construct.

Fluorescence experiments:

General procedures. All fluorescence spectra were recorded using a Fluoromax 3 instrument (Horiba Jobin Yvon) at 25 °C. The samples were each excited at the wavelength appropriate for the fluorescent peptide. The slit widths were set to 3 nm for excitation and 6 nm for emission. The data points were collected at 0.5 nm increments with a 0.1 s integration period. All spectra were corrected for intensity using the manufacturer-supplied correction factors and corrected for background fluorescence by subtracting a blank scan of the buffer system.

KR peptide study in dioxane/water. Concentrated stocks of each of the purified peptides in the series were prepared in deionized H_2O and quantified by UV-visible spectrometry using the known or measured extinction coefficients of the corresponding fluorophores (Table 4-1). Samples of each peptide were then prepared to a final concentration of 5 μM in either TBS buffer or dioxane containing 18-crown-6 (5 mM) as an additive to enhance solubility. This was done using a 10 mL volumetric flask. The samples were then transferred to a 100 μL quartz cuvette for measurement. This process was repeated in triplicate for both solvent systems. The fold-increase measured for each fluorescent peptide at the wavelength of maximum emission in dioxane was calculated by integrating the area under the curve spanning a 5 nm window centered on the wavelength of interest. The area measured in dioxane was then divided by the area measured in TBS buffer. The results of three trials were then averaged and the error calculated from the standard deviation and the Student's t-value for a 90% confidence interval.

Ca^{2+}-CaM-M13 mutant study. Concentrated stocks of each of the purified peptides in the series were prepared in deionized H_2O and quantified by UV-visible spectrometry using the known or measured extinction coefficients of the corresponding fluorophores. A concentrated

stock solution of the CaM-His_6 construct was also prepared in TBS buffer and quantified by measuring the absorbance in 6 M guanidinium chloride using the predicted extinction coefficient ($\varepsilon_{280\ nm}$ = 2980 cm^{-1} M^{-1}) based on residue composition.[44] Additionally, stocks of $CaCl_2$ (2 mM) and ethylene diamine tetraacetic acid (EDTA, 5 mM) were prepared. From these stock solutions, four experiments were conducted in triplicate as shown in Table 4-6.

Table 4-6. Experimental conditions for Ca^{2+}-CaM-M13 mutant study

Experiment	M13 (10 μM)	EDTA (40 μM)	CaM-His6 (15 μM)	$CaCl_2$ (200 μ)
●	✓	✓		
△	✓	✓	✓	
○	✓	✓	✓	✓
□	✓	✓		✓

The fold-increase measured for each fluorescent peptide at the wavelength of maximum emission under condition '○' was calculated by integrating the area under the curve spanning a 5 nm window centered on the wavelength of interest. The area measured for condition '○' was then divided by the area measured for conditions '●' and '△' to calculate the two reported ratios. The results of three trials were averaged and the reported errors were calculated from the standard deviations and the Student's t-value for a 90% confidence interval.

Titration of $M13_{4DMN}$ peptide with Ca^{2+}-CaM. This experiment was conducted at 25 °C in TBS buffer (pH 7.4) containing 200 μM $CaCl_2$ and 0.1% BSA. The BSA was added to prevent nonspecific adsorption of the CaM construct or the mutant M13 peptide to the walls of the quartz cuvette or pipette tips. The $M13_{4DMN}$ peptide was dissolved in the buffer system to an

initial concentration of 10.2 nM and was gradually diluted to 9.9 nM as the titrant was added. Due to the low signal-to-noise ratio obtained using standard fluorescence instrumentation, lower concentrations of the fluorescent M13 peptide gave less reliable results. The titrant was a stock solution of the CaM construct (920 μM). The total CaM concentration was varied from 0 nM to 22.9 nM as fluorescence spectra were collected at each increment. Due to the low concentration of the fluorescent peptide, the excitation slit width was opened to 10 nm and the integration period extended to 0.2 s. The data from nine replicate titrations were imported into SPECFIT/32™ Global Analysis System for Windows (version 3.0.39) to calculate the K_d of the interaction. The results of the nine trials were then averaged and the error calculated from the standard deviation and the Student's t-value for a 95% confidence interval. The data processing of a typical titration under these conditions is illustrated in Figure 4-6.

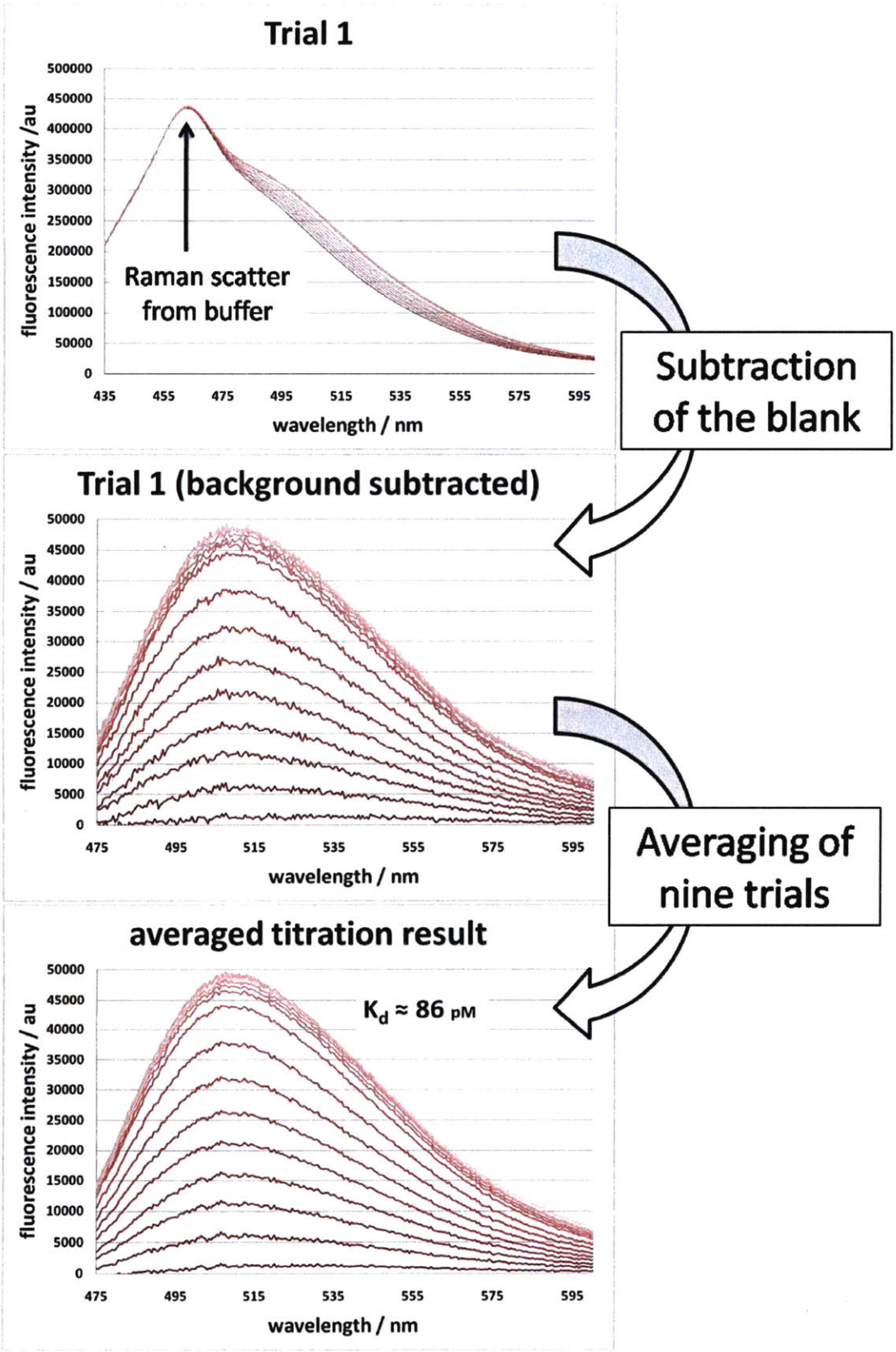

Figure 4-6. Titration of the $M13_{4DMN}$ peptide with Ca^{2+}-CaM.

Acknowledgments

This research was supported by NSF CHE-0414243 (BI), the NIH Cell Migration Consortium (GM064346), and the Biotechnology Training Program (T32-GM08334). Special thanks to Dr. Matthieu Sainlos (MIT) for his helpful advice and insight. The Department of Chemistry Instrumentation Facility (NSF CHE-9808061, DBI-9729592, and CHE-0234877) and the Biophysical Instrumentation Facility for the Study of Complex Macromolecular Systems (NSF-0070319) are also gratefully acknowledged.

References

(1) Pawson, T.; Nash, P. Assembly of cell regulatory systems through protein interaction domains. *Science* **2003**, *300*, 445-452.
(2) Vicente-Manzanares, M.; Webb, D. J.; Horwitz, A. R. Cell migration at a glance. *J. Cell. Sci.* **2005**, *118*, 4917-4919.
(3) Zamir, E.; Geiger, B. Molecular complexity and dynamics of cell-matrix adhesions. *J. Cell. Sci.* **2001**, *114*, 3583-3590.
(4) Velazquez-Campoy, A.; Ohtaka, H.; Nezami, A.; Muzammil, S.; Freire, E. Isothermal titration calorimetry. *Curr. Protoc. Cell. Biol.* **2004**, *Chapter 17*, Unit 17 18.
(5) Lebowitz, J.; Lewis, M. S.; Schuck, P. Modern analytical ultracentrifugation in protein science: a tutorial review. *Protein Sci.* **2002**, *11*, 2067-2079.
(6) Young, K. H. Yeast two-hybrid: so many interactions, (in) so little time. *Biol. Reprod.* **1998**, *58*, 302-311.
(7) Dormán, G. In *Bioorganic chemistry of biological signal transduction*; Springer Berlin: Heidelberg, 2001, p 169-225.
(8) Jares-Erijman, E. A.; Jovin, T. M. FRET imaging. *Nat. Biotechnol.* **2003**, *21*, 1387-1395.
(9) Lakowicz, J. R. *Principles of fluorescence spectroscopy*; 3rd ed.; Springer: New York, 2006.
(10) Vazquez, M. E.; Rothman, D. M.; Imperiali, B. A new environment-sensitive fluorescent amino acid for Fmoc-based solid phase peptide synthesis. *Org. Biomol. Chem.* **2004**, *2*, 1965-1966.
(11) Vazquez, M. E.; Blanco, J. B.; Imperiali, B. Photophysics and biological applications of the environment-sensitive fluorophore 6-*N,N*-dimethylamino-2,3-naphthalimide. *J. Am. Chem. Soc.* **2005**, *127*, 1300-1306.
(12) Reactive derivatives of these three fluorophores are availiable through a number of companies such as Molecular Probes® and AnaSpec, Inc.
(13) Zuhlke, R. D.; Pitt, G. S.; Deisseroth, K.; Tsien, R. W.; Reuter, H. Calmodulin supports both inactivation and facilitation of L-type calcium channels. *Nature* **1999**, *399*, 159-162.

(14) Torok, K.; Cowley, D. J.; Brandmeier, B. D.; Howell, S.; Aitken, A.; Trentham, D. R. Inhibition of calmodulin-activated smooth-muscle myosin light-chain kinase by calmodulin-binding peptides and fluorescent (phosphodiesterase-activating) calmodulin derivatives. *Biochemistry* **1998**, *37*, 6188-6198.

(15) Tsalkova, T. N.; Davydova, N. Y.; Halpert, J. R.; Davydov, D. R. Mechanism of interactions of α-naphthoflavone with cytochrome P450 3A4 explored with an engineered enzyme bearing a fluorescent probe. *Biochemistry* **2007**, *46*, 106-119.

(16) Zhang, J.; Wallar, B. J.; Popescu, C. V.; Renner, D. B.; Thomas, D. D.; Lipscomb, J. D. Methane monooxygenase hydroxylase and B component interactions. *Biochemistry* **2006**, *45*, 2913-2926.

(17) Nitz, M.; Mezo, A. R.; Ali, M. H.; Imperiali, B. Enantioselective synthesis and application of the highly fluorescent and environment-sensitive amino acid 6-(2-dimethylaminonaphthoyl) alanine (DANA). *Chem. Commun. (Camb.)* **2002**, 1912-1913.

(18) Ding, F. X.; Lee, B. K.; Hauser, M.; Davenport, L.; Becker, J. M.; Naider, F. Probing the binding domain of the saccharomyces cerevisiae α-mating factor receptor with fluorescent ligands. *Biochemistry* **2001**, *40*, 1102-1108.

(19) Hagihara, M.; Fukuda, M.; Hasegawa, T.; Morii, T. A modular strategy for tailoring fluorescent biosensors from ribonucleopeptide complexes. *J. Am. Chem. Soc.* **2006**, *128*, 12932-12940.

(20) Wang, Q. Z.; Lawrence, D. S. Phosphorylation-driven protein-protein interactions: A protein kinase sensing system. *J. Am. Chem. Soc.* **2005**, *127*, 7684-7685.

(21) Weber, G.; Farris, F. J. Synthesis and spectral properties of a hydrophobic fluorescent probe: 6-propionyl-2-(dimethylamino)naphthalene. *Biochemistry* **1979**, *18*, 3075-3078.

(22) Prendergast, F. G.; Meyer, M.; Carlson, G. L.; Iida, S.; Potter, J. D. Synthesis, spectral properties, and use of 6-acryloyl-2-dimethylaminonaphthalene (Acrylodan). A thiol-selective, polarity-sensitive fluorescent probe. *J. Biol. Chem.* **1983**, *258*, 7541-7544.

(23) Blumenthal, D. K.; Takio, K.; Edelman, A. M.; Charbonneau, H.; Titani, K.; Walsh, K. A.; Krebs, E. G. Identification of the calmodulin-binding domain of skeletal muscle myosin light chain kinase. *Proc. Natl. Acad. Sci. U.S.A.* **1985**, *82*, 3187-3191.

(24) Ikura, M.; Clore, G. M.; Gronenborn, A. M.; Zhu, G.; Klee, C. B.; Bax, A. Solution structure of a calmodulin-target peptide complex by multidimensional NMR. *Science* **1992**, *256*, 632-638.

(25) Kawahashi, Y.; Doi, N.; Takashima, H.; Tsuda, C.; Oishi, Y.; Oyama, R.; Yonezawa, M.; Miyamoto-Sato, E.; Yanagawa, H. *In vitro* protein microarrays for detecting protein-protein interactions: application of a new method for fluorescence labeling of proteins. *Proteomics* **2003**, *3*, 1236-1243.

(26) Ozawa, T.; Nogami, S.; Sato, M.; Ohya, Y.; Umezawa, Y. A fluorescent indicator for detecting protein-protein interactions in vivo based on protein splicing. *Anal. Chem.* **2000**, *72*, 5151-5157.

(27) Ozawa, T.; Umezawa, Y. Detection of protein-protein interactions in vivo based on protein splicing. *Curr. Opin. Chem. Biol.* **2001**, *5*, 578-583.

(28) Kajihara, D.; Abe, R.; Iijima, I.; Komiyama, C.; Sisido, M.; Hohsaka, T. FRET analysis of protein conformational change through position-specific incorporation of fluorescent amino acids. *Nat. Methods* **2006**, *3*, 923-929.

(29) Crivici, A.; Ikura, M. Molecular and structural basis of target recognition by calmodulin. *Annu. Rev. Biophys. Biomol. Struct.* **1995**, *24*, 85-116.

(30) This structure rendered using PyMol v0.99 (DeLano Scientific LLC).
(31) Olwin, B. B.; Edelman, A. M.; Krebs, E. G.; Storm, D. R. Quantitation of energy coupling between Ca2+, calmodulin, skeletal muscle myosin light chain kinase, and kinase substrates. *J. Biol. Chem.* **1984**, *259*, 10949-10955.
(32) Venkatraman, P.; Nguyen, T. T.; Sainlos, M.; Bilsel, O.; Chitta, S.; Imperiali, B.; Stern, L. J. Fluorogenic probes for monitoring peptide binding to class II MHC proteins in living cells. *Nat. Chem. Biol.* **2007**, *3*, 222-228.
(33) Gao, Z. H.; Krebs, J.; VanBerkum, M. F.; Tang, W. J.; Maune, J. F.; Means, A. R.; Stull, J. T.; Beckingham, K. Activation of four enzymes by two series of calmodulin mutants with point mutations in individual Ca2+ binding sites. *J. Biol. Chem.* **1993**, *268*, 20096-20104.
(34) Findlay, W. A.; Martin, S. R.; Beckingham, K.; Bayley, P. M. Recovery of native structure by calcium binding site mutants of calmodulin upon binding of sk-MLCK target peptides. *Biochemistry* **1995**, *34*, 2087-2094.
(35) Summerer, D.; Chen, S.; Wu, N.; Deiters, A.; Chin, J. W.; Schultz, P. G. A genetically encoded fluorescent amino acid. *Proc. Natl. Acad. Sci. U.S.A.* **2006**, *103*, 9785-9789.
(36) Wang, J.; Xie, J.; Schultz, P. G. A genetically encoded fluorescent amino acid. *J. Am. Chem. Soc.* **2006**, *128*, 8738-8739.
(37) Cohen, B. E.; McAnaney, T. B.; Park, E. S.; Jan, Y. N.; Boxer, S. G.; Jan, L. Y. Probing protein electrostatics with a synthetic fluorescent amino acid. *Science* **2002**, *296*, 1700-1703.
(38) Turcatti, G.; Nemeth, K.; Edgerton, M. D.; Meseth, U.; Talabot, F.; Peitsch, M.; Knowles, J.; Vogel, H.; Chollet, A. Probing the structure and function of the Tachykinin Neurokinin-2 receptor through biosynthetic incorporation of fluorescent amino acids at specific sites. *J. Biol. Chem.* **1996**, *271*, 19991-19998.
(39) Dufau, I.; Mazarguil, H. Design of a fluorescent amino acid derivative usable in peptide synthesis. *Tetrahedron Lett.* **2000**, *41*, 6063-6066.
(40) Chan, W. C.; White, P. D. *Fmoc solid phase peptide synthesis: a practical approach*; Oxford University Press: New York, 2000.
(41) Hancock, W. S.; Battersby, J. E. New micro-test for detection of incomplete coupling reactions in solid-phase peptide-synthesis using 2,4,6-trinitrobenzene-sulphonic acid. *Analytical Biochemistry* **1976**, *71*, 260-264.
(42) Hachmann, J.; Lebl, M. Alternative to piperidine in Fmoc solid-phase synthesis. *J. Comb. Chem.* **2006**, *8*, 149-149.
(43) Sainlos, M.; Imperiali, B. Tools for investigating peptide-protein interactions: peptide incorporation of environment-sensitive fluorophores via on-resin derivatization. *Nat. Protoc.* **2007**, *2*, 3201-3209.
(44) Gasteiger, E.; Gattiker, A.; Hoogland, C.; Ivanyi, I.; Appel, R. D.; Bairoch, A. ExPASy: the proteomics server for in-depth protein knowledge and analysis. *Nucleic Acids Res.* **2003**, *31*, 3784-3788.

Chapter 5: A comparative study of the 4-DMN thiol-reactive agents with other commercial solvatochromic fluorophores

A significant portion of the work described in this chapter has been submitted for publication in:

Loving, G.; Imperiali, B. Thiol-reactive derivatives of the solvatochromic 4-*N,N*-dimethylamino-1,8-naphthalimide fluorophore: A highly sensitive toolset for the detection of biomolecular interactions. *Bioconjug. Chem.* Submitted on July 17, 2009.

Introduction

The solvatochromic properties of many environment-sensitive fluorophores have been exploited in a wide range of biological applications such as detecting protein-peptide binding events,[1-6] monitoring changes in protein allostery,[7-12] and reporting various forms of post-translational modification.[13,14] Since both intra- and intermolecular interactions of many proteins often involve a dynamic veiling and unveiling of discrete hydrophobic clefts or pockets within the topology of these macromolecules, an appropriately placed solvatochromic fluorophore can provide a general and facile method of detecting protein function or activation. Due to the adaptable nature of these tools for addressing an array of problems in the biological sciences, many classes of solvatochromic fluorophores are now commercially available in reactive forms ready for direct conjugation to proteins and other relevant biomolecules.[15] This diversity offers greater prospects of identifying fluorescent constructs with signaling characteristics suitable for study.

A common application of solvatochromic fluorophores is the development of constructs in which the measured fluorescence change is integrally coupled to a perturbation in a specific aspect of protein structure. Such an approach is particularly advantageous when structural changes are too subtle to be detected by other fluorescence-based methods such as Förster resonance energy transfer (FRET)[16] and fluorescence polarization (FP).[17] However, a practical limitation often encountered when using many of the commercially available solvatochromic probes is that the magnitude of the observed fluorescence change rarely approaches the maximum potential obtained in the context of a typical solvent comparison study (Chapter 4).[6] The reasons for this observation are varied, but can frequently be attributed in part to the high

degree of intrinsic fluorescence exhibited by these fluorophores in water as well as insufficient sensitivity to changes in the local environment.

This chapter describes the development of a new series of cysteine modifying agents, **3-3** through **3-6** (Chart 5-1), based on the solvatochromic fluorophore 4-DMN. The principle advantage of this fluorophore, along with other members of the dimethylaminophthalimide family, is that it exhibits extremely low fluorescence quantum yields when exposed to polar protic solvents like water (Chapter 4).[6] This greatly reduces background signal thereby creating the effect of 'on-off' or 'switch-like' changes in the observed emission intensity with the potential to exceed ratios of 1000-fold. Furthermore, as described in Chapter 2, it has been determined that this fluorophore possesses significantly greater chemical stability than the other dimethylaminophthalimide dyes we have investigated[6] making it particularly suitable for applications that require prolonged exposure to a wide range of aqueous conditions relevant for most biological applications.

Much of the former work with the dimethylaminophthalimide dyes in the Imperiali group focused on the development of fluorescent amino acids for incorporation into small peptide-based probes designed to recognize and report binding to discrete protein motifs such as 14-3-3 domains,[18] SH2 domains,[3] and PDZ domains.[19] While these efforts have proved highly successful, the work described in this chapter aims to expand the scope of applications to include the integration of these tools into native proteins. However, several fundamental differences must be considered when applying these tools in proteins versus short peptides. With increasing peptide length, the polymer chain exhibits greater potential for adopting higher order structure[20] leading, in some instances, to significant changes in the local environment of the attached fluorophore. Such changes may include the degree of solvent exposure, the frequency of

collisional quenching, and the emergence of local electrostatic fields. Additionally, the arrangement of the polymer chain around the dye could restrict certain vibrational modes responsible for non-radiative decay processes that compete with fluorescence. The influence of such structural elements and the effects they impart on the photophysical properties of the fluorophore are difficult to predict and can often complicate efforts toward developing useful fluorescent protein probes that utilize the full potential of the fluorescent tool. Hence, empirical screening approaches are typically required, leading us to focus on the development of a series of cysteine-labeling agents. This approach offers a direct and facile method for the site-selective incorporation of these probes into proteins.

This study identifies key variables that influence the fluorescent response of labeled proteins to changes in protein structure providing a general framework for understanding the ways in which solvatochromic tools may best be applied. Additionally, it reveals a systematic approach to developing future fluorescent protein probes for detecting various biomolecular interactions. The members of this new series of thiol-modifying agents vary according to the linker type and the nature of the electrophilic group necessary for cysteine labeling (Chart 5-1). Using the calcium-sensing protein calmodulin as a model system for our study, we demonstrate the power of this suite of solvatochromic tools to develop highly effective sensors of dynamic biomolecular interactions.

Chart 5-1. Thiol-reactive derivatives of 4-DMN and other commercially available solvatochromic fluorophores

4-DMN thiol-reactive dyes

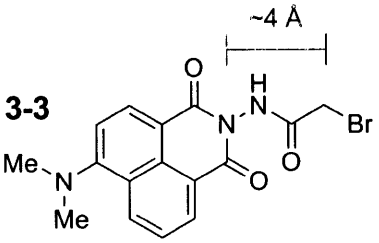

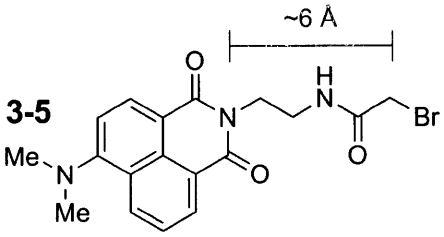

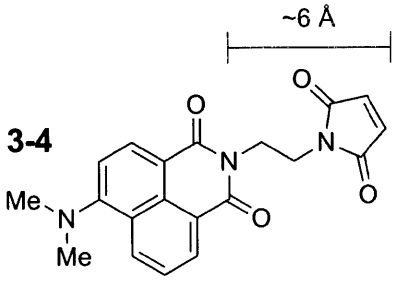

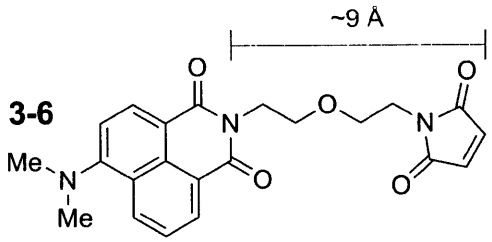

Commercial thiol-reactive dyes

MDCC

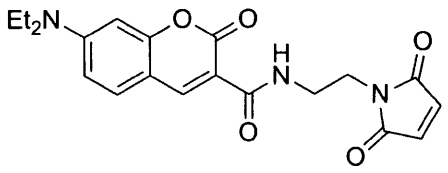

IANBD

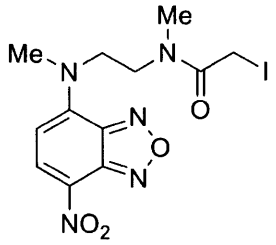

BADAN

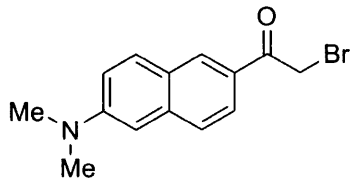

IAEDANS

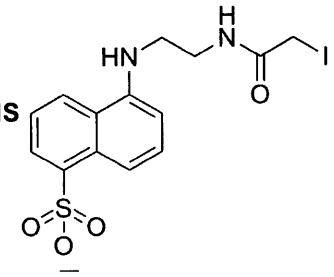

PyMPO

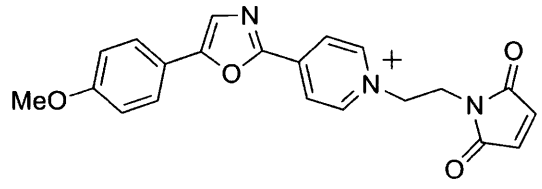

Results

The calcium binding protein calmodulin (CaM), which has been extensively characterized by a number of research groups,[21] was selected as the model system for a comparative study to evaluate the performance of the 4-DMN cysteine modifying agents **3-3** through **3-6**. CaM is a soluble protein that responds to sudden influxes of cytosolic Ca^{2+} levels[22] by rapidly chelating as many as four of these cations through specialized Ca^{2+}-binding motifs called EF-hands. The binding event induces an allosteric change in the N- and C-terminal domains of the protein resulting in the formation of two hydrophobic pockets, which can then bind critical hydrophobic residues of certain peptide motifs that are recognized by the protein (Figure 5-1).[21,23] One advantage to using calmodulin is that the wild-type protein is devoid of native cysteine residues. This characteristic affords considerable freedom in selecting discrete sites for cysteine mutagenesis and subsequent modification by a thiol-reactive agent. The exceptional attributes offered by this unique system provides a useful benchmark for our studies since numerous research groups[12,24-28] over the last 30 years have attempted to develop CaM-based calcium sensors by labeling the protein at a variety of sites with various solvatochromic probes. However, despite extensive efforts, the reported changes in fluorescence emission are modest and typically encumbered by high background fluorescence, which strongly limits the utility of these constructs in certain applications such as fluorescence microscopy.

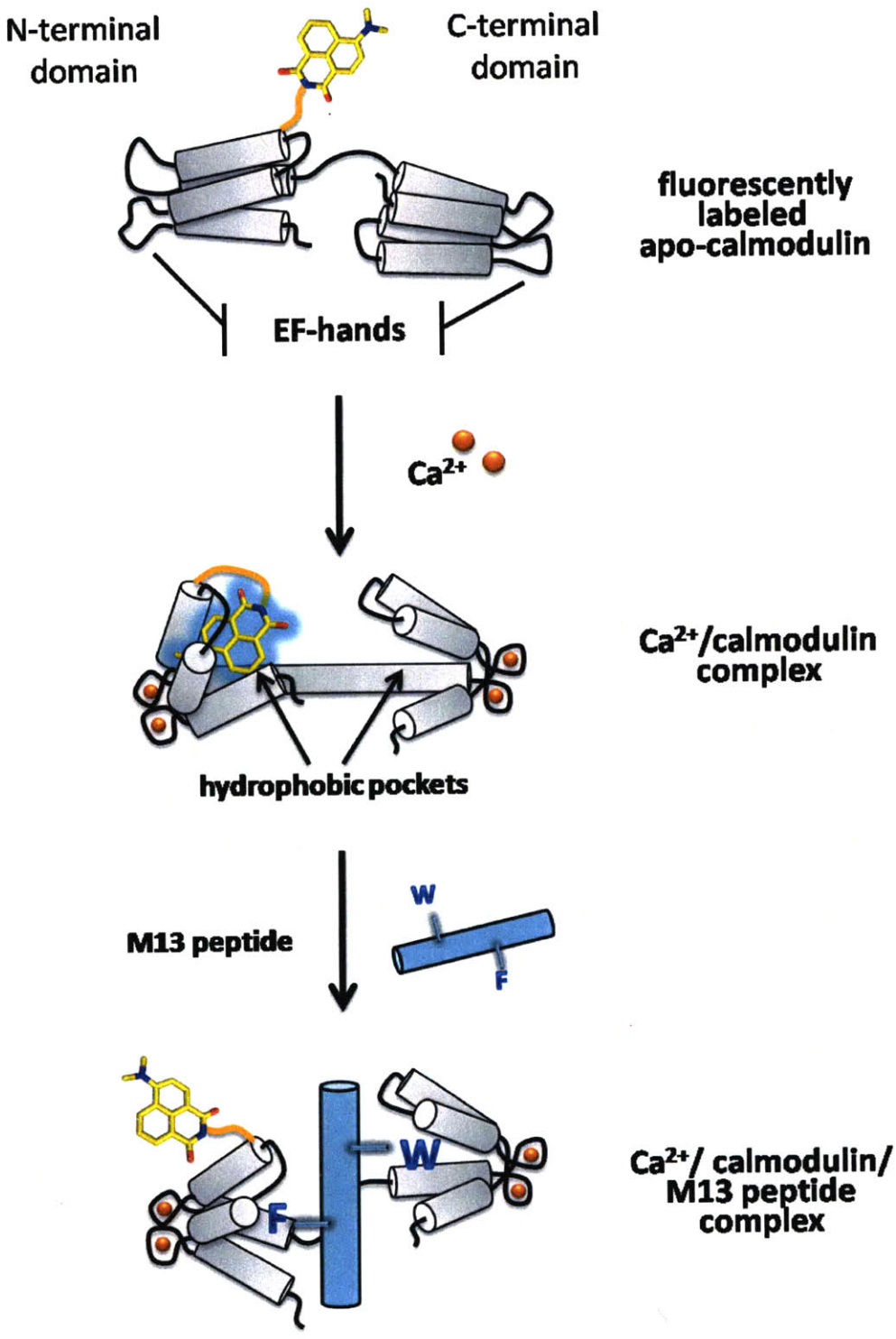

Figure 5-1. Ca^{2+} activation of a CaM mutant (grey) results in the burying of an attached solvatochromic fluorophore (yellow) within one of the newly formed hydrophobic pockets. In response, the fluorophore exhibits a dramatic increase in fluorescence intensity. Subsequent addition of the M13 peptide (cyan) can displace the fluorophore from the pocket through insertion of an aromatic side-chain from the phenylalanine or tryptophan residue indicated here using the single-letter notation for amino acids.

Based on careful examination of available X-ray and NMR structures of calmodulin in the apo-state,[29] as well as the calcium-bound[30] and calcium-peptide-bound[31] states, seven sites were selected for cysteine mutagenesis (Figure 5-2). The basis for the selection process was the identification of residues that are relatively solvent exposed when the protein exists in the apo-state and do not appear to play an important functional role that might be disrupted through mutagenesis and labeling. By exploring multiple sites spanning the breadth of the protein structure, it is possible to resolve trends that are site-dependent from those that are site-independent and to better ascertain the robustness of those trends. Site-directed mutagenesis was performed on the wild-type template to introduce cysteine residues at two sites on the N-terminal domain (E11C and S38C), two sites within the linker region (M76C and E87C), and three sites in the C-terminal domain (N111C, E114C, and M145C).

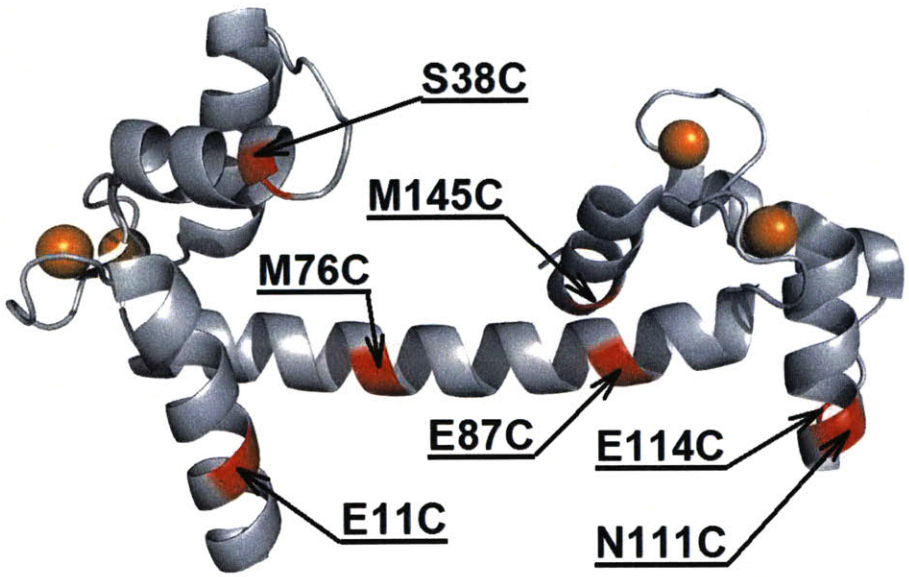

Figure 5-2. Crystal structure of the Ca^{2+}-CaM complex deposited by Rupp et. al. (PDB entry 1UP5).[30] The structure indicates the seven sites selected for cysteine mutagenesis (red). The bound calcium ions are indicated by spheres (yellow).

In addition to the 4-DMN derivatives **3-3** through **3-6**, five commercially available solvatochromic fluorophores were also included in this study for comparison (Chart 5-1). These fluorophores provide a representative sampling of the major classes of solvatochromic probes that are currently available and commonly used at this time. The reagents vary fundamentally in size, shape, and hydrophobicity and each exhibits distinct photophysical properties.[15] For the comparison, we focused on common dyes that were available as thiol-reactive labeling agents possessing dimensions similar to that of the 4DMN derivatives. With a total of nine fluorescent labeling agents and seven cysteine mutants of calmodulin, sixty-three possible fluorescent constructs were prepared for evaluation. The wild-type CaM construct was included as a control in the labeling experiments, although no significant background labeling was observed.

In order to gauge the capacity of each labeling agent to report a change in the structural state of the calmodulin mutants, fluorescence spectra were collected in the presence and absence of saturating calcium. Additionally, since the Ca^{2+}-CaM complex is capable of binding certain peptide motifs with high affinity, a known peptide binding partner commonly referred to as the M13 peptide[32] was also introduced to the fluorescent constructs, in the presence and absence of calcium, to observe whether further changes in the emission spectra occur. The constructs were compared by measuring the ratio of fluorescence intensity at the wavelength of maximum emission of the Ca^{2+}-CaM complex to that of the apo-state for the three the examined conditions (saturating Ca^{2+}, saturating M13 peptide, and saturating Ca^{2+} with the M13 peptide).[33] For brevity, the results of three representative mutants are shown in Figure 5-3 (panels a-c). The remaining data sets are located at the end of the Experimental section of this chapter (Figure 5-7).

A common feature observed among most of the cysteine mutants of this study was the tendency to exhibit higher fluorescence intensity in the Ca^{2+}-bound state compared to that of the full Ca^{2+}-CaM-M13 peptide complex (Figure 5-3a,b). This propensity for the labeled constructs to display a diminished fluorescent signal in the presence of a native peptide-binding partner was general for all of the solvatochromic fluorophores, with exception to the two charged species IAEDANS and PyMPO included in this study. The effect is attributed to a process of competitive displacement in which the fluorophore and ligand both compete for occupancy of the same hydrophobic binding site thereby increasing the average exposure of the fluorophore to the surrounding solvent environment. However, this behavior was by no means a rule as many constructs included in this study, particularly those of the M145C mutant (Figure 5-3c), exhibited the greatest fluorescence intensity for the Ca^{2+}-CaM-M13 peptide complex.

A number of key trends emerged from the fluorescence screen. One among these was a pronounced dependence of the measured fluorescence change on the linker type for the 4-DMN series of compounds **3-3** through **3-6**. For instance, the E11C mutant exhibited a strong bias for the shortest linker of the series (4 Å) whereas the trend was the reverse for the S38C mutant, which yielded the best response with linkers of intermediate to longer length (6-9 Å). This result was largely site-dependent and yielded no clear pattern for determining the optimal linker type *a priori*. Hence, the process of identifying a construct with the desired fluorescence properties may best be accomplished through an empirical approach utilizing the set of 4-DMN-labeling agents as a combined suite.

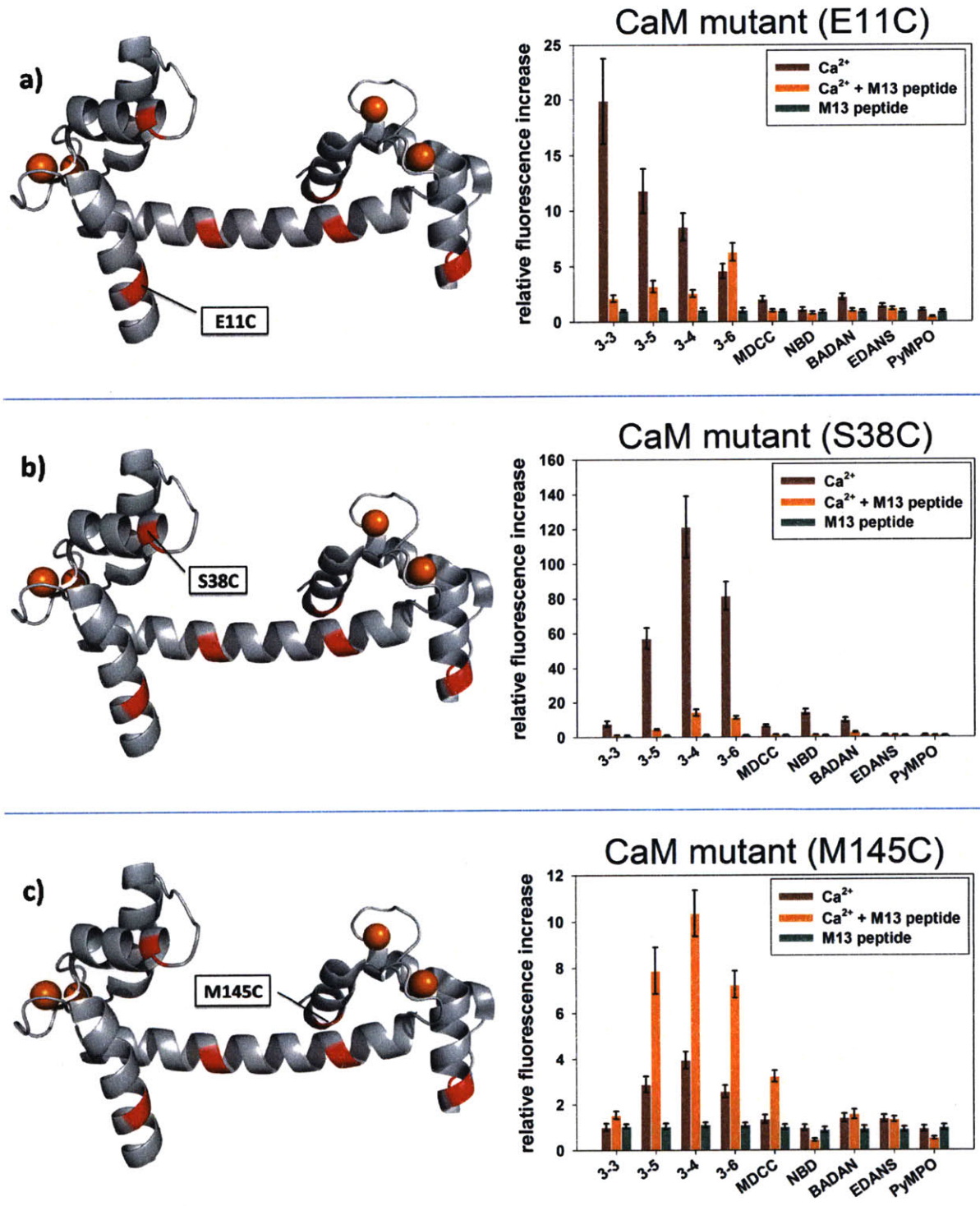

Figure 5-3. Histograms indicating the fluorescence results obtained from three of the cysteine mutants examined in this study. The vertical bars represent the ratio of fluorescence intensity measured at the wavelength of maximum emission under the condition that yielded the brightest state for each construct with respect to that of the apo-state. The fluorophores are indicated along the horizontal axis below the associated results. For each condition, saturating levels of Ca^{2+} and/or the M13 peptide were used. The indicated errors represent the 90% confidence intervals determined from three trials.

The next revealed trend was the marked ability of the calmodulin cysteine mutants labeled with the 4-DMN derivatives, **3-3** through **3-6**, to produce greater signal increases in response to the presence of saturating calcium (or calcium plus the M13 peptide) over those modified by the other dyes considered in the study. Although in some cases these differences were modest, the overall trend demonstrated that this property was robust and relatively site-independent. This is particularly apparent for the S38C mutant (Figure 5-3b) labeled with compound **3-4**, which showed a greater than one hundred-fold increase in emission intensity upon binding calcium. Among the commercially available fluorophores, IANBD was the closest by comparison exhibiting only a fifteen-fold increase in intensity. Although the influence of linker type, which played a crucial role in obtaining optimal results with the 4-DMN fluorophore, was not examined when comparing the other commercial fluorophores, the limiting factor for those dyes was largely due to the high degree of intrinsic fluorescence that each exhibits in aqueous environments. This high background effectively reduces the maximum attainable signal-to-noise ratio despite these dyes being good fluorophores.

Results of the study also suggest that certain factors known to enhance hydrophilicity can negatively influence the capacity of a solvatochromic fluorophore to respond to perturbations within the local topology of the protein surface. This was particularly apparent between the two charged dyes included in the series (IAEDANS and PyMPO). Neither dye displayed significant changes in emission properties when the associated cysteine mutants were exposed to combinations of Ca^{2+} and the M13 peptide. By bearing a formal positive or negative charge, the energetic cost of desolvating these fluorescent species may negate any benefit gained by burying the aromatic ring systems deep within a hydrophobic pocket formed as the result of a conformational change to the protein structure. This would greatly impact the equilibrium of the

buried versus solvated state making these probes less sensitive to such structural dynamics despite otherwise exhibiting good solvatochromic properties. Although this trend was relatively site-independent for the mutants of the calmodulin protein, it is expected that these probes could be better suited for applications where the possibility of charge complementarity exists or where other molecular driving forces are responsible for the partitioning of the probes between two distinct environments.[34]

Discussion

In developing this series of 4-DMN cysteine labeling agents, an essential question we wished to address was whether there was value in utilizing an assortment of linker types or if this simply introduced an element of redundancy. The results of this study strongly indicate that the linker type does play a critical role in influencing the magnitude of the fluorescent response. For a solvatochromic probe to function optimally, it must directly interact with a feature of interest. If this feature happens to be a hydrophobic pocket located far from the point of attachment on the protein surface, then a longer linker would clearly be favored over one that is unable to reach (Figure 5-4a). However, a caveat of using a longer linker is that the greater range may inadvertently increase the probability that the fluorophore will encounter and bind a shallow hydrophobic patch that is unaltered by the structural state of the protein. Such a static interaction would produce and undesirable increase in the fluorescence background. In this instance a shorter linker could prove better suited (Figure 5-4b). In fact this appears to be the case for mutant E11C where compound **3-3** produced a much greater increase in fluorescence intensity than compound **3-6** upon the addition of saturating Ca^{2+}. Both constructs displayed comparable emission intensities in the Ca^{2+} bound state. However, the apo-state of the construct labeled with

3-6 exhibited a fluorescence background that was roughly five-fold greater than that of the construct with the shortest linker resulting in the smaller observed increase.

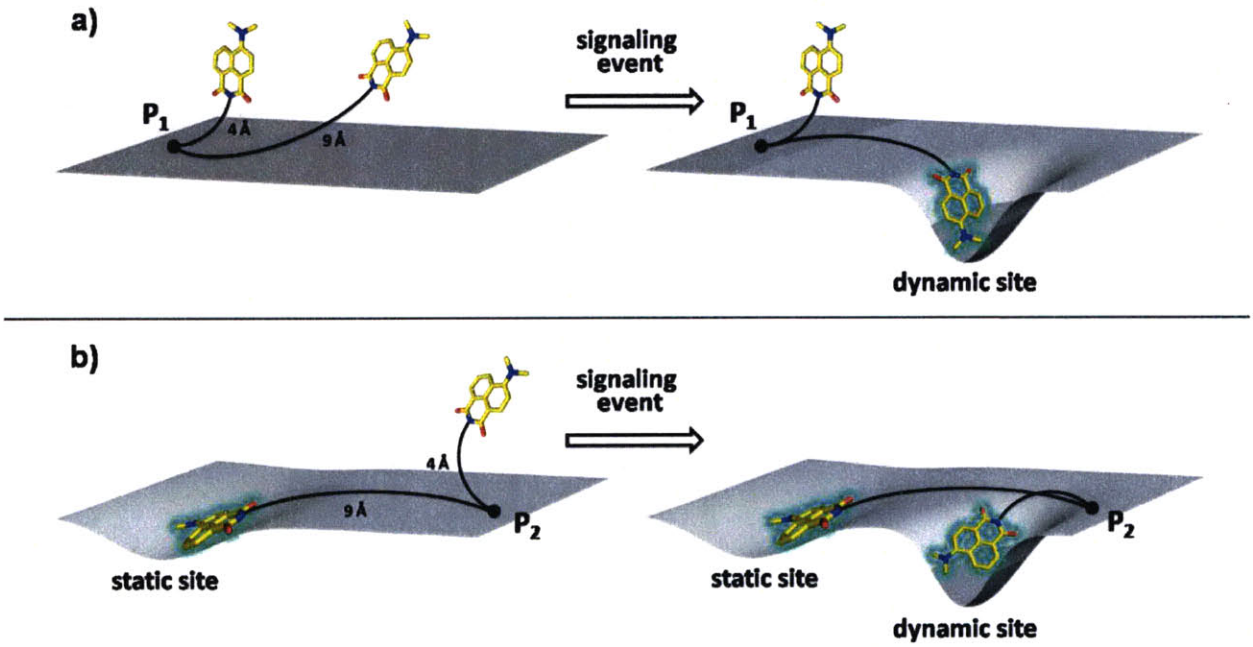

Figure 5-4. (a) Attachment point P_1 is located far from a hydrophobic pocket formed upon a structural change in the protein. Here, a longer linker is preferred to a shorter one. (b) Attachment point P_2 is located near the hydrophobic pocket formed in response to a structural change. Such sites may favor shorter linkers as longer linkers could tend to allow the fluorophore to encounter non-specific hydrophobic patches that remain static with regard to the dynamics of protein topology. This would result in higher background fluorescence.

Interference by background fluorescence is a phenomenon that affects all solvatochromic fluorophores and extends beyond the model system used in this study. Solvatochromic fluorophores often display somewhat different emission properties when appended to globular proteins such as calmodulin.[35] A bulky hydrophobic fluorophore protruding into the surrounding solvent environment demands a large enthalpic cost due to disruption of the dense network of hydrogen-bonded water molecules. Consequently, the probe will exhibit a strong tendency to associate with any hydrophobic clefts or pockets formed by structural elements within the immediate vicinity to minimize this exposure. The degree of background fluorescence

associated with these non-specific interactions is largely site-dependent for a fluorophore of a given linker-type. This interference is further compounded by any intrinsic fluorescence already produced by the probe in water. A convenient method we have developed for measuring the background resulting from such effects involves comparing the emission spectra of the construct under both natured (TBS buffer pH 7.4) and denatured conditions (TBS buffer pH 7.4 with 6.67 M guanidine hydrochloride). This was performed with all sixty-three fluorescently labeled calmodulin constructs and the results summarized in Figure 5-6 located in the Experimental section of this chapter. Although site-dependent background fluorescence appeared to be a critical limitation to many of the commercial dyes, this issue proved much less consequential for the 4-DMN derivatives due to the negligible degree of intrinsic fluorescence exhibited by these probes in water.

An ideal site for labeling would be one that precludes the solvatochromic fluorophore from forming any surface associations of this sort until a structural change in the protein has occurred. In practice, however, identifying an optimal labeling site is often challenging even when exceptional structural data for the protein is available. As a result, screening of a strategically selected series of cysteine mutants is typically required. When applied in combination with the series of 4-DMN labeling agents, this approach allowed us to readily identify a number of fluorescent mutants that respond sensitively and selectively to the formation of the Ca^{2+}-CaM complex. Additionally, although the 4-DMN labeled M145C mutants showed only a modest selectivity for the Ca^{2+}-CaM-M13 peptide complex over that of the Ca^{2+}-CaM complex, it is possible that a more extensive screen could yield a construct with greatly improved properties permitting access to a set powerful sensors of either state.

Conclusion

In this study, the 4-DMN derivatives **3-3** through **3-6** were evaluated and compared with five other well-established solvatochromic fluorophores to address a number of critical factors pertaining to the successful application of such tools in detecting specific types of bimolecular interactions. These factors include the importance of linker type, the influence of hydrophobicity, and the deleterious effects of high intrinsic fluorescence.

Due to the rarity with which solvatochromic fluorophores exhibit the maximum potential fluorescence changes when used in many biological applications, the large intrinsic fluorescence exhibited by many of these probes in aqueous environments represents a critical issue that can ultimately be limiting. This matter is further compounded by the strong tendency for these probes to show a marked enhancement in fluorescent signal when appended to proteins as a result of non-specific topological interactions. Because the 4-DMN derivatives possess such low intrinsic fluorescence in water, these effects are significantly less consequential.

Linker variety is a fundamental component to designing sensors that incorporate solvatochromic dyes and is a feature that is not typically examined systematically. Often, the linker is considered a passive component of fluorescent labeling agents, serving merely to connect the dye to the target molecule without interfering with native properties like function or solubility. Here, we demonstrate that linkers play a more active role and can be a vital element in the optimization of the fluorescent response. When applied in combination with cysteine-scanning mutagenesis, the number of fluorescent constructs is greatly expanded thereby increasing the potential for obtaining a sensor with the desired properties. We therefore present this series of labeling agents as a combined suite that offers the excellent properties of the 4-

DMN dye in a format ready to meet the strict demands required by a wide spectrum of applications ranging from high-throughput screening assays to fluorescence microscopy.

Experimental

Tris-buffered saline. All references to solutions prepared in TBS buffer pertain to the following recipe.

10× TBS Buffer:

60.6 g Tris-HCl
87.7 g NaCl

Dissolve the measured salts in 800 mL of distilled H_2O and adjust the pH to 7.3 with concentrated HCl. Then increase the volume to 1 L. Upon diluting the 10× TBS buffer ten-fold with distilled H_2O, the pH should be 7.4. The final 1× TBS concentrations are 50 mM Tris-HCl, 150 mM NaCl, and pH 7.4.

Synthesis of the M13 peptide. The peptide used in this study represents a truncated form of the originally described M13 peptide discovered by Blumenthal *et al.*[32] The sequence encompasses only the minimum residues required to bind the Ca^{2+}-CaM activated complex. The residue numbering refers to that of the original fragment.

M13 Peptide

Residue #	N-term	2	3	4	5	6	7	8	9	10	11	12	13	14	15	16	17	18	19	C-term
Sequence	H_2N-	R	R	W	K	K	N	F	I	A	V	S	A	A	N	R	F	K	K	-$CONH_2$

The M13 peptide was prepared using standard Fmoc-based solid-phase peptide synthesis techniques (SPPS)[36] with 0.17 mmol/g loading Fmoc-NovaPEG Rink Amide resin LL (Cat. No. 01-64-0483, Novabiochem®). Fmoc-protected amino acids with the standard side-chain protecting groups were used: Fmoc-Ala-OH, Fmoc-Phe-OH, Fmoc-Ile-OH, Fmoc-Lys(Boc)-OH, Fmoc-Asn(Trt)-OH, Fmoc-Arg(Pbf)-OH, Fmoc-Ser(tBu)-OH, Fmoc-Val-OH, and Fmoc-Trp(Boc)-OH. Synthesis of the peptide began by coupling the first seven residues (positions 13-19) with an ABI 431A peptide synthesizer (Applied Biosystems). The synthesis was performed

on the 40 μmol scale using 4 equiv of the Fmoc amino acids in each cycle. It had been discovered from earlier attempts at making the M13 peptide that the coupling efficiency was extremely low for residues incorporated after the alanine at position 10 in the sequence. This problem was overcome by using a pseudoproline dipeptide, Fmoc-Val-Ser($\Psi^{Me,Me}$pro)-OH (Cat. No. 05-20-1001, Novabiochem), for positions 11-12 in place of Fmoc-Val-OH and Fmoc-Ser(tBu)-OH. The remaining residues were coupled manually using 6 equiv of the Fmoc amino acids. The building blocks were dissolved to a final concentration of 50 mM in DMF containing a 1:1 mixture of HOBt/HBTU (50 mM each) with *N,N*-diisopropylethylamine (100 mM, 12 equiv). Each coupling reaction was allowed to proceed at room temperature for 30-45 min. The coupling efficiency was monitored using the TNBS test.[37] Removal of the Fmoc group prior to each coupling step was performed using a 20% 4-methylpiperidine solution[38] in DMF (3 × 5 min). A Boc-Arg(Pbf)-OH residue was incorporated at the N-terminus of the peptide in order to yield the free α-amino group following cleavage from the solid support. The M13 mutant peptide was cleaved from the resin using a solution of 96:2:2 TFA/H_2O/EDT for 3 hrs. The cleavage cocktail was then filtered and evaporated. The crude peptide was triturated with cold diethyl ether (3 × 10 mL) and purified by HPLC using a Waters 600E HPLC with a Waters 600 automated control module and Waters 2487 dual wavelength absorbance detector set at 228 and 280 nm. The separation was performed using a preparative YMC-pack, C_{18}, 20 × 250 mm reverse-phase column. A YMC-pack, C_{18}, 4.6 ×150 mm reverse-phase column was used for analytical HPLC. The following analytical HPLC method was used to characterize the peptide:

Time (min)	Flow Rate (mL/min)	H_2O % (with 0.1% TFA)	MeCN % (with 0.1% TFA)	Gradient
initial	1.00	93	7	linear
5.0	1.00	93	7	linear
40.0	1.00	0	100	linear

Retention time (min)	ESI-MS (m/z) $[M+xH]^{x+}$ calcd	ESI-MS (m/z) $[M+xH]^{x+}$ found
21.6	740.9 [M+3]	740.6 [M+3]
	555.9 [M+4]	555.7 [M+4]
	444.9 [M+5]	444.8 [M+5]

The peptide mass was determined by ESI-MS on a Mariner electrospray mass spectrometer (PerSeptive Biosystems).

Subcloning of codon-optimized CaM gene into the pET-14b vector. The synthetic CaM construct ordered from Bio Basic Inc. was designed for optimal expression in *E. coli.* The gene was inserted into a high-copy pUC-57 vector for ease of amplification. The product was delivered as a lyophilized powder and also as a stab of transformed DH5α cells in LB agar with carbenicillin. A sterile loop was dipped in the stab and swabbed over a fresh LB agar plate containing carbenicillin (50 μg/mL). The plate was incubated overnight at 37 °C. The next day, a colony was selected and amplified in order to isolate the vector using a Qiagen Plasmid Miniprep kit. The DNA was then quantified by Abs at 260 nm (0.11 μg/μl).

Sequence of codon-optimized CaM gene.

```
ATGGCAGATCAACTGACTGAAGAACAGATTGCGGAATTTAAAGAAGCATTCAGCCTGTTC
GACAAAGATGGCGATGGCACCATTACGACCAAGGAGCTGGGTACGGTGATGCGTTCTCTG
GGTCAGAACCCAACTGAGGCAGAACTGCAGGATATGATCAACGAGGTTGATGCTGACGGT
AATGGCACCATCGACTTCCCGGAATTCCTGACCATGATGGCCCGTAAAATGAAAGACACC
GATTCCGAAGAAGAAATCCGTGAGGCTTTCCGTGTATTCGACAAAGACGGTAACGGCTAC
ATTTCTGCGGCGGAACTGCGCCATGTGATGACCAACCTGGGCGAAAAACTGACCGACGAA
GAAGTTGACGAGATGATCCGCGAAGCTGATATCGACGGTGATGGTCAGGTCAACTATGAA
GAATTTGTTCAGATGATGACTGCGAAGCACCACCACCACCACCAC
```

Translation of codon-optimized CaM gene.

```
MADQLTEEQIAEFKEAFSLFDKDGDGTITTKELGTVMRSLGQNPTEAELQDMINEVDADG
NGTIDFPEFLTMMARKMKDTDSEEEIREAFRVFDKDGNGYISAAELRHVMTNLGEKLTDE
EVDEMIREADIDGDGQVNYEEFVQMMTAKHHHHHH
```

A double digestion of the amplified pUC-57(CaM) vector was performed simultaneously with the double digestion of the pET-14b vector. The reaction conditions were as follows:

pET-14b vector:		pUC-57 vector:	
1.28 µL	pET-14b (2.34 µg/µL)	27.0 µL	pUC-57 (0.11 µg/µL)
41.2 µL	dH_2O (sterile)	15.5 µL	dH_2O (sterile)
5.0 µL	10× NEB buffer 2	5.0 µL	10× NEB buffer 2
0.5 µL	100× BSA	0.5 µL	100× BSA
1.0 µL	XhoI	1.0 µL	XhoI
1.0 µL	NcoI	1.0 µL	NcoI
50.0 µL	total volume	50.0 µL	total volume

The reactions were allowed to proceed for 1 hr at 37 °C before stopping with the addition of 12.5 µL of 5× DNA loading buffer. The both reaction mixtures were then loaded onto a 1% agarose gel and resolved at 110 V. The desired restriction products (the CaM insert of the pUC-57 vector and the linearized pET-14b expression vector) were cut from the gel and isolated using a QIAquick™ Gel Extraction kit. The subcloning vector and insert were then quantified on 1% agarose gel by comparing band intensities to those of the NEB 2-Log DNA ladder.

Two ligation reactions were assembled: one containing both the CaM insert and the pET-14b vector, and the other with only the pET-14b vector as a negative control. The reaction conditions were as follows:

vector (control)		vector + insert	
0.3 μL	pET-14b (120 ng/μL)	0.3 μL	pET-14b (120 ng/μL)
3.2 μL	dH_2O (sterile)	1.0 μL	CaM insert (15 ng/μL)
1.0 μL	T4 DNA ligase	2.2 μL	dH_2O (sterile)
0.5 μL	10× T4 ligase buffer	1.0 μL	T4 DNA ligase
		0.5 μL	10× T4 ligase buffer
5.0 μL	total volume	5.0 μL	total volume

Note- There were 36 μg of pET-14b vector in each reaction and 15 μg of the insert in the ligation. The insert is 480 bp and the vector is 4500 bp. This corresponds to a 4:1 molar ratio of insert to vector.

The reactions were allowed to proceed for 16 hrs at 16 °C. The reactions were then used to transform two 30 μL batches of DH5α cells plated on LB/agar with 50 μg/mL carbenicillin. The next day, no colonies were observed for the negative control. Three colonies from the non-control plate were selected and amplified for sequencing. All selected colonies were determined to be the desired construct. The new vector, pET-14b[CaM], was transformed into BL21-Gold(DE3) competent cells from Stratagene for protein expression.

Cysteine mutagenesis of wild-type CaM gene. These seven cysteine mutants of the CaM construct were prepared by site-directed mutagenesis using the following set of PAGE-purified primers along with the corresponding reverse compliments ordered on the 50 nmole scale from Operon:

E11C-
CTGACTGAAGAACAGATTGCGTGCTTTAAAGAAGCATTCAGCCTG

S38C-
GGGTACGGTGATGCGTTGTCTGGGTCAGAACCC

M76C-
CCTGACCATGATGGCCCGTAAATGCAAAGACACCGATTCCG

E87C-
CCGATTCCGAAGAAGAAATCCGTTGCGCTTTCCGTGTATTCGAC

N111C-
CTGCGCCATGTGATGACCTGCCTGGGCGAAAAACTGACC

E114C-
GTGATGACCAACCTGGGCTGCAAACTGACCGACGAAGAAG

M145C-
CTATGAAGAATTTGTTCAGATGTGCACTGCGAAGCACCACCACC

Upon receiving the primers, stock solutions were prepared in sterile water (125 ng/μl). The reactions were assembled accordingly:

5.0 μL	10× Pfu Turbo rxn buffer.
0.5 μL	pET14b vector [CaM] (20 ng/μL)
1.0 μL	fwd primer (125 ng/μL)
1.0 μL	rev primer (125 ng/μL)
2.5 μL	dNTP's (10 mM each)
40.0 μL	dH_2O (sterile)
50.0 μL	total volume

A control reaction was also performed in which the primers were excluded from the reaction mixture. Next, 1 μL of Pfu Turbo (2.5 U/μL, Stratagene) was added to each reaction. The reaction solutions were mixed thoroughly by gentle pipetting, centrifuged briefly and loaded into an MJ-mini PCR machine from Bio-Rad. The PCR method employed was as follows:

PCR method:

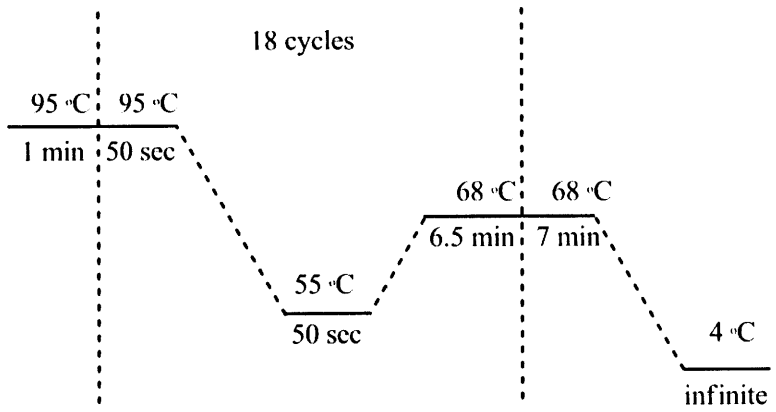

After the PCR reaction was complete the parent vector was digested by adding 1 μL of DpnI (20 U/μL) to each reaction mixture. The reactions were then mixed with gentle pipetting and incubated at 37 °C for 1.5 hrs each. The reaction mixtures were then used to transform XL1-blue DH5α cells obtained from Stratagene. Colonies from each transformation were selected and submitted for sequencing to confirm the desired constructs were obtained. The DNA from each of the chosen colonies was isolated using a Qiagen Miniprep kit.

Expression and purification of wild-type CaM and cysteine mutants. The calmodulin constructs were designed with a C-terminal hexahistidine tag for easy purification of the expressed product. The CaM-His_6 mutants were transformed in BL21-Gold(DE3) competent cells from which 20% glycerol stocks were prepared for subsequent protein expression. The stocks were used to inoculate 5 mL LB-broth starter cultures containing carbenicillin (50 μg/mL). The starter cultures were allowed to grow overnight in a 37 °C shaker at 225 rpm. The next day, the starter cultures were used to inoculate 1 L LB-broth cultures containing carbenicillin (50 μg/mL) and grown at 37 °C with agitation at 225 rpm. The cultures were

allowed to grow to an $OD_{600nm} \approx 0.5$ after which the 1 L shaker flasks were transferred to a 25 °C shaker (225 rpm) for induction. The cells were induced with 0.1 mM IPTG and shaken for 4 hrs before harvesting at 5000 × g (4 °C). The pellets were then resuspended in a 0.9% NaCl aqueous solution (30 mL) and transferred to 50 mL conical tubes to be repelleted for storage at -80 °C.

On the day of the protein preparation, the pellets were thawed at room temperature and resuspended in the following lysis buffer:

4 mL	10× TBS buffer
400 µL	NP-40 Alternative
4 mL	glycerol
40 mg	lysozyme
6 mg	dithiothreitol
40 µL	Protease Cocktail III (Calbiochem)
40 mL	final vol. after diluting with dH_2O

Once the pellets were fully resuspended, the cells were sonicated using a Branson Sonifier 450 at 50% power with a 30% duty cycle for 2 min at 4 °C. The lysates were then transferred to 45 mL polycarbonate bottles and spun at 100,000 × g in a Type 28 rotor from Beckman Coulter to pellet DNA and other cellular debris. Meanwhile, a 5 mL bed of Ni-NTA agarose resin obtained from Qiagen was pre-equilibrated in TBS buffer for each construct. After the spin, the clarified supernatants were transferred to clean 50 mL conical tubes and mixed with the pre-equilibrated Ni-NTA agarose resin. The samples were tumbled gently on a rotisserie at 4 °C for 1 hr to allow binding of the His-tagged proteins. The resin was then recovered by passing the lysates through 20 mL spin columns obtained from Bio-Rad. The resin was washed first with 4 mL of TBS buffer, then 4 mL of 10 mM imidazole in TBS buffer and then with 4 mL of 20 mM imidazole in TBS buffer at 4 °C. The protein was then eluted in 6 × 1 mL fractions of 250 mM imidazole in TBS buffer at 4 °C. The fractions were assayed for protein and combined appropriately. The imidazole was removed by dialysis using a 3.5 kDa MWCO Slide-A-Lyzer

dialysis cassette from Pierce. The protein solutions were dialyzed against 3 × 2 L changes of TBS buffer. The protein concentrations were then quantified using the Bio-Rad protein assay solution. Protein yields were ~80 mg/L for the purified CaM mutants.

SDS PAGE (15% polyacrylamide) analysis was performed on the proteins to confirm purity by Coomassie staining (Figure 5-5). Western blotting of the gel also confirmed the presence of the poly-histidine tag when probed with the mouse anti-his IgG. After transferring to nitrocellulose for 1 hr at 4 °C under 100 V, the nitrocellulose membrane was blocked with nonfat dry milk (3 g) in TBS buffer (30 mL) for approximately 4 hrs. The milk solution was then poured off and the membrane washed with TBST buffer (3 × 30 mL for 5 min each wash). Next, a 1:10,000 dilution in TBST (15 mL) of the mouse anti-his IgG was added to the nitrocellulose and incubated for 1 hr. The antibody solution was poured off and the nitrocellulose membrane was again washed with TBST buffer (3 × 30 mL) for 5 min each wash). A 1:10,000 dilution of the goat anti-mouse IgG(H+L) alkaline phosphatase conjugate in TBST (15 mL) was added to the nitrocellulose and incubated for 1 hr. The antibody solution was poured off and the nitrocellulose membrane was again washed with TBST buffer (3 × 30 mL) for 5 min each wash). Last, 10 mL of 1-Step™ NBT/BCIP from Pierce was added and incubated with the nitrocellulose until the band was visible. The nitrocellulose was then washed with dH_2O and dried.

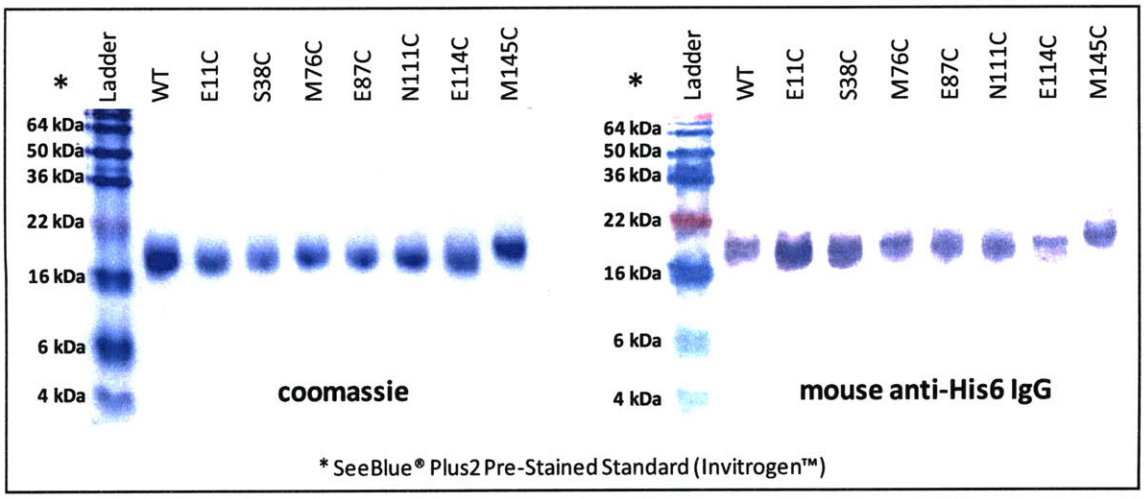

Figure 5-5. Coomassie and western blot of the cysteine mutants of the CaM-His_6 construct.

ESI-MS of expressed CaM constructs. The cysteine mutants of the CaM-His_6 protein were also analyzed by mass spectrometry (Table 5-1) to confirm the identity of the isolated protein products. All eight of the expressed products matched the calculated molecular weights determine from the primary structures minus the N-terminal methionine due to methionine aminopeptidase activity in *E. coli.*

Table 5-1. Mass spectrometry of expressed CaM-His_6 mutants

CaM-His6 construct	ESI-MS (m/z) $[M+xH]^{x+}$ calcd	ESI-MS (m/z) $[M+xH]^{x+}$ found
Wild-type	1948.7 [M+9]	1948.1 [M+9]
	1753.9 [M+10]	1755.2 [M+10]
	1594.6 [M+11]	1593.8 [M+11]
E11C	1945.8 [M+9]	1945.1 [M+9]
	1751.3 [M+10]	1750.5 [M+10]
	1592.2 [M+11]	1591.4 [M+11]
S38C	1950.5 [M+9]	1950.2 [M+9]
	1755.5 [M+10]	1754.7 [M+10]
	1596.0 [M+11]	1595.3 [M+11]
M76C	1945.6 [M+9]	1944.9 [M+9]
	1751.1 [M+10]	1750.3 [M+10]
	1592.0 [M+11]	1591.3 [M+11]
E87C	1945.8 [M+9]	1945.3 [M+9]
	1751.3 [M+10]	1750.6 [M+10]
	1592.2 [M+11]	1593.4 [M+11]
N111C	1947.5 [M+9]	1946.7[M+9]
	1752.8 [M+10]	1752.2 [M+10]
	1593.6 [M+11]	1592.9 [M+11]
E114C	1945.8 [M+9]	1944.9 [M+9]
	1751.3 [M+10]	1752.7 [M+10]
	1592.2 [M+11]	1591.2 [M+11]
M145C	1945.6 [M+9]	1945.1 [M+9]
	1751.1 [M+10]	1751.5 [M+10]
	1592.0 [M+11]	1591.4 [M+11]

The protein masses were determined by ESI-MS on a Mariner electrospray mass spectrometer (PerSeptive Biosystems).

Fluorescent labeling and isolation of calmodulin cysteine mutants. The following procedure was performed on each of seven cysteine mutants of calmodulin (E11C, S38C, M76C, E87C, N111C, E114C, and M145C) as well as the wild-type, which served as a control to determine whether any of the labeling agents exhibited non-specific labeling under the selected reaction conditions. All eight of the calmodulin constructs were labeled separately with one of the nine fluorophores examined in this study [4-DMN derivatives **3-3** through **3-6**, 7-diethylamino-3-((((2-maleimidyl)ethyl)amino)carbonyl)coumarin (MDCC), *N,N'*-dimethyl-*N*-(iodoacetyl)-*N'*-(7-nitrobenz-2-oxa-1,3-diazol-4-yl)ethylenediamine (IANBD), 6-bromoacetyl-2-dimethylaminonaphthalene (BADAN), 5-((((2-iodoacetyl)amino)ethyl)amino)naphthalene-1-sulfonic acid (IAEDANS), and 1-(2-maleimidylethyl)-4-(5-(4-methoxyphenyl)oxazol-2-yl)pyridinium methanesulfonate (PyMPO)][15] to yield the seventy-two possible combinations. Following the expression and purification of each calmodulin mutant, the protein concentration was adjusted to 100 μM in TBS (pH 7.4) containing 1 mM of the reducing agent tris(2-carboxyethyl)phosphine (TCEP) and allowed to incubate at 4 °C overnight. The proteins were then analyzed by SDS-PAGE gel under non-reducing conditions to confirm that the cysteine mutants were in the fully reduced state. Aliquots of each protein (0.6 mL) were then transferred to clear 1.7 mL microcentrifuge tubes to which 6 μL of the respective cysteine labeling agent was added from a 100 mM stock solution in DMSO. The final concentration of the labeling agent in each reaction was 1 mM. The reaction mixtures were inverted 4-6 times immediately following the addition of the labeling agent and allowed to react overnight in the dark at 4 °C. The following day, the microcentrifuge tubes containing the reaction mixtures were spun at 16,000 g for 5 min at 4 °C to pellet any insoluble material before transferring the protein solutions to a 0.5 mL centrifugal filtering device (Millipore Ultrafree®-MC, Durapore PVDF

0.22 μm). The samples were spun again at 16,000 g for 5 min at 4 °C. The excess unreacted labeling agent in each reaction mixture was then removed using a 5 mL HiTrap™ desalting column obtained from GE Healthcare Life Sciences. The desalting columns were preequilibrated with TBS buffer (pH 7.4). The eluted fractions containing the labeled proteins were then quantified using the Bio-Rad protein assay where a stock solution of wild-type calmodulin of predetermined concentration was used to generate the standard curve. The labeling efficiency was determined by measuring the absorbance of the fluorophore for each construct at the corresponding wavelength of maximum absorption (λ_{max}). The calculated fluorophore concentration was then compared to the quantified protein concentration to compute the extent of protein labeling (Table 5-2).

Table 5-2. Labeling efficiencies obtained for each of the CaM-His_6 constructs

			Labeling ratio of CaM Mutants:							
Fluorophore:	**Abs_{max} (nm)**	**ε (cm^{-1} M^{-1})[a]**	**Wild-type**	**E11C**	**S38C**	**M76C**	**E87C**	**N111C**	**E114C**	**M145C**
3-3	440	8800	0.01	0.64	0.16	0.47	0.62	0.62	0.84	0.55
3-5	440	8800	0.04	0.85	0.41	0.61	0.70	0.78	0.84	0.50
3-4	440	8800	0.00	0.81	0.63	0.60	0.62	0.69	0.84	0.53
3-6	440	8800	0.00	0.72	0.67	0.60	0.60	0.65	0.79	0.67
MDCC	419	50000	0.00	0.42	0.35	0.30	0.28	0.25	0.31	0.21
IANBD	478	25000	0.01	0.56	0.18	0.46	0.47	0.43	0.52	0.31
BADAN	387	21000	0.01	0.53	0.31	0.43	0.43	0.42	0.48	0.31
IAEDANS	336	5700	0.00	0.30	0.25	0.27	0.39	0.32	0.52	0.30
PyMPO	412	23000	0.02	0.60	0.52	0.45	0.47	0.43	0.50	0.41

[a]The extinction coefficients of the commercial dyes were obtained from the suppliers (AnaSpec, Inc. and Molecular Probes®). The extinction coefficient for 4-DMN was determined using compound **3-13** as a standard (see Appendix section A-1).

Fluorescence studies of calmodulin mutants. Upon isolating the fluorescently labeled calmodulin constructs, stock solutions of each were prepared at 30 μM in TBS buffer (pH 7.4).

Stock solutions of $CaCl_2$ (2 mM), EDTA (5 mM), guanidine hydrochloride (8 M) and the M13 peptide[32] (1 mM) were also prepared in TBS buffer (pH 7.4) and filtered through a 0.2 μm Nalgene® cellulose acetate syringe filter prior to use. The fluorescence spectra of each construct was then measured in triplicate under five different conditions: 1) calmodulin construct only (5 μM); 2) calmodulin construct (5 μM) with $CaCl_2$ (200 μM); 3) calmodulin construct (5 μM) with $CaCl_2$ (200μM) plus M13 peptide (10 μM); 4) calmodulin construct (5 μM) with M13 peptide (10 μM); 5) calmodulin construct (5 μM) with guanidine hydrochloride (6.67 M). Additionally, each of these experimental conditions included 40 μM EDTA to ensure that no extraneous calcium, which may have been carried through the protein preparation, interfered with any of the fluorescence measurements. The samples were loaded in a 96 well black Polysorp Fluoronunc plate from NUNC™ and the fluorescence spectra were measured for each condition using a SPECTRAmax GEMINI XS plate reader from Molecular Devices. The total sample volume for each well was 200 μL. The excitation and emission settings selected for each construct are listed in Table 5-3.

Table 5-3. Emission and excitation settings for SPECTRAmax GEMINI XS plate reader

Fluorophore	exc (nm)	em (nm)
1-4	405	440-660
MDCC	400	430-650
IANBD	455	490-710
BADAN	365	400-620
IAEDANS	336	440-660
PyMPO	412	440-660

Denaturing of fluorescent CaM constructs to determine background emission. There exist two primary sources of background fluorescence directly associated with a solvatochromic fluorophore when used to develop a fluorescent protein probe. The first involves the intrinsic fluorescence exhibited by the fluorophore when fully solvated by water. The second is a ramification of appending the fluorophore to the surface of a globular protein. This frequently results in a change in the photophysical properties of the fluorophore that would be expected if it were participating in some type of non-specific interaction with the local topology of the attached protein. By denaturing the protein in a concentrated solution of guanidine hydrochloride, the secondary and tertiary structures that may contribute to this effect are disrupted permitting one to determine the degree of background emission generated (Figure 5-6).

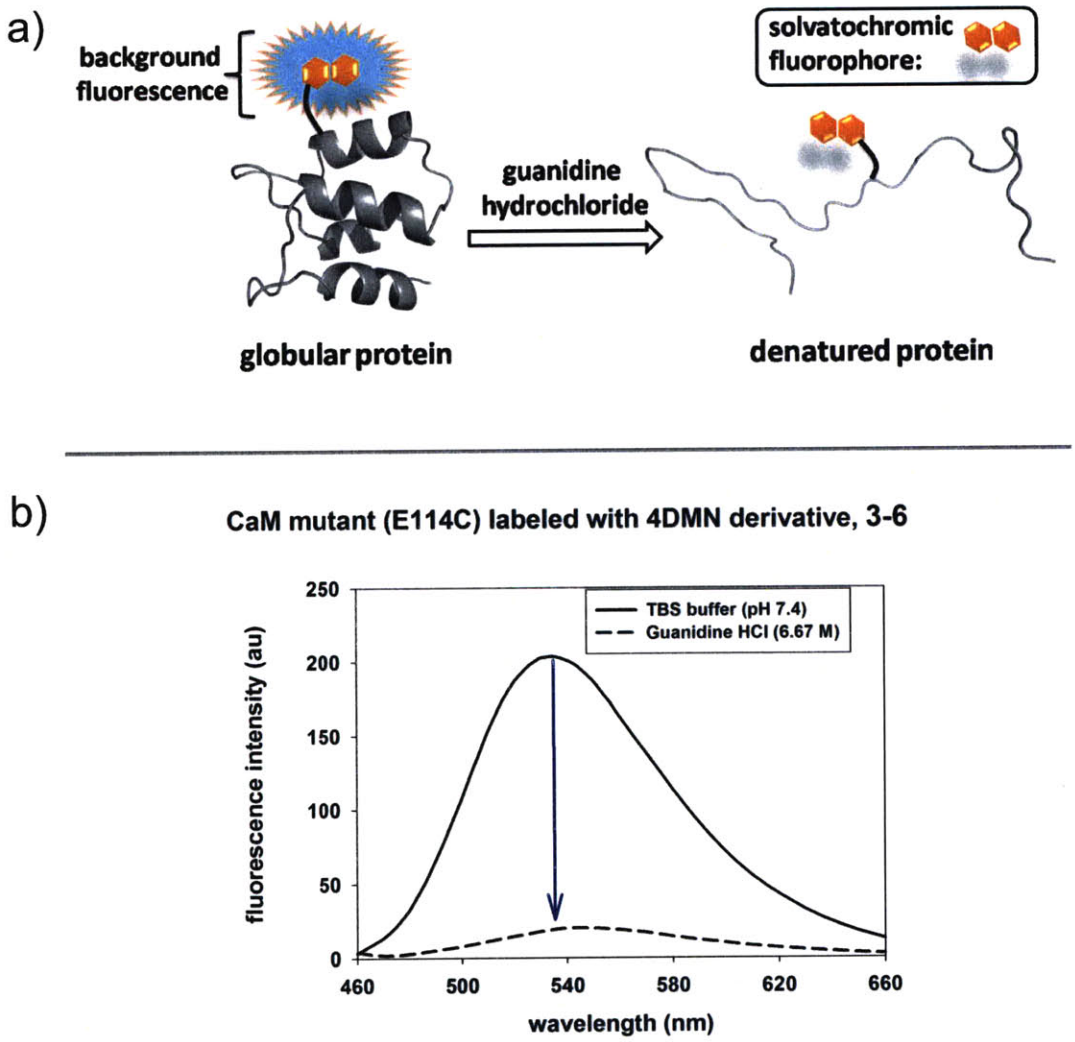

Figure 5-6. (a) Graphic depicting the tendency of solvatochromic fluorophore to exhibit background fluorescence when appended to a globular protein until denatured, thus fully exposing the fluorophore to the aqueous environment. (b) Example of a typical fluorescent response of a labeled CaM mutant under both natured and denatured conditions (TBS buffer versus guanidine hydrochloride solution at pH 7.4)

A series of experiments was conducted on each of the sixty-three fluorescent CaM constructs prepared in this study in which the degree of background fluorescence associated with the appending of the fluorophore to the protein was determine by measuring the emission spectra of the constructs in TBS buffer (pH 7.4) and guanidine hydrochloride (6.67 M, pH 7.4) and calculating the ratio of intensity at the wavelength of maximum emission in the natured state. The results of this work are displayed in Figure 5-7.

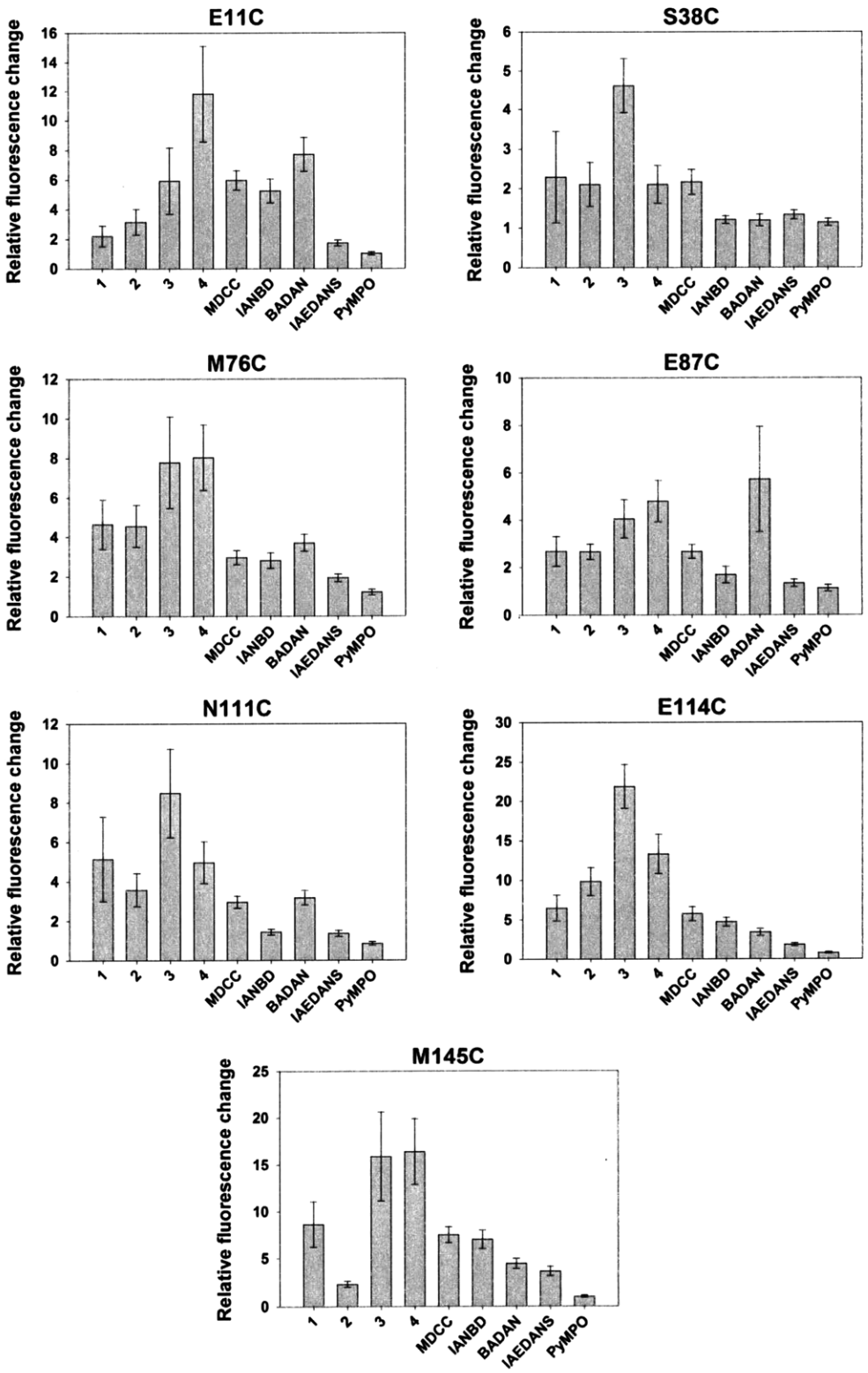

Figure 5-7. The fluorescent constructs were measured at a concentration of 5 μM in TBS buffer (pH 7.4) and guanidine hydrochloride (6.67 M, pH 7.4). The vertical bars represent the magnitude of the ratio of fluorescence in TBS buffer over that of the construct in the guanidine solution. A greater ratio indicates high initial background

fluorescence due to non-specific interactions of fluorophore with local features of the attached protein. Indicated errors represent the 90% confidence interval for three trials.

Fluorescence data for CaM mutants M76C, E87C, N111C, and E114C. The results of Figure 5-8 reflect the ratio of emission intensity of the CaM mutants under the three indicated conditions with respect to the apo-state. Measurements were made at the wavelength of maximum emission for the calcium bound state.

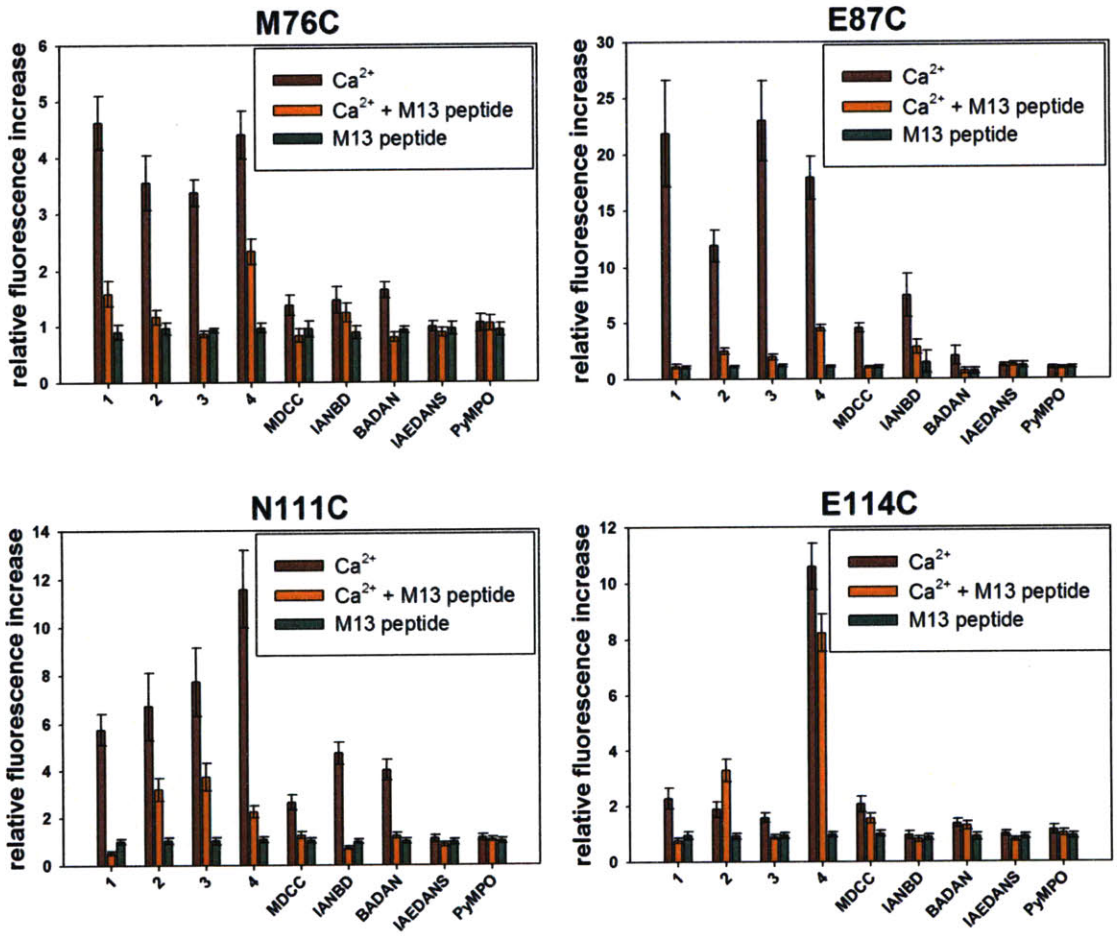

Figure 5-8. The fluorescent CaM constructs were maintained at a concentration of 5 μM for these measurements. The Ca^{2+} and M13 peptide were introduced at saturating levels of 200 μM and 10 μM respectively. Indicated errors represent the 90% confidence interval calculated from three trials.

Acknowledgments

This research was supported by NSF CHE-0414243 (BI), the NIH Cell Migration Consortium (GM064346), and the Biotechnology Training Program (T32-GM08334). I thank Dr. Matthieu Sainlos (MIT) for his helpful advice and insight. The Biophysical Instrumentation Facility for the Study of Complex Macromolecular Systems (NSF-0070319) is also gratefully acknowledged.

References

(1) Venkatraman, P.; Nguyen, T. T.; Sainlos, M.; Bilsel, O.; Chitta, S.; Imperiali, B.; Stern, L. J. Fluorogenic probes for monitoring peptide binding to class II MHC proteins in living cells. *Nat. Chem. Biol* **2007**, *3*, 222-228.

(2) Vazquez, M. E.; Nitz, M.; Stehn, J.; Yaffe, M. B.; Imperiali, B. Fluorescent caged phosphoserine peptides as probes to investigate phosphorylation-dependent protein associations. *J. Am. Chem. Soc.* **2003**, *125*, 10150-10151.

(3) Vazquez, M. E.; Blanco, J. B.; Imperiali, B. Photophysics and biological applications of the environment-sensitive fluorophore 6-*N,N*-dimethylamino-2,3-naphthalimide. *J. Am. Chem. Soc.* **2005**, *127*, 1300-1306.

(4) Wang, Q. Z.; Lawrence, D. S. Phosphorylation-driven protein-protein interactions: A protein kinase sensing system. *J. Am. Chem. Soc.* **2005**, *127*, 7684-7685.

(5) Enander, K.; Choulier, L.; Olsson, A. L.; Yushchenko, D. A.; Kanmert, D.; Klymchenko, A. S.; Demchenko, A. P.; Mely, Y.; Altschuh, D. A peptide-based, ratiometric biosensor construct for direct fluorescence detection of a protein analyte. *Bioconjug. Chem.* **2008**, *19*, 1864-1870.

(6) Loving, G.; Imperiali, B. A versatile amino acid analogue of the solvatochromic fluorophore 4-*N,N*-dimethylamino-1,8-naphthalimide: A powerful tool for the study of dynamic protein interactions. *J. Am. Chem. Soc.* **2008**, *130*, 13630-13638.

(7) Zhu, J. G.; Pei, D. H. A LuxP-based fluorescent sensor for bacterial autoinducer II. *ACS Chem. Biol.* **2008**, *3*, 110-119.

(8) Hibbs, R. E.; Talley, T. T.; Taylor, P. Acrylodan-conjugated cysteine side chains reveal conformational state and ligand site locations of the acetylcholine-binding protein. *J. Biol. Chem.* **2004**, *279*, 28483-28491.

(9) Cohen, B. E.; Pralle, A.; Yao, X. J.; Swaminath, G.; Gandhi, C. S.; Jan, Y. N.; Kobilka, B. K.; Isacoff, E. Y.; Jan, L. Y. A fluorescent probe designed for studying protein conformational change. *Proc. Natl. Acad. Sci. U.S.A.* **2005**, *102*, 965-970.

(10) Hahn, K.; Debiasio, R.; Taylor, D. L. Patterns of elevated free calcium and calmodulin activation in living cells. *Nature* **1992**, *359*, 736-738.

(11) Dattelbaum, J. D.; Looger, L. L.; Benson, D. E.; Sali, K. M.; Thompson, R. B.; Hellinga, H. W. Analysis of allosteric signal transduction mechanisms in an engineered fluorescent maltose biosensor. *Protein Sci.* **2005**, *14*, 284-291.

(12) SchauerVukasinovic, V.; Cullen, L.; Daunert, S. Rational design of a calcium sensing system based on induced conformational changes of calmodulin. *J. Am. Chem. Soc.* **1997**, *119*, 11102-11103.
(13) Post, P. L.; Trybus, K. M.; Taylor, D. L. A genetically-engineered, protein-based optical biosensor of myosin-II regulatory light-chain phosphorylation. *J. Biol. Chem.* **1994**, *269*, 12880-12887.
(14) Cassidy, P. B.; Dolence, J. M.; Poulter, C. D. Continuous fluorescence assay for protein prenyltransferases. *Meth. Enzymol.* **1995**, *250*, 30-43.
(15) Haugland, R. P.; Spence, M. T. Z.; Johnson, I. D.; Basey, A. *The handbook : a guide to fluorescent probes and labeling technologies*; 10th ed.; Molecular Probes: Eugene, OR, 2005.
(16) Vogel, S. S.; Thaler, C.; Koushik, S. V. Fanciful FRET. *Sci. STKE* **2006**, *2006*, re2.
(17) Goulko, A. A.; Zhao, Q.; Guthrie, J. W.; Zou, H.; Le, X. C. In *Springer Series on Fluorescence*; 1st ed.; Wolfbeis, O. S., Ed.; Springer: New York, 2008; Vol. 5, p 303-322.
(18) Vazquez, M. E.; Rothman, D. M.; Imperiali, B. A new environment-sensitive fluorescent amino acid for Fmoc-based solid phase peptide synthesis. *Org. Biomol. Chem.* **2004**, *2*, 1965-1966.
(19) Sainlos, M.; Iskenderian, W. S.; Imperiali, B. A General screening strategy for peptide-based fluorogenic ligands: probes for dynamic studies of PDZ domain-mediated interactions. *J. Am. Chem. Soc.* **2009**, *131*, 6680-6682.
(20) Hill, D. J.; Mio, M. J.; Prince, R. B.; Hughes, T. S.; Moore, J. S. A field guide to foldamers. *Chem. Rev.* **2001**, *101*, 3893-4011.
(21) Crivici, A.; Ikura, M. Molecular and structural basis of target recognition by calmodulin. *Annu. Rev. Biophys. Biomol. Struct.* **1995**, *24*, 85-116.
(22) Berridge, M. J.; Bootman, M. D.; Roderick, H. L. Calcium signalling: dynamics, homeostasis and remodelling. *Nat. Rev. Mol. Cell Biol.* **2003**, *4*, 517-529.
(23) Yap, K. L.; Kim, J.; Truong, K.; Sherman, M.; Yuan, T.; Ikura, M. Calmodulin target database. *J. Struct. Funct. Genomics* **2000**, *1*, 8-14.
(24) Torok, K.; Trentham, D. R. Mechanism of 2-chloro-(epsilon-amino-Lys75)-[6-[4-(N,N-diethylamino)phenyl]-1,3,5-triazin-4-yl]calmodulin interactions with smooth muscle myosin light chain kinase and derived peptides. *Biochemistry* **1994**, *33*, 12807-12820.
(25) Milikan, J. M.; Bolsover, S. R. Use of fluorescently labelled calmodulins as tools to measure subcellular calmodulin activation in living dorsal root ganglion cells. *Pflugers Arch.* **2000**, *439*, 394-400.
(26) Olwin, B. B.; Storm, D. R. Preparation of fluorescent labeled calmodulins. *Meth. Enzymol.* **1983**, *102*, 148-157.
(27) Nakanishi, J.; Nakajima, T.; Sato, M.; Ozawa, T.; Tohda, K.; Umezawa, Y. Imaging of conformational changes of proteins with a new environment/sensitive fluorescent probe designed for site specific labeling of recombinant proteins in live cells. *Anal. Chem.* **2001**, *73*, 2920-2928.
(28) Hahn, K. M.; Waggoner, A. S.; Taylor, D. L. A calcium-sensitive fluorescent analog of calmodulin based on a novel calmodulin-binding fluorophore. *J. Biol. Chem.* **1990**, *265*, 20335-20345.
(29) Zhang, M.; Tanaka, T.; Ikura, M. Calcium-induced conformational transition revealed by the solution structure of apo calmodulin. *Nat. Struct. Biol.* **1995**, *2*, 758-767.

(30) Rupp, B.; Marshak, D. R.; Parkin, S. Crystallization and preliminary X-ray analysis of two new crystal forms of calmodulin. *Acta Crystallogr. D Biol. Crystallogr* **1996**, *52*, 411-413.
(31) Ikura, M.; Clore, G. M.; Gronenborn, A. M.; Zhu, G.; Klee, C. B.; Bax, A. Solution structure of a calmodulin-target peptide complex by multidimensional NMR. *Science* **1992**, *256*, 632-638.
(32) Blumenthal, D. K.; Takio, K.; Edelman, A. M.; Charbonneau, H.; Titani, K.; Walsh, K. A.; Krebs, E. G. Identification of the calmodulin-binding domain of skeletal muscle myosin light chain kinase. *Proc. Natl. Acad. Sci. U.S.A.* **1985**, *82*, 3187-3191.
(33) For the fluorescent constructs of the M145C CaM mutant, all fluorescence measurements were made at the wavelength of maximum emission for the Ca^{2+}-CaM-M13 peptide complex instead of the of the Ca^{2+}-CaM complex since this state generally exhibited greater emission intensity.
(34) Savalli, N.; Kondratiev, A.; Toro, L.; Olcese, R. Voltage-dependent conformational changes in human Ca(2+)- and voltage-activated K(+) channel, revealed by voltage-clamp fluorometry. *Proc. Natl. Acad. Sci. U.S.A* **2006**, *103*, 12619-12624.
(35) We have observed similar effects in our work with SH2 domains, PDZ domains and the regulatory light-chain of myosin.
(36) Chan, W. C.; White, P. D. *Fmoc solid phase peptide synthesis: a practical approach*; Oxford University Press: New York, 2000.
(37) Hancock, W. S.; Battersby, J. E. New micro-test for detection of incomplete coupling reactions in solid-phase peptide-synthesis using 2,4,6-trinitrobenzene-sulphonic acid. *Anal. Biochem.* **1976**, *71*, 260-264.
(38) Hachmann, J.; Lebl, M. Alternative to piperidine in Fmoc solid-phase synthesis. *J. Comb. Chem.* **2006**, *8*, 149-149.

Chapter 6: Development of a fluorogenic sensor of Cdc42 activity

The work described in this chapter was performed in close collaboration with fellow colleague Brenda Goguen from the Imperiali laboratory.

Introduction

The emergence of complex cellular behavior through fundamental biomolecular interactions has come to represent a basic tenet of cell biology. The normal growth and development of a living cell requires it to continually receive information from the immediate environment and respond appropriately. This process often occurs through an elaborate network of molecular events involving specific proteins capable of assuming multiple signaling states. The state of a protein involved in a particular signal transduction pathway may be defined by various forms of posttranslational modification such as phosphorylation. However, structural changes can also play an important role. Due to the essential functions of these proteins, pathologies often result in instances where normal activity is impaired or defective. Hence, methods to interrogate the activities of such regulatory elements are highly sought after.

The protein Cdc42 is a small guanosine triphosphatase (GTPase) that is a member of the Rho-family of GTPases.[1] This family of proteins plays an important role in regulating the dynamics that underlie many cellular processes including cytokinesis, vesicle trafficking, cell migration, and morphogenesis.[2,3] Many of these activities involve the integration of various extracellular signals relayed though specialized membrane receptors and transmitted through intracellular signal transduction pathways. These pathways then converge to activate Rho-GTPases like Cdc42, which are then responsible for coordinating the reorganization of the actin cytoskeleton.[1]

Like other GTPases, Cdc42 can exist in two different states: a GTP-bound complex and a GDP-bound complex. The operative state is the Cdc42-GTP complex, which is capable of binding certain effector proteins. The Cdc42-GDP complex is typically inactive. The exchange of a GDP molecule for GTP induces an allosteric change in Cdc42 that can lead to a 1000-fold

increase in affinity for the GTPase-binding domains (GBDs) of some effector proteins.[4] It has been shown that the GBDs of many effector proteins exert an autoinhibitory effect that may be abated upon binding to Cdc42-GTP.[5] Since a number of these effectors are protein kinases, the binding of Cdc42 activates the catalytic activity of these enzymes.

There are several proteins that are known to regulate the activation and localization of Cdc42. These include guanine nucleotide exchange factors (GEFs), GTPase activating proteins (GAPs), and GDP dissociation inhibitors (GDIs).[3] Additionally, Cdc42 is subject to various forms of post-translational modification such as prenylation and phosphorylation.[6] The activation of Cdc42 is tightly regulated, both spatially and temporally, through the opposing functions of GEFs and GAPs (Figure 6-1). Rho-GTPases are intrinsically slow at promoting GTP hydrolysis to GDP. Likewise, the exchange rate of a GDP molecule for a GTP molecule is also slow.[3] These two processes are facilitated by GEF and GAP activity. The GEF "switches" Cdc42 to the active state by catalyzing the displacement of a bound GDP with GTP, thus inducing the necessary structural change required for the protein to bind its effectors. GAPs compete kinetically with GEFs to promote hydrolysis of the Cdc42-bound GTP molecule in order to reverse this effect.[3] Therefore, the existence of Cdc42 in the operative state can be extremely transient, requiring an effector protein to be in close proximity in order to intercept the Cdc42-GTP complex and become activated.

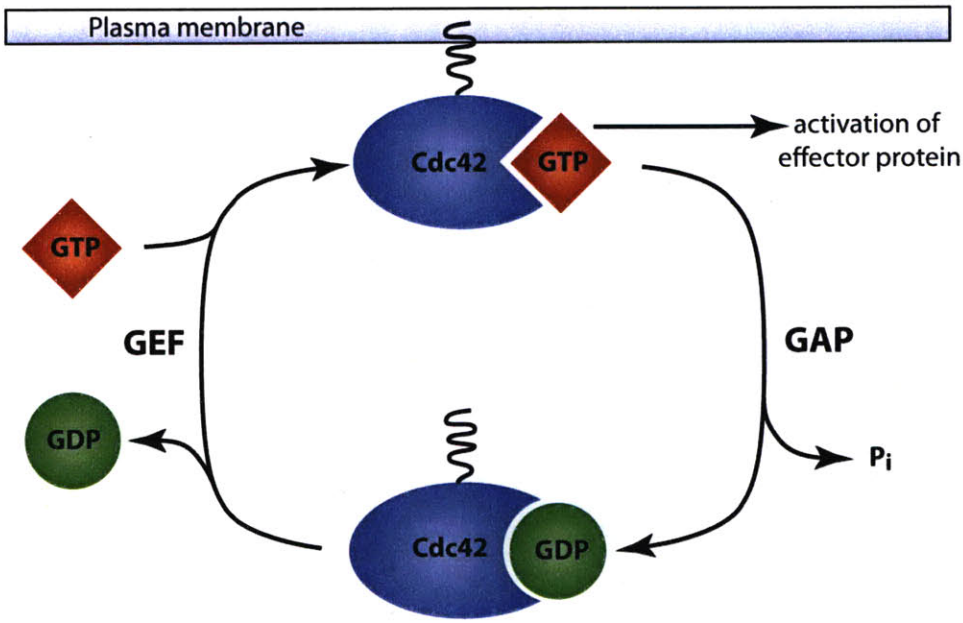

Figure 6-1. Regulation of Cdc42 activity by guanine nucleotide exchange factors (GEFs) and GTPase activating proteins (GAPs).

An additional level of Cdc42 regulation is imposed by GDIs.[3] These proteins can bind the Cdc42-GDP complex and block GEF activity. GDIs are also capable of solubilizing prenylated Cdc42 and sequestering it from the plasma membrane. The interaction of GDIs with Rho-GTPases is further regulated through the actions of GDI displacement factors (GDFs)[3] and by direct phosphorylation of the GTPases.[6]

Studies of the subcellular localization of Cdc42 have shown that much of the protein is concentrated at the Golgi apparatus.[7] The presence of the protein has also been detected at the plasma membrane as well as various vesicular structures within the cytosol.[8] However, the abundance of Cdc42 within a localized region of a cell does not necessarily imply that this is where the protein is most active. In order to determine the regions within the cell that GEF-mediated activation of Cdc42 occurs during fibroblast adhesion and spreading, researchers of the Hahn laboratory developed a new fluorescent biosensor.[9] In 2004, a report by Nalbant *et al.*[9] described the design of small peptide motif derived from the Cdc42-binding domain of the

protein WASP that was labeled with a fluorescent merocyanine derivative called I-SO[10] (Figure 6-2). The probe, named MeroCBD, was demonstrated to respond selectively to the presence of Cdc42-GTP over that of the Cdc42-GDP complex by exhibiting an overall 2.8-fold increase in fluorescence intensity.

The GTPase-binding domain of many Cdc42 effectors is a highly conserved sequence of residues known as the CRIB (Cdc42- and Rac-Interactive Binding) motif.[11] In designing MeroCBD, researchers in the Hahn laboratory utilized an available NMR structure of the complex between Cdc42 and the CRIB motif of the protein WASP (PDB entry 1CEE)[12] to identify potential residues of the peptide sequence that could be replaced by a cysteine for covalent modification with I-SO. They selected three residues (I223, D264, and F271 of WASP) for mutagenesis. The constructs were expressed in *E. coli* and purified using a C-terminal hexahistidine tag before labeling with the solvatochromic dye. The emission spectrum of each construct was then examined in the presence of Cdc42-GDP and Cdc42-GTPγS[13] in order to determine whether the two states could be distinguished by a measurable difference in fluorescence intensity. Based on their evaluation, the I-SO labeled construct of the F271C mutant yielded the best result.

Further characterization of the probe showed that it was a highly selective sensor capable of discriminating between the activation of Cdc42 and that of closely related GTPases such as RhoA and Rac. The probe was then deployed to detect the kinetics of Cdc42 activation in fMetLeuPhe (fMLP) peptide-stimulated human neutrophil lysates. A variant of the probe design, which included an enhanced green fluorescent protein (EGFP), was also used as a ratiometric sensor of endogenous Cdc42 activity in MEF/3T3 fibroblasts.[9]

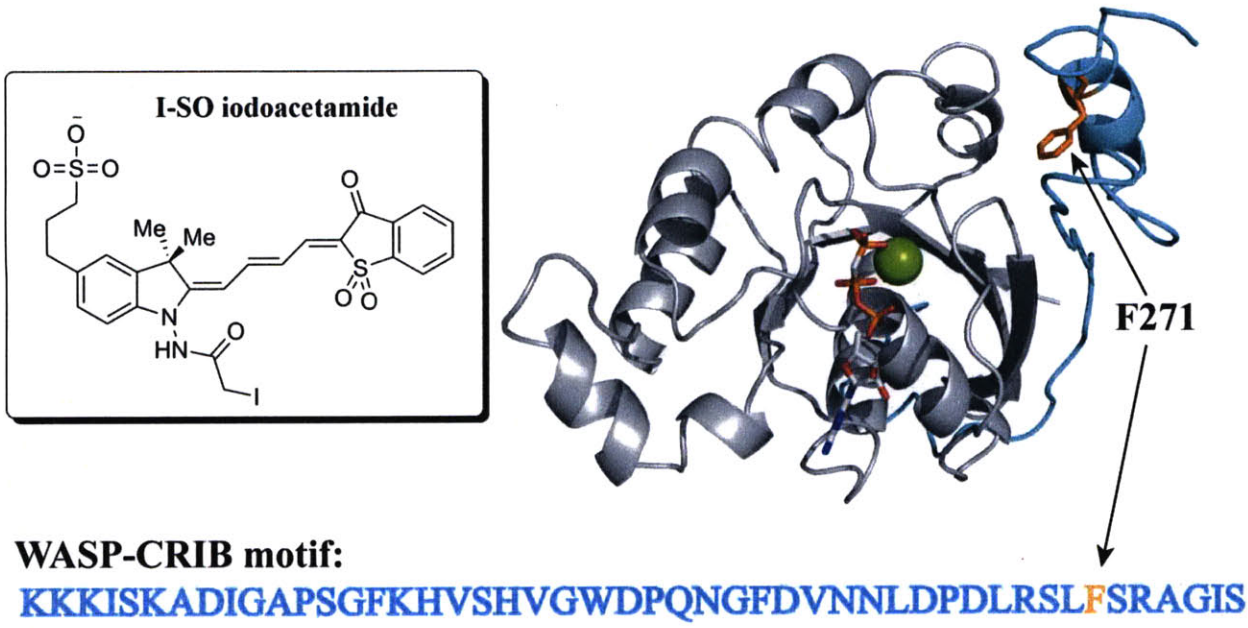

Figure 6-2. Cdc42-GTPPCP (grey) complex with WASP CRIB motif (cyan).[12] The sequence for the WASP CRIB motif is indicated below the structure with the single-letter notation for amino acids. The phenylalanine residue F271 (gold) that was selected by Nalbant *et al.* as the site for cysteine mutagenesis and labeling with I-SO iodoacetamide is indicated by the two arrows.

This chapter describes recent work, performed in collaboration with fellow colleague Brenda Goguen, to develop a second-generation Cdc42 biosensor based on the original design described by Nalbant *et al.* Athough MeroCBD was shown to be an effective probe, it was limited by small changes in fluorescence intensity and by the fact that its affinity for Cdc42 was determined to be roughly 2-fold weaker than that of the wild-type WASP CRIB motif. In response, we conjectured that the fluorescent derivatives of 4-DMN described in the previous chapters might prove valuable for overcoming both of these issues. The superb "switch-like" fluorescence properties and discrete size of the 4-DMNA amino acid make it an excellent candidate for incorporation at position 271 of the WASP CRIB peptide. Two approaches to the design of this sensor are currently under investigation. The first involves the chemical modification of a WASP CRIB F271C mutant peptide using the 4-DMN thiol-reactive agents (**3-**

3 through **3-6**), while the second entails the introduction of the 4-DMNA amino acid via semisynthesis and expressed protein ligation (EPL). At present, much of the work in this project area has focused on the former of these two approaches with the preliminary results shown here.

Results and Discussion

6-1. Design considerations for a second-generation Cdc42 biosensor

The CRIB motif of Wiskott-Aldrich syndrome protein (WASP) binds with high affinity ($K_d = 77 \pm 9$ nM)[9] to Cdc42-GTP. This interaction activates WASP allowing it to then activate the Arp2/3 complex, which is responsible for initiating the polymerization of actin filaments.[11] Based on the success of the fluorescent MeroCBD probe, we decided to focus on the same site (F271) of the WASP CRIB domain for the incorporation of the 4-DMN fluorophore. The NMR structure of this complex (Figure 6-2) shows that a prominent hydrophobic contact is formed between the side chain of F271 and residues V36, F37, L67, and L70 of Cdc42. A similar contact involving a tryptophan residue is revealed in the crystal structure of Cdc42-GTPPCP bound to the CRIB domain of human P21-activated kinase 6 (Pak6) (Figure 6-3a). This information, in combination with the fact that the MeroCBD probe exhibits weaker affinity for Cdc42 compared to wild-type WASP,[9] led us to reason that this interaction is potentially important and may be preserved by substituting the smaller 4-DMNA amino acid at position 271 (Figure 6-3b) instead of the larger I-SO dye.

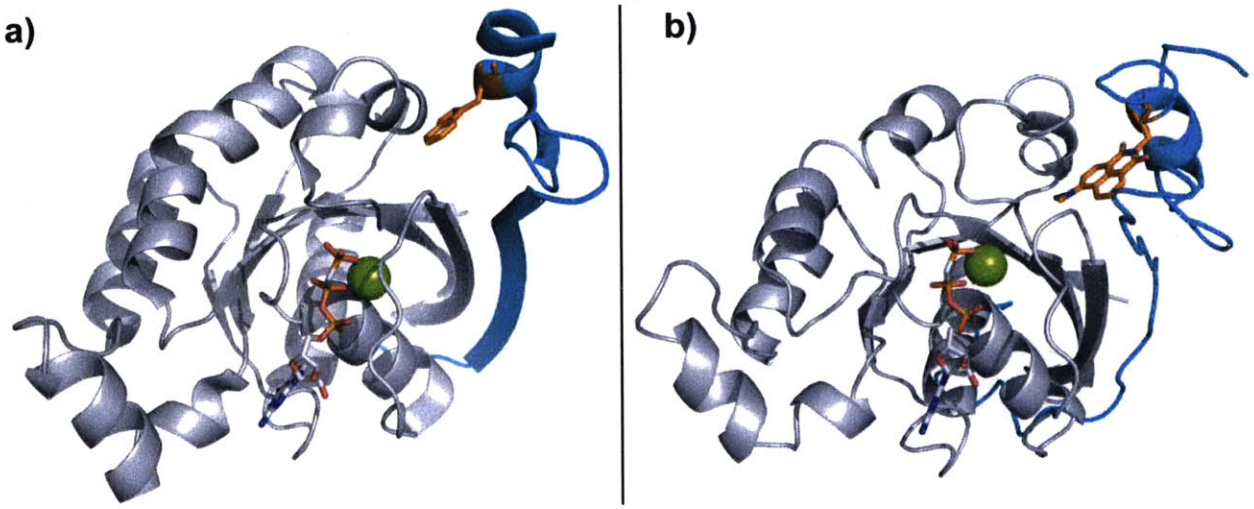

Figure 6-3. (a) Crystal structure of Cdc42-GTPPCP (grey) with the CRIB domain of Pak6 (cyan) (PDB entry 2ODB). The Trp40 residue of Pak6 is indicated in gold. (b) The NMR structure of Cdc42-GTPPCP (grey) in complex with the WASP CRIB domain (cyan) (PDB entry 1CEE). The phenylalanine residue at position 271 of the WASP CRIB domain is replaced with 4-DMNA to illustrate how the mutant construct might interact with activated Cdc42.

In addition to developing a fluorogenic probe that utilizes the advantageous properties of the 4-DMNA amino acid, we also elected to use the 4-DMN thiol-modifying agents described in Chapters 3 and 5 to label an F271C mutant of the WASP CRIB motif. Here, the MeroCBD probe provides an additional benchmark for evaluating the efficacy of these new fluorescent tools. The two probe designs are illustrated in Figure 6-4.

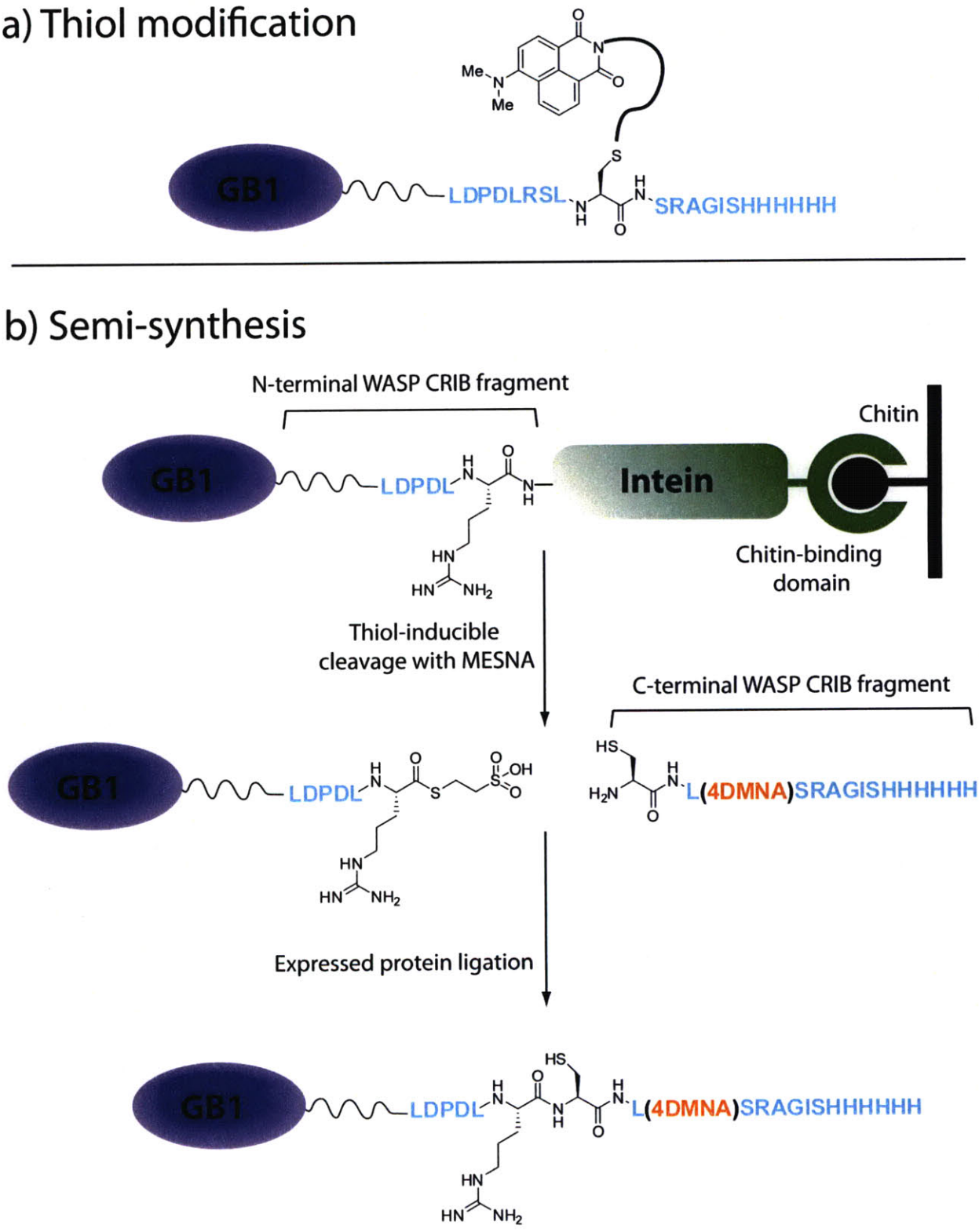

Figure 6-4. Fluorescent biosensors of Cdc42 activation derived from a GB1 fusion of the WASP CRIB domain (cyan). The GB1 domain (purple) is a 55 amino acid sequence that enhances expression, solubility, and stability of small protein motifs.[14] (a) A 4-DMN modified F271C mutant of the GB1-WASP CRIB domain. (b) The 4-DMNA amino acid (gold) is incorporated into a synthetic peptide bearing an N-terminal cysteine residue. The N-terminal

fragment of the sensor is prepared as a thioester by expressing it as a fusion with a modified intein that bears a chitin-binding domain on the C-terminus. The N-terminal fragment is then liberated from the intein through thiol-inducible cleavage using MESNA. The expressed N-terminal thioester is then ligated to the synthetic C-terminal peptide via a reversible transthioesterification step, followed by an irreversible intramolecular S→N acyl transfer resulting in the formation of an amide bond.

The probe design displayed in Figure 6-4a can be prepared in a straightforward manner through direct chemical modification of a cysteine side chain with one of the thiol-reactive 4-DMN derivatives (**3-3** through **3-6**). Both constructs in Figure 6-4 were designed to include a GB1 domain located at the N-terminus of the sensor. The GB1 domain is a 55 amino acid sequence that has been shown to enhance expression and solubility of small protein motifs.[14] Based on prior experience in the Imperiali laboratory, this domain has been found to be extremely useful for applications of this type.

The alternative probe design is illustrated in Figure 6-4b. Here the 4-DMNA amino acid is incorporated directly into the peptide backbone of the WASP CRIB domain at position 271. This would be achieved using a method known as expressed protein ligation (EPL).[15-17] With this approach, the N-terminal fragment of the construct is expressed as a fusion with a modified intein that contains a chitin-binding domain at the C-terminus. Following expression of the protein in *E. coli*, the product is isolated by binding to chitin resin. The target protein fragment is then liberated from the intein as a reactive thioester through a thiol-induced cleavage reaction using sodium 2-mercaptoethane sulfonate (MESNA). The C-terminal fragment of the construct is prepared synthetically via solid phase peptide synthesis. Once the two fragments are obtained, the next step is the ligation reaction, which begins with a reversible transthioesterification step followed by an irreversible intramolecular S→N acyl transfer resulting in the formation of an amide bond. Here, we designed the final product such that it contains a hexahistidine tag to help facilitate purification.

6-2. Development and validation of a fluorogenic Cdc42 sensor based on the fluorescence properties of the 4-DMN dye

(The experiments and associated results described herein represent the work of fellow colleague Brenda Goguen).

In developing a new Cdc42 sensor based on the design shown in Figure 6-4a, each the of 4-DMN thiol-labeling agents (**3-3** through **3-6**) was screened to determine which could produce the greatest fluorescence change. For this experiment, four fluorescent constructs of the GB1-WASP CRIB (F271C) mutant were prepared. The fluorescent constructs were then examined at the same concentration (1 μM) under the three conditions shown in Figure 6-5. The results illustrate that although some of the constructs produce a much brighter signal in the presence of Cdc42-GTPγS, the ratio of fluorescence intensity between the GTPγS-bound state versus the GDP-bound state is uncorrelated. Since the construct labeled with compound **3-3** exhibited the largest overall enhancement in fluorescence (8.5-fold), it was used in the remaining experiments.

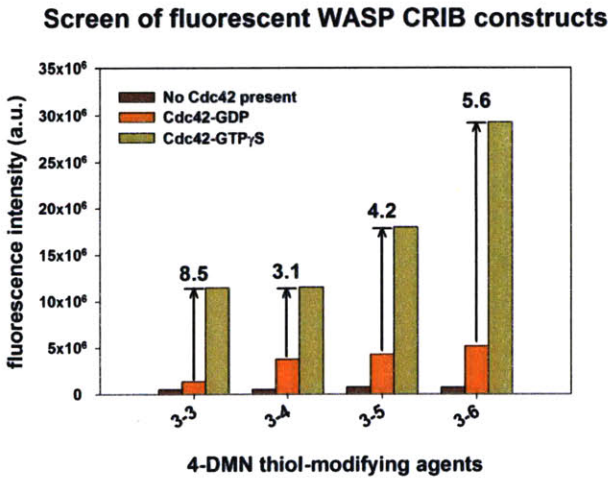

Figure 6-5. Screen for second-generation Cdc42 biosensor. The histograms represent the fluorescence intensity measured for each construct GB1-WASP CRIB (F271C) mutant labeled with one of the four 4-DMN thiol-labeling agents (**3-3** through **3-6**). The emission intensities were measured at the wavelength of maximum emission in the presence of the Cdc42-GTPγS complex. The concentration of the fluorescent constructs in these experiments was 1 μM and Cdc42 was 5 μM when present.

Although the fluorescent response of the WASP construct labeled with **3-3** was an improvement over the 2.8-fold fluorescence increase reported for the MeroCBD probe, it was still minor compared to the potential of the 4-DMN fluorophore. It was determined that this was due primarily to the fact that the experiment was conducted at concentrations of the WASP construct and Cdc42 that far exceed the native K_d value for the WASP-Cdc42-GTP complex (77 ± 9 nM).[9] Since WASP is capable of binding the Cdc42-GDP complex with a K_d value of roughly 35 μM,[12] then it was estimated that as much as 11% of the fluorescent sensor could have been bound resulting in an artificially high emission intensity. To test this hypothesis, the concentrations of the biosensor and Cdc42 were reduced to determine whether the ratio of fluorescence intensity could be increased (Figure 6-6). Here, the biosensor was maintained at 100 nM, while Cdc42, in the GDP- and GTPγS-bound forms, was introduced at 2 μM. At these concentrations, the percentage of fluorescent biosensor predicted to be bound to Cdc42-GTPγS versus Cdc42-GDP should be approximately 96% and 5%, respectively. This is confirmed by the data shown in Figure 6-6, where the measured ratio of fluorescence intensity now exceeds 20-fold. Future experiments will reveal whether the ratio can further be improved by using more physiologically relevant concentrations that are closer to the K_d of the WASP-Cdc42-GTP complex.

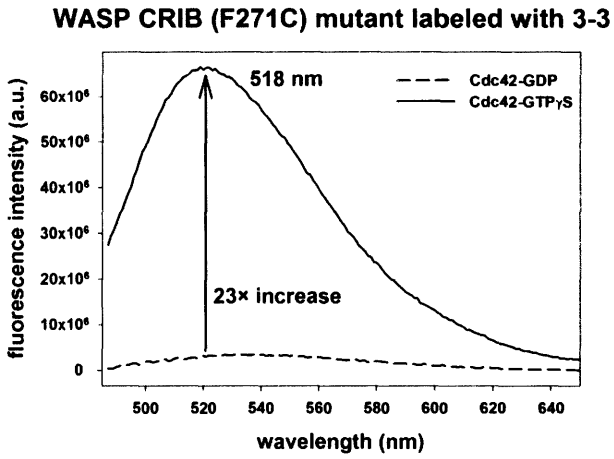

Figure 6-6. Fluorescence spectra of the WASP CRIB (F271C) mutant labeled with compound **3-3**. The biosensor in this experiment is maintained at 100 nM and the Cdc42 protein, in both the GDP- and GTPγS-bound forms, is introduced at 2 μM.

In order to validate the selectivity of the fluorescent biosensor derived from the WASP CRIB domain, a series of control experiments were performed. A double mutant of the CRIB domain (H246D, H249D) that abrogates binding to Cdc42 was prepared. Additionally, a Cdc42 mutation (Q61L) that renders the protein constitutively active was also prepared. For ease of discussion, these two constructs are referred to as the CRIB mutant and Cdc42(Q61C), respectively. The CRIB wild-type and CRIB mutant domains were examined in combination with the Cdc42 wild-type and Cdc42(Q61C) mutant. The Cdc42 constructs were preincubated with saturating concentrations of either GDP or GTPγS. In all, a total of eight experiments were conduct and the results shown in Figure 6-7.

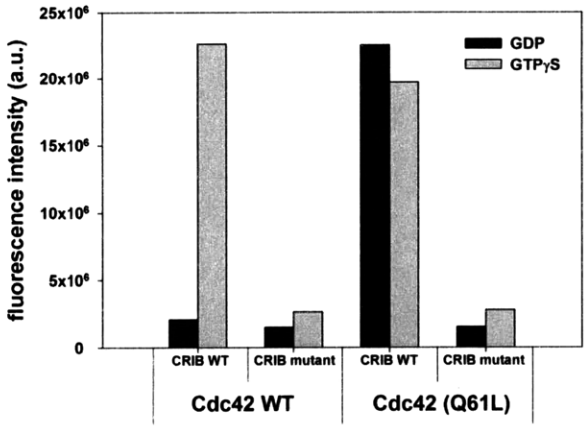

Figure 6-7. Control experiments of the WASP CRIB biosensor labeled with compound **3-3**. The CRIB WT and mutant constructs are maintained at 500 nM while the Cdc42 wild-type and Q61L mutant are introduced at 5 μM. The fluorescence measurements were made at 518 nm.

The results of this series of experiments agree strongly with the predicted outcomes. The CRIB mutant shows relatively little change in response to the nucleotide-bound state of Cdc42. Only the wild-type CRIB is capable of responding. Furthermore, the wild-type CRIB shows little ability to discriminate between Cdc42(Q61L) that was preincubated with GDP versus that which was preincubated with GTPγS.

Conclusions

Preliminary work with the Cdc42 sensor described in section 6-2 has revealed the great potential of this design and the power of the 4-DMN derivates to produce large changes in fluorescence intensity — particularly when used in the study of biomolecular interactions. Future investigations will examine the affinity of this biosensor for Cdc42-GTP to determine whether the presence of the fluorophore disrupts binding in any way. Furthermore, efforts will continue to focus on the incorporation of the 4-DMNA amino acid at position 271 of the WASP CRIB domain in order to see if further improvements in the fluorescent response can be attained.

If successful, this work could lay the foundation for the development of a new array of fluorescent sensors of other known GTPases.

The key focus of this thesis has been to develop new fluorescent tools capable of operating in complex cellular environments and the method for incorporating them into proteins. The criteria for meeting such challenges are numerous and demanding. In Chapters 2 and 4, it was shown that the 4-DMN fluorophore exhibits significantly enhanced chemical stability while retaining many of the excellent photophysical properties that are characteristic of the dimethylaminophthalimide family. This opens the door to exploring new applications that were previously inaccessible using the 4-DMAP and 6-DMN fluorophores. Chapters 4 and 5 demonstrated two distinctly different approaches in which the power the 4-DMN dye may be utilized to obtain valuable information regarding the dynamics of biomolecular interactions. The 4-DMNA amino acid offers the advantage of smallness with a size comparable to that of the natural amino acid tryptophan. Alternatively, the 4-DMN thiol-modifying agents provide a convenient method for the incorporation of the fluorophore into proteins and other important biomolecules. Work toward the validation of these tools in the previous chapters has facilitated our understanding of contexts in which they may best be applied and influenced the design of improved sensors, such as that described in this chapter, which we anticipate will be of great value in future cellular studies.

Experimental

Tris-buffered saline. All fluorescence experiments were conducted in the following buffer system:

1× TBS (pH 7.9)

1 mM	dithiothreitol (DTT)
50 mM	Tris-HCl
50 mM	NaCl
5 mM	$MgCl_2$

Nucleotide exchange protocol. In order to prepare the purified Cdc42 protein in the GDP-bound or GTPγS-bound state, the protein was initially incubated at a concentration of 100 μM in the presence of EDTA (25 mM) and the corresponding GDP or GTPγS nucleotide (1 mM) for 30 minutes at 30 °C. After this period, $MgCl_2$ was added to a final concentration of 35 mM and incubated an addition 15 minutes at room temperature.

Fluorescence experiments:

Screening of the 4-DMN thiol-reactive agents. After isolating the GB1-WASP CRIB F217C mutant and labeling it with each of the four 4-DMN thiol-modifying agents (**3-3** through **3-6**), the fluorescent constructs were screened to determine which produced the largest fluorescent change in response to the presence of Cdc42-GTPγS compared to Cdc42-GDP. The constructs were adjusted to a final concentration of 1 μM and Cdc42 was 5 μM. The excitation wavelength selected for these experiments was 408 nm with the slit width of the light source set at 5 nm. The emission spectrum of each construct was collected from 450-650 nm under both conditions.

Comparison of GB1-WASP CRIB F217C(3-3) fluorescence at 100 nM in presence of Cdc42-GDP vs. Cdc42-GTPγS. In order to reduce the amount of background fluorescence produced by nucleotide-independent binding of the GB-WASP CRIB biosensor to Cdc42, the concentration of both components were reduced. The fluorescent GB1-WASP CRIB domain was maintained at 100 nM for the two examined conditions. Cdc42-GDP and Cdc-GTPγS were then introduced at 2 μM. The excitation wavelength selected for these measurements was 435 nm. The emission spectra were collected from 450-650 nm. The ratio of fluorescence intensity for the two conditions was calculated at the wavelength of maximum emission for the complex of GB1-WASP CRIB with Cdc42-GTPγS.

Control studies with of GB1-WASP CRIB and Cdc42 mutants. For this set of experiments, two sets of fluorescently labeled GB1-WASP CRIB constructs were used. Both possessed the F271C mutation for modification with the 4-DMN derivative **3-3**; however, one also contained a second pair of mutations (H246D and H249D) to prevent it from interacting with Cdc42. These two constructs are referred to as the CRIB wild-type and the CRIB mutant for simplicity. Two Cdc42 constructs were also used in these experiments. One was the wild-type and the other contains a Q61L mutation that renders the construct constitutively active. All four combinations of the two GB1-WASP CRIB constructs and two Cdc42 constructs were examined in the presence of saturating GDP as well as GTPγS. The final concentrations of GB1-WASP CRIB constructs and Cdc42 mutants used in the experiments were 500 nM and 5 μM, respectively. The samples were excited at 435 nm and the emission spectra collected from 450-650 nm. The slit width of the light source was set to 10 nm.

Cloning of WASP CRIB and Cdc42 constructs:

GB1-WASP CRIB gene sequence. The following gene sequence was synthesized by Bio Basic Inc. and delivered in a pUC-57 vector. The construct was codon-optimized for expression in *E. coli*. The coding region begins at the first ATG (**bold**) that appears in the sequence.

```
TATACCATGGGTCAGTATAAACTGGCACTGAACGGTAAAACTCTGAAAGGTGAAACCACCACCGA
GGCTGTAGACGCGGCTACCGCCGAAAAAGTGTTTAAACAATACGCCAACGATAACGGCGTGGATG
GTGAATGGACTTACGACGATGCGACGAAAACCTTCACTGTCACCGAAAAGAAAAAGATCTCCAAA
GCTGACATCGGTGCGCCAAGCGGCTTCAAACACGTTTCTCACGTTGGTTGGGACCCTCAGAACGG
CTTCGACGTTAATAACCTGGATCCGGATCTGCGCTCTCTGTGCTCTCGTGCAGGCATTTCCCACC
ACCACCATCATCACTAACTCGAG
```

GB1-WASP CRIB amino acid sequence. The following is the translated gene product. The highlighted region indicates the residues of the GB1 domain and the cysteine at position 271 is shown in bold face.

```
MGQYKLALNGKTLKGETTTEAVDAATAEKVFKQYANDNGVDGEWTYDDATKTFTVTEKKKISKAD
IGAPSGFKHVSHVGWDPQNGFDVNNLDPDLRSLCSRAGISHHHHHH
```

Subcloning of GB1-WASP CRIB gene into pET-14b vector. A double digestion of the amplified pUC-57(GB1-WASP CRIB) vector was performed simultaneously with the double digestion of the pET-14b vector. The reaction conditions were as follows:

pET-14b vector:		pUC-57 vector:	
42.5 µL	pET-14b (20 ng/µL)	15.0 µL	pUC-57 (0.11 µg/µL)
0.0 µL	dH_2O (sterile)	27.5 µL	dH_2O (sterile)
5.0 µL	10× buffer D	5.0 µL	10× buffer D
0.5 µL	100× BSA	0.5 µL	100× BSA
1.0 µL	XhoI	1.0 µL	XhoI
1.0 µL	NcoI	1.0 µL	NcoI
50.0 µL	total volume	50.0 µL	total volume

The reactions were allowed to proceed for 1 hr at 37 °C before stopping with the addition of 12.5 μL of 5× DNA loading buffer. The both reaction mixtures were then loaded onto a 1% agarose gel and resolved at 110 V. The desired restriction products (the GB1-WASP CRIB insert of the pUC-57 vector and the linearized pET-14b expression vector) were cut from the gel and isolated using a QIAquick™ Gel Extraction kit. The subcloning vector and insert were then quantified on 1% agarose gel by comparing band intensities to those of the NEB 2-Log DNA ladder.

Two ligation reactions were assembled: one containing both the GB1-WASP CRIB insert and the pET-14b vector, and the other with only the pET-14b vector as a negative control. The reaction conditions were as follows:

vector (control)		vector + insert	
1.0 μL	pET-14b (50 ng/μL)	1.0 μL	pET-14b (50 ng/μL)
1.0 μL	dH_2O (sterile)	1.0 μL	GB1-WASP CRIB insert
1.0 μL	T4 DNA ligase	1.0 μL	T4 DNA ligase
3.0 μL	2× Ligafast buffer	3.0 μL	2× Ligafast buffer
6.0 μL	total volume	6.0 μL	total volume

Note- Used a 4:1 molar ratio of insert to vector.

The reactions were allowed to proceed for 15 minutes at room temperature. The reactions were then used to transform two 30 μL batches of DH5α cells plated on LB/agar with 50 μg/mL carbenicillin. The next day, no colonies were observed for the negative control. Three colonies from the non-control plate were selected and amplified for sequencing. One of the selected colonies was determined to be the desired construct. The new vector, pET-

14b(GB1-WASP CRIB), was transformed into BL21-Gold(DE3) competent cells from Stratagene for protein expression.

Subcloning of GB1-WASP CRIB N-terminal fragment into pTWIN1 and pTWIN2 vectors. In order to clone the N-terminal fragment of the GB1-WASP CRIB domain into the pTWIN vectors obtained from New England Biolabs® Inc., the following primer set was ordered.

Primers for pTWIN1&2:

Forward:

(NdeI)

GGTGGT**CATATG**GGTCAGTATAAACTGGC

Reverse:

(SapI)

GGTGGTT**GCTCTTC**CGCAGCGCAGATCCGGATCCAGGTTATTA

The desired insert was amplified by PCR using the following reaction conditions:

6.0 µL	dNTP mix (10 mM each)
1.2 µL	Forward primer (100 µg/µL)
1.2 µL	Reverse primer (100 µg/µL)
1.0 µL	DNA template (200 ng/µL)
30 µL	10× Pfu reaction buffer
254.6 µL	sterile dH_2O
6.0 µL	Pfu Turbo (Stratagene)
300.0 µL	Total reaction volume

Once the reaction components were assembled in the PCR tubes and mixed, the tubes were centrifuged briefly and loaded into an MJ-mini PCR machine from Bio-Rad. The following PCR method was employed.

PCR method:

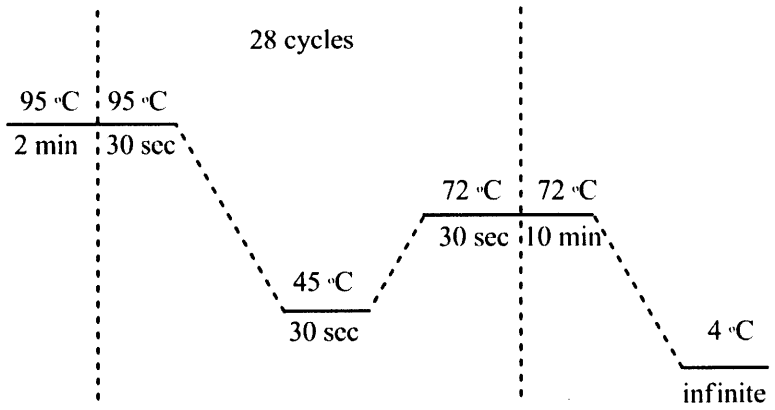

After the PCR was complete, the amplified insert was isolated using the Wizard® SV Gel and PCR Clean-Up System from Promega and quantified by UV absorbance at 260 nm. The insert was then digested using the following reaction conditions:

GB1-WASP CRIB insert:

4.0 µL	insert (500 ng/µL)
36.0 µL	dH_2O (sterile)
5.0 µL	10× buffer 4
0.5 µL	100× BSA
2.5 µL	NdeI
2.5 µL	SapI
50.0 µL	total volume

The restriction reaction run for 3 hours at 37 °C before it was stopped by adding 12.5 µL of 5× DNA loading buffer and transferring to a 1% agarose gel and run at 110 V. The gel was then soaked in ethidium bromide and visualized on the transilluminator. The band corresponding to the insert was excised and purified using the Wizard® SV Gel and PCR Clean-Up System from Promega. The DNA was then quantified by UV absorbance at 260 nm.

Two separate reactions were then assembled to ligate the insert into the two pTWIN vectors. The following reaction conditions were applied:

pTWIN1		pTWIN2	
1.36 μL	vector (36.7 ng/μL)	0.95 μL	vector (52.7 ng/μL)
0.18 μL	dH_2O (sterile)	0.59 μL	dH_2O (sterile)
0.46 μL	insert (30 ng/μL)	0.46 μL	insert (30 ng/μL)
1.00 μL	T4 DNA ligase	1.00 μL	T4 DNA ligase
3.00 μL	2× Ligafast buffer	3.00 μL	2× Ligafast buffer
6.00 μL	total volume	6.00 μL	total volume

The reactions were allowed to proceed for 15 minutes at room temperature. The reactions were then used to transform two 30 μL batches of DH5α cells plated on LB/agar with 50 μg/mL carbenicillin. The next day, no colonies were observed for the negative control. Three colonies from each of the non-control plates were selected and amplified for sequencing. The constructs were transformed into BL21-Gold(DE3) competent cells from Stratagene for protein expression.

Solid phase peptide synthesis of C-terminal fragment of GB1-WASP CRIB domain:

Residue #:																
N-term	**269**	**270**	**271**	**272**	**273**	**274**	**275**	**276**	**277**	**278**	**279**	**280**	**281**	**282**	**283**	C-term
H_2N-	C	L	4-DMNA	S	R	A	G	I	S	H	H	H	H	H	H	-$CONH_2$

The C-terminal peptide component of the fluorescent biosensor design illustrated in Figure 6-4a was prepared using standard Fmoc-based solid-phase peptide synthesis techniques (SPPS).[18] The peptide was prepared using 0.17 mmol/g loading Fmoc-NovaPEG Rink Amide resin LL (Cat. No. 01-64-0483, Novabiochem®). Fmoc-protected amino acids with the standard

side-chain protecting groups were used: Fmoc-4DMNA-OH, Fmoc-Ala-OH, Fmoc-Ile-OH, Fmoc-Leu-OH, Fmoc-Gly-OH, Fmoc-His(Trt)-OH, Fmoc-Arg(Pbf)-OH, Fmoc-Ser(tBu)-OH, and Fmoc-Cys(Trt)-OH. The synthesis was performed on the 40 μmol scale using 4 equiv of the Fmoc amino acids in each cycle. All of the building blocks were dissolved to a final concentration of 50 mM in DMF containing a 1:1 mixture of HOBt/HBTU (50 mM each) with *N,N*-diisopropylethylamine (100 mM, 12 equiv). Each coupling reaction was allowed to proceed at room temperature for 30-45 min. The coupling efficiency was monitored using the TNBS test.[19] Removal of the Fmoc group prior to each coupling step was performed using a 20% 4-methylpiperidine solution[20] in DMF (3 × 5 min). The N-terminal cysteine residue was left as a free amine for ligation to the N-terminal GB1-WASP CRIB fragment. The peptide was cleaved from the resin using a solution of 96:2:2 TFA/H_2O/EDT for 3 hrs. The cleavage cocktail was then filtered and evaporated. The crude peptide was triturated with cold diethyl ether (3 × 10 mL) and purified by HPLC using a Waters 600E HPLC with a Waters 600 automated control module and Waters 2487 dual wavelength absorbance detector set at 228 and 280 nm. The separation was performed using a preparative YMC-pack, C_{18}, 20 × 250 mm reverse-phase column. A YMC-pack, C_{18}, 4.6 ×150 mm reverse-phase column was used for analytical HPLC. The following analytical HPLC method was used to characterize the peptide:

Time (min)	Flow Rate (mL/min)	H_2O % (with 0.1% TFA)	MeOH % (with 0.1% TFA)	Gradient
initial	1.00	95	5	linear
5.0	1.00	95	5	linear
40.0	1.00	0	100	linear

Table 6-1: Characterization of the purified C-terminal GB1-WASP CRIB peptide

HPLC Ret. Time (min)	$[M+xH]^{x+}$ Calc.	$[M+xH]^{x+}$ found
26.9	1937.9 (1+)	—
	969.5 (2+)	970.1 (2+)
	646.7 (3+)	647.4 (3+)

Peptide mass determined by ESI-MS on a Mariner electrospray mass spectrometer (PerSeptive Biosystems).

Acknowledgments

This research was supported by NSF CHE-0414243 (BI), the NIH Cell Migration Consortium (GM064346), and the Biotechnology Training Program (T32-GM08334). I thank Brenda Goguen (MIT) for her hard work, thoughtfulness, and dedication to this project. The Biophysical Instrumentation Facility for the Study of Complex Macromolecular Systems (NSF-0070319) is also gratefully acknowledged.

References

(1) Sinha, S.; Yang, W. Cellular signaling for activation of Rho GTPase Cdc42. *Cell. Signal.* **2008**, *20*, 1927-1934.

(2) Heasman, S. J.; Ridley, A. J. Mammalian Rho GTPases: new insights into their functions from in vivo studies. *Nat. Rev. Mol. Cell Biol.* **2008**, *9*, 690-701.

(3) Bement, W. M.; Miller, A. L.; von Dassow, G. Rho GTPase activity zones and transient contractile arrays. *Bioessays* **2006**, *28*, 983-993.

(4) Leung, D. W.; Rosen, M. K. The nucleotide switch in Cdc42 modulates coupling between the GTPase-binding and allosteric equilibria of Wiskott-Aldrich syndrome protein. *Proc. Natl. Acad. Sci. U.S.A.* **2005**, *102*, 5685-5690.

(5) Bishop, A. L.; Hall, A. Rho GTPases and their effector proteins. *Biochem. J.* **2000**, *348*, 241-255.

(6) Forget, M. A.; Desrosiers, R. R.; Gingras, D.; Beliveau, R. Phosphorylation states of Cdc42 and RhoA regulate their interactions with Rho GDP dissociation inhibitor and their extraction from biological membranes. *Biochem. J.* **2002**, *361*, 243-254.

(7) Erickson, J. W.; Zhang, C. J.; Kahn, R. A.; Evans, T.; Cerione, R. A. Mammalian Cdc42 is a brefeldin A-sensitive component of the Golgi apparatus. *J. Biol. Chem.* **1996**, *271*, 26850-26854.
(8) Cerione, R. A. Cdc42: new roads to travel. *Trends Cell Biol.* **2004**, *14*, 127-132.
(9) Nalbant, P.; Hodgson, L.; Kraynov, V.; Toutchkine, A.; Hahn, K. M. Activation of endogenous Cdc42 visualized in living cells. *Science* **2004**, *305*, 1615-1619.
(10) Toutchkine, A.; Kraynov, V.; Hahn, K. Solvent-sensitive dyes to report protein conformational changes in living cells. *J. Am. Chem. Soc.* **2003**, *125*, 4132-4145.
(11) Hoffman, G. R.; Cerione, R. A. Flipping the switch: The structural basis for signaling through the CRIB motif. *Cell* **2000**, *102*, 403-406.
(12) Abdul-Manan, N.; Aghazadeh, B.; Liu, G. A.; Majumdar, A.; Ouerfelli, O.; Siminovitch, K. A.; Rosen, M. K. Structure of Cdc42 in complex with the GTPase-binding domain of the 'Wiskott-Aldrich syndrome' protein. *Nature* **1999**, *399*, 379-383.
(13) GTPγS is a non-hydrolyzable analogue of GTP.
(14) Bao, W. J.; Gao, Y. G.; Chang, Y. G.; Zhang, T. Y.; Lin, X. J.; Yan, X. Z.; Hu, H. Y. Highly efficient expression and purification system of small-size protein domains in Escherichia coli for biochemical characterization. *Protein Expr. Purif.* **2006**, *47*, 599-606.
(15) Dawson, P. E.; Muir, T. W.; Clark-Lewis, I.; Kent, S. B. Synthesis of proteins by native chemical ligation. *Science* **1994**, *266*, 776-779.
(16) Hackeng, T. M.; Griffin, J. H.; Dawson, P. E. Protein synthesis by native chemical ligation: expanded scope by using straightforward methodology. *Proc Natl Acad Sci U S A* **1999**, *96*, 10068-10073.
(17) Muir, T. W.; Sondhi, D.; Cole, P. A. Expressed protein ligation: A general method for protein engineering. *Proc. Natl. Acad. Sci. U.S.A.* **1998**, *95*, 6705-6710.
(18) Chan, W. C.; White, P. D. *Fmoc solid phase peptide synthesis: a practical approach*; Oxford University Press: New York, 2000.
(19) Hancock, W. S.; Battersby, J. E. New micro-test for detection of incomplete coupling reactions in solid-phase peptide-synthesis using 2,4,6-trinitrobenzene-sulphonic acid. *Analytical Biochemistry* **1976**, *71*, 260-264.
(20) Hachmann, J.; Lebl, M. Alternative to piperidine in Fmoc solid-phase synthesis. *J. Comb. Chem.* **2006**, *8*, 149-149.

Appendix: Useful information

A-1. Determination of the extinction coefficient of 4-DMN (Beer-Lambert plot)

In order to accurately measure the extinction coefficient (ε) of 4-DMN, it was necessary to identify a species that is fully soluble at the required concentrations in TBS buffer (pH 7.4). Compound **3-13** was determined to remain soluble in TBS buffer for days at concentrations as high as 90 μM. Three separate stock solutions of **3-13** were prepared in a 1 L volumetric flask to a final concentration of roughly 90 μM. This concentration corresponds to approximately 25 mg/L. The standard, which had been stored as a solid under high vacuum overnight to desiccate, was weighed on a micro balance into a 7 mL glass vial. The material was then dissolved in 1 mL of spectroscopic grade DMSO and immediately transferred to a 1 L volumetric flask to be diluted in freshly filtered TBS buffer (pH 7.4). The final concentrations of the three stock solutions were 89.7 μM, 88.6 μM, and 89.3 μM. Serial dilutions from these stock solutions were then prepared by making four successive two-fold dilutions. The absorption spectrum of each solution was collected from 220 nm to 600 nm. This enabled the determination of ε for multiple wavelengths. The data corresponding to the absorbance of the chromophore at each wavelength were plotted as a function of the known concentrations of the measured solutions and fitted by linear regression. The slopes of the lines represent the value of ε (M^{-1} cm^{-1}) for each wavelength. The results are summarized in Table A-1 with the associated error for each value indicated by a 90% confidence interval (C. I.) for the three trials. By knowing the ε value at each wavelength, it is possible to resolve the contribution of 4-DMN to the absorption spectrum of a molecule that contains multiple chromophores with overlapping absorption bands.

Table A-1. Molar extinction coefficients for compound **3-13** in TBS (pH 7.4)

wavelength (nm)	ε_{ave} (M^{-1} cm^{-1})	90% C. I.[a] (M^{-1} cm^{-1})
280	9520	800
285	9126	600
290	8496	419
295	7414	231
300	5969	126
305	4674	93
310	3772	22
315	3032	45
320	2538	22
325	2237	41
330	2310	41
335	2007	39
340	2170	20
345	2552	30
350	2300	23
355	2534	21
360	3032	23
365	3581	32
370	4171	18
375	4784	16
380	5365	13
385	5917	16
390	6415	6
395	6867	2
400	7240	11
405	7578	6
410	7871	9
415	8120	9
420	8335	24
425	8517	24
430	8662	25
435	8765	28
440	8808	18
445	8773	22
450	8645	22
455	8410	23
460	8068	22
465	7609	23
470	7056	17
475	6431	16
480	5733	7
485	4925	2
490	4093	9
495	3335	8
500	2602	14
505	1950	19
510	1381	28
515	936	27
520	597	27
525	366	31
530	217	30
535	130	35
540	76	33
545	43	35
550	26	37
555	14	33
560	11	32
565	10	33
570	8	44
575	6	39
580	11	35
585	9	40
590	11	35
595	10	38
600	14	32

(a) The confidence intervals (C. I.) were calculated using the standard deviation determined from three trials and the appropriate value obtained from the student's t-distribution.

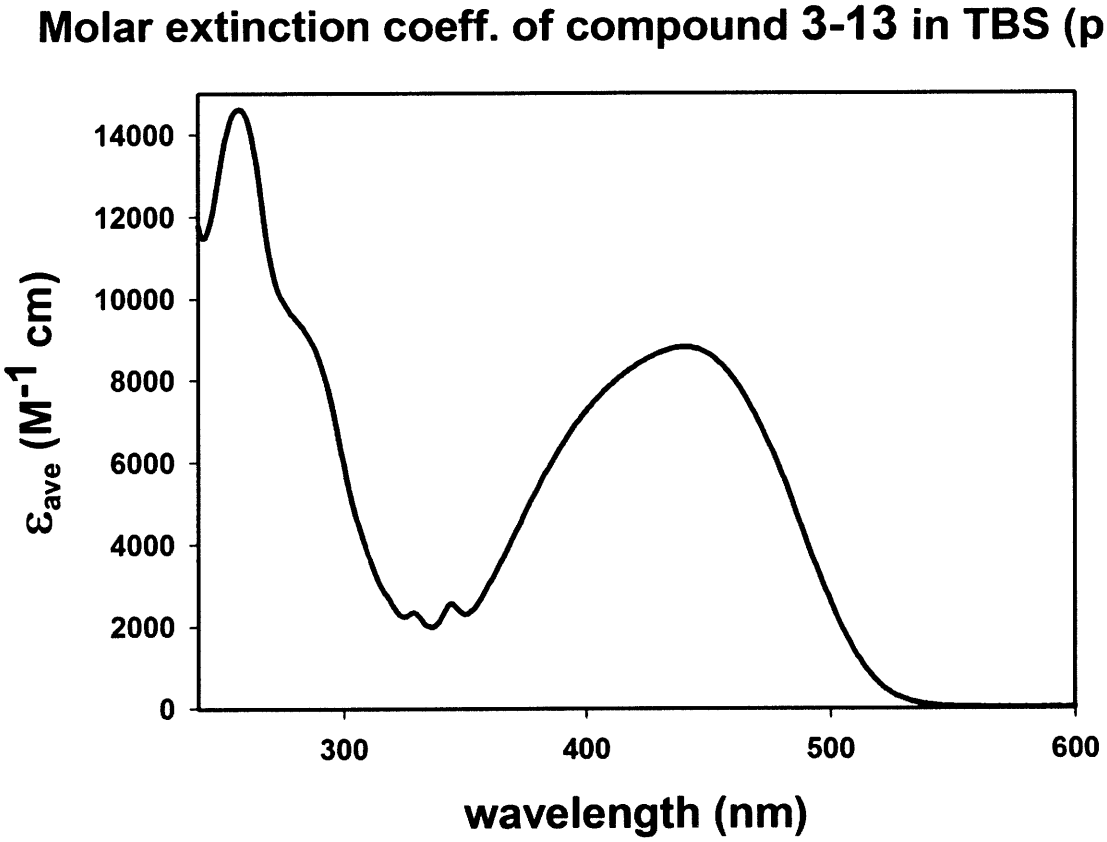

Figure A-1. Graph of the averaged results of three Beer-Lambert plots to determine the molar extinction coefficient of compound **3-13** as a function of wavelength.

A-2. Emission spectra of 4-DMN in solvents of varying polarity

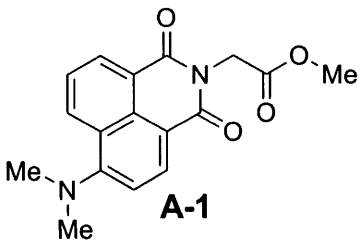

To better illustrate the solvatochromic properties of the 4-DMN fluorophore, compound **A-1** was synthesized and dissolved to a final concentration of 20 μM in the following organic solvents: diethyl ether, benzene, toluene, chloroform, dioxane, tetrahydrofuran (THF), ethyl acetate, acetone, 3-propanol, ethanol, acetonitrile, methanol, and dimethyl sulfoxide (DMSO). The samples were then excited at 375 nm and the emission spectra

collected from 390 nm to 730 nm. The compound exhibits the greatest emission intensity in diethyl ether with an emission maximum at 490 nm. The least emission intensity was observed in DMSO with an emission maximum at 530 nm.

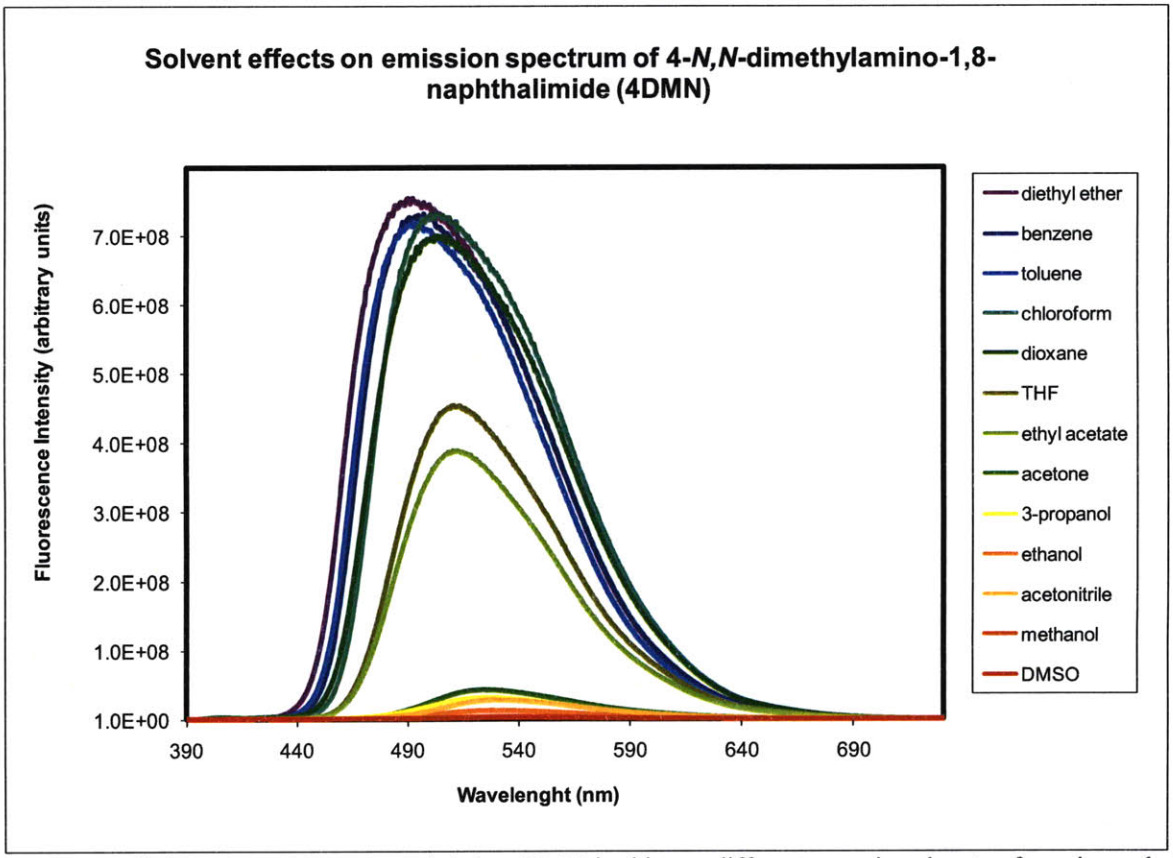

Figure A-2. Emission spectra of compound **A-1** at 20μM in thirteen different organic solvents of varying polarity. The fluorophore exhibits the greatest emission intensity in diethyl ether with an emission maximum at 490 nm. The least emission intensity was observed in DMSO with an emission maximum at 530 nm.

A-3. Improved synthesis of the 4-DMAP anhydride (A-2)

Due to the challenges of synthesizing the 4-DMAP anhydride **A-2** on a multigram scale using the sublimation method described by Vazquez *et al.*[1], and the following alternative approach was developed. This protocol is significantly faster and higher yielding.

Scheme A-1. Improved conditions for the preparation of 4-DMAP anhydride (**A-2**)

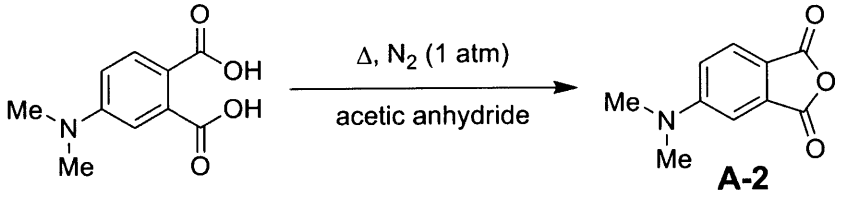

Conversion of the diacid precursor of **A-2** to the anhydride is performed by dissolving the starting material (1.00 g, 4.78 mmol) in 239 mL of acetic anhydride. The solution is prepared in a 500 mL round-bottom flask equipped with a reflux condenser and charged with N_2 gas. The temperature is raised to 140 °C and the reaction is allowed to reflux for 2 hrs. The pale yellow color of the starting material will change to a brilliant fluorescent yellow as the reaction proceeds. Caution – the aniline nitrogen will oxidize rapidly if air is allowed to contaminate the reaction while at high temperature. Once the reaction is complete, the temperature is reduced before removing the acetic anhydride by rotary evaporation. The isolated product is then placed under high vacuum overnight to remove any residual acetic anhydride. The desired product is obtained in quantitative yield (0.91 g, 4.78 mmol).

Reference

(1) Vazquez, M. E.; Rothman, D. M.; Imperiali, B. A new environment-sensitive fluorescent amino acid for Fmoc-based solid phase peptide synthesis. *Org. Biomol. Chem.* **2004**, *2*, 1965-1966.

Curriculum Vitae

Galen S. Loving

30 Chester St. #16 • Somerville, MA 02144 • Phone: 857-991-8017 • Email: gsloving@gmail.com

---

EDUCATION

Massachusetts Institute of Technology, Cambridge, MA — Sept. 2003 – Sept. 2009
Doctor of Philosophy in Organic Chemistry
Thesis supervisor: Professor Barbara Imperiali

University of Kansas, Lawrence, KS — Jan. 1998 – May, 2003
Bachelor of Science in Chemistry, completed Chemistry Honors Program; graduated with Highest Distinction, GPA 4.00/4.00

EXPERIENCE

Massachusetts Institute of Technology, Cambridge, MA — Sept. 2003 – present
Graduate Research Assistant; Thesis supervisor: Professor Barbara Imperiali
Thesis title: New Tools Derived from the Solvatochromic 4-*N,N*-Dimethylamino-1,8-naphthalimide Fluorophore for the Detection of Biomolecular Interactions

- Developed and characterized a new unnatural amino acid containing the solvatochromic fluorophore 4-*N,N*-dimethylamino-1,8-naphthalimide (4-DMN) as the side-chain group. This residue was prepared as an Fmoc-protected building block for solid-phase peptide synthesis and used to prepare fluorescent probes for the direct detection of protein—protein interactions. Fluorescent probes were prepared for SH2 domains, PDZ domains and the calcium-sensing calmodulin protein and were observed to produce 10^3—10^4 fold fluorescence increases upon binding to target proteins.

- Developed a series of cysteine-modifying agents derived from the 4-DMN fluorophore for covalent modification of proteins. These probes were shown to sensitively detect allosteric changes in the calmodulin protein upon addition of calcium. The linker region of these chemical probes was determined to play an important role toward obtaining optimal fluorescent responses. A comparative study of the 4-DMN series of cysteine-modifying agents with members of other commercially available solvatochromic fluorophores showed that 4DMN typically exhibits the strongest fluorescent response to changes in the local solvent environment.

- Examined the pH dependence and kinetics of hydrolysis of the 6-*N,N*-dimethylamino-2,3-naphthalimide (6-DMN) and 4-*N,N*-dimethylaminopthalimide (4-DMAP) fluorophores previously studied in our laboratory. These experiments revealed that 6-DMN and 4-DMAP are particularly susceptible to hydrolysis under alkaline conditions (≥ pH 8) while the 4-DMN fluorophore possess much greater stability over a wide range of chemical and thermal conditions.

- In process of engineering a new fluorescent sensor for imaging the spatial and temporal activation of Cdc42 (a small GTPase of the Rho-subfamily) within living cells.

- Applied the amber codon suppression methodology to incorporate unnatural amino acids of 6-DMN, 4-DMAP, and 4-DMN into the SH2 domain of the adapter protein Crk using an *in vitro* transcription/translation system (*E. coli* T7 S30 extract). Employed a semi-synthetic approach to prepare a series of tRNA charged with these unnatural amino acids to be incorporated through suppression of the amber stop codon (TAG) during protein translation.

AstraZeneca R&D Boston, Waltham, MA Sept 2006 –Nov. 2006
Research Assistant, Assay Development group of the Infection Division
Developed a fluorescence-based assay for high throughput screening of potential small molecule anti-microbial agents. The assay focused on a novel class of therapeutic targets and was designed to meet the demanding requirements of large-scale automated screening using a plate reader format.

University of Kansas, Lawrence, KS Sept. 2001 – May 2003
Undergraduate Research Assistant, Supervisor: Professor Richard Givens
Examined structure/activity relationships between derivatives of the photo-cleavable *para*-hydroxy phenacyl (pHP) protecting groups. Synthesized the 5-(2-bromoacetyl)-2-hydroxybenzoic acid caging group for coupling to various biologically active agents in order to measure the effects of the electron withdrawing carboxylate group on the quantum yield and kinetics of uncaging.
Synthesized lariat crown ethers and cryptands containing photo-cleavable bonds for the facile capture and release bound metal cations.

TEACHING

Supervisor, Undergraduate Research Opportunities Program, Cambridge, MA
- Trained an undergraduate student in the synthesis of a series of novel fluorescent compounds. Topics included basic organic synthesis techniques, flash column chromatography, NMR, fluorescence, and mass spectrometry. Jan 2009 – May 2009

Massachusetts Institute of Technology, Cambridge, MA
Teaching Assistant, Chemical Tools for Assessing Biological Function
- Prepared and graded problems sets focused on reviewing current primary literature related to the course material. Taught a short tutorial on the use of PDB viewing software such as PyMOL and DeepView Swiss-Pdb Viewer. February 2006 – May 2006

Massachusetts Institute of Technology, Cambridge, MA

Teaching Assistant, Organic Chemistry I

- Taught two recitations per week, maintained the course website, graded problem sets and exams, proctored exams, and met with students outside of class time to discuss difficult concepts. Jan. 2004 – May 2004

Massachusetts Institute of Technology, Cambridge, MA

Teaching Assistant, Laboratory Chemistry

- Taught two five-hour laboratory classes per week. Prepared weekly lectures on the experiments to be conducted, demonstrated proper laboratory techniques, supervised student activities within the laboratory setting, prepared and administered weekly quizzes on important concepts discussed in the formal lecture portion of the course, proctored and graded exams. Sept. 2003 – Dec 2003

SKILLS

Solid-phase peptide synthesis, protein preparation and purification, organic synthesis, cloning, large-scale preparation and isolation of DNA, experience with cell-free transcription/translation systems, and experience with RNA work. Possess an extensive background in fluorescence spectroscopy. Responsible for the maintenance and operation of our laboratory ESI-TOF mass spectrometer, Beckman ultracentrifuges, and HPLC systems.

AWARDS AND FELLOWSHIPS

MIT Biotechnology Training Program (MIT/BTP) Fellow	*May 2004-2007*
American Institute of Chemistry Award	*May 2003*
Jacob Kleinberg Award for Outstanding Undergraduate Research	*May 2002*
Max W. Barlow Book Award for Excellence in Organic Chemistry	*May 2001*
Fassnacht Chemistry Career Scholarship	*May 2001*
Proctor and Gamble Book Award for Excellence in Organic Chemistry	*May 2000*

PUBLICATIONS AND PATENTS

Loving, G. and Imperiali, B., A versatile amino acid analogue of the solvatochromic fluorophore 4-*N,N*-dimethylamino-1,8-naphthalimide: a powerful tool for the study of dynamic protein interactions. *J. Am. Chem. Soc.* **130** (41), 13630 (2008).

Loving, G. and Imperiali, B., Thiol-reactive derivatives of the solvatochromic 4-*N,N*-dimethylamino-1,8-naphthalimide fluorophore: a highly sensitive toolset for the detection of biomolecular interactions. *Submitted on 17 July 2009 to Bioconjug. Chem.*

Imperiali, B. and Loving, G., *Peptides incorporating environmentally-sensitive fluorophores for investigating protein-protein interactions*. Application: US Patent No. 2007-710789
2008206885 (20070226. 2008).

Imperiali, B. and Loving, G., *Peptides incorporating environmentally-sensitive fluorophores for investigating protein-protein interactions*. Application: WO Patent No. 2008-US2485
2008106104 (20080226. 2008).

POSTERS

Loving, Galen and Imperiali, Barbara, New tools for detecting protein-protein interactions and changes in protein allostery using derivatives of the environment-sensitive fluorophore 4-*N,N*-dimethylamino-1,8-naphthalimide. *Abstracts of Papers, 236th ACS National Meeting, Philadelphia, PA, United States, August 17-21, 2008*, BIOL (2008).